Imidazoquinazolinone Based Inhibitors of Phosphodiesterase 3

Timothy R. Blackmore

B.Med.Chem (Hons)

A thesis submitted in fulfillment of the requirements for the degree of Doctor of Philosophy.

Medicinal Chemistry

Monash Institute of Pharmaceutical Sciences

Monash University

2012

MONASH University
Pharmacy and Pharmaceutical Sciences

Contents

Front Matter ..... **i**
Statement of Originality i
General Declaration ii
Acknowledgements iv
Abbreviations and Acronyms v
Abstract vii
Chapter 1: Introduction **1**
1.1 Background 1
1.2 PDE3 Genes and Protein Sequence \ Structure 2
1.3 Expression 5
1.4 Transcription and Translation 6
1.5 Phosphorylation and protein complexes of PDE3 7
1.6 Effects of PDE3 Inhibition 9
1.6.1 PDE3A Inhibition 9
1.6.2 PDE3A Knockout Mice 11
1.6.3 PDE3B Inhibition 12
1.6.4 PDE3B Knockout Mice 12
1.7 PDE3 Inhibitors and Heart Disease 13
1.8 PDE3 Inhibitors in the Clinic 15
1.9 Isoform Selective Inhibition 18
Chapter 2: Synthesis and Evaluation of Imidazoquinazolinone PDE3 Inhibitors **21**
2.1 Background 21
2.1.1 Known imidazoquinazolinone PDE3 inhibitors 21
2.1.2 Literature Synthesis of Imidazoquinazolinones 24
2.2 Results and Discussion 27
2.2.1 Selection of Compounds for Synthesis 27
2.2.2 Chemistry 28
2.2.3 Biochemical Assays 33
2.3 Conclusions 40
Chapter 3: Molecular Modeling **42**
3.1 Background 42
3.1.1 Early Applications of Computational Chemistry in PDE3 Inhibition 42
3.1.2 Reports of Computational Chemistry Using PDE3B Crystal Structures 43
3.2 Results and Discussion 45
3.2.1 Preparation and Validation of Models of PDE3A and PDE3B 45
3.2.2 Docking of Known PDE3 inhibitors into the PDE3A and PDE3B Models 54
3.2.3 Docking of Imidazoquinazolinone Analogues 57
3.3 Design of Novel Imidazoquinazolinones to Probe PDE3A and PDE3B Binding Sites 62

3.4 Conclusions 66
Chapter 4: Novel Imidazoquinazolinone PDE3 Inhibitors 67
4.1 7-Aminoimidazoquinazolines 67
4.1.1 Reported Inhibitory Activity of 7-aminoIMQ Derivatives and Analogues 67
4.1.2 Reported Synthetic Approaches 68
4.2 Results and discussion 70
4.2.1 Linear Synthesis of 7-piperazinyl-IMQ 70
4.3.2 Cross-Coupling Reactions of 7-bromo-IMQ 72
4.3.3 Detailed Examination of Buchwald-Hartwig Conditions 75
4.3.4 Optimization of Buchwald-Hartwig Conditions 78
4.3.5 7-aminosubstituted-IMQ Analogues 81
4.4 Biochemical Assays 86
4.5 Structure Activity Relationships 89
4.6 Conclusions 94
Chapter 5: Imidazolidin-4-ones 95
5.1 Outline 95
5.1.1 Fragment Based Drug Design 96
5.1.2 Imidazolidin-4-ones as Fragments 97
5.1.3 Literature Syntheses of IMD and Derivatives 98
5.2 Results and Discussion 99
5.2.1 Synthesis of 4-Imidazolinone 99
5.2.2 Design of Substituted 4-Imidazolinones Fragment Scaffolds 102
5.2.3 Synthesis of Imidazolidin-4-one Based Fragments 103
5.4 Biochemical Assays Versus PDE3 110
5.6 Conclusion 112
Chapter 6 Experimental 113
Computational Methods 113
General Information 114
General Methods 115
Chapter Two Compounds 118
Chapter Four Compounds 128
Chapter Five Compounds 140
References 156
Appendix A 173
A.1 Molecular docking of PDE3A inhibitors into the PDE3A homology model 173
A.2 Docking of reported MERCK1 analogues. 174
Appendix B 177
Monash University Declaration for Thesis Appendix B 177
IMIDAZOLIDIN-4-ONES: Their Syntheses and Applications 178

Early Reports: 179
Cyclization by addition of Nitrogen 183
Imidazolidin-4-one by ring expansion and contraction 184
Other routes to imidazolin-4-ones 188
Imidazolidin-4-ones in synthesis 190
As Organic Catalysts 193
Imidazolidin-4-ones in Medicinal Chemistry 195
Pro drugs 197
Conclusion 199
References and Notes 200

Front Matter

Statement of Originality

To the best of the author's knowledge and belief, this thesis contains no material which has been accepted for the award of any other degree or diploma in any university or other institution, and contains no material previously published or written except where due reference is made.

TIMOTHY R. BLACKMORE

General Declaration

Monash University, Monash Research Graduate School. Declaration for thesis based or partially based on conjointly published or unpublished work

In accordance with Monash University Doctorate Regulation 17/ Doctor of Philosophy and Master of Philosophy (MPhil) regulations the following declarations are made:

I hereby declare that this thesis contains no material which has been accepted for the award of any other degree or diploma at any university or equivalent institution and that, to the best of my knowledge and belief, this thesis contains no material previously published or written by another person, except where due reference is made in the text of the thesis.

This thesis includes 1 original paper published in a peer reviewed journal. The core theme of the thesis is the search for novel inhibitors of phosphodiesterase 3A and 3B. The ideas, development and writing up of all the papers in the thesis were the principal responsibility of myself, the candidate, working within the theme of Medicinal Chemistry and Drug Action under the supervision of Associate Professor Philip Thompson and Dr David Manallack. The co-author of the paper is Associate Professor Philip Thompson.

In the case of Appendix B my contribution to the work involved the following:

Thesis Chapter	Publication title	Publication status	Nature and extent of candidate's contribution
Appendix B	Imidazolidin-4-ones: Their syntheses and applications	Published	Literature review and manuscript preparation

I have not renumbered sections of submitted or published papers in order to generate a consistent presentation within the thesis.

Signed: ……

Date: ……

Acknowledgements

First and foremost I would like to thank my supervisor Dr Philip Thompson for his guidance, and mentorship as well as his unwavering encouragement and support throughout this project. I would also like to thank Dr David Manallack for his input, particularly with the computational chemistry work.

Thanks to everyone in the Thompson group who made my candidature so much fun. My friends and fellow students who have shared the trials and tribulations with me; Diana Neale, William Nguyen, Susan Northfield, Jo-anne Pinson, Michelle Camarino, Jacob Nankervis, Brittany Howard, Michelle Miller, Syazwani Amran, and Oscar Lui. Thanks to the post-docs in the lab who have taught me throughout my candidature, and have helped solve all kinds of problems; Gerard Moloney, Simon Mountford, Kade Roberts, Ian Jennings, and Joyce Zheng. Thanks to Jason Dang for performing the mass spectrometry experiments, and teaching me to use a variety of equipment.

I would also like to those in other labs whose friendship I have enjoyed in and outside of my time at Monash; Christopher Opie, Mark Agostino, Jennifer La, Joshua Gosling, Vladimir Moudretski, Brad Doak, Wendy Zeng, Yanni Chin, Fiona McRobb, Natalie Vinh, Amelia Vom, Mansha Vazirani,

I would particularly like to thank my friends and housemates James Buist, Asher Rogers and Ashleigh Cooper for encouraging me throughout the years and for putting up with my student ways.

Finally I would like to thank my family for getting me to where I am now. The support of my parents Heather Peters, and Don Blackmore; and my step-parents Colleen Blackmore, and Graham Peters; has been incredible and a great comfort to me. I would also like to thank my inspiring sister Lucy Hearn and her wonderful family.

Abbreviations and Acronyms

Å	Angstrom
ACN	Acetonitrile
AMP	Adenosine monophosphate
Ar	Aryl
BINAP	2,2'-bis(diphenylphosphino)-1,1'-binaphthyl
Boc	*tert*-butyloxycarbonyl
°C	Degrees Celsius
^{13}C-NMR	Carbon-13 nuclear magnetic resonance
cAMP	Cyclic adenosine monophosphate
celite	Diatomaceous earth
CHF	Chronic heart failure
CLogP	Calculated logarithm of the partition coefficient
Conc.	concentrated
Da	Dalton
DCM	Dichloromethane
DEPT	Distortionless Enhancement by Polarization Transfer
DIPEA	*N,N*-diisopropylethylamine
DMF	N,N-dimethylformamide
DMP	4,4-dimethyl-1H-pyrazol-5(4H)-one
DMSO	Dimethylsulfoxide
ESI	Electrospray ionization
equiv	equivalence
FBDD	Fragment Based Drug Design
h	Hours
^{1}H-NMR	Proton nuclear magnetic resonance
HBTU	O-(Benzotriazol-1-yl)-N,N,N′,N′-tetramethyluronium hexafluorophosphate
HCTU	O-(6-Chlorobenzotriazol-1-yl)-N,N,N′,N′-tetramethyluronium hexafluorophosphate
HPLC	High performance liquid chromatography
HRMS	High Resolution Mass Spectrometry
HMBC	Heteronuclear Multiple Bond Correlation
HSQC	Heteronuclear Single Quantum Coherence
HTVS	High throughput virtual screening
IC_{50}	Concentration at which 50% inhibition occurs
IMD	Imidazolidin-4-one
IMQ	Imidazoquinazolinone, or 3,5-dihydroimidazo[2,1-b]quinazolin-2(1H)-one

°K	Degrees Kelvin
LiHMDS	Lithium bis(trimethylsilyl)amide
MDP	(R)-5-methyl-4,5-dihydropyridazin-3(2H)-one
MEK	Methyl Ethyl Ketone
MS	Mass Spectrometry
MW	Molecular Weight
NMR	Nuclear magnetic resonance
$Pd_2(dba)_3$	Tris(dibenzylideneacetone)dipalladium(0)
PDE	Phosphodiesterase
PKA	Protein Kinase A
PKB	Protein Kinase B
PKG	Protein Kinase G
ppm	Parts per million
pTSA	*para*-Toluene sulfonic acid
RT	Room temperature
RMSD	Root mean square deviation
SAR	Structure activity relationships
Sat.	Saturated
SP	Standard precision
TBAB	Tetra-n-butylammonium bromide
TBTU	O-(Benzotriazol-1-yl)-N,N,N',N'-tetramethyluronium tetrafluoroborate
TFA	Trifluoroacetic acid
THF	Tetrahydrofuran
TLC	Thin layer chromatography
VdW	Van der Waals
VSMC	Vascular smooth muscle cells
XP	Extra precision

Abstract

Phosphodiesterases (PDE) catalyze the deactivation of cyclic adenosine monophosphate (cAMP) and cyclic guanosine monophosphate (cGMP). Inhibiting a cell's PDE increases the level of cAMP or cGMP in the cytosol, enhancing the cells response to stimuli. Selectively inhibiting a PDE subtype can cause a specific cell or tissue type to elicit a therapeutic response. In the past PDE3 inhibitors were designed as cardiac inotropic agents to replace cardiac glycosides and sympathomimetic drugs. Though they were effective, limitations due to serious side effects arose and PDE3 inhibitors were largely abandoned. Further research has found two isoforms of PDE3; PDE3A which is responsible for PDE3 inhibitors inotropic and antithrombotic effects, and PDE3B which is involved in the insulin signaling pathway. The majority of literature PDE3 inhibitors have not been examined for isoform selectivity between PDE3A and PDE3B. Inhibitors that select for either subtype will assist in delineating the physiological roles of these isoforms and may show improved therapeutic profiles.

A variety of known and novel PDE3 inhibitors based on an imidazoquinazolinone scaffold were synthesized and screened against each isoform. A literature PDE3 inhibitor was found to be 13 fold selective for PDE3A over PDE3B and is the most selective PDE3A inhibitor identified to date. An improved synthetic route to analogous compounds was established. This approach was used to design and synthesize a focused library of compounds. From this library several potent novel PDE3 inhibitors were identified.

Inspired by the structures known PDE inhibitors a series of novel compounds incorporating an imidazolidin-4-one ring were synthesized. The synthesis and derivatization of this structural motif was explored in an effort to use Fragment Based Drug Design to develop novel ligands for PDE inhibition or other therapeutic targets.

Chapter 1: Introduction

A shock of adrenaline springs loose the system of cyclic adenosine monophosphate (cAMP) synthesis, stimulating the soma with a sanguine surge; soon a phosphodiesterase suppresses the swell of second messenger slowly settling, and sobering the spirit.

1.1 Background

When an extracellular receptor binds a signalling molecule such as adrenaline, that signal can be propagated to the cell's internal components via a second messenger. Many cell types do so via the cAMP-dependant pathway, in which cAMP is produced to function as the second messenger. In response to the binding of a signalling molecule to a G-protein coupled receptor (GPCR), adenylyl cyclase is activated to produce cAMP from adenosine triphosphate (ATP). The produced cAMP activates cAMP-dependant protein kinase (PKA), which goes on to catalyse the phosphorylation of other proteins, leading to the hallmark cell responses of that original extracellular binding event. The signal is terminated by cyclic nucleotide phosphodiesterase (PDE) enzymes which convert cAMP to AMP, consequently attenuating the cells response. An analogous pathway exists where guanosine triphosphate (GTP) is converted to the second messenger cyclic guanosine monophosphate (cGMP) by guanylate cylase (GC). cGMP then activates target intracellular proteins such as protein kinase G (PKG). cGMP activity is also deactivated by PDEs converting it to guanosine monophosphate (GMP). If the PDE enzyme is inhibited the concentration of cAMP and/or cGMP increases and so too does the cell's response.[1] Pharmacological PDE inhibitors thus amplify the native cyclic nucleotide signal and have been very effective in treating a number of diseases through this mechanism. Moreover, specific tissues can be targeted through the different types of phosphodiesterase they express.

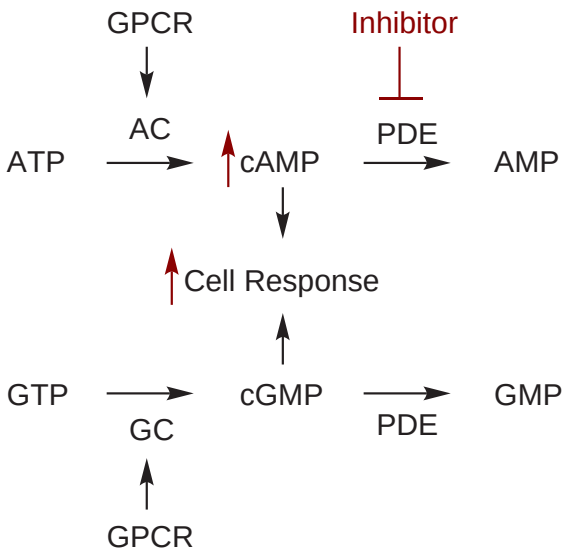

Figure 1 Phosphodiesterase inhibition in the cAMP signal transduction pathway.

A total of 11 families of cyclic nucleotide phosphodiesterase enzyme have been identified, and each family is further sub-divided into isoforms and splice variants. The families vary in their regulation, structure, and susceptibility to different inhibitors. Expression of the different PDE subtypes varies between tissues, cell types, and sub-cellular location. Affinity for cAMP vs. cGMP varies significantly between families but less so within them. Members of the PDE1, 2, 3, 10 and 11 families are able to hydrolyse both cAMP and cGMP, while PDE4, 7, and 8 are cAMP specific, and PDE5, 6, and 9 are cGMP specific.[2-4] There are several successful drugs that act through the inhibition of particular PDE families, eg. sildenafil, a PDE5 inhibitor; and cilostazol, a PDE3 inhibitor. This thesis is focused on inhibitors of the PDE3 family.[4]

PDE3 was originally described pharmacologically as, "low *K*m, cGMP-inhibited cAMP PDE". PDE3 has higher affinity for cGMP than cAMP (K_m of 30 μM vs. 90 μM) but have a higher turnover of cAMP than cGMP (k_{cat} of 30 min^{-1} vs. 6 min^{-1}).[5] The enzyme hydrolyses cGMP so slowly that it can be considered to be inhibited by it.[6-8] In some cases an increase in cGMP can cause an increase in cAMP due to inhibition of PDE3 by cGMP, this can lead to cross talk within a cell between the two second messenger systems.[9, 10]

1.2 PDE3 Genes and Protein Sequence \ Structure

In the PDE3 family there are two subtypes, named PDE3A and PDE3B that are produced from two separate genes.[11, 12] PDE3A is located on chromosome 11, and PDE3B on chromosome 12.[13, 14] Each of the

genes are between ~121 kb and ~312 kb long in mice or humans and contain 16 exons.[15] Interestingly, human PDE3 subtypes are better matched to rat PDE3 subtypes than they are with each other within one species. Polymorphisms in PDE3B were being investigated as contributing factors of non-insulin dependant diabetes mellitus and obesity, however no correlating single nucleotide polymorphism has been found.[16, 17]

All mammalian PDEs share a conserved catalytic core composed of about 270 amino acids, which is found towards to the C-terminal. Similarity is very high (>80%) in this region between members of the same PDE family, and is significant across families (~25-40%). The high sequence homology translates into structural homology which typically includes a variable C-terminal region and a variable regulatory N-terminal region. The structural organization of PDE3 subtypes, PDE3A and PDE3B are identical. Both members of the PDE3 family have a 44 amino acid insert within the catalytic domain sequence, this insert's sequence differs significantly between PDE3A and PDE3B, and is absent in all other PDEs families.

The catalytic domain of PDE isoforms contain two characteristic sequences, a $HisAsp(X)_2His(X)_4$ Asn motif, and two putative metal binding domains $His(X)_3His(X)_{24\text{-}26}Glu$. Together these motifs form a binuclear divalent metal-binding site in most PDEs. In PDE3 the 44 amino acid insert exists within the first of the two metal binding domains, producing a larger gap separating the second histidine from the glutamic acid than the usual 24-26 residues. PDE3 are also unique amongst PDE isoforms in that they use manganese, magnesium or cobalt ions, rather than zinc, which is used in most other PDE enzymes. This is an important distinction as replacing the native metal ion with Zinc has an inhibitory effect on PDE3A.[18]

The N-terminal and the C-terminal domains are more varied across all the PDE families.[6-8, 19] The N-terminal region contains a regulatory domain that can arbitrarily divided into two regions, region one contains a large hydrophobic domain consisting of 5-6 transmembrane helices, region two contains phosphorylation sites for both PKA and protein kinase B (PKB) and a membrane targeting sequence.[4]

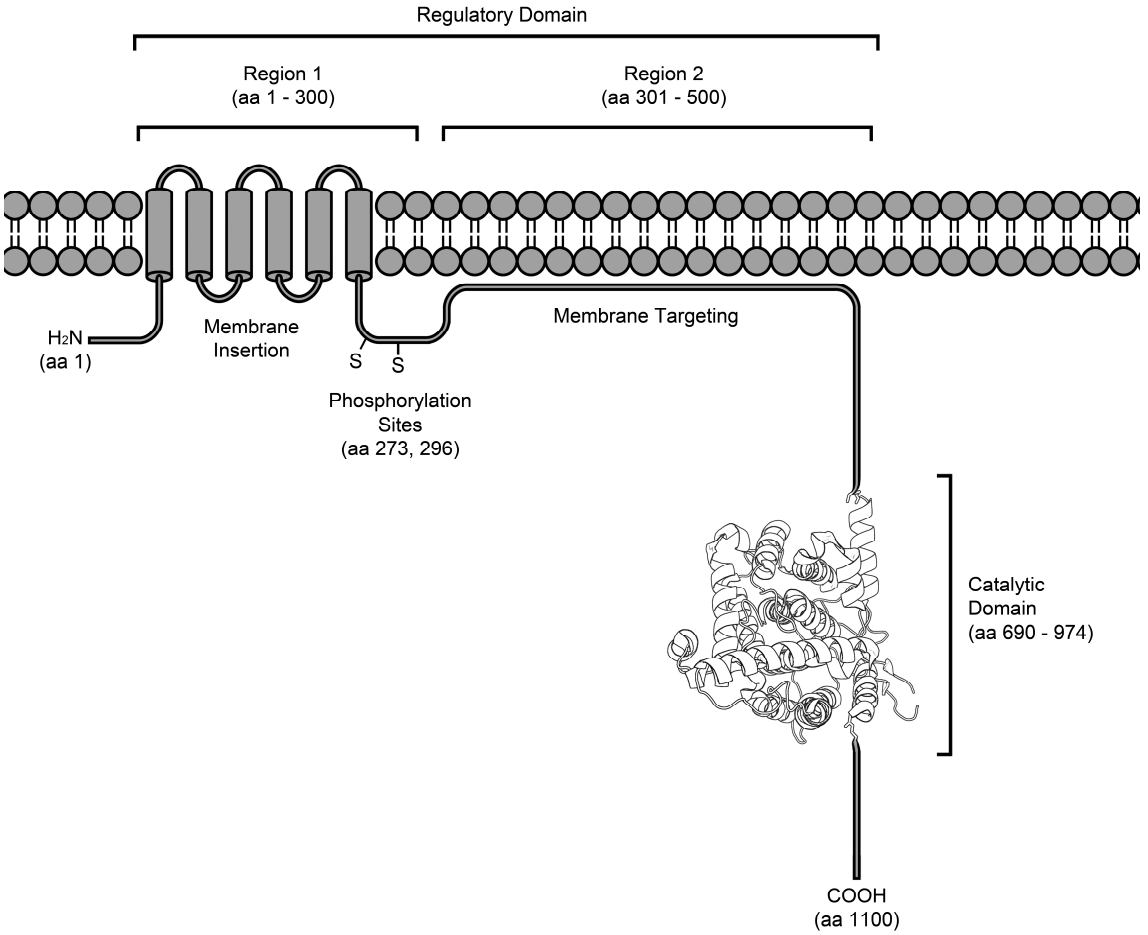

Figure 2 Overview of PDE3B catalytic and regulatory domains.[15]

Studies of truncated PDE3 isoforms have shown that the N-terminal domain is not necessary for activity.[20] There is low homology in the C-terminal domain between isoforms as well but no specific functions associated with them. The limits of the catalytic domain of human PDE3B have been refined by deletion mutagenesis, it was reported that the smallest active construct begins between Glu665 and Tyr667 and ends at Lys1073.[21] Similar yet less definitive results have been reported for human PDE3A in which the catalytic domain begins near Asp680 and ends somewhere between Glu1051 and Pro1108.[22] The minimum catalytic domain of rat PDE3B is equivalent to human PDE3B residues 654 – 1086, the catalytic domain of mouse PDE3B is equivalent to human PDE3B residues 624 – 1112.[22, 23] It was found that the when the 44-amino acid insert is deleted the rat PDE3B enzyme can no longer function.[22] Neither were mutations of the putative β-turns at either end of the insert tolerated.[24]

1.3 Expression

While the second messenger molecule cAMP is found in many different tissue and cell types, the location of different PDE subtypes is tightly controlled. The combination of tissue specific localization and direct amplification of cell response make specific PDEs attractive targets in a number of disease states. Inhibitors that are selective for a single isoform of PDE are useful because they only affect tissue types that express that isoform. A famous example of a selective PDE inhibitor is sildenafil, which inhibits PDE5 which is expressed in corpus cavernosum, as a safe and orally available treatment for erectile dysfunction.

The two subtypes of the PDE3 family are expressed separately in some tissue types but overlap in some others. The overriding distinction is that PDE3A is predominantly expressed in the cardiovascular system, while PDE3B is expressed in tissues responsible for the metabolism of glucose and lipids. More specifically the PDE3A isoform is found predominantly in platelets, oocytes, megakaryocytes, heart and vascular smooth muscle. Whereas the PDE3B isoform is expressed predominantly in white and brown adipocytes, hepatocytes, pancreatic beta cells, renal collecting duct epithelium, and developing spermatocytes. There are many intricacies to PDE3A / PDE3B expression not covered by the generalization that PDE3A is cardiovascular and PDE3B is in energy homeostasis. Studies of rat developing rat brains indicate that both PDE3 isoforms are expressed in the brain, however while PDE3B is expressed uniformly across the brain while PDE3A is expressed in different regions at different stages of development.[4, 25-27] Although PDE3A closely associated with platelets, T-lymphocytes and monocyte derived macrophages are dominated by PDE3B.[28, 29]

To aid the characterization of both PDE3A and PDE3B physiological roles, knockout mice have been produced and compared, their phenotypes confirmed that PDE3A plays a significant role in the cardiovascular system, particularly in regards to platelet aggregation; and PDE3B has a complex role in energy homeostasis.[30, 31]

While PDE3A and PDE3B are expressed in other tissues there are often PDEs from other families also present, which leads to further complexities. In cells that contain multiple types of PDE, selectively inhibiting just one isoform of PDE can have a significantly different outcome than inhibiting another. This may seem counterintuitive as both PDEs are converting cAMP to AMP, but is likely a result of subcellular

localization, which is where the concentration of cAMP is not uniform across the entire cytosol instead distinct pools of cAMP exist due to the location of the enzymes that produce and degrade it.[32] In adipocytes the majority of PDE3s are found in the microsomal fractions.[33] In platelets they are more abundant in the cytosol,[34] and in rat myocardium and vascular smooth muscle PDE3A is cytosolic and PDE3B is found in particulate fractions.[35] These differences in subcellular localization are attributed to differences in the N-terminal region between isoforms and their transcriptional variants.

1.4 Transcription and Translation

There are three known transcription variants of PDE3A, and only one known for PDE3B. The single full length PDE3B has been shown to associate with the cell membrane.[36] The three PDE3A variants are all generated from the PDE3A gene but undergo either an altered transcription, or post transcription processing. The full length PDE3A1 (PDE3A-136) contains a group of transmembrane helices, one PKB phosphorylation site two PKA phosphorylation sites, and a membrane targeting region, this variant binds to membranes. PDE3A2 (PDE3A-118) is missing the transmembrane helices and one phosphorylation site, it is found in the cytosol and membrane associated cell fractions, finally PDE3A3 (PDE3A-94) is missing both N-terminal hydrophobic domains and all three phosphorylation sites, which causes it to be cytosolic.[35, 37-39] Wechsler et al. hypothesize that the full length PDE3A1 is produced when the transcription begins at the A1 site, and PDE3A2 and PDE3A3 when transcription begins at the A2 site. They further suggest that PDE3A2 and PDE3A3 are a result of alternate translation sites within the shorter transcript.[40] Since the N-terminus is home to a membrane association domain and sites for activation by phosphorylation, different transcript variants and truncated mutants have different sensitivities to activation pathways due to both localization and activation.[4, 37, 38, 40]

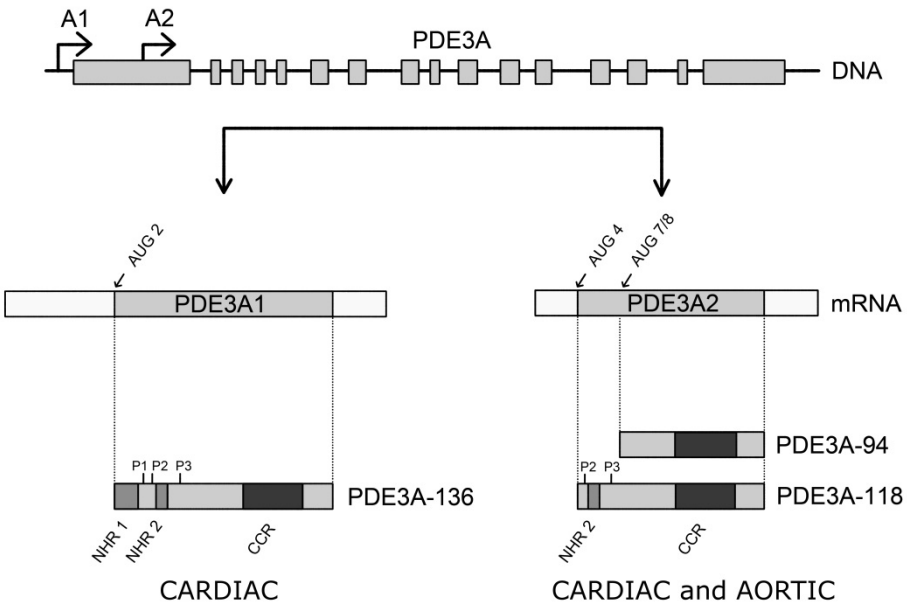

Figure 3 Suggested origins of the three truncations of PDE3A Top – PDE3A exons with two transcription sites, Left – Translation of full length PDE3A1, Right – Alternate translation sites and products for PDE3A2 and PDE3A3. Reproduced with permission.[40]

PDE3B is found associated with the cell membrane, more specifically it is found to associate with caveolae, which are detergent resistant invaginations of the plasma membrane. There may be some interaction between PDE3 and caveolin (which stabilizes caveolae) as they are present in the same structure, and have both been associated with cAMP and insulin pathways.[41-43]

1.5 Phosphorylation and Protein Complexes of PDE3

In addition to the enzymes subcellular location it is also important to consider its interactions with other proteins and what affect they have on activity. An important protein-protein interaction for PDE3 is where elevated levels of cAMP activate PKA, and PKA activates PDE3 by phosphorylating sites in its regulatory domain, once activated PDE3 increases its turnover of cAMP completing a negative feedback loop. PDE3s are likely to exist as dimers in solution, as they possess a dimer interface that is conserved between PDE3 and PDE4 and mutations at this site in PDE4 disrupt oligomerization in solution.[44] Dimerization that is present in the PDE3 crystal structures is therefore unlikely to be an artifact of crystallization, it is expected that this also holds true for the full length enzyme.[45]

PDE3 isoforms form complexes with a number of other proteins, not just with themselves. During purification PDE3B elutes as large protein complexes of ~670 kDa and >4000 kDa, these large complexes only exist if the N-terminal domain is present.[20, 23, 36, 41] These complexes have been found to contain phosphorylated PDE3B with other signaling proteins such as insulin receptor substrate (IRS)-1, phosphatidylinositol-3-kinase (PI3K) p85, protein kinase B (PKB), heat shock protein (HSP)-90, phosphoprotein phosphatase (PP)-2A and 14-3-3.[15, 41] Complexes of PDE3 with other signaling proteins may play a role in combining and modulating responses from multiple signal sources. Formation of these signaling complexes as well as phosphorylation of PDE3B is triggered by insulin and can be blocked by pre-treatment with a PI3K inhibitor.[15]

Additional reports indicate that in adipocytes, the antilipolytic response to insulin is mediated by the phosphorylation and activation of PDE3B by PKB. This has been shown by inhibiting PDE3B, after which adipocytes no longer respond to insulin.[46] Additionally insulin has no effect on lipolysis in adipocytes that have been activated with cAMP analogues, that cannot be hydrolyzed by PDEs.[47] Finally, cells that express a modified constitutively active mutant of PKBα have phosphorylated PDE3B, with or without the addition of insulin-like growth factor 1 (IGF-1).[48] Similarly PDE3B is activated in pancreatic β-cells by IGF-1 and in hepatocytes by insulin and cAMP-increasing hormones.[26, 49, 50] PDE3s are also activated by insulin-like growth factor 1 (IGF-1) or by elevated levels of cAMP.[51] Protein phosphatase 2A (PP2A) is responsible for the dephosphorylation of PDE3B and protein phosphatase 1 for PDE3A.[52, 53]

PDE3A is activated by phosphorylation at as many as five different sites by different kinases resulting in distinct protein-protein interactions.[54] Activation of platelet PDE3A via PAR-1 is dependent on the activation of PKC; however activation triggered by thrombin goes via PKB and $P2Y_{12}$. Once activated via PKC PDE3A associates with 14-3-3 proteins. Alternative signaling molecules such as PGE_1 and forskolin also activate platelet PDE3A, however in these cases only one site (Ser312) is phosphorylated and there is no subsequent association with 14-3-3.[53, 55] There is evidence of a prothrombotic interaction between PDE3A and the leptin receptor in platelets.[56]

1.6 Effects of PDE3 Inhibition

1.6.1 PDE3A Inhibition

An array of physiological responses can be induced by inhibition of the PDE3A subtype. These responses can be characterized as inotropic, lusitropic, vasodilating, platelet deactivating, anti proliferative and bronchodilating. The mechanisms by which these responses are induced are outlined in this section.

In myocardium PDE3 inhibition increases the concentration of cAMP, which activates PKA. PKA effects phosphorylation of calcium channels on both the cell membrane, and the sarcoplasmic reticulum (SR), SR-associated phospholamban, and troponin I. Consequently, there is more Ca^{2+} moving into the cell through the cell membrane and the SR during systole, and the SR recovers more Ca^{2+} during diastole. These effects combined lead to increased flux of cytosolic Ca^{2+} and therefore increase the extent of contraction and relaxation, the overall effect is inotropic.[4]

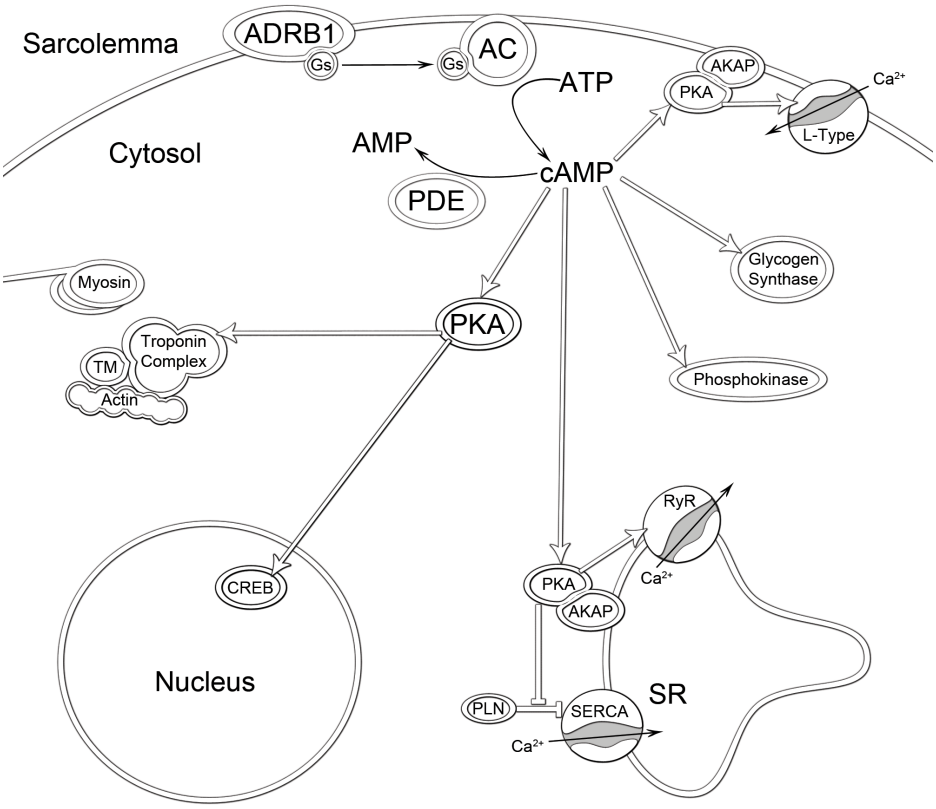

Figure 4 β_1-adrenergic receptor signal transduction in cardiac myocytes. ADRB1 = β_1-adrenoceptor AC = adenylate cyclase, Gs = Stimulative regulative G-protein, AKAP = A-kinase anchor protein, PKA = protein kinase A, L-Type = L-Type calcium channel, ATP = adenosine triphosphate, cAMP = cyclic adenosine monophosphate, AMP = adenosine monophosphate, PDE = phosphodiesterase, TM = Tropomyosin, RyR = Ryanodine receptor, SERCA = Sarco/Endoplasmic reticulum calcium ATPase, SR = Sarcoplasmic Reticulum, PLN = phospholamban, CREB = cAMP response-element binding. Adapted from Movsesian et al.[57]

Rat vascular smooth muscle cells (VSMC) express both membrane bound PDE3B and cytosolic PDE3A.[35] PDE3 inhibitors are known to act as vasodilators through VSMC; this is likely to be a result of higher concentrations of cAMP cross-activating protein kinase G (PKG) which is usually activated by cGMP.[58]

Endogenous antithrombotics such as adenosine, prostacyclin and prostaglandin D_2 cause platelets to produce cAMP via adenylyl cyclase. PDE3 inhibitors prevent the degradation of cAMP in platelets causing a similar increase in concentration and antithrombotic effect.

A report found that the PDE3 inhibitor Cilostazol suppresses the proliferation of rat aortic smooth muscle cells.[59] There is also evidence that the same drug reduces restenosis after percutaneous transluminal coronary angioplasty or coronary atherectomy.[60, 61] These effects combine to make PDE3 inhibition a target for treatment of several disease states, particularly chronic heart failure (CHF). However, PDE3 inhibitors have been contraindicated in CHF patients which is discussed in Section 1.8.

PDE3 inhibitors cause relaxation of airway smooth muscle, even though there are several other types of PDE present in the associated tissues. This could be of use in treatment of asthma and chronic obstructive pulmonary disease.[62]

1.6.2 PDE3A Knockout Mice

PDE3A and PDE3B knockout mice were produced and studied to confirm and further investigate which subtype is responsible for which physiological effects. In these studies it was found that PDE3B expression is upregulated by cAMP and that PDE3A is not.[63] Cultured VSMCs from the aortas of PDE3A and PDE3B knockout mice show that PDE3A is required for mitogen induced proliferation.[64]

Mice lacking PDE3A are protected pulmonary thromboembolism caused by collagen and epinephrine however; the same mice showed an increase in heart rate and a decrease in arterial blood pressure and left ventricular pressure. The increase in heart rate led to the suggestion that PDE3A is largely responsible for cAMP metabolism in sinoatrial nodal pacemaker cells, which are responsible for regulating heart rate.[30]

Female PDE3A knockout mice develop normally except that they are completely infertile. Oocyte maturation is completely arrested in prophase I due to high levels of cAMP persistently activating PKA and thereby blocking maturation-promoting factor and mitogen-activated protein kinase (MAPK). This mechanism could lead to the development of new non-hormonal contraceptive agents. The advantage of this approach is that it would not interfere with the normal menstrual cycle. However, unless the oocyte can be specifically targeted there may be a risk of cardiovascular side effects.[65]

1.6.3 PDE3B Inhibition

There are two opposing sides to the role of PDE3B in diabetes; these have been investigated in PDE3B knockout mice. Type 2 diabetes (T2D) is characterized by dysregulation of adipose tissue activity, leading to development of hyperglycemia and dyslipidemia. Patients with T2D have increased levels of nonesterified free fatty acid (FFA), this increase leads to systemic insulin resistance.[66, 67] As discussed previously, PDE3B is required for the antilipolytic action of insulin. If PDE3B is inhibited in adipocytes lipolysis could run out of control, increasing the level of FFAs in circulation. Some evidence of this occurring in the diabetic disease state exists where diabetic patients and diabetic animal models have shown decreased PDE3 activity and / or expression in adipose tissue.[68, 69] Conversely PDE3B inhibition potentiates the secretion of insulin by pancreatic β-cells in response to incretins (e.g. GLP-1) which would be beneficial for treating T2D. Other potentially beneficial effects are increased thermogenesis and reduced inflammation in adipose tissue.

1.6.4 PDE3B Knockout Mice

To investigate the balance of these beneficial and risk inducing effects PDE3B knockout mice were produced, they were found to develop and behave similarly to the wild type (WT). They were fertile and had an unaltered lifespan, overall the KO mice were slightly heavier yet they were found to have less gonadal adipose tissue and smaller adipocytes. A greater response was seen in KO mice than WT upon injection of catecholamines which caused an increase in the circulating levels of lipolysis products (FFA and glycerol), presumably from adipocytes. Basal levels of FFA and glycerol did not vary between the wild-type and KO, but fasting levels did. It was found that without active PDE3B insulin is unable to control catecholamine stimulated lipolysis in adipocytes. The liver of KO mice was less sensitive than a WT mice's to the inhibitory effect of insulin on endogenous glucose production.[31]

When stimulated by incretins, the pancreatic β-cells of KO mice released more insulin than WT mice. While the KO mice did eventually become insulin resistant, they were not hyperglycaemic and therefore not diabetic.[31]

Treatment of WT mice and rats with PDE3 inhibitors results in a similar mix of these diabetogenic and potentially therapeutic responses i.e. Increases in lipolysis, insulin secretion and endogenous glucose production.[70, 71] Negative control mice that over express PDE3B in pancreatic β-cells, secrete less insulin in response to glucose. They are also more likely than WT mice to develop diabetes like-symptoms if fed a high fat diet.[72]

It appears that PDE3B inhibition in adipocytes and hepatocytes is liable to induce T2D, while the same inhibition in pancreatic β-cells could offer a treatment through increased insulin secretion. Whether an inhibitor could be selectively delivered to tissues that offer therapeutic outcomes is beyond the scope of this investigation.

1.7 PDE3 Inhibitors and Heart Disease

It was through the use of selective inhibitors that much of the early work in understanding the different PDE family's tissue expression and function was accomplished. PDE3 is selectively inhibited by cilostamide, cilostazol, milrinone, enoximone, siguazodan, trequinsin, OPC-3911, lixazinone and others.

PDE3 inhibitors have a long and chequered history in clinical trials, in some trials they failed so completely that the class could be considered as inherently flawed. At the heart of PDE3 inhibitors failure is the increased risk or mortality that comes with prolonged use in patients with chronic heart failure (CHF), a disease state that they had been designed to treat. The mechanism by which PDE3 inhibitors side effects may arise is discussed, followed by several examples of drugs that have failed from the negative side effects, and others that have succeeded despite them. In other trials certain off-target or compensatory effects in combination with targeting different patient groups have led to resounding successes.[73-77]

Currently PDE3 inhibitors can be used for short term treatment of acute CHF where they provide similar effects as β-adrenergic receptor agonists. In both approaches, the increase in cAMP concentration in cardiomyocytes is pivotal to the therapeutic effect.

There are some other limitations to using PDE3 inhibitors to treat CHF. Studies of the left ventricle muscle of patients in different stages of CHF found that the inotropic effect of PDE3 inhibitors decreases as the disease progresses. The decrease in PDE3 inhibitor efficacy has been linked to a decrease in PDE3 activity which in turn was linked to a lack of PDE3 enzyme.[78, 79] A lack of PDE3 to inhibit could limit the

efficacy of these drugs in treating CHF even if the dangerous side effects could be overcome. There has been some disagreement as to the extent that PDE3 is down regulated in heart failure, while it can be shown that PDE3 is down regulated, the effect may be to contribute to the progression of heart failure, or conversely aide in compensating the disease state.[80]

Further investigation of PDE3's role in heart failure may have discovered the mechanism by which increased levels of cAMP can increase mortality. Hydrolysis of cAMP in cardiac tissue is predominantly carried out by both PDE3 and PDE4. While prolonged inhibition of PDE3 increased rat neonatal cardiac myocyte apoptosis, prolonged PDE4 inhibition did not. This indicates that myocyte apoptosis is linked to a cAMP pool that is regulated by PDE3 not PDE4.[81]

Other studies of the link between PDE3 inhibition and cardiac myocyte apoptosis revealed that it is mediated by cAMP response element binding protein (CREB) and inducible cAMP early repressors (ICER). Usually ICER expression is transient, where the presence of ICER prevents further production of itself. If an elevated level of ICER is maintained it could prevent CREB-regulated gene expression, which may have pathological outcomes. It has been shown that persistent ICER induction promotes cardiac myocyte apoptosis, yet temporary induction does not. Elevated levels of ICER can be sustained by inhibition of PDE3A through a positive feedback loop in which PDE3A transcription is down regulated by ICER, a lack of PDE3A increases levels of cAMP, cAMP activates PKA and PKA stabilizes ICER.[78, 81, 82] If this is the mechanism by which PDE3 inhibitors increase mortality of chronic heart failure patients, it is not yet clear why PDE3 inhibitors are safe to use in other disease states.

Some have suggested that the decreased levels of cAMP found in the cardiac tissue of CHF patients is a protective mechanism, and that treatments that increase the concentration cAMP are therefore inherently dangerous.[5]

1.8 PDE3 Inhibitors in the Clinic

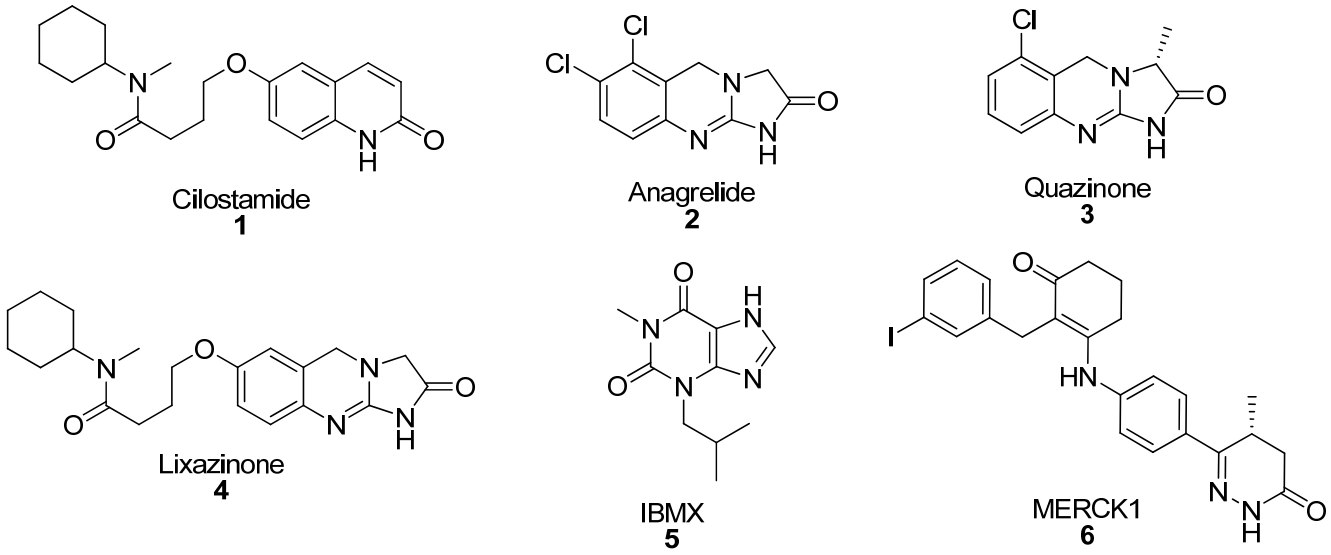

Figure 5 Examples of PDE3 inhibitors.

As discussed previously, increasing levels of cAMP leads to activation of PKA which increases the amplitude of Ca^{2+} cycling in cardiac myocytes. This inotropic action is supplemented by concurrent vasodilation which reduces total peripheral resistance, which is attributed to increased cAMP levels activating PKG in VSMC. These combined effects make PDE3 inhibition an opportune target for treating heart failure. Despite appearing to be a promising target to treat heart failure, clinical results were generally far from ideal.

The PDE3 story begins with a number of inotropic compounds that were discovered and trialled in animals and then in humans with dilated cardiomyopathy which is a type of heart failure that involves dysregulation of both receptor sensitivity to native ligands and cAMP production. These compounds were eventually found to be PDE3 inhibitors which were reversing the decreased cAMP levels in the systemic and pulmonary vasculature.[83] PDEs in the cardiovascular system became a target for treating this and related disease states via this mechanism.

Amrinone was found to be an efficacious inotropic agent before it's mechanism of action had been identified.[84] The first large scale, randomized, double-blind and placebo controlled clinical trial of a PDE3 inhibitor (amrinone) was to treat chronic congestive heart failure. In this multi-centre trial it was found that amrinone didn't improve cardiac function over conventional treatments.[85] These findings were re-affirmed in another double-blind trial which used a higher dosage (200 mg three times daily instead of 113 ± 33 mg three

times daily).[86] Over the subsequent years a number other PDE3 inhibitors were identified and trialled these included milrinone, enoximone, indolidan, vesnarinone and pimobendan and the mechanism of action for these drugs (PDE3 inhibition) was identified.[75] None of these turned out to be the orally active treatment for CHF that was sought. In fact, it was found in a large trial (1088 patients) that milrinone treatment significantly increased the risk of mortality in patients with chronic heart failure.[76] A meta-analysis of some 14 clinical trials of PDE3 inhibitors reached the same conclusion.[75] PDE3 inhibitors became generally accepted to increase the risk of death when used to treat CHF long term, which had been the disease they were most closely associated with. Afterwards PDE3 inhibitors fell out of favour with many pharmaceutical companies.

Despite their limitations there are some aspects of cardiovascular disease where PDE3 inhibitors are used today. For example, short term therapy is not associated with the same risk. Milrinone has been used extensively as short term intravenous therapy of severe congestive heart failure and for low output states following cardiac surgery. An alternative approach was to lower the dosages to increase safety. A clinical trial found that low dose enoximone improves exercise capacity without increased risk of cardiac events but was found to lack clinical utility in later trials.[87]

Some of the newer inhibitors had improved risk/benefit profiles while others were augmented by additional modes of action. A number of newer PDE3 inhibitors were investigated, and some were brought to market with alternate modes of action, for use in heart failure or other disease states.

Early clinical trial results found that vesnarinone might not increase risk of adverse cardiac events due to its multiple modes of action (it also modulates ion channels) however it was later found that the same risks were in fact present.[73, 75, 88] However, despite the increased risk of mortality associated with vesnarinone, some late stage patients were prepared to accept the risk in exchange for the increase in quality of life offered by the treatment. Saterinone is an α-adrenoceptor antagonist and a PDE3 inhibitor, this additional mode of action enhances the vasodilatory effect of PDE3 inhibition.[89] Levosimendan is a potent inhibitor of PDE3, but its inotropic action is predominantly through calcium sensitization. In a large clinical trial it was found to be as safe and effective as dobutamine, and superior to dobutamine in patients also taking β-blockers or with a history of CHF.[90, 91]

Cilostazol is another example of a successful PDE3 inhibitor with multiple modes of action; it was approved for use in Japan (as Pletal) in 1988 to treat the symptoms of peripheral arterial occlusive disease. Initially known to be a PDE3 inhibitor (IC_{50} = 0.2 μM), it was later found to also inhibit the uptake of adenosine (IC_{50} 5-10 μM), the safety of cilostazol compared to other PDE3 inhibitors has been attributed to this additional mechanism of action. The increase in adenosine around platelets and smooth muscle cells adds to the vasodilatory and antiplatelet action of cilostazol. The same increase of adenosine around cardiac myocytes subtracts from the inotropic action of cilostazol. By dulling the cardiac effects, cilostazol gains a measure of safety, but is obviously less useful where increased cardiac output is the desired outcome.[92-97]

The fact that inhibition of adenosine uptake is an important aspect of cilostazol's action is demonstrated when its antithrombotic effect is nullified in the presences of a A_{2A} adenosine receptor antagonist or by adenosine deaminase.[95] Interestingly cilostazol is 50 times more potent in *in vivo* experiments than in *in vitro* equivalents, suggesting that there may be even more mechanisms of action.[98] A key advantage of cilostazol over other antithrombotic agents such as aspirin and clopidogrel is that cilostazol does not increase bleeding time. The exact reason for this has yet to be elucidated.[99] Another useful aspect of cilostazol is that it also has an antiproliferative effect on vascular smooth muscle cells due to its PDE3 inhibition.[100]

Aside from the cardiovascular effects, cilostazol has positive side effects on lipid metabolism and is neuroprotective. Cilostazol's neural protective effects were demonstrated by reducing the cerebral infarct size following ischemia in rats.[101] Patients with peripheral vascular disease and type II diabetes who took cilostazol were found to have decreased plasma triglycerides, and increased levels of the omega-3 fatty acid docosahexaenoic acid.[102] Being neuroprotective, antithrombotic and vasodilatory makes cilostazol effective in preventing the recurrence of stroke.[103] Another possible advantage is that cilostazol does not inhibit PDE4 (IC_{50} > 100 μM) whereas the milrinone does (IC_{50} 16 μM).[104] Some have suggested the cilostazol's safety profile is a consequence of this as it decreases the effect it has on cAMP levels in cardiac myocytes, which express both PDE3 and PDE4.[105] However the same concept does not seem to apply to cilostamide, which can cause tachycardia and has even greater PDE3/PDE4 selectivity than cilostazol.[106]

Today cilostazol has been approved for use in the USA, UK, Ireland, Japan and Australia and elsewhere for treatment of intermittent claudication and peripheral arterial occlusive disease. However, it is contraindicated in patients with a history of heart failure.

Several PDE3 inhibitors based on the imidazoquinazolinone scaffold have been reported. Some examples are quazinone, lixazinone, anagrelide.[4] Anagrelide is an imidazoquinazolinone based drug with both anti-platelet and anti-PDE3 activity.[107] In phase I clinical trials it produced thrombocytopenia in patients,[108] this effect was later used to treat patients with myeloproliferative disorders, where it appears to inhibit the production of platelets.

Lixazinone is another imidazoquinazolinone based PDE3 inhibitor, it was designed as a hybrid by combining structural elements of two earlier PDE3 inhibitors, specifically the side chain of cilostamide with the imidazoquinazolinone core of anagrelide. It was found to have haemodynamic effects and inhibit platelet aggregation in dogs and monkeys, and was later taken into clinical trials.[109, 110]

1.9 Isoform Selective Inhibition

During development of most of the PDE3 inhibitors discussed in this Chapter, the existence of PDE3B was largely unknown. As a consequence there is a multitude of compounds that are known to inhibit PDE3A, and virtually nothing is known of their activity against PDE3B.

For example, there is a great deal of published information about the structure activity relationship (SAR) between imidazoquinazolinones (anagrelide and lixazinone) and PDE3A. Across a series of 5 publications from 1976 to 1987 no less than 212 imidazoquinazolinones were synthesized and assessed for PDE3A-related functions.[111-115]

Yet only lixazinone has been examined with respect to isoform selectivity for PDE3A vs. PDE3B. It is 4 fold more potent against short forms PDE3A than full length PDE3B. This indicates that the binding mode of lixazinone is sensitive to changes between the N-terminus or between isoforms. On the basis of these results, Kenan et al suggest that it may be possible to design *"more specific Lixazinone-like PDE3A inhibitors*".[23]

There have just been a few reports that indicate that it is possible for inhibitors to distinguish between PDE3A and PDE3B. Notably a report by Edmondson et al. which includes **7** (Figure 6) which is the

most PDE3B selective compound identified to date (33 fold, IC_{50} values of 150 nM at 3A and 4.5 nM at 3B).[116] Also a series of 2-(biphenyl-4-ylmethylsulfonyl)-N-(2-hydroxyethyl)acetamides such as compound **9** that were reported in a patent as selective for PDE3B, but have not appeared in peer reviewed literature.[117]

Nikpour et al. designed and synthesized a series of compounds including **8** that were predominantly found to be more potent at PDE3A than PDE3B (up to ~4 fold).[118] Finally cilostamide is reported to be non-selective (IC_{50} values of 16 nM at PDE3A and 18 nM at PDE3B) by Snyder, however Kim et al. reported that it is ~4 fold selective for PDE3A (IC_{50} values of 18 nM at PDE3A and 69 nM at PDE3B).[119, 120] Three reported PDE4 inhibitors were shown to have some off target activity at PDE3, and are slightly more potent at PDE3B.[121]

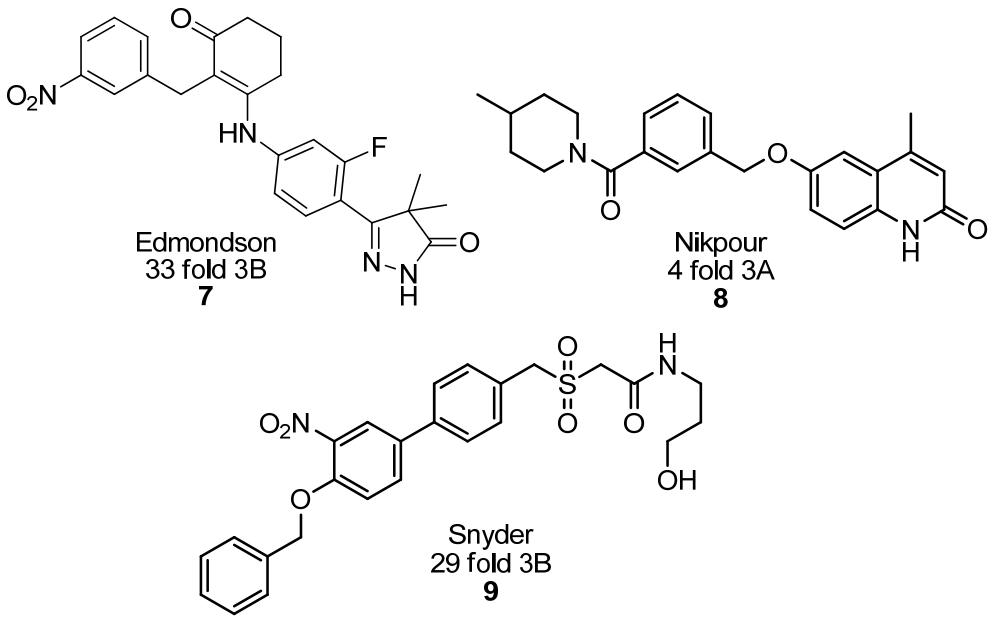

Figure 6 Examples of PDE3A and PDE3B isoform selecting inhibitors.

The combination of these reports indicates that it is possible to develop isoform selective inhibitors, that lixazinone may be primed for isoform selectivity, and that there is demand for new compounds that will increase understanding of PDE3 inhibitor selectivity, mechanism of action, and shortcomings, which could lead to improved treatments for an array of disease states.

The hope for subtype selective inhibitors of PDE3A or PDE3B is their potential to treat diabetes or obesity in the case of PDE3B inhibition, or mitigate the negative side effects of PDE3A inhibition. If isoform specific inhibitors are realized, this could lead to better characterization and management of any negative

effects. It is hoped that the invention of subtype selective inhibitors could also enhance understanding of subtype localization and function.

Due to compartmentalization of cAMP pools in cardiac myocytes, that the negative side effects of chronic PDE3 inhibition could possibly be mitigated by inhibiting different subtypes of PDE3.[122] By effecting just one of either cytosolic or membrane bound PDE3A it may be possible to raise either the background level of cAMP or the level of cAMP at the membrane that is produced in response to stimuli. There is evidence that the length of N-terminal domain can affect the activity of some inhibitors (e.g. lixazinone).[23] It may be that this could be modeled using PDE3A or PDE3B selective inhibitors in mice because they express both PDE3A and PDE3B in their cardiac tissue,[123] where PDE3B is only found associated with the membrane.

Against all the preceding literature, this PhD thesis has set out to explore the following questions. First, do the imidazoquinazolinone class of PDE3 inhibitors represented by lixazinone and anagrelide exhibit any levels of isoform selectivity that could be exploited by further applications of medicinal chemistry? Second, can the binding of this and other classes of PDE3 inhibitors to PDE3A or PDE3B be accurately described using computational modeling and therefore used in new inhibitor design? Third, can new members of the imidazoquinazolinone class be identified that exhibit promising activity? Finally, can the imidazoquinazolinone structure be reverse engineered to generate new chemotypes for drug discovery?

Chapter 2: Synthesis and Evaluation of Imidazoquinazolinone PDE3 Inhibitors

A plethora of patented and published products are proven to prevent PDE3 performance; perhaps a portion of the particularly potent prototypes will profess a proclivity for PDE3A or PDE3B.

2.1 Background

The imidazoquinazolinone (IMQ) family of heterocyclic compounds include some of the most widely studied inhibitors of PDE3 – anagrelide (**2**), quazinone (**3**), and lixazinone (**4**). Previous evaluation of IMQs has involved assessment of them as platelet aggregation inhibitors or as inhibitors of cAMP-PDE activity from platelet lysates. Both of these assay formats are reasonable surrogates for PDE3A inhibition as PDE3A is the dominant PDE in platelets. As these compounds were developed before the identification of the two PDE3 isoforms, PDE3A and PDE3B there has not really been consideration of their relative isoform selectivities.

To investigate these ideas, a range of IMQs were synthesized and evaluated as inhibitors of PDE3A and PDE3B. Examples were chosen from different stages of the drug design process that led to the development of lixazinone (**4**) and summarized below, beginning with the simplest example, imidazoquinazolinone (**10**) itself, through to highly elaborated analogues with strong inhibitory potency reported versus PDE3A.

2.1.1 Known imidazoquinazolinone PDE3 inhibitors

In 1975, IMQ (**10**) was reported as an inhibitor of collagen-induced platelet aggregation (EC_{50} of 2 mg/ml). In the early patent data, it was shown that substitution at the 7 position of **10** can alter the activity - a chloro, bromo, methoxy or nitro group improved activity, while a 7-amino analogue had reduced activity. In general though, small substitutions right around the aromatic ring are tolerated.[124] The same group also reported that 6-methyl-IMQ (**11**) was a potent inhibitor of ADP-induced platelet aggregation and "*may be of value in the treatment of platelet disorders*".[125] The 6,7-dichloro derivative, anagrelide (**2**) was patented in

1976.[112] Ishikawa et al replaced the aromatic ring with a thiophene which diminished activity. However, adding lipophilic substituents to the thiophene ring restored its potency.[126]

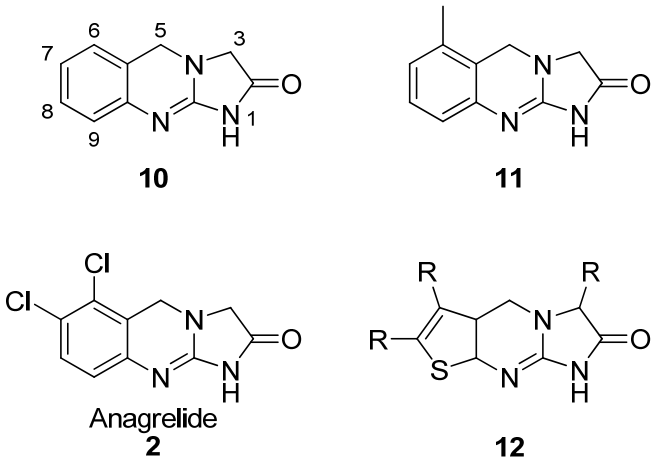

Figure 7 Unsubstituted IMQ, 6-methyl-IMQ, anagrelide and template structure from Ishikawa et al.[126]

Researchers at Syntex generated numerous analogues in the development of lixazinone (**4**) and reported their potency against PDE3 from platelets and as platelet aggregation inhibitors.[127] Combining the N-cyclohexyl-N-methyl-4-oxybutyramide side chain of another potent PDE3 inhibitor, cilostamide (**1**) with the IMQ core of anagrelide (**2**), gave lixazinone (**4**), which was more potent than either of the parent compounds. They also investigated a range of different lactam heterocycles but none exceeded imidazoquinazolinone in terms of potency.

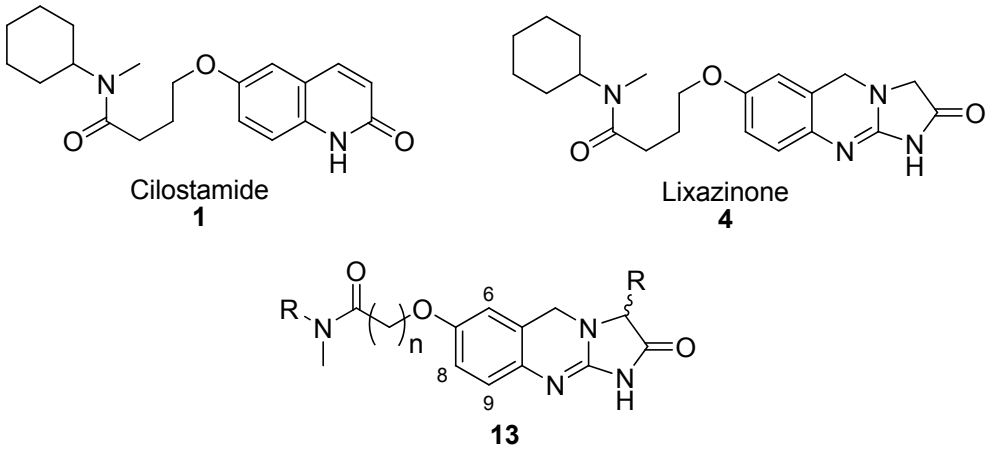

Figure 8 Cilostamide, Lixazinone and optimization template.

The group performed in depth SAR studies of the lixazinone scaffold predominantly following the template structure **13**. It was shown that the optimum position to attach the side chain was the 7 position;

moving the side chain to the 8 position reduced activity, and moving it to the 6 or 9 positions completely abolished activity. They also reported that the hydrophobic nature of the N-cyclohexyl-N-methyl moiety of **4** markedly increased potency, yet replacing the cyclohexyl group with aromatic substituents was detrimental. Some variation in the chain length ($(CH_2)_{4\text{-}6}$) was tolerated, but very short linkers of only one methylene were not. Methyl and hydroxymethyl substitution at the lactam methylene groups were tolerated, and the *R*-configuration was more potent than the *S*-configuration.[111] Fused or pendant heteroaryl rings (**14** and **15** respectively) were examined but found to be inferior to lixazinone (**4**). The SAR suggested the existence of a secondary pocket in the binding site distinct from the core binding site, in agreement with the earlier pharmacophores.[128] Finally, a related series of IMQ pro-drugs were evaluated but did not improve the drugs oral bioavailability.[110] This marked the last interest in IMQ based structures as PDE3 inhibitors for many years.

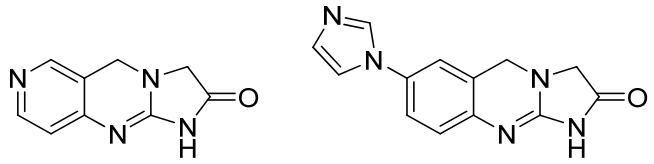

14 **15**

Figure 9 Examples analogues from Venuti et al.[129]

A series of isomeric imidazoquinolinone (**16**) analogues were produced by workers at Bristol Myers Squibb. The unsubstituted imidazoquinolinone (**16**) core was found to be equipotent with the unsubstituted IMQ (**10**) and in general terms, the remainder of the SAR matched that of the corresponding IMQs.[130, 131] One notable inclusion was the 4-oxy-1-(piperazin-1-yl)butan-1-one structures (**17**), and a variety substitutions (benzyl, cyclohexyl, and derivatized phenyls) were well tolerated as were isosteric replacements of the side chain's amide component (ureas, sulfones, sulfonamides and tetrazoles).[132, 133]

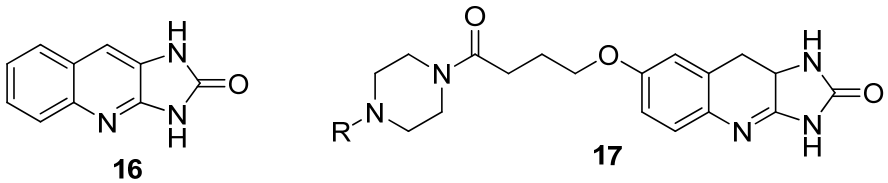

16 **17**

Figure 10 Example compounds reported by Meanwell et al.[131-133]

While this represents a large body of work, it is important to remember that all of the SAR discussed above was developed against PDE3A or surrogate assays. There was no assay or SAR of the class for PDE3B across this intense period of medicinal chemistry research.

2.1.2 Literature Synthesis of Imidazoquinazolinones

The literature reports described above included a variety of methods for synthesizing substituted IMQs. The most widely used approach is shown in Scheme 1, exemplified for the parent molecule **10**. The 2-nitrobenzylglycine ester (**28)** was prepared by reductive amination of 2-nitrobenzaldehyde (**18**) with glycine ethyl ester. Alternatively alkylation has been achieved by treating ethyl glycinate with 2-nitrobenzyl chloride.[124]

The nitro group of **19** has been reduced to a primary amine (**20**) via catalytic hydrogenation or alternatively using iron or tin with hydrochloric acid.[134] Treatment of **29** with cyanogen bromide yielded cyanamide (**21**) which was not isolated, but instead the addition of ammonia induced intramolecular cyclization which forms **10**.

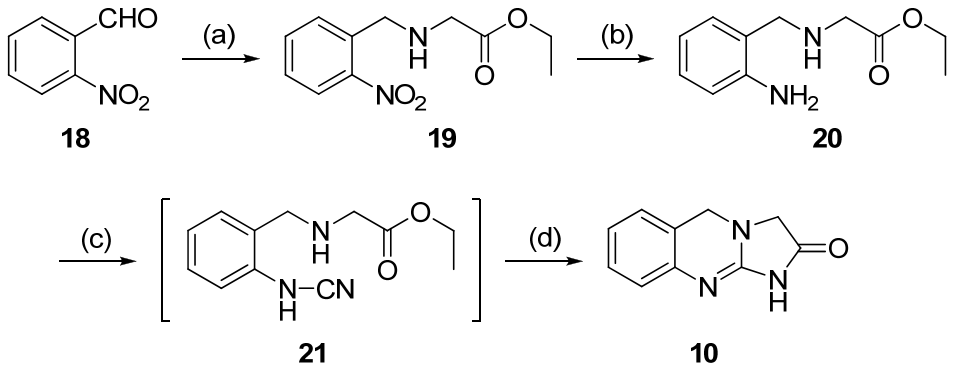

Scheme 1 Example synthesis of unsubstituted IMQ. Reagents and conditions: (a) GlyOEt, $NaCNBH_3$, EtOH, RT, 4 h (b) 10% Pd-C, H_2, EtOH, RT, 16 h (c) CNBr, EtOH, RT, 16 h (d) conc. NH_4OH, EtOH, RT, 1 h.

The reductive amination and catalytic hydrogenation steps of the synthesis are high yielding, and the final cyclization results in the product precipitating from solution allowing for ready isolation. On the other hand, stoichiometric amounts of toxic cyanogen bromide are required for this final step that needs to be washed away and safely disposed of.

The synthesis of many substituted analogues begins with the synthesis of the corresponding substituted 2-nitrobenzaldehyde. IMQs bearing alkyl groups, halides, ethers, thioethers, and sulfonyl groups have all been prepared in this way. Even in the synthesis of lixazinone (**4**) (Scheme 2), the extended side chain was appended to the 5-hydroxy-2-nitrobenzaldehyde (**22**) via **23**. This intermediate (**24**) was then subjected to the same ring forming steps as in Scheme 1 to give lixazinone (**4**). It should be noted that Venuti and others found that the potentially divergent alkylation of hydroxy-IMQ was unsuccessful, probably due to competing alkylation at the ring nitrogen atoms.

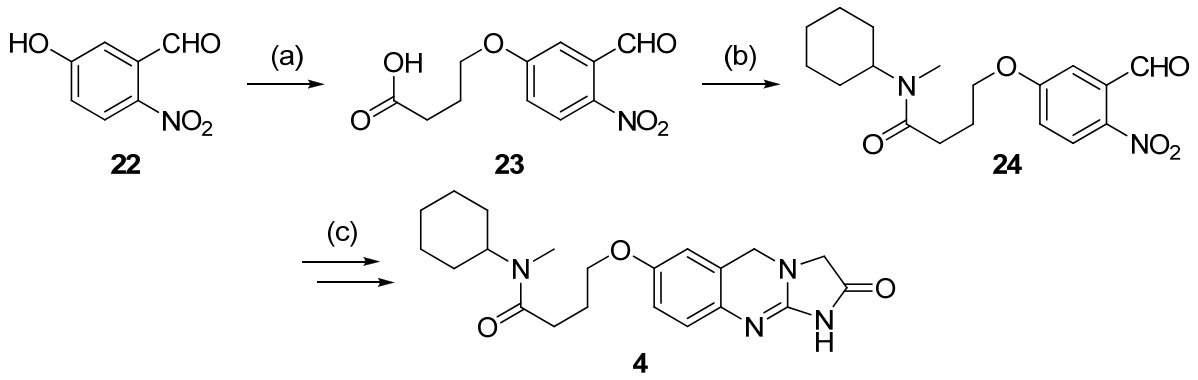

22 **23** **24** **4**

Scheme 2 Literature synthesis of lixazinone.[127] Reagents and conditions: (a) ethyl-4-bromobutyrate, K_2CO_3, N_2, DMF, 100 °C, 1 h; KOH, H_2O, EtOH (b) $C_2O_2Cl_2$, C_6H_6, DMF, RT, 1 h; N-methylcyclohexylamine, Na_2CO_3, THF, H_2O, RT, 1 h (c) as per Scheme 1.

In Scheme 3 substitution at the lactam methylene of the IMQ is achieved by using α-amino acid esters in the reductive amination with **25** to give **26**, thereby including a chiral centre in the final IMQ (**27**).[111, 127]

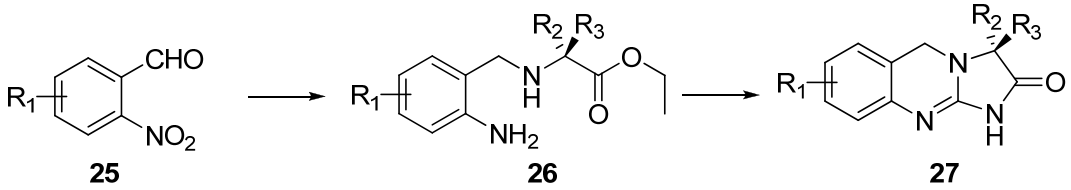

25 **26** **27**

Scheme 3 Chiral substitution at the lactam methylene.

Srivastava et al[135] have recently adapted the synthesis for the solid phase (Scheme 4), effectively replacing the ethyl ester by ester attachment to Wang resin (**28**). Reduction of the nitro group (**29**) to an amine (**30**), demanded the use of stannous chloride as a replacement for heterogeneous palladium on carbon, which is ill suited for solid phase synthesis. Cyclization proceeded through intermediate **31** to give IMQ (**10**)

upon resin cleavage. A variation of this method was also published that gives IMQs substituted at three positions, the aromatic ring, lactam methylene and lactam nitrogen.[136]

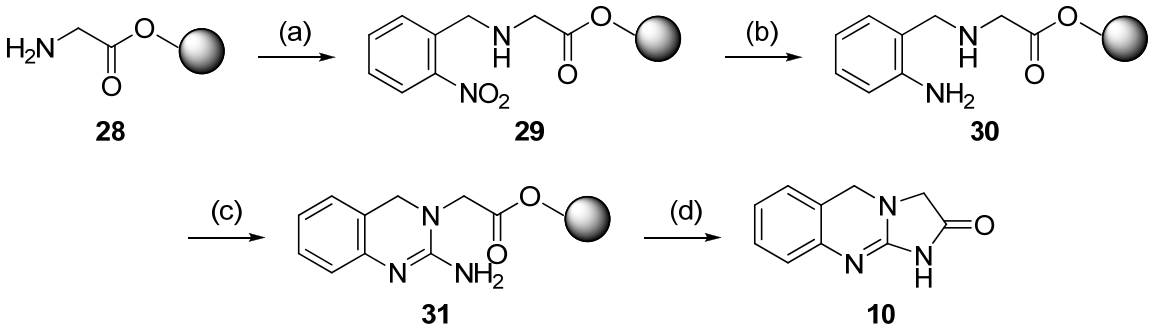

Scheme 4 Solid phase synthesis of imidazoquinazolinone.[135] Reagents and conditions: (a) $NaCNBH_3$, AcOH, trimethylorthoformate, RT, 2 h (b) 2M $SnCl_2$, DMF, RT, 5 h (c) CNBr, DMF, EtOH, RT, 16 h (d) TFA, DCM, RT, 2 h.

An alternate synthesis of anagrelide was reported by Yamaguchi et al[137] and is shown in Scheme 5, it begins with 2,4,5,6-tetrachloroquinazoline (**32**) being reduced with sodium borohydride to 2,5,6-trichloro-3,4-dihydroquinazoline (**33**). The resulting secondary amine (**33**) is alkylated with ethyl bromoacetate to give **34**. Cyclization is induced by treatment with ammonium hydroxide to give anagrelide (**2**). The advantage of this method is that it does not require cyanogen bromide, however it begins with a less readily available material and the steps use slightly harsher conditions.

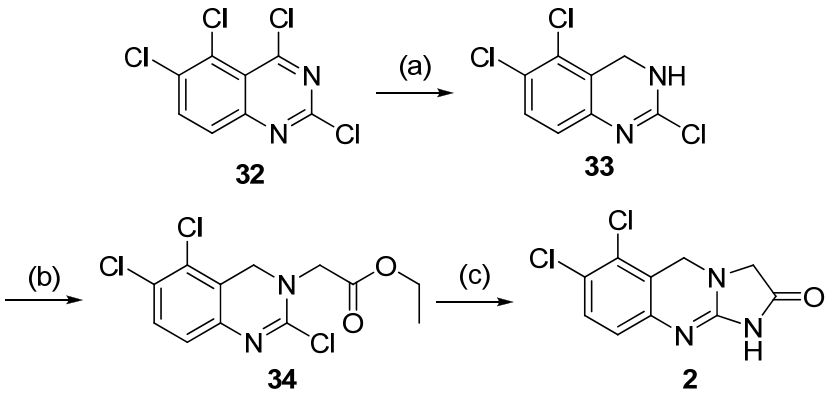

Scheme 5 Alternate synthesis of anagrelide.[137] Reagents and conditions: (a) $NaBH_3$, $CHCl_3$, EtOH, RT, 2 h (b) ethyl bromoacetate, KCO_3, MEK, reflux, 3 h (c) 10% NH_4OH, 120 °C, 16 h.

As outlined in this section, there is a wealth of opportunity for derivatization during construction of the tricyclic ring system. When developing analogues of lixazinone (**4**), the most frequently reported method was to produce the appropriate nitrobenzaldehyde precursor and subject it to the tricyclic ring construction

sequence. This approach and variations of it were undertaken to reproduce a number of literature analogues in this work.

2.2 Results and Discussion

2.2.1 Selection of Compounds for Synthesis

As there was basically no data available on the SAR of PDE3B inhibition by imidazoquinazolinone a range of molecules were targeted which aim to identify potential points of divergence from what has been observed in PDE3A inhibition. These relate to structural variants of lixazinone (Figure 11), as well as anagrelide and quazinone. Simple substituents on the IMQ ring, and points of elaboration that lead out to the extended lixazinone structure were examined.

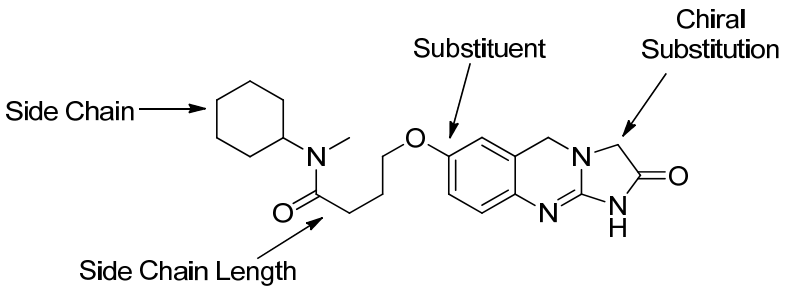

Figure 11 Lixazinone template and design strategies.

As such compounds bearing simpler substituents (**35-38**) to the more elaborate ones incorporating longer side chains (**39-42**) that could extend toward a secondary binding site or including simple chiral substitutions were targeted. Finally, the extended substituents found on highly potent compounds reported by Venuti et al[111] (**43**) and Meanwell et al[132] (**44**) were reproduced to determine if the increase in potency was specific to PDE3A. The reported IC_{50} values are shown in Table 1.

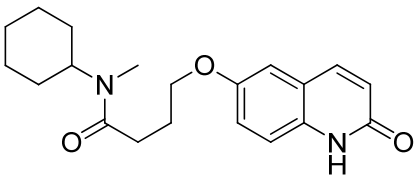

Cilostamide
1

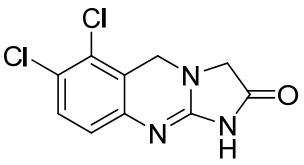

Anagrelide
2

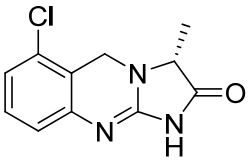

Quazinone
3

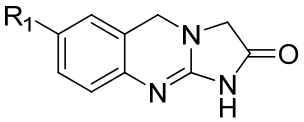

10, 35-38

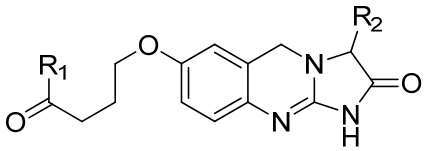

39-44

#	R_1	R_2	Lit. Platelet PDE IC_{50} (nM)
Cilostamide **1**	-	-	170 [127]
Anagrelide **2**	-	-	80 [127]
Quazinone **3**	-	-	240 [129]
10	H	-	8800 [129]
35	Cl	-	1500 [129]
36	Br	-	-
37	OCH_3	-	1500 [129]
38	OH	-	3300 [129]
39	OCH_2CH_3	H	240 [111]
40	OCH_2CH_3	(R)-CH_3	-
41	OH	H	280 [111]
42	OH	(R)-CH_3	-
43	*$N(C_6H_{11})CH_2CH_2OCOC_6H_5$	H	0.94 [111]
44	*$N(CH_2CH_2)_2NCH_2C_6H_{11}$	H	6 [132]

Table 1 Targeted compounds and corresponding platelet PDE IC_{50} values from literature.

2.2.2 Chemistry

The literature route to IMQ (**10**) was recapitulated to establish the synthetic methods required for building the compound library and to characterize the spectroscopic properties of the IMQ ring system. Firstly, 2-nitrobenzaldehyde (**18**) underwent reductive amination with glycine ethyl ester hydrochloride

using sodium cyanoborohydride in good yield (**19**, 93%).[138] ^{1}H-NMR analysis of this intermediate (**19**) showed that the characteristic aromatic peaks were well distributed from 7.9 – 7.3 ppm and included some well-defined ^{4}J coupling. Further upfield in the ^{1}H-NMR spectrum, there are two singlets, the first at 4 ppm represents the methylene adjacent to the aryl ring and the second at 3.3 ppm was assigned to the methylene between the secondary amine and the carbonyl, and the characteristic ethyl ester signals appear at 4.1 and 1.2 ppm.

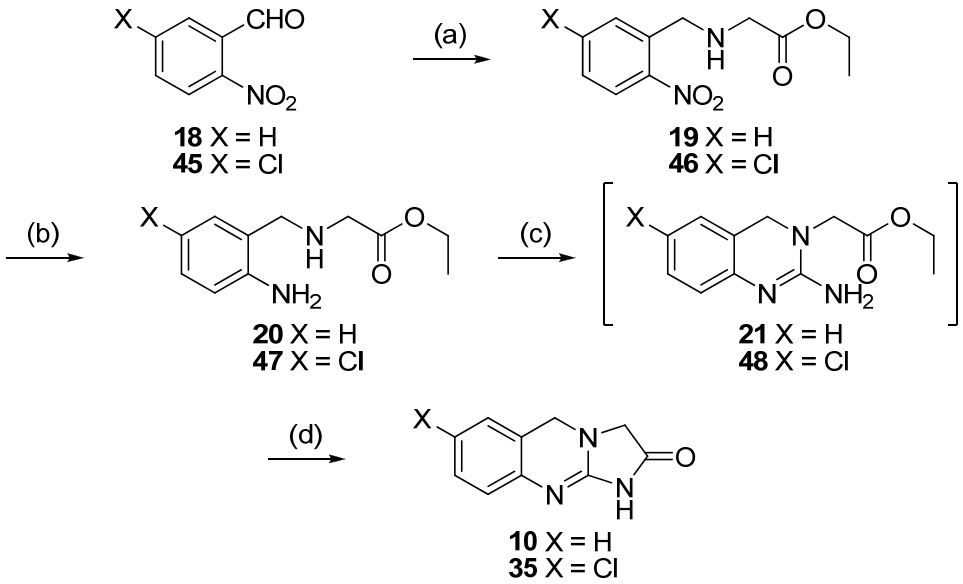

Scheme 6 Synthesis of IMQs. Reagents and conditions: (a) GlyOEt, $NaCNBH_3$, EtOH, RT, 4 h (b) 10% Pd-C, H_2, EtOH, RT, 16 h (c) CNBr, EtOH, RT, 16 h (d) conc. NH_4OH, EtOH, RT, 1 h.

Catalytic hydrogenation with palladium on carbon under atmospheric hydrogen converted the nitro group of **19** to a primary amine (**20**) in quantitative yield. In the ^{1}H-NMR of this intermediate, the transformation from the deactivating nitro group to the activating amino group shifts the aromatic signals down field by almost 1 ppm leaving them between 7.1 and 6.6 ppm; the signal for the benzylic methylene protons is also shifted down field from 4 to 3.8 ppm, while the remaining signals did not change significantly.

The final stage of ring construction is the cyclization using cyanogen bromide, it is hypothesized to proceed via the cyanamide intermediate (**21**) shown in Scheme 6.[125] Addition of concentrated ammonium hydroxide triggers the intramolecular ring cyclization. The decreased solubility of the fused ring system (**10**) causes it to precipitate out of solution in good yield (59%). Post cyclization the ^{1}H-NMR signals of the aryl

ring are bunched closer together between 7.3 and 7.1; the two singlets are shifted down field to 4.7 for the aryl adjacent methylene and 4.2 for the carbonyl adjacent methylene. The ^{13}C-NMR was assigned using HSQC and HMBC experiments which showed the carbonyl carbon resonance at 168.5 ppm and the guanidinyl carbon at 153.8 ppm. The signals of the carbonyl and guanidinyl carbons along with the quaternary carbons of the aryl ring were not detected in all of the analogues in this work; this was attributed to the low solubility of the ring system which made it difficult to obtain sufficient signal, even in DMSO. All of the quaternary carbon signals were obtained for the unsubstituted IMQ (**10**), and analogues with extended side chains, ethyl ester (**39**) and amide (**43**), for which solubility was not an issue.

The 7-chloro substituted derivative (**35**) was also prepared in this manner and in comparable yields (three steps, **46** 96%, **47** 98%, **35** 38%). It was noted that the high yields and simple isolation of the desired products, typically allowed us to forego purification of intermediates which significantly reduced the labour required.

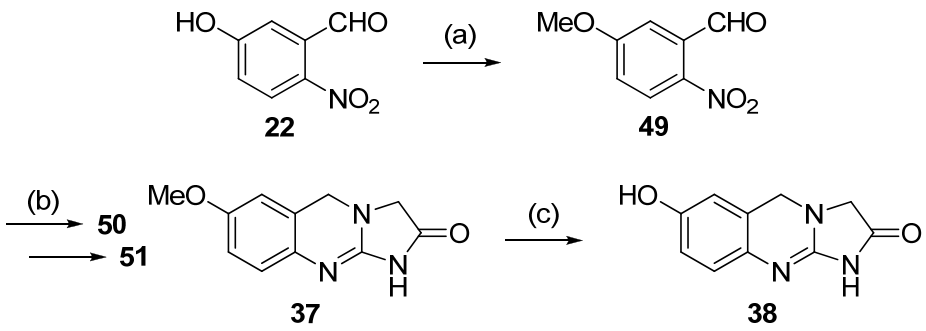

Scheme 7 Synthesis of 7-methoxy-IMQ and 7-hydroxy-IMQ. Reagents and conditions: (a) Cs_2Co_3, MeI, DMF, RT, 3 d (b) as per Scheme 6 (c) conc. HBr, 110 °C, 1 h.

The synthesis of 7-methoxy-IMQ (**37**) was reported in the original patent by Beverung et al[112] and was repeated in this work (Scheme 7). To begin, 5-hydroxy-2-nitrobenzaldehyde (**22**) was treated with methyl iodide to give 5-methoxy-2-nitrobenzaldehyde (**49**) in quantitative yield with the corresponding methyl group appearing in the ^{1}H-NMR at 4 ppm. The tricyclic ring system was constructed as described in Scheme 6 albeit with a decreased yield (three steps, **49** 88%, **50** 89%, **51** 13%) which was attributed to the smaller reaction scales. The methoxy signal could be tracked through around 3.6 ppm in the ^{1}H-NMR of each of the products. The 7-methoxy group was deprotected to the corresponding phenolic derivative (**38**) by treatment with hydrobromic acid in good yield (92%).

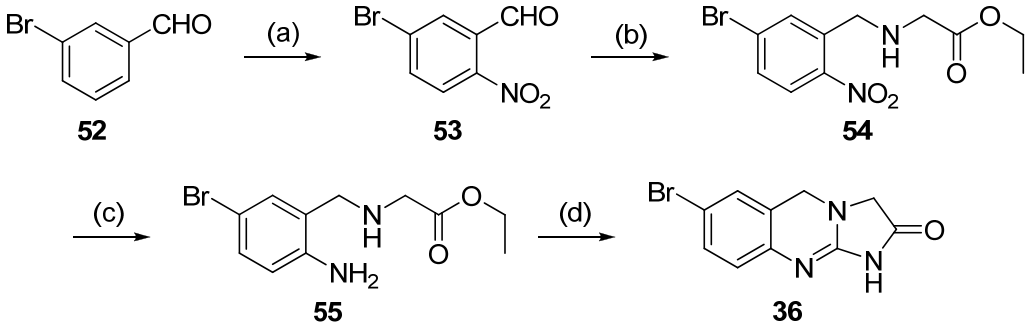

Scheme 8 Revised synthesis of 7-bromo-IMQ. Reagents and conditions: (a) conc. HNO_3, H_2SO_4, 0 °C, 3 h (b) GlyOEt, $NaCNBH_3$, EtOH, RT, 4 h (c) Fe, 1 M HCl, EtOH, H_2O, 45 °C, 2 h (d) CNBr, EtOH, RT, 16 h; conc. NH_4OH, EtOH, RT, 1 h.

The synthesis of the 7-bromo-IMQ analogue (**36**) demanded some adaptations but was achieved on a multi-gram scale, providing a stockpile of a common precursor with a useful synthetic handle. First, the precursor 5-bromo-2-nitrobenzaldehyde (**53**) was prepared by nitration of 3-bromobenzaldehyde (**52**) in 66% yield. Reductive amination gave **54** in 64% yield. Catalytic hydrogenation of **54** caused hydrogenolysis of the bromine substituent yielding compound **20**. Selective reduction of **54** to yield the amine **55** was achieved using iron and HCl according to the method of Diedrich et al[139] Curiously the product of the Iron/HCl reduction gave a parent ion in the ESI-MS that corresponded to a cyclic compound (**56**) while ^{1}H-NMR indicated the expected structure, suggesting that this cyclization was occurring only in the mass spectrometer. The desired cyclization was achieved as before to give **36** in 79% yield. The presence of the bromo group was confirmed by the characteristic 1:1 signal in mass spectrometry of the intermediates and target compound.

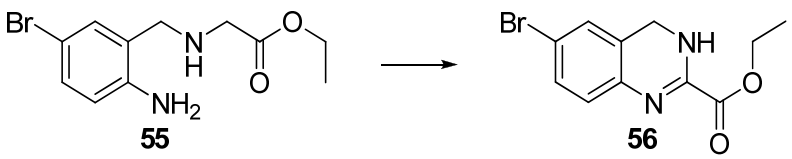

Scheme 9 Suggested cyclization to explain anomalous mass spectrometry result.

Compounds **39-42** were prepared by a common sequence that began with the synthesis of the ester **57** in quantitative yield. This precursor was then reacted with glycine methyl ester to give **58** in moderate yield (49%) and the synthesis continued as previously to the corresponding IMQ derivative **39** with good yields obtained (**58** 49%, **60** 69%, **39** 57%). The same synthesis was then pursued, but using D-alanine methyl ester (R = Me, *R*-enantiomer). The reductive amination product **59** was obtained in 93% yield and the

IMQ synthesis via **61** (72%) to the corresponding IMQ (**40**). The cyclization yield of compound (**40**) was significantly reduced (17%) compared to the glycine derived equivalent (**39** 57%). The R-methyl group was observed in ^{1}H-NMR as a doublet at 1.3 ppm, the lactam methine overlapped with the ether methylene to give a multiplet, and the IMQ methylene adjacent to the aryl ring was observed as two geminal coupled doublets at 4.56 and 4.43 ppm. The two esters **39** and **40** were then hydrolysed to reveal the corresponding carboxylic acids (R = H, **41** 98%, R = Me, **42** 65%).

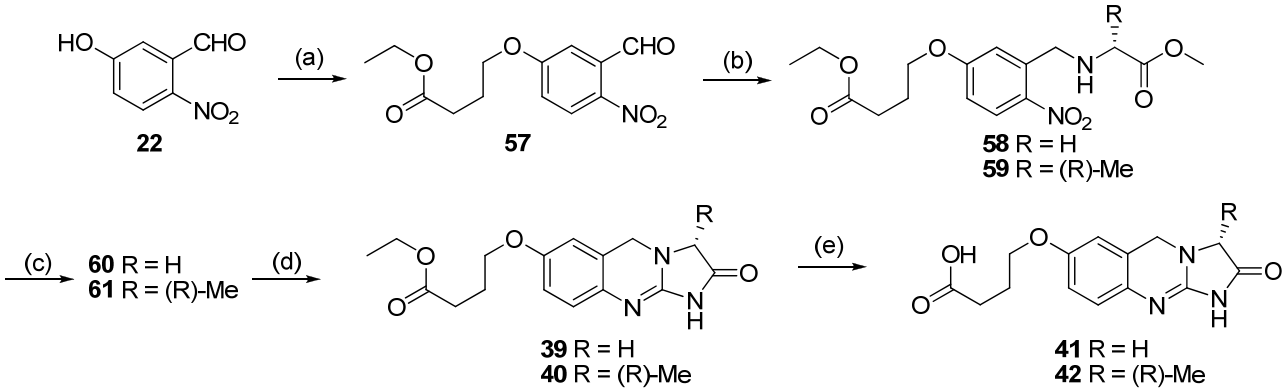

Scheme 10 Synthesis with ethyl-4-oxybutyrate side chain and (R)-methyl group. Reagents and conditions: (a) ethyl-4-bromobutyrate, K_2CO_3, DMF, 100 °C, 1 h (b) for R = Me, D-AlaOMe, for R = H, GlyOMe, $NaCNBH_3$, EtOH, RT, 4 h (c) 10% Pd-C, H_2, EtOH, RT, 16 h (d) CNBr, EtOH, RT, 16 h (e) NaOH, water, EtOH, RT, 1 h.

The final two compounds of the series were produced by coupling the carboxylic acid side chain of **41** to the appropriate amine. To couple 2-(cyclohexylamino)ethyl benzoate an activated ester of the carboxylic acid (**41**) was first formed with TBTU. This reaction produced **43** in quite low yield (12%). Coupling 1-(cyclohexylmethyl)piperazine was achieved using EDC, in comparison the conditions of this reaction were milder but the yield of **44** was inferior (6%). While the low yields may be due to a variety of reasons, in particular losses during purification, this is consistent with the fact that earlier groups constructed the completed side chains on precursor 2-nitrobenzaldehydes prior to constructing the IMQ ring. Certainly the preparation of these products was hampered by limited solubility in organic solvents. The target compounds were characterized by ^{1}H-NMR and HR-MS, which corresponded to the expected values. There was insufficient material to obtain ^{13}C-NMR spectra of **44**, however, sufficient material was available to conduct in vitro assays.

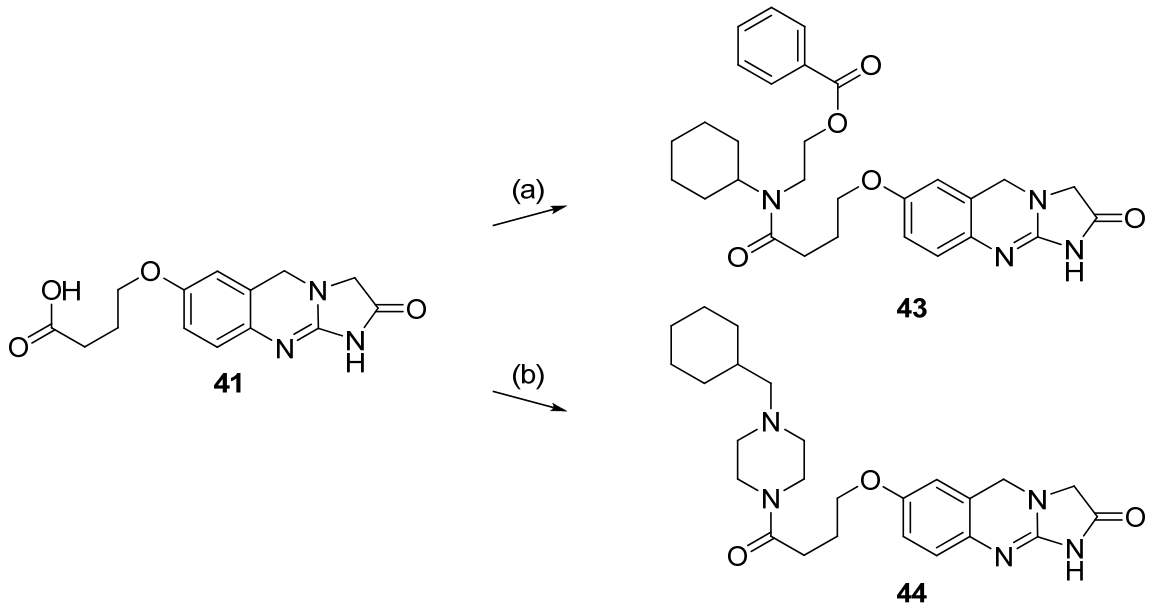

Scheme 11 Extended side chain analogues via amide coupling. Reagents and conditions: (a) 2-(cyclohexylamino)ethyl benzoate, TBTU, DIPEA, DMF, 80 °C, 2 h (b) 1-(cyclohexylmethyl)piperazine, EDC, Et_3N, THF, RT, 24 h.

In summary, the synthesis of these 11 compounds provided an excellent base for the characterization of the IMQ class as inhibitors of PDE3A and PDE3B which had not previously been done. The syntheses though largely following reported methods also gave a strong basis for understanding the pivotal steps and flagged certain substituents for which the synthetic steps needed to be adapted.

2.2.3 Biochemical Assays

PDE inhibition assays were conducted at BPS Bioscience (San Diego) using a fluorescence polarization-based assay of fluorescently-labeled cAMP hydrolysis as outlined in Figure 12. In brief, hydrolysis of the fluorescently labeled cAMP yields the fluorescently labeled AMP, which is immobilized by a binding agent producing a change in fluorescent polarization that is indicative of the amount of hydrolysed substrate present. Both the enzymatic reaction and binding agent steps proceed for one hour. The assay format has been applied for numerous PDE inhibitors and the results are generally in agreement with assay data from alternate formats.

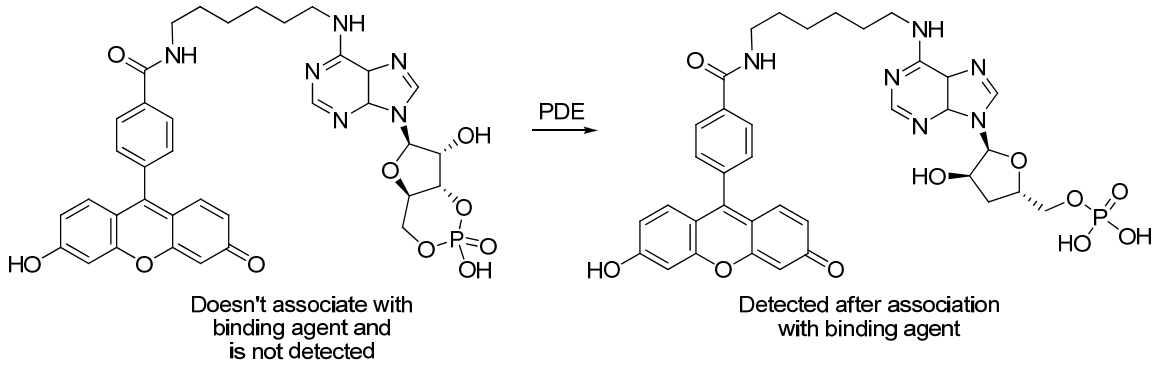

Figure 12 Overview of PDE activity assay format.

Compounds were assayed against recombinant human PDE3A (amino acids 484-1141) and PDE3B (amino acids 592-end) that were expressed with N-terminal GST tags in Baculovirus infected Sf9 cell expression systems.

Dose response curves were obtained for three commercially available PDE3 inhibitors: cilostamide (**1**), anagrelide (**2**), and quazinone (**3**). Anagrelide (**2**) was found to be very potent, with IC_{50} values of 35 nM at PDE3A and 100 nM at PDE3B, making it 3-fold selective for PDE3A. Cilostamide (**1**) was confirmed to have similar activity as anagrelide (**2**) with IC_{50} values of 22 nM at PDE3A and 48 nM at PDE3B. Quazinone (**3**) is less potent at both isoforms with IC_{50} values of 180 nM at PDE3A and 230 nM at PDE3B showing almost no selectivity between isoforms.

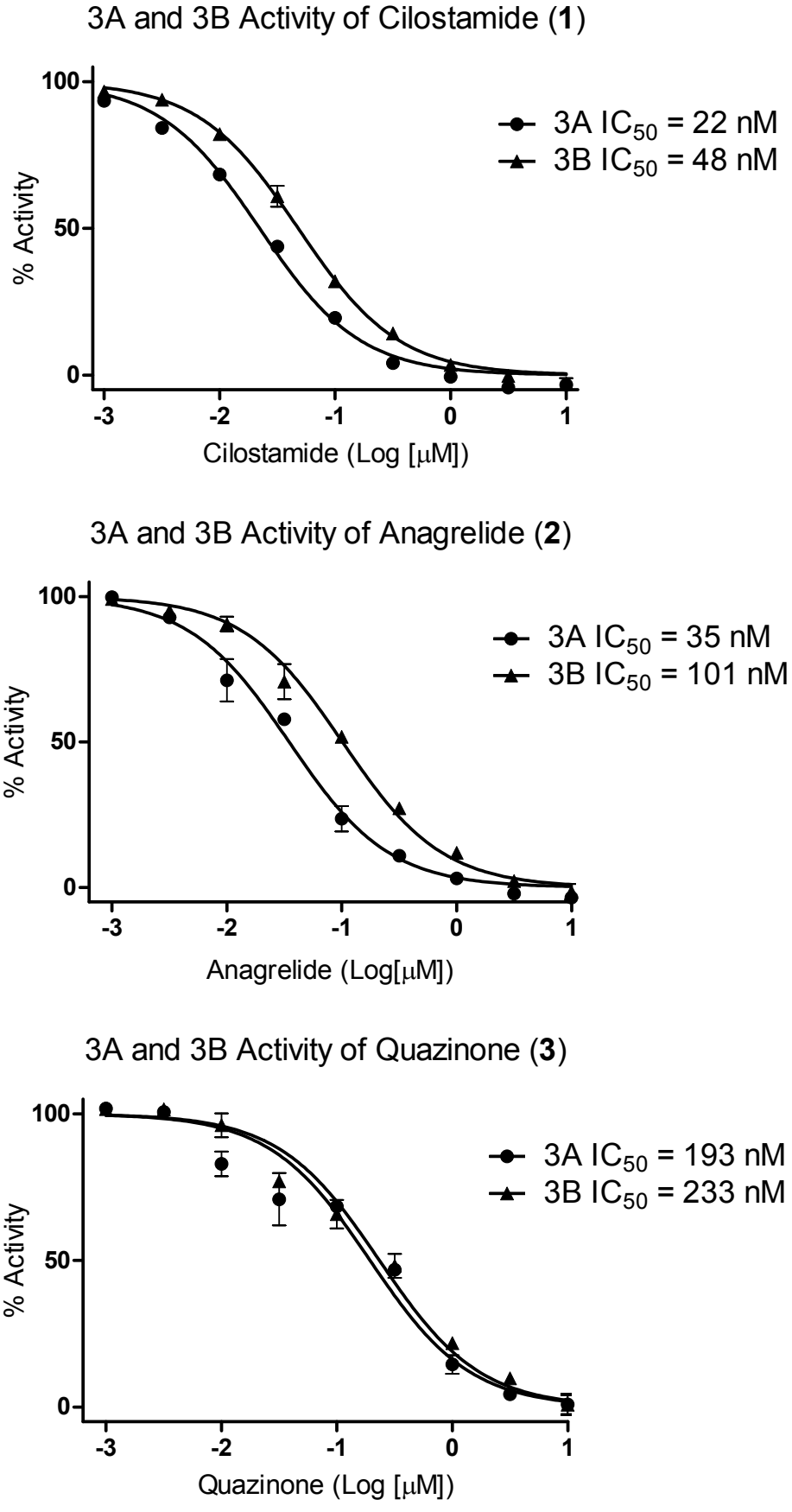

Figure 13 Dose response curves of known PDE3 inhibitors.

The results for the screen of the synthesized compounds **10** and **35-44** are summarized in Table 2; assay concentrations were chosen to be close to the literature IC_{50} for PDE3A as reported: the unsubstituted IMQ (**10**) was screened at 1000 nM, analogues **35-42** were screened at 500 nM and the analogues **43-44** were screened at 50 nM.

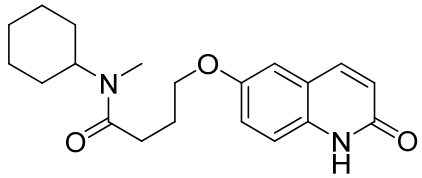

Cilostamide
1

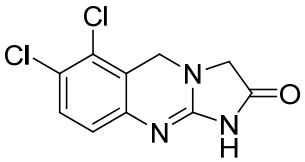

Anagrelide
2

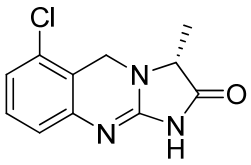

Quazinone
3

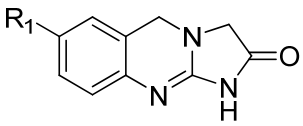

10, 35 - 38

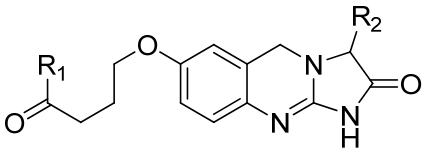

39 - 44

#	R_1	R_2	% Inhibition			IC_{50} (nM)	
			[nM]	3A	3B	3A	3B
Cilostamide **1**	-	-				22	48
Anagrelide **2**	-	-				35	100
Quazinone **3**	-	-				180	230
10	H	-	1000	72	60		
35	Cl	-	500	57	10	610	1900
36	Br	-	500	82	39		
37	OCH_3	-	500	82	46		
38	OH	-	500	65	14	750	2700
39	CH_2CH_3	H	500	93	66		
40	CH_2CH_3	(R)-CH_3	500	71	41		
41	OH	H	500	92	78		
42	OH	(R)-CH_3	500	65	43		
43	*$N(C_6H_{11})CH_2CH_2OCOC_6H_5$	H	50	99	92	0.17	2.3
44	*$N(CH_2CH_2)_2NCH_2C_6H_{11}$	H	50	83	53	17	24

Table 2 Activity assay results.

The screening data showed that all the compounds inhibited PDE3A by more than 50% at the concentration tested, and although compound **10** showed only a marginal difference between PDE3A and PDE3B some of the substituted analogues showed more marked differences. Of these compounds **35** and **38** showed poor inhibition of PDE3B at the chosen 500 nM. A number of the compounds showed almost complete blockade at the test concentration, including the two most potent analogues **43** and **44**. These four compounds were thus selected for further analysis by IC_{50} determinations against both isozymes (Figures 14 and 15). Compounds **35** and **38** show similar but modest selectivity for PDE3A of approximately 3-fold. Compound **43** on the other hand shows a significant 13-fold selectivity with a sub-nanomolar IC_{50} versus PDE3A. Compound **44** was potent but basically non-selective against the two isoforms.

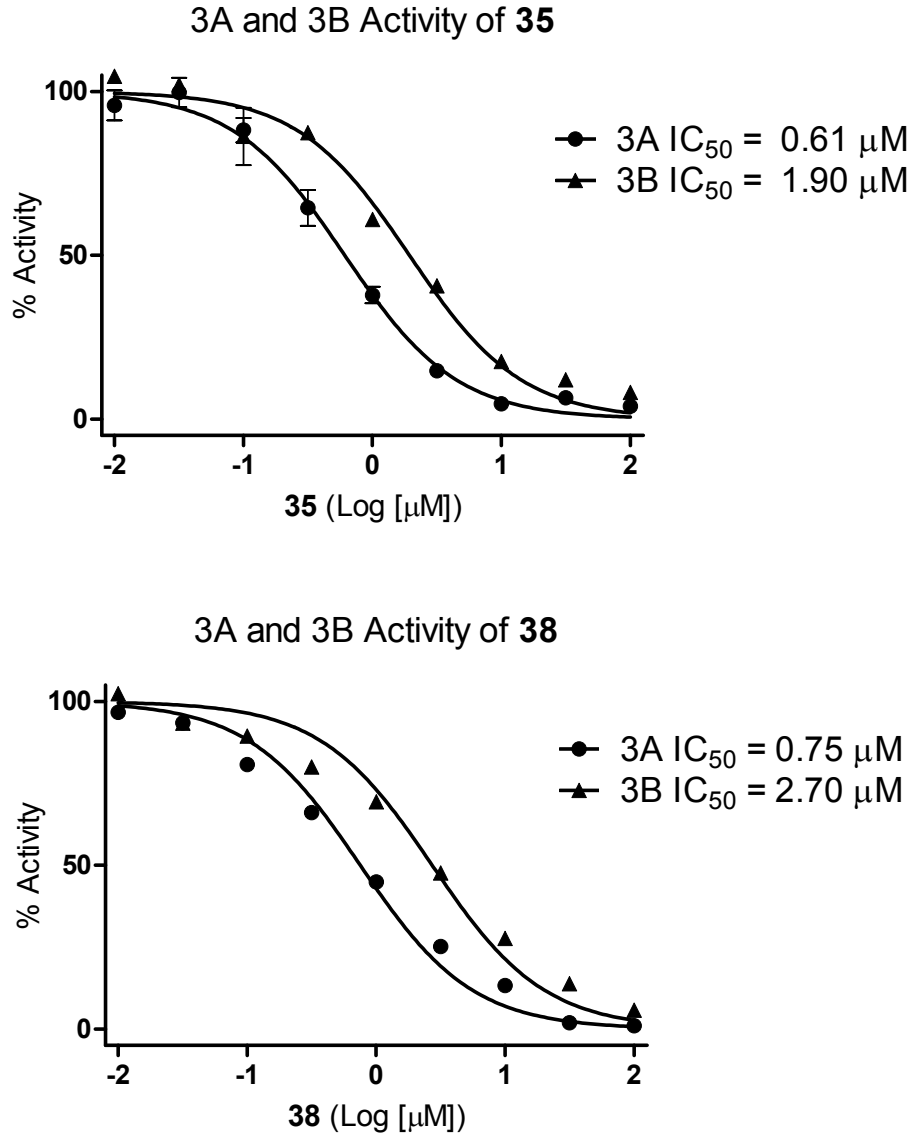

Figure 14 Dose response curves of 35 **and** 38

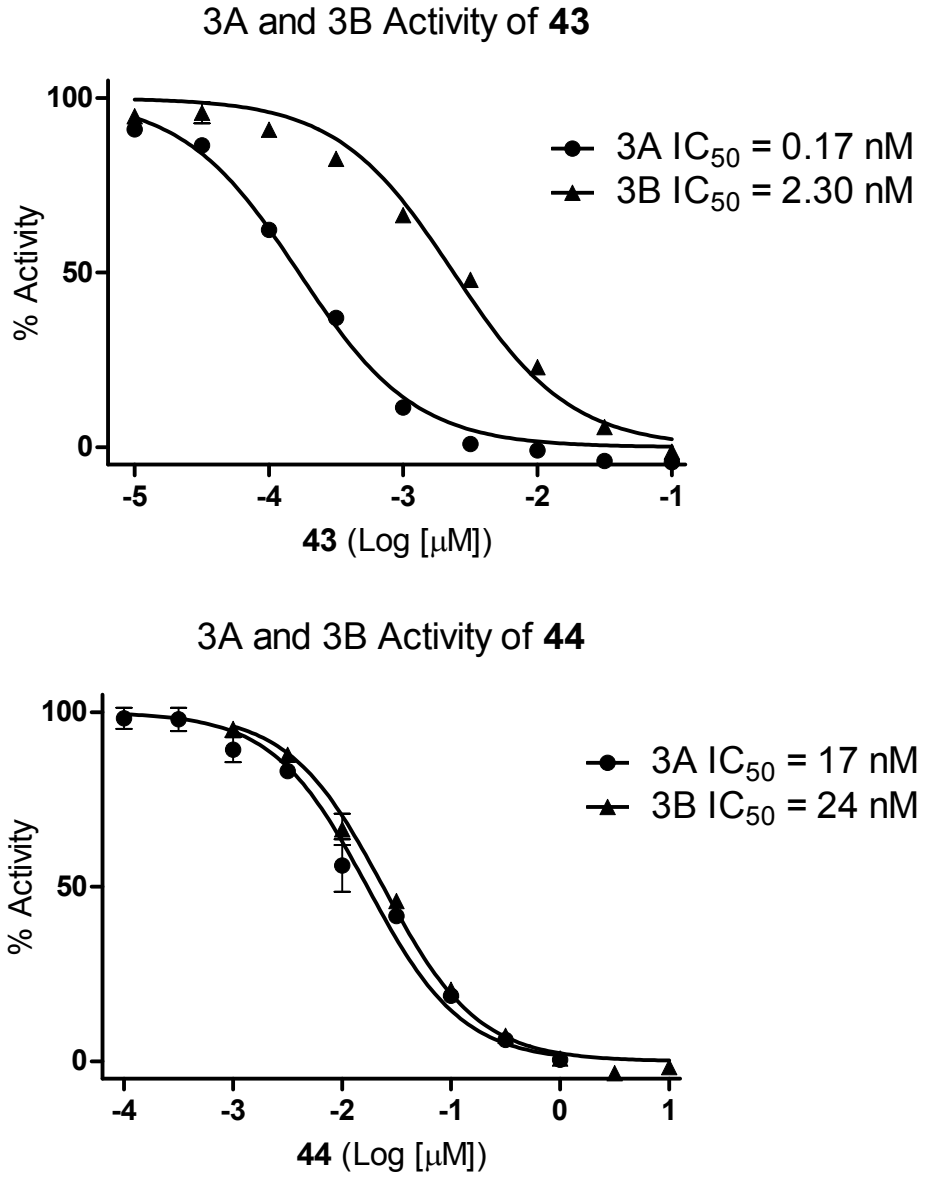

Figure 15 Dose response curves of 43 **and** 44**.**

The collective results of the screening assays and the dose response curves show a number of results relevant to this project. Firstly, the assays provide the first measurement of inhibition for many of these compounds against recombinant PDE3A. The inhibitory potency was in general terms found to be consistent with reported values from PDE activity from platelet lysates. Secondly, PDE3B assays were provided for all the IMQ compounds for the first time. They show that PDE3B inhibition was generally comparable to PDE3A inhibition, but in no case was PDE3B inhibition stronger. Three compounds show evidence of PDE3A preference, most notably the most potent compound **43** which had a PDE3A IC_{50} of 0.17 nM, 13-fold more potent than at PDE3B.

This data allows the first attempt to identify structural features that might contribute to isoform selectivity. Quazinone (**3**) is significantly less potent than Anagrelide (**2**) this is likely due to either the addition of an R-methyl on the lactam ring of quazinone (**3**), or the lack of substitution at the 7 position or both. The addition of an R-methyl group in other analogues reported here (**40** and **42**) causes a small decrease in potency, but seems to have little effect on selectivity. This suggests that the substitution at the 7 position is responsible for both an increase in potency and a small degree of selectivity for PDE3A.

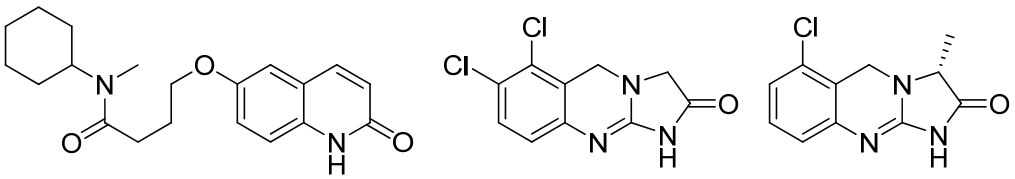

Figure 16 Comparison of commercial PDE3 inhibitors structure-activity.

Cilostamide (**1**) was found to be as potent as anagrelide (**2**) at PDE3A which is interesting considering the significantly higher molecular weight of cilostamide (**1**) (MW = 384) compared anagrelide (**2**) or quazinone (**3**) (MW = 256 and 215 respectively) cilostamide (**1**) was also slightly more potent at PDE3B. All three commercial PDE3 inhibitors examined are far more potent than the unsubstituted analogue produced in this study which has an estimated IC_{50} above 1000 nM at both isoforms.

The results for the series of analogues featuring small electronegative functional groups substituted at the 7 position show that this functionality provides an increase in potency and PDE3A selectivity over the unsubstituted scaffold. The larger bromo (**36**) seems to be more potent than the chloro (**35**) which follows reported results from a platelet aggregation (PDE3A) assay by Venuti et al, where larger halogens are more potent.[129] The IC_{50} values for the chloro (**35**) and hydroxy (**38**) analogues show are both 3-4 fold more potent against PDE3A than PDE3B. Overall there appears to be relatively small changes in activity associated with variation of electronegative substituents at the 7 position.

Analogues with an ethyl butanoate connected by an ether linkage at the 7 position (**39**, **40**, **41**, **42**) show an increase in potency over the 7-methoxy analogue (**37**). A relatively small change in potency was observed when the ester side chain was hydrolysed to a carboxylic acid. This could indicate that the side

chain is hydrogen bonding to the receptor and that the hydrophobic ethyl group confers little inhibitory activity. The addition of an (R)-methyl group at the lactam methylene ($\mathbf{R_2}$) onto analogues with the either ethyl 4-(2-oxo)butanoate (**40**) or 4-(2-oxo)butanoic acid (**42**) side chains, decreased the potency at both isoforms. Curiously, the equivalent modification in lixazinone is reported to give a small increase in potency.[111]

The two analogues with extended side chains were both found to be potent but show a difference in selectivity. While compound **44** is almost equipotent between the two isoforms, **43** is 13 times more active against PDE3A than PDE3B making it the most PDE3A selective inhibitor identified to date. When the results are analyzed solely by how the substituents affect the isoform selectivity it becomes apparent that all of the small substitutions are similarly selective for PDE3A, it is only with the extended side chain of **43** that significant changes in selectivity are observed.

2.3 Conclusions

The purpose of this study was to gather information on the isoform selectivity of a range of PDE3 inhibitors of the IMQ class. With this information in hand, decisions could be made regarding the pursuit of novel isoform selective PDE inhibitors.

The two best known IMQ PDE3 inhibitors anagrelide (**2**) and lixazinone (**4**) have similar potency, but the elaboration of the parent IMQ structure is quite contrasting. In anagrelide (**2**), 6,7-dichloro-substitution leads to approximately 30-fold enhance potency. In lixazinone (**4**) this is achieved by an elaborated 7-substituent. In neither case, does this make a marked change in PDE3A/3B selectivity. In fact we could determine, just one analogue for which a promising level of selectivity could be obtained. The most potent compound of the series **43** achieves a 13-fold selectivity for PDE3A.

From these results, and also drawing on the studies of Edmondson et al[116] it can be concluded that there is a secondary binding site that is accessible to extended side chains which may be able to interact with it to achieve selectivity. However, the selectivity observed to date is not sufficient to constitute truly selective compounds. Moreover, the molecules are quite large which compromises them as potential therapeutics and also adds quite a synthetic challenge. It is concluded, that other parameters should be sought to generate isoform selectivity. One other that has been examined here is the position adjacent to the lactam

amide. The D-alanine derived compounds **40** and **42** were less potent and no more selective than their glycine derived equivalents, so this may not be productive.

Other pathways to explore include, changes to the substituent linkage. The butyrate ether chain is inherently flexible, and the multiple rotatable bonds may allow the one molecule to access different binding orientations of the PDE3A and PDE3B binding sites. It might be desirable to examine new pendant groups from the IMQ ring that confer more rigidity into the molecules.

From a synthesis perspective, it is important to have a method of appending side chains rapidly and efficiently. The IMQ core should be a template precursor as it would remain a constant. In order to design further analogues, particularly those with novel structures and chemistries, it was decided to examine the SAR of PDE3 inhibitors and isoform selective inhibitors in more detail. To this end a computational chemistry investigation was undertaken which is the subject of the next Chapter.

Chapter 3: Molecular Modeling

A computer crisply calculates the co-ordinates of chemical components contained in a catalytic cave, by counting the contributions of complimentary and clashing contacts it compiles a catalogue of compounds for consideration.

3.1 Background

3.1.1 Early Applications of Computational Chemistry in PDE3 Inhibition

The use of computational chemistry as a means to understand the molecular basis of PDE3 inhibition goes back to the 1980's. These first reports attempted to correlate specific physicochemical properties of known inhibitors with their potency, and thereby define pharmacophores for PDE3 selective inhibition.[128, 140, 141] A pharmacophore is a set of steric and electronic features that represent favourable interactions with a specific biological target, determined by comparing the structure of ligands with the desired activity and finding features in common. A pharmacophore can be thought of as a ligand-based representation of the binding site, useful for designing new ligands with the same activity. Moos et al[141] proposed a pharmacophore for PDE3 inhibitors based upon the substituted 4,5-dihydropyridazin-3(2H)-one template shown in Figure 17.

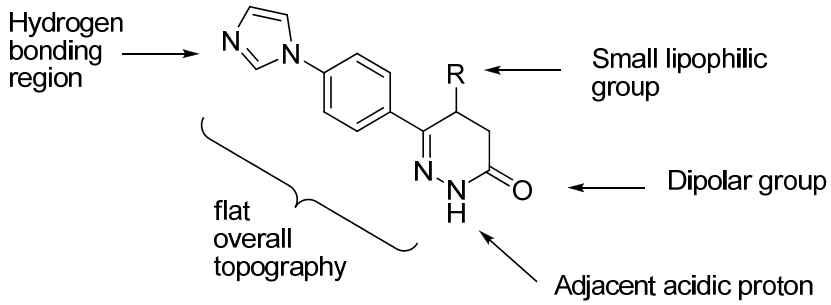

Figure 17 Common features of PDE3 selective inhibitors. Adapted from Moos et al.[141]

Pharmacophores for PDE3 ligand binding were progressively developed that could to an extent predict a ligand's potency and selectivity for PDE3.[142] As information regarding the PDE3 sequence and likely structure became available, attempts were made to predict what amino acid residues in the catalytic site were involved in these interactions.[143] As the field of molecular modeling advanced so did its application

to PDE3 inhibitor design, from predominantly pharmacophore/QSAR based approaches to simulations of the ligand/protein interaction - molecular docking.

There are well recognised limitations in the docking approach that limit their accuracy; first, the protein structure utilized is a model, both in respect of the starting topology, which may be derived by analogy to a homologous protein, but also in that a continuous dynamic system is being approximated with discrete steps between static structures. Secondly, approximations of quantum mechanical effects must be used such that the accuracy of the simulation is compromised which is compounded by limitations in computing resources. On the other hand ligand docking experiments are able to define broad areas of favourable / unfavourable interactions with polar and non-polar groups, suggest specific key interactions and the binding site residues involved can be identified. The increased understanding of the binding site afforded by this approach aids the design of ligands that can adequately complement the topography and polarity of the active site.[144]

Fossa et al[145] developed a homology model of the PDE3A catalytic site based on a combination of the PDE4B2B crystal structure[146] and a considerable body of PDE3A mutagenesis data. From this homology model they could explain the binding of several structural elements that are found in potent PDE3 inhibitors. One of the finer details uncovered by these experiments was that the lactam group common to PDE3-selective inhibitors was interacting with a glutamine residue, a feature later confirmed through crystallographic studies.

3.1.2 Reports of Computational Chemistry Using PDE3B Crystal Structures

The next important improvement in the understanding of PDE3 inhibition came with the report of two x-ray crystal structures of PDE3B in 2004.[45] The structures were solved with MERCK1 (**6**), a PDE3B selective inhibitor solved to a resolution of 2.4 Å and with the non-selective PDE inhibitor IBMX solved to 2.9 Å. With few differences between the PDE3A and PDE3B sequences in the catalytic domain, a model of PDE3A based on the crystal structure of PDE3B can be expected to be much more accurate than those derived from PDE4. No crystal structures of PDE3A have yet been reported.

Despite this pivotal data becoming available, there have been few analyses of PDE3 inhibition using computational methods, perhaps reflecting industry's low interest in this target. Recently, Nikpour et al[118]

did use a computational approach to design novel PDE3 inhibitors (**63**), specifically aiming for compounds that would selectively increase cardiac contractile force without affecting the frequency of contractions. They aimed to produce these ligands based on vesnarinone (**62**) using molecular docking as the main design tool. Interestingly, they found that a poor correlation was obtained between the predicted K_i and experimentally determined IC_{50} values using results from the lowest energy conformer. On the other hand when they selected only a specific family of conformers this binding mode gave a strong correlation. Given that the researchers needed to effectively disregard the most favoured theoretical conformer suggests this process is limited in predictive design, especially with other chemotypes.

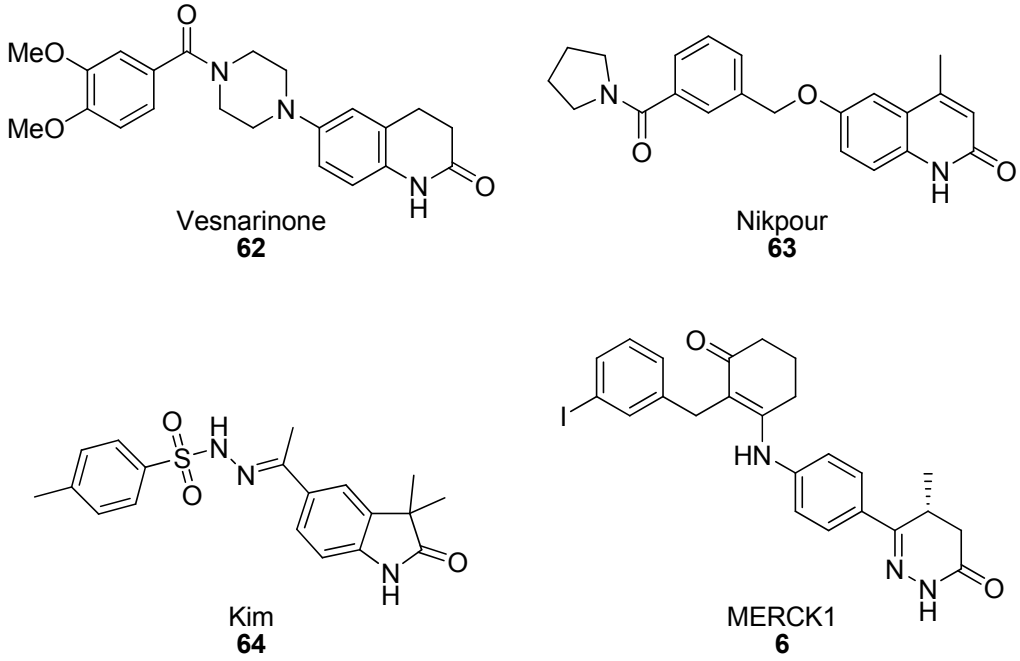

Figure 18 Vesnarinone, and several PDE3 inhibitors that were discovered or optimized using computational chemistry.

Kim et al[120] used a virtual screening approach to identify new lead PDE3 inhibitors. Beginning with a virtual library of some 3000 diverse "lead-like" compounds, docking identified 80 compounds that bound in a low energy conformation. These 80 compounds were screened for adipocyte lipolysis activity and four structurally unrelated leads were identified. The most potent of the four (**64**) has IC_{50} values of 14.8 nM at PDE3A and 88.4 nM at PDE3B. Of the four compounds, two contained a lactam ring fused to a phenyl ring that is commonly seen in PDE3 inhibitors. The remaining two compounds did not have any significant overlap with other known inhibitors.

From these limited literature examples we can conclude that molecular modeling and in particular molecular docking can simulate the binding of PDE3 inhibitors. However it must also be acknowledged that it is not a simple process and effective use of docking in PDE3 inhibitor design is not straightforward. Even more difficult are experiments that seek to understand the molecular basis for PDE3A or PDE3B selectivity.

In this Chapter, a series of molecular modeling experiments are described that were devised and executed to aid understanding and design of PDE3 inhibitors. Firstly a model of PDE3A was developed based upon the PDE3B crystal data, with a focus on differences that can be exploited for selective inhibitor design. Secondly, a variety of docking experiments were performed to establish if a method was available that would correlate theoretical binding energies with experimental enzyme inhibition. This series looked at (i) the ability of docking to recapitulate binding observed in crystal structures, (ii) the ability of docking to predict inhibitory potency across a range of PDE3 inhibitors in the literature, then (iii) narrowing in on specific inhibitor classes, including the new data on IMQs described in Chapter 2. Finally, the information was combined in an attempt to develop a strategy for the design of new compounds with the potential to show reasonable potency or isoform selectivity for either of the PDE3 isoforms. From this work a new series of ligands was designed which form the basis of Chapter 4.

3.2 Results and Discussion

3.2.1 Preparation and Validation of Models of PDE3A and PDE3B

3.2.1.1 Analysis of x-ray data

The first task was to develop and analyse structural models of PDE3A and PDE3B for use in molecular docking. The two PDE3B crystal structures are similar and correspond to the generalized structural fold of the PDE class.[45] There are 14 residues (res 767 - 781) in the 44 amino acid loop (res 755 - 798) unique to PDE3A and 3B (Section 1.2) that are not resolved in either crystal structure which is attributed to a high degree of protein mobility in the loop. There is another region between the 15th and 16th helices (1016 – 1052) for which no density was observed.

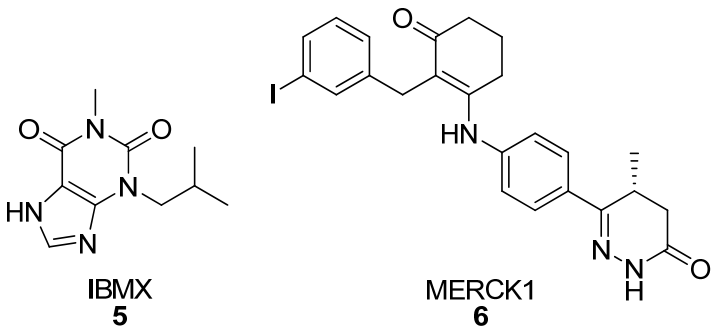

Figure 19 Non-specific PDE inhibitor IBMX and PDE3 selective inhibitor MERCK1 are included in the two available PDE3B crystal structures.

The other characteristic region of the active site of PDE3 is the metal ion binding region - a complex network of amino acids and water molecules which hold two solvated magnesium ions in place. The first metal ion interacts with four residues, (Nτ-His741, Nτ-His821, COOH-Asp822, and COOH-Asp937) and two water molecules, one of which is shared with the second metal ion. The second metal interacts with the side chain of Asp822 and the remaining co-ordination sites are filled with water molecules. These water molecules form hydrogen bonds with a number of residues (Asp822, Glu851, His737, His825, Thr893) and two hydrogen bonds with carbonyls from the backbone chain of His 821 and Thr893.

IBMX (**5**) and MERCK1 (**6**) have binding site interactions commonly observed for PDE inhibitors in general. Most notable are the hydrophobic or Pi-stacking interactions between the inhibitor's aromatic ring and Phe991 and Ile 955 which form a hydrophobic clamp.[45] Another common aspect of ligand binding is the hydrogen bonding between the ligands and a conserved glutamine residue, Gln988. It should be noted that the carboxamide side chain conformation of Gln988 is flipped between the two crystal structures. The flipping of Gln988 is thought to be the reason that PDE3 isoforms can accommodate both cAMP and cGMP.[147] It has been suggested that IBMX (**5**) binds in the enzyme's cGMP binding conformation, and MERCK1 (**6**) binds as cAMP would.[45, 148]

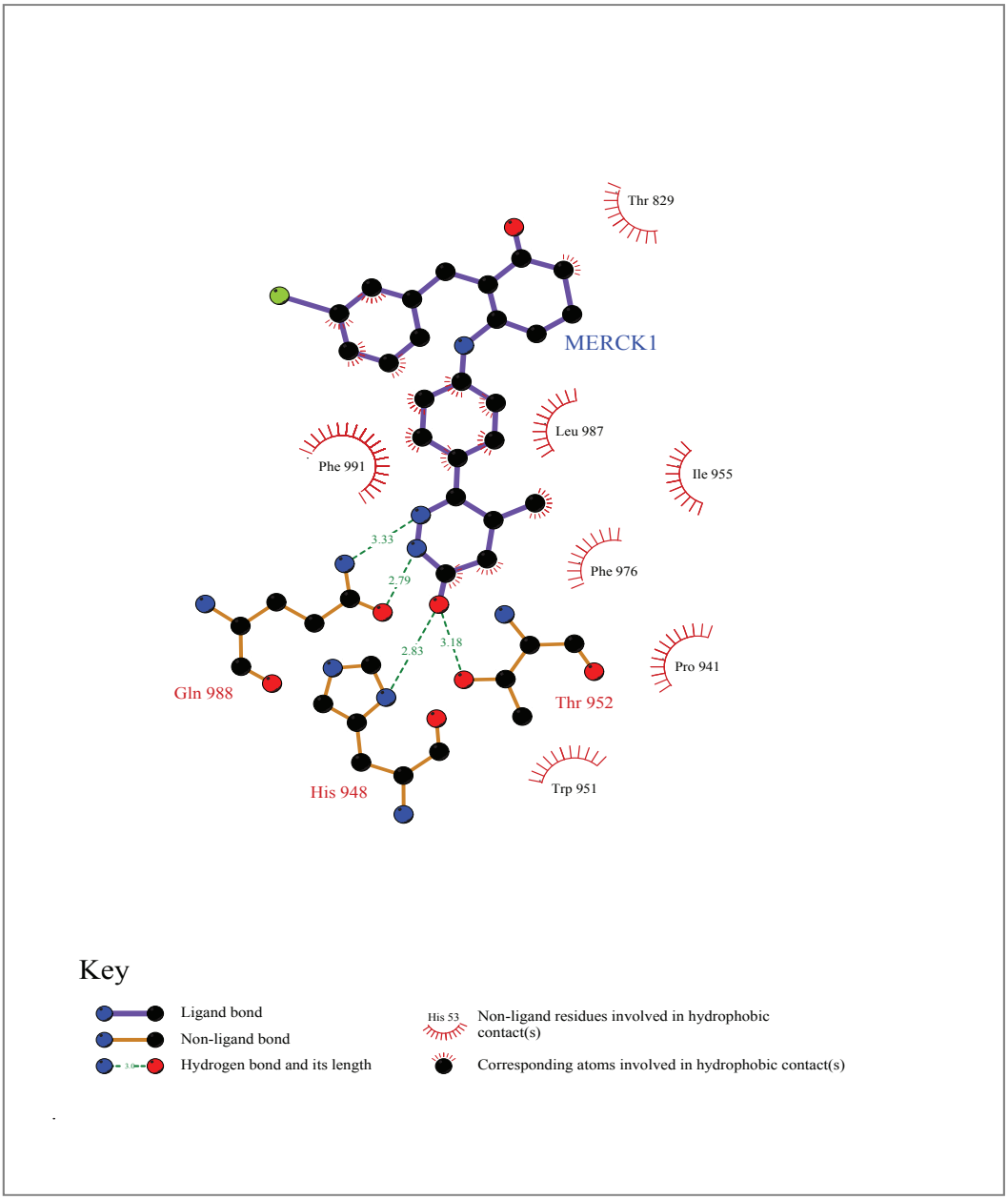

Figure 20 Ligplot diagram of the interactions between MERCK1 (6) and the PDE3B binding site

While IBMX (**5**) is a pan-PDE inhibitor, MERCK1 (**6**) is selective for PDE3, and it has been hypothesized that the source of PDE3 selectivity is the ability to access one residue - His948 (His961 in PDE3A) which in other PDE enzymes is concealed. PDE3 has a unique glycine residue Gly940 (Gly953 in PDE3A) that exposes the histidine which can then interact with the pyridazinone carbonyl of MERCK1 (**6**). It seems likely that a similar interaction provides the basis for selectivity for many inhibitors of the PDE3 family that have comparable binding motifs including the imidazoquinazolinone inhibitors that are the focus of this thesis.

The regions of the crystal structures that have not been solved (PDE3B residues 767-781 and 1016-1052) may have an important bearing on ligand binding. There are some sequence differences between PDE3A and PDE3B in these flexible loops, which may form an important region of heterogeneity between the two isoforms' active sites. Evidence that the non-conserved 44-amino acid insert interacts with the active site was reported by Hung et al[149] who showed that a cAMP analogue (Sp-adenosine-3,5-cyclic-S-(4-bromo-2,3-dioxobutyl) monophosphorothioate) covalently binds to Tyr807 in PDE3A which is within the insert. They also found that in a Tyr807Ala mutant the same inhibitor does not covalently bind, and in the wild type and Tyr807Cys mutant (the equivalent residue in PDE3B is Cys792) it does. A series of alanine mutations on the insert also exhibited an altered k_{cat} which indicates that the loop may play a role in catalysis.[149, 150] This evidence suggests that because some of the insert is missing in the crystal structure, the active site that it describes may be incomplete or not represent the active conformation of the enzyme. It is not known how this will affect docking studies that use this structure.

The homology model of PDE3A was created using the PDE3B enzyme model as a template. PDE3A and PDE3B share an overall 67% homology. For residues within 15 Å of the active site, the homology increases to 95%, and the majority of amino acids that don't match are substituted for similar residues (Figure 21).[118, 151] As shown in Figure 22 none of the non-conserved residues present in the crystal structure directly interact with the MERCK1 ligand (**6**).

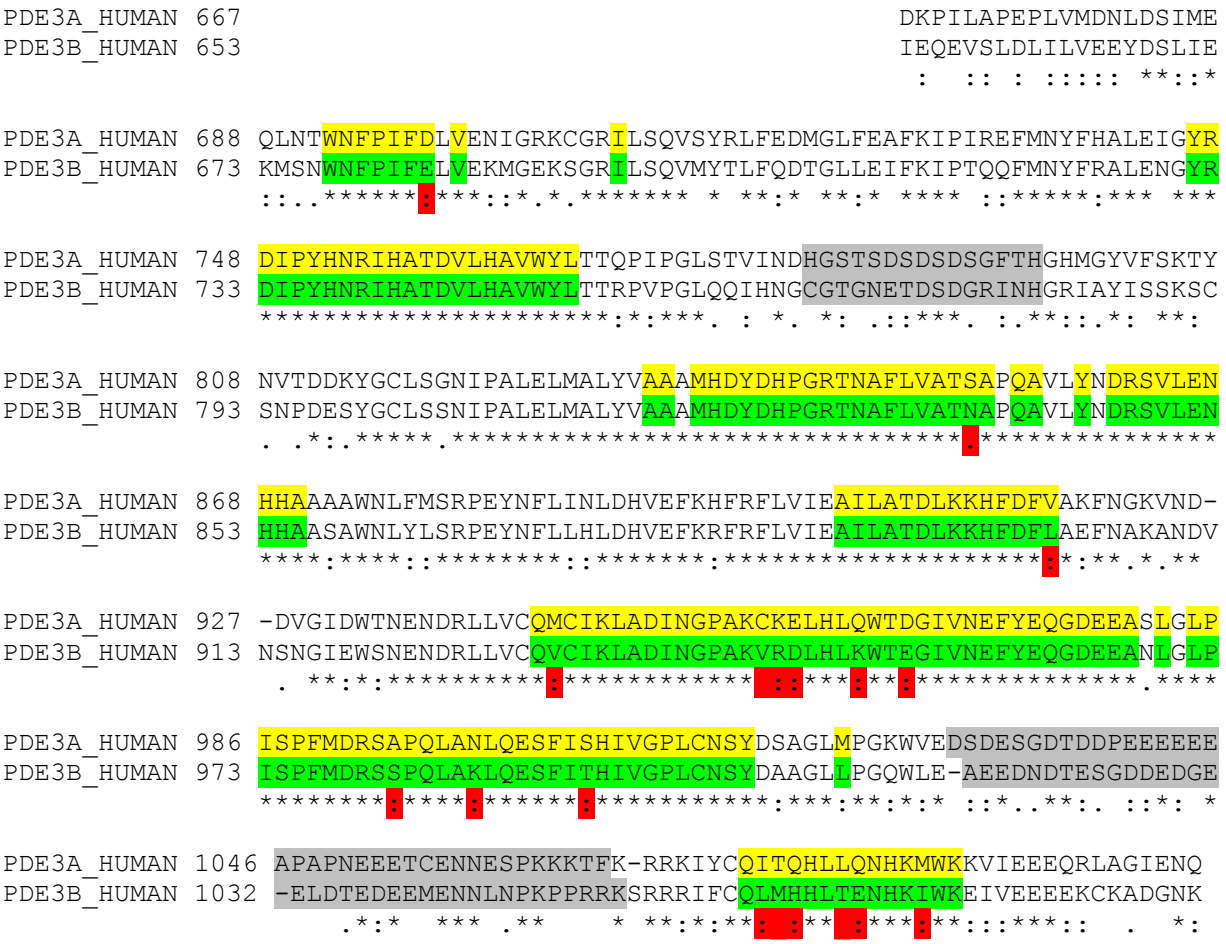

Divergent 3A residues within 15 Å of bound ligand
Divergent 3B residues within 15 Å of bound ligand
Heterogeneous positions within 15 Å of bound ligand
Inserts not included in crystal structure

An * (asterisk) indicates positions which have a single, fully conserved residue.
A : (colon) indicates conservation between groups of strongly similar properties - scoring > 0.5 in the Gonnet PAM 250 matrix.
A . (period) indicates conservation between groups of weakly similar properties - scoring =< 0.5 in the Gonnet PAM 250 matrix[152]

Figure 21 Sequence alignment of PDE3A and PDE3B catalytic domains.

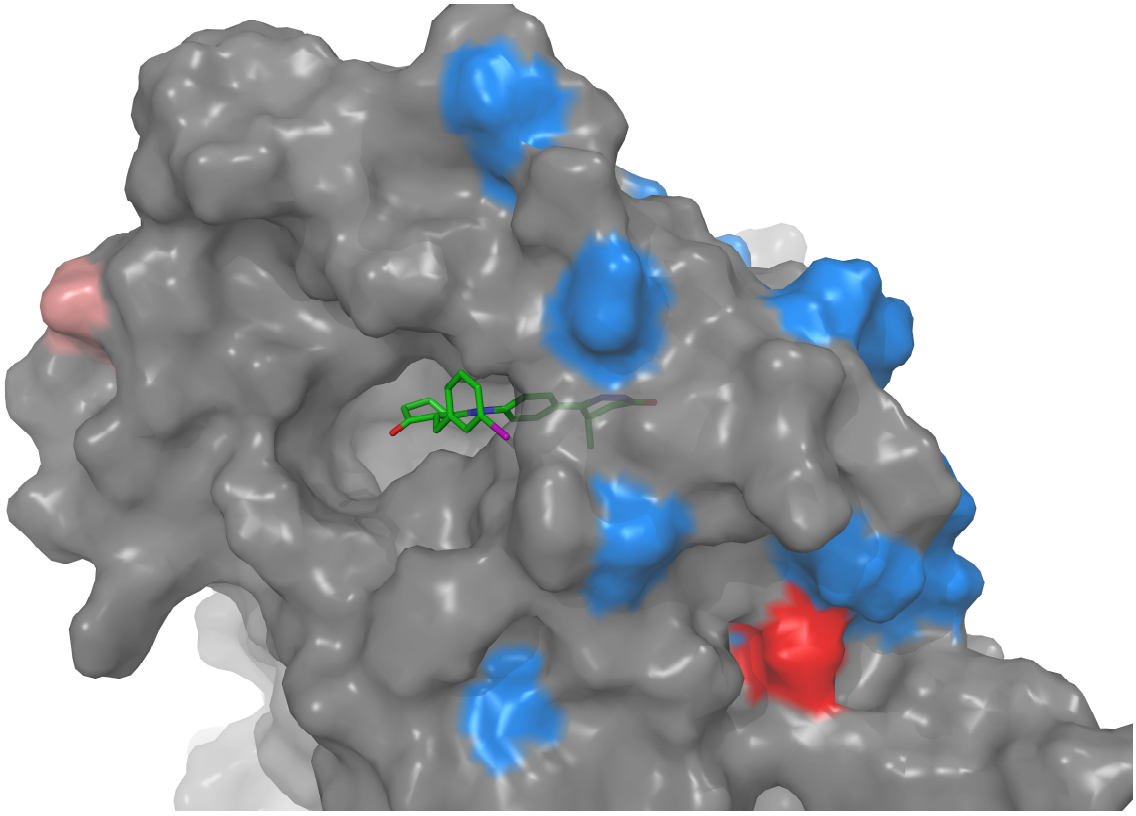

Figure 22 Heat map of non-conserved residues within 15 Å of ligand, none of which directly interact with the ligand (Grey – identical, Blue – similar, Pink – weakly similar, Red – divergent).

3.2.1.2 Preparation of the models

A crystal structure is not used directly in molecular docking experiments, but is used to prepare an enzyme model. The crystal co-ordinates of PDE3B (1SO2) contains four monomers in the crystal unit, the structure is poorly defined in multiple regions as described above, and no density for protons is observed.

The model for PDE3B was built by first isolating a single monomer; then hydrogen atoms were added to the crystal structure and missing side chains were added and optimized. To further prepare the enzyme model the following adjustments were made; metal ions were assigned an appropriate formal charge, bond orders were assigned, the proteins hydrogen bonding network was optimized, and finally a limited minimization was used to ease strained bonds and angles as well as any steric clashes.

The construction of the homology model for PDE3A was achieved using the program PRIME.[153] Specific residues were added, deleted and mutated to match the PDE3A sequence. Sequence loops that were missing in the PDE3B structure were subsequently also missing in the PDE3A structure. As expected the

resulting model of PDE3A was very similar to the PDE3B template (RMSD 0.11 Å). The high homology between the two isoforms means that the homology model should be a good representation of the structure of PDE3A. On the other hand, there are such few differences between the PDE3B crystal structure and the PDE3A homology model that their utility in the design of isoform selective compounds may be limited.

Finally, one other feature that was given consideration was the hydration of the binding site. Over 100 water molecules are defined in the first subunit of the 1SO2 structure. In an attempt to consider the influence of binding site water molecules, three separate models of PDE3B were prepared. In model A, all of the water molecules that were further than 5 Å from a heterogeneous group (i.e. not protein) were removed leaving a total of 20 water molecules, 6 of which were bound to the two metal ions. In model B, only the 6 metal-bound waters were included while a third model (C) was prepared where all waters were deleted. It was expected that the model (C) with naked metal ions would not be representative of a biological system, yet it may show potential for the ligand to interact in the location of the co-ordinated water molecules. It was anticipated that just one of these models would prove suited to further studies.

*3.2.1.3 Docking of MERCK1 (**6**) – Validation of Docking*

Molecular docking experiments were performed using GLIDE[154] for all docking simulations. This program has been shown to provide reasonable results for docking small molecules into proteins, and demonstrating superior results over alternate software packages.[155, 156]

The GLIDE algorithm offers three different docking modes, from least to most computationally intensive they are; High Throughput Virtual Screening (HTVS), Standard Precision (SP), and Extra Precision (XP). The different options of both enzyme preparation (retaining 20, 6 or 0 waters) and docking method (HTVS vs. SP vs. XP) were all applied to dock the MERCK1 (**6**) ligand back into the PDE3B enzyme model. The ability to reproduce the crystal structure binding pose of MERCK1 (**6**) was measured by root mean square deviation (RMSD) of heavy atoms. The results are summarized in Table 3.

Run #	Model	Docking Method	RMSD (Å)	Matching Pose
1	A	HTVS	0.85	Yes
2	B	HTVS	2.42	No*
3	C	HTVS	3.95	No
4	A	SP	0.59	Yes
5	B	SP	2.22	No*
6	C	SP	5.11	No
7	A	XP	0.63	Yes
8	B	XP	0.71	Yes
9	C	XP	0.73	Yes

Table 3 Reproducing MERCK1 binding mode using different PDE3B enzyme models (A – 20 waters, B – 6 waters, C – 0 waters) and docking methods (HTVS – High Throughput Virtual Screening, SP – Standard Precision, XP – eXtra Precision). * Indicates that only the iodophenyl ring was flipped.

The correct binding pose was reproduced in 5 of the 9 experiments, notably all those using Model A (Runs 1, 4, 7) and all those using the XP docking method (Runs 7, 8, 9). In 2 others from Model B (Runs 2, 5) the basic pose matched the structure but with a flipped conformation of the iodophenyl group. Two of the trials with model C failed and gave different binding modes (Runs 3, 6). It is clear that the inclusion of water molecules in the model affects the docking result except in the case of XP docking. The pose with the iodophenyl ring flipped compared to the crystal structure as shown in Figure 23 appears to be a feasible alternate conformer.

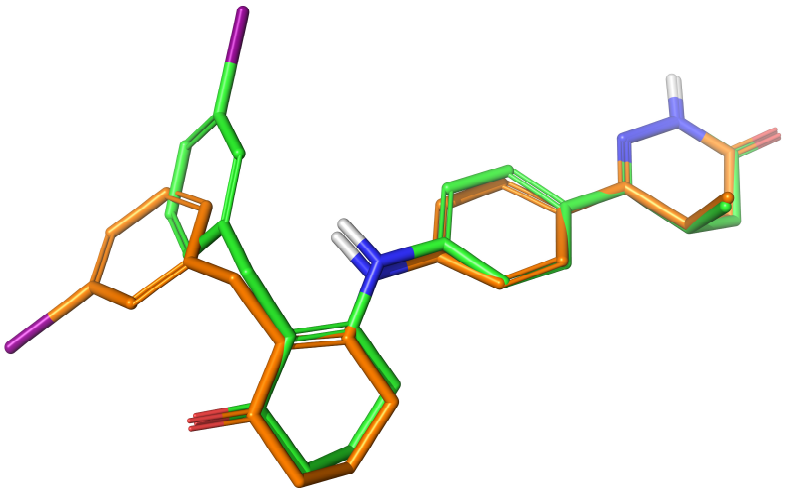

Figure 23 Comparison of docking results of MERCK1 in model B with matching pose (green – XP docking) and flipped iodophenyl ring (Orange – SP docking).

When the model with 20 waters (A) was used, the correct pose was predicted with each method. This shows that the presence of the additional water molecules aid in docking, however this may only hold true when docking the original ligand back in, which the waters are already positioned to accommodate and may provide an unrealistic templating effect.

It was clear that when the waters coordinating the metal were removed, the results were negatively affected, although less so when using XP docking. Both HTVS and SP methods produced reasonable binding poses when using the 6 water model, in both cases the orientation of the iodophenyl ring was incorrect, but the rest of the molecule matched reasonably well. Interestingly, the lowest RMSD was produced by SP rather than XP docking although there was little discernible difference between the two best poses and the crystal structure ligand.

After consideration of the results described above model (B) with 6 metal-bound waters was chosen for use in further investigations. This model gave the correct pose with an RMSD very close to the best result, and may allow for the docking of structurally diverse ligands given the removal of extraneous water molecules. The XP docking mode was best able to produce the correct binding mode for MERCK1 (**6**) in model B. This also confirmed that GLIDE has reasonable predictive ability using these conditions. All subsequent docking was performed using GLIDE in extra precision (XP) mode.

MERCK1 is just 3-fold more potent at PDE3B than PDE3A and so would be expected to adopt a comparable pose in both models. The PDE3A homology model was also evaluated by docking MERCK1 (**6**) and the predicted binding mode for MERCK1 (**6**) was virtually identical to that observed for the PDE3B crystal structure (RMSD = 0.38 Å). The docking scores for MERCK1 (**6**) were comparable between the PDE3A and PDE3B docking experiments (-11.84 vs. -12.08 respectively) which is reflected in the affinity of MERCK1 (**6**) for both enzymes. The gScore function gives a measure of the energy of the binding interaction, as such the most potent compounds should have the lowest scores. A representative formula used to calculate gScores is included in the experimental section.

In summary in this preliminary phase, models for PDE3A and PDE3B had been developed which gave reasonable approximations of the crystal data and might be expected to provide guidance in understanding the principle elements of ligand binding to PDE3 isoforms.

3.2.2 Docking of Known PDE3 Inhibitors into the PDE3A and PDE3B Models

In an attempt to determine how the docking results obtained from these models related to reported assay data, two more docking experiments were carried out. Firstly, a series of 21 known PDE3A inhibitors with diverse scaffolds were docked into the PDE3A model (Appendix A). The results were somewhat disappointing, despite a general ability to select a binding pose entirely consistent that shown by MERCK1, that is with the heterocyclic end group projecting deep into the adenosine binding pocket, no correlation was observed between the ligands docking scores and reported IC_{50} values.[148] For example, imazodan with an IC_{50} of 6 μM, was ranked 19th in terms of potency but was 3rd ranked by the scoring function. The most potent of the series, OPC-33540 was ranked 13th. The scoring function was clearly unable to represent the key binding features of these ligands.

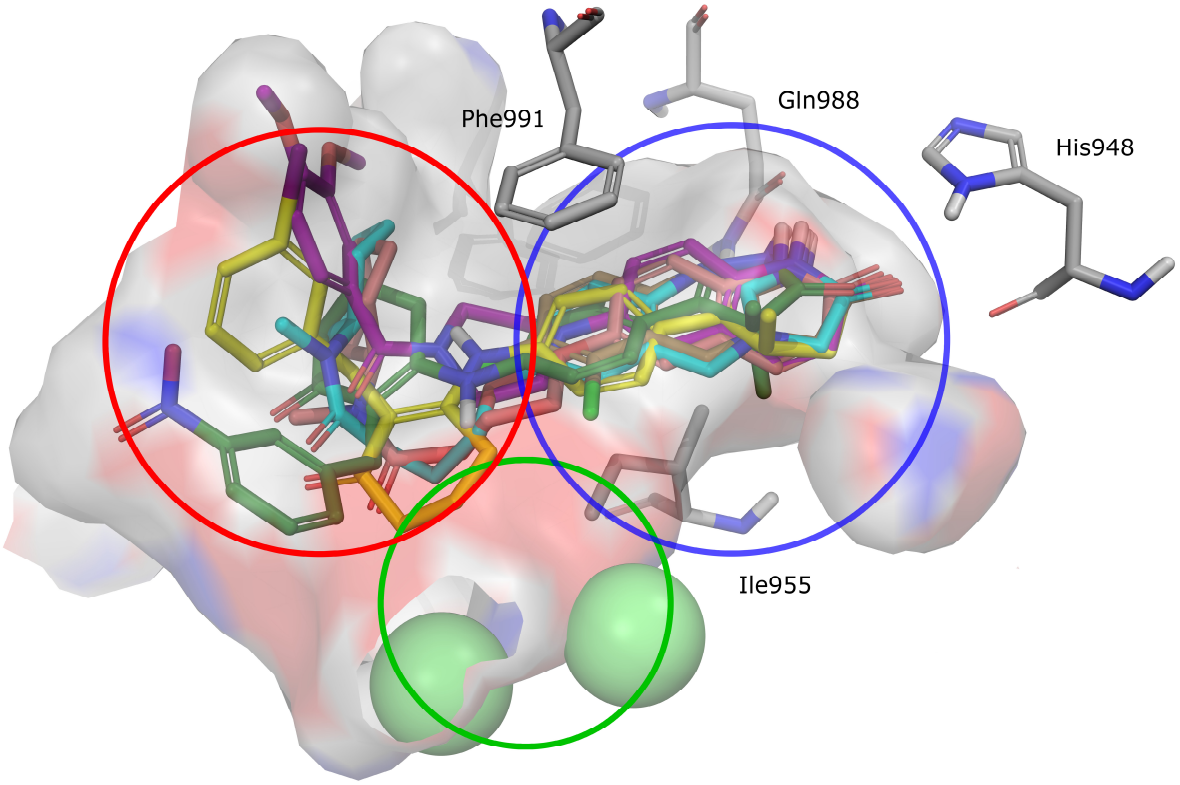

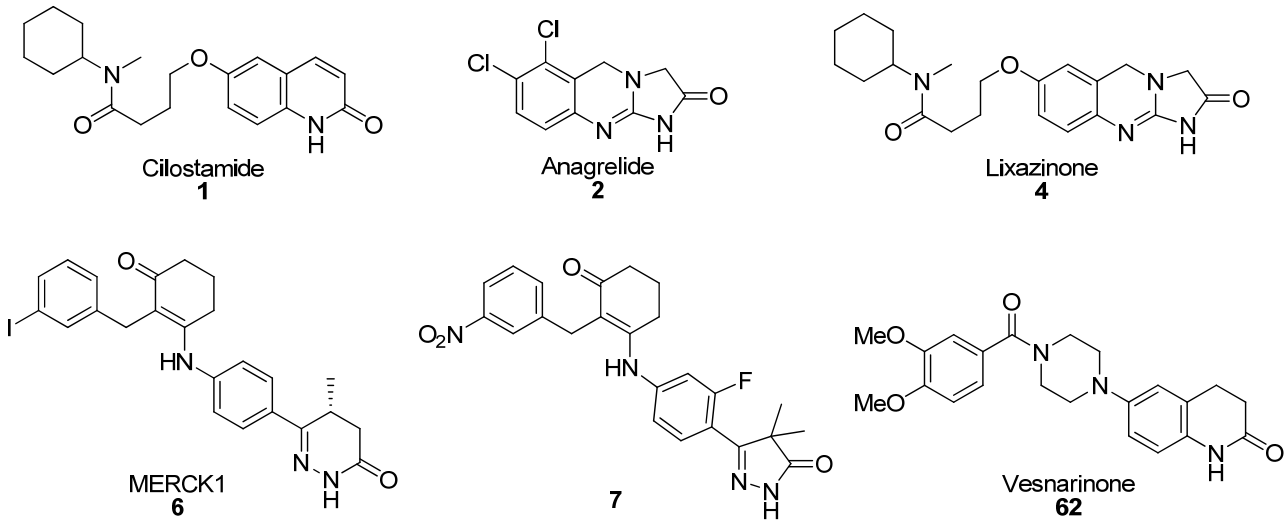

Figure 24 PDE3B binding site surface with docked PDE3 inhibitors overlaid. 6 **(yellow),** 7 **(green), Cilostamide (pink), Anagrelide (brown), Lixazinone (cyan), Vesnarinone (purple). Blue circle – core binding region, Green circle – metal binding region, Red circle – secondary binding region.**

Unsurprisingly then a second series of experiments to ascertain if the models could approximate the reported selectivity data also failed. A series of analogues based on the PDE3B-selective series described by

Edmondson et al[116] were docked into both the PDE3A and PDE3B models. The docking score rankings against PDE3A and PDE3B didn't correlate to the observed PDE3B selectivity of the compounds. Compound **7** which was the most selective for PDE3B (33 fold) was predicted to be among the least PDE3B selective compounds of the series. The compound predicted to be most selective was one of the least selective (Appendix A).

While the gScore gave no indication about the basis of affinity or selectivity, visual inspection of the docked solutions did yield some possible clues for consideration in design. In some analogues such as **65**, substitution on the central aryl ring caused it to be twisted out of plane compared to the unsubstituted analogue. In certain analogues the substituent on the central aryl ring when docked in PDE3A was flipped 180º in PDE3B. Given that in some examples, this substitution also generated 8-10 fold selectivity for PDE3B in vitro, this aspect of the binding mode could be an important feature for isoform selectivity.

The compound class exemplified by **7** yielded more selective compounds than the class including **65**. A large amount of selectivity is derived from substitution on the terminal aryl ring. In the docking solutions this ring is positioned towards the opening of the binding site. It has been suggested that the flexible 44 amino acid insert of PDE3 may interact with the binding site in this region and in doing so provide a source of heterogeneity between the two isoforms and this could explain how substitution at the terminal aryl ring of these analogues has a significant effect on isoform selectivity. While representing an undefined region from crystallography, this secondary binding site may be an important contributor to selectivity in extended analogues.

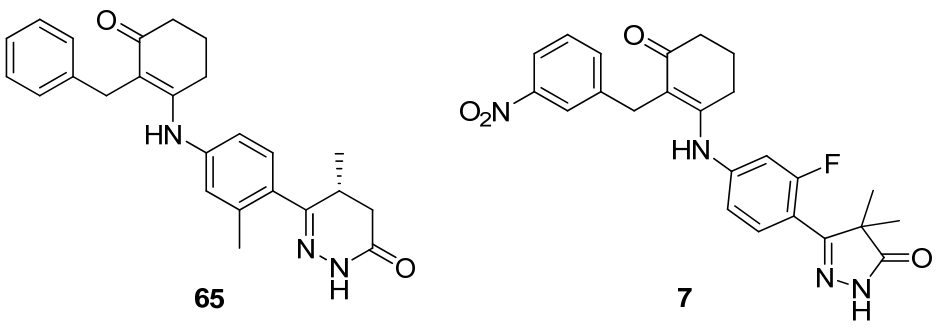

Figure 25 PDE3B selective ligands reported by Edmondson et al.[116]

In summary, manual inspection of the docking results for PDE3 inhibitors identified some aspects of the ligands binding mode that may be important for determining isoform selectivity. The two most

significant contributors appear to be decoration of both the phenyl ring in the core binding region and the phenyl ring within the secondary binding region.

3.2.3 Docking of Imidazoquinazolinone Analogues

The next series of experiments explored inhibitors that had been synthesized in this current study as well as related compounds. As described above lixazinone (**4**) binds in a very similar manner to MERCK1 (**6**) (Figure 26). This pose is entirely consistent with potent selective inhibition of PDE3 isoforms.

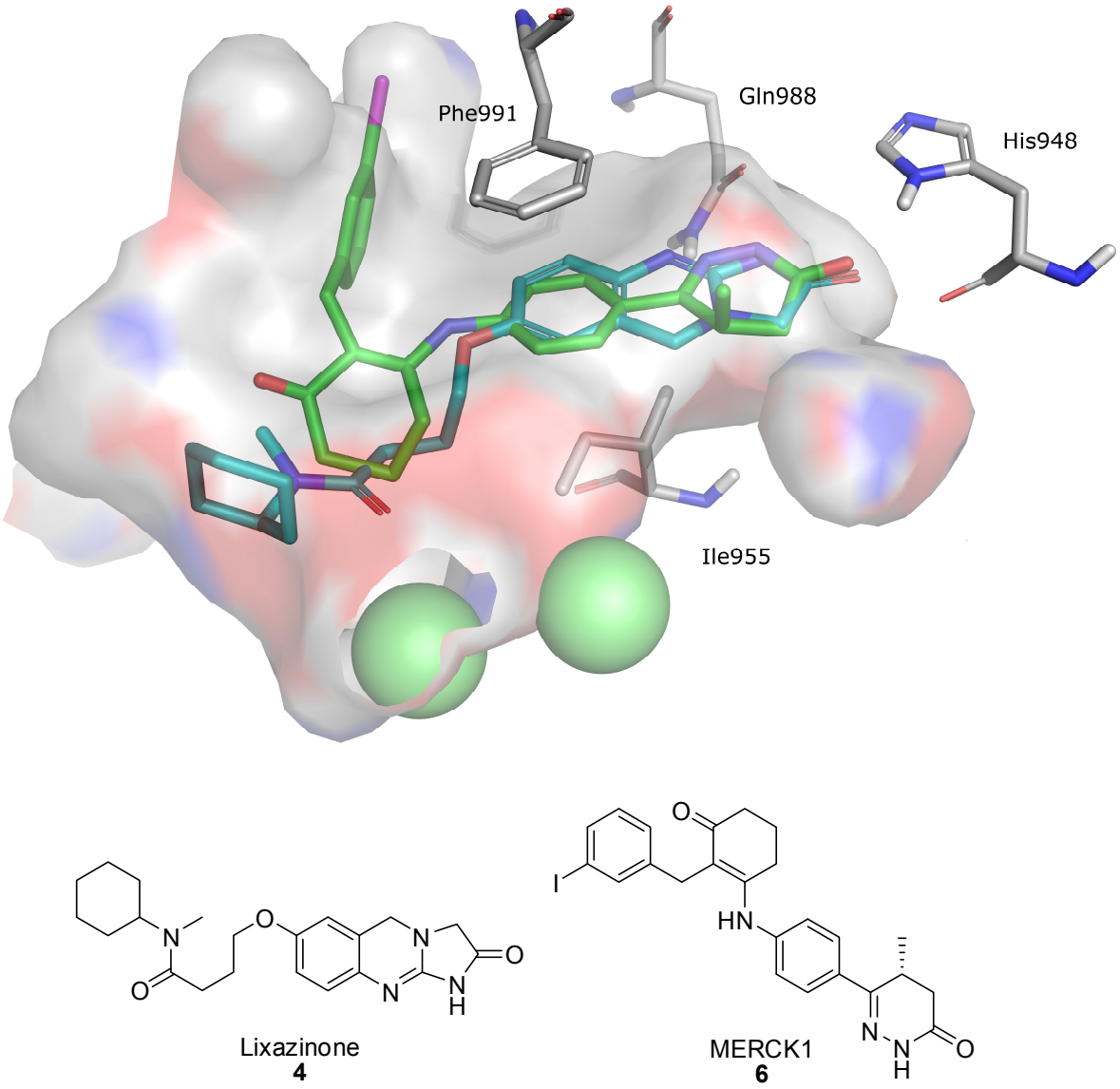

Figure 26 Overlay of MERCK1 (green) and Lixazinone (teal) in the PDE3B binding site with key residues

In the docking solution of unsubstituted IMQ (**10**) this core binding pose is conserved (Figure 27) and the binding site interactions in detail include a hydrogen bond between the His948 side chain and the carbonyl group of the ligand and two paired hydrogen bonds between the Gln988 side chain and two of the guanidine-like nitrogens. Finally there are two interactions with the IMQs aryl ring; a hydrophobic interaction with Ile955 and pi-stacking with Phe991.

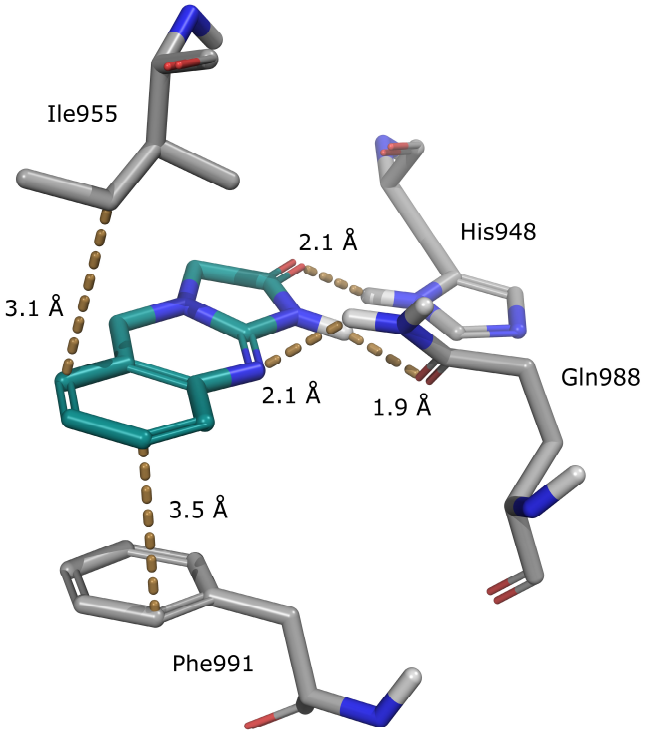

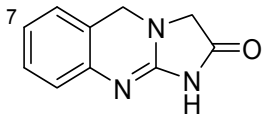

10

Figure 27 Key interactions between the IMQ scaffold (10**) and the PDE3B binding site.**

The compounds bearing small substitutions around the aromatic ring (**35**, **36**, **37**, **38**) all produced the same pose as shown for **10**, in which the 7-position, with or without an electronegative group, projects toward the two metal ions and their coordinated waters. However, these substituents do not project far enough to make a direct interaction with this region.

Analogues with extended side chains such as an ethyl-4-butanoate (**39**) or a butanoic acid (**41**) side chain all docked into PDE3B in the same manner as **35-38**. The carboxylic acid or ethyl ester group which

forms the terminus of these analogue's side chains were consistently positioned within the metal binding region where they formed hydrogen bonds with the metal bound waters. The docking solutions into PDE3A were the same.

The highly potent analogues **43** and **44** gave similar poses when docked into PDE3B (Figure 28) and PDE3A (not shown). In both compounds the carboxamide section of the side chain was drawn towards the metal binding region, leaving the attached non-polar groups positioned via hydrophobic interactions in the secondary binding region. The results gave no indication of the origins of the selectivity observed in **43** (13-fold for PDE3A) compared to **44** (non-selective).

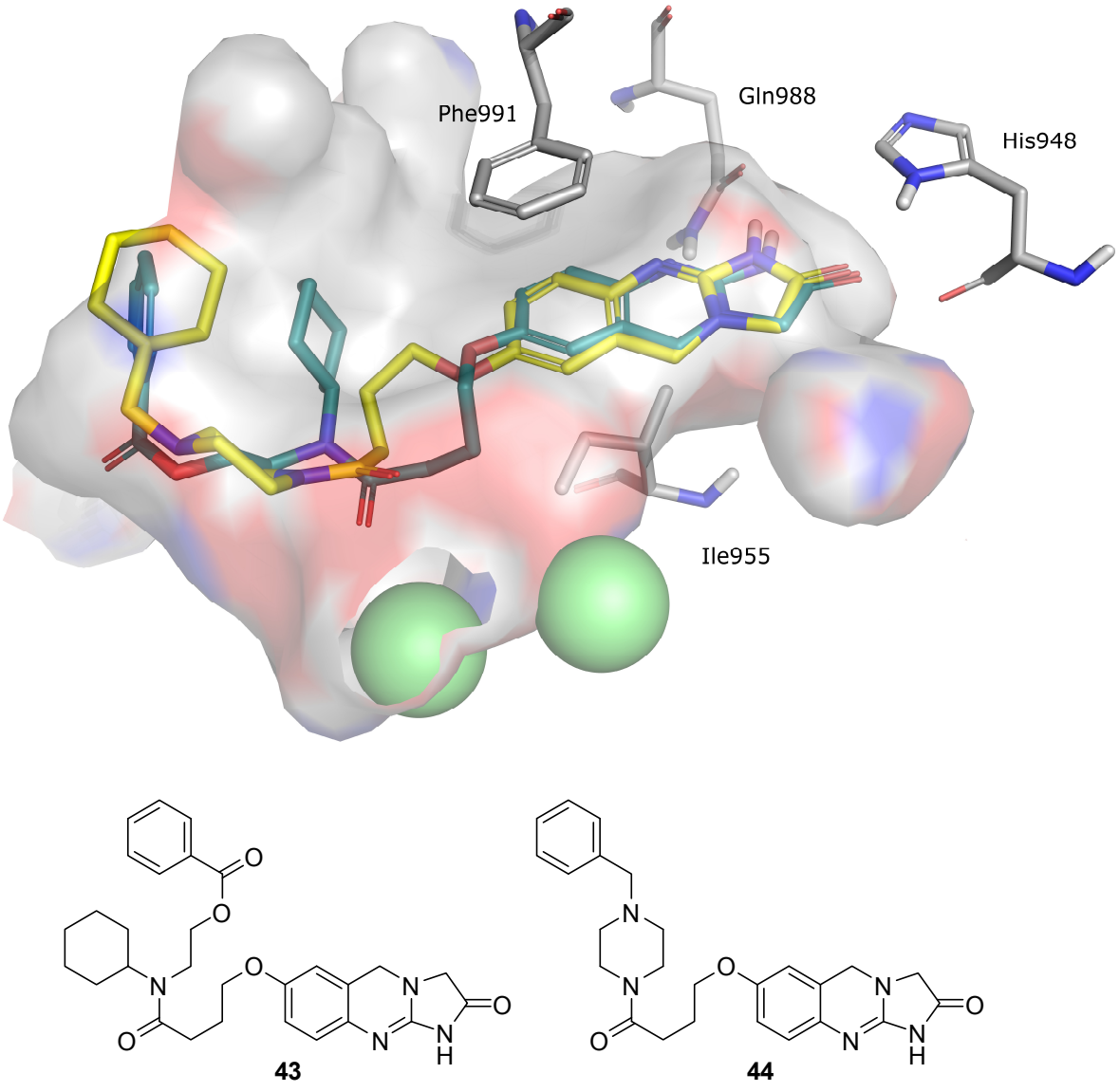

Figure 28 Overlay of 43 **(aqua), and** 44 **(yellow) in the PDE3B binding site.**

The chiral compounds **40** and **42** have lower affinity than their nor-methyl counterparts. They contain (R)-methyl groups on the lactam methylene, that are accommodated by a small hydrophobic recess within the core binding region, however these compounds exhibited a slightly different binding pose compared to their glycine-derived analogues (**39** and **41**) which may explain the lost affinity. The bulk and position of the methyl group also alters the position of the scaffold within the core binding region. While the change in position was small, this difference would likely have a significant cumulative effect across the entire scaffold. In the earlier studies of IMQs substituted at the lactam methylene Venuti et al found that a methyl group in either the R or S configuration could be tolerated, although the R configuration was favoured. R- or S-hydroxy-methyl substituents were also tolerated with a small loss in potency. Analogues with larger substituents for both the R and S configurations were reported to be at least a 100 fold less potent.[111]

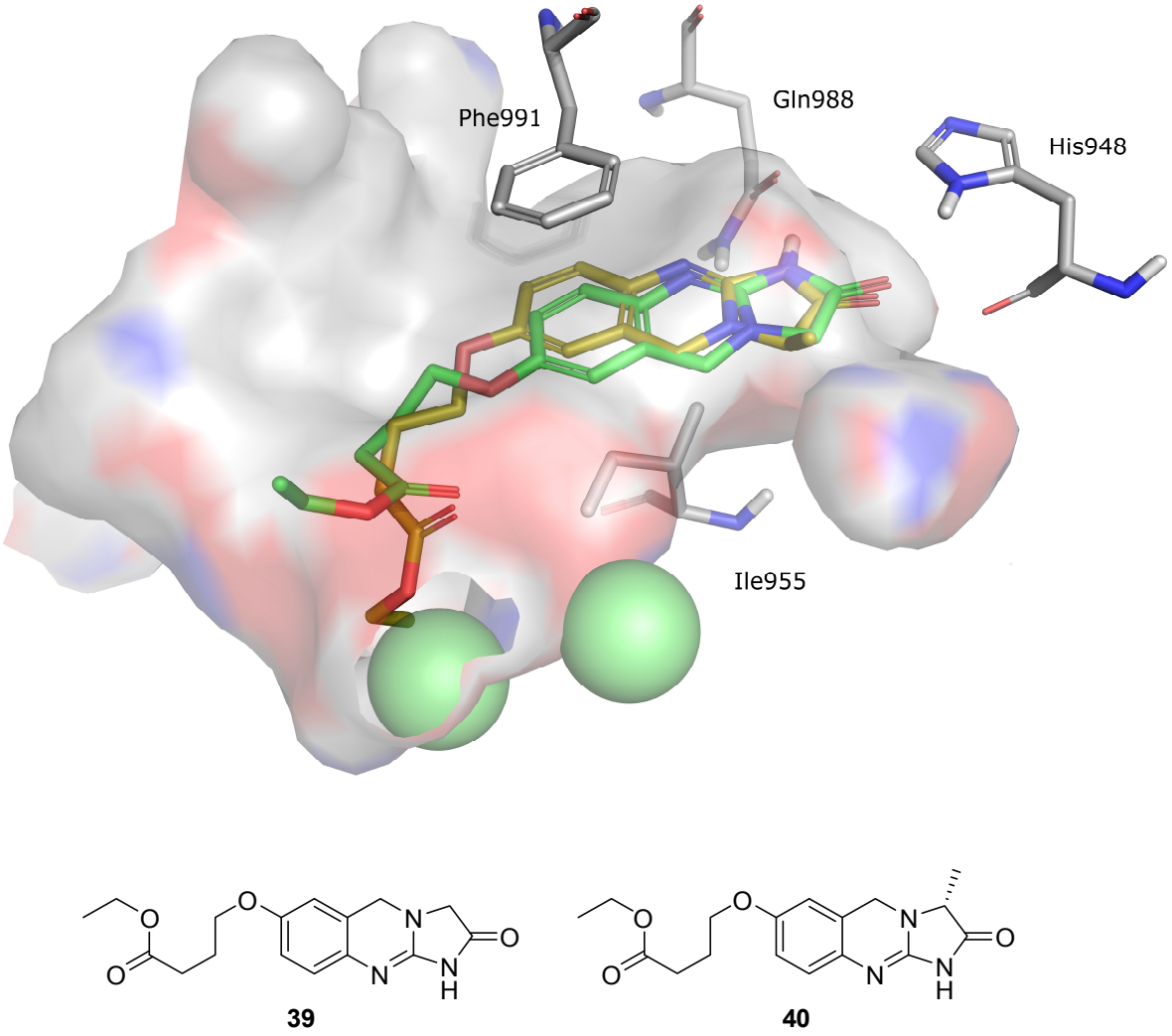

Figure 29 Variation in poses with (R)-methyl group (40 gold) and without (39 green) in the PDE3B binding site (surface)

It is clear from the accumulated activity and modeling data that the nature of the side chain has a major contribution to both the potency and selectivity observed, and this study revealed a number of elements that seem likely to drive binding affinity, such as core scaffold orientation, carbonyl derived interactions with metal associated water and a secondary hydrophobic binding site. However, even with all the available data there is little indication of what influences selectivity for either PDE3A or PDE3B. What had become apparent was that in these analogues, there were neither compounds with sufficient bulk and rigidity to exploit dynamic differences between the two isoforms to generate truly selective inhibitors. Nor was there a particularly broad survey of functional groups that might impart further isoform selective interactions. To develop a greater understanding of the source of isoform selectivity, analogues with a wide

variety of side chains must be produced in order to probe the binding site. The subject of the next phase of this docking study was to design a series of ligands that could explore this.

3.3 Design of Novel Imidazoquinazolinones to Probe PDE3A and PDE3B Binding Sites

Molecular docking studies offered only limited insight to explain why some compounds were more potent than others. Likewise, predictions of selectivity seemed to be largely beyond the scope of these models and docking regimes. It was considered that virtual screening could be used to survey potential new analogues of the IMQ class to identify which residues the ligands would interact with, particularly toward the proposed secondary binding region, where there appears to be some isoform specific interactions available.

To conduct this phase of the work, a strategy was adopted that included a consideration of synthetic parameters introduced in Chapter 2, and in this case the process was narrowed to a series of novel products including 7-amino-IMQ derivatives. Relatively few of these are described in the literature, possibly due to the fact that much of this research into IMQ's was performed before the development of one of the key amine forming reactions in organic synthesis, the palladium catalysed Buchwald-Hartwig amination of aryl halides.[157] As such our library would be largely composed of new chemical entities. To construct the library the ChemAxon program REACTOR,[158] a high performance virtual synthesis engine was implemented.

The virtual screen evaluated compounds for several potentially useful characteristics; particularly that the molecule extended toward the secondary binding site, and would be placed against the boundaries of the binding site, as a result of rigidity or conformational restriction. In order to find compounds that exploited the secondary binding pocket for selectivity, finding the right linker was be important. The desired linker would be amenable to derivatization and ideally would contribute some potency or selectivity itself, rather than functioning solely as a linker.

The screening protocol is summarized in Figure 30. The virtual library was constructed by creating model analogues where an available amine was attached to the IMQ scaffold at the 7-position. Any resultant analogues with a molecular weight above 500 were discarded.

It had been established that a more modular synthesis would be required to efficiently produce a wide variety of substituted IMQ analogues. It was also economical for us to begin with an in-house library of

precursor building blocks, but otherwise any available chemical with a primary or secondary amine was used to construct the virtual library.

The virtual library was screened in two ways. Firstly, compounds were selected if they gave significantly different binding modes and/or gScores between the PDE3A and PDE3B models. As described above, there was no validation of the gScores as a predictor of selectivity but the inability to adopt the same pose in PDE3A versus PDE3B was seen as a useful indicator.

Secondly, compounds were selected that showed different binding modes and/or gScores between the standard PDE3B model described above and an alternate model where Van der Waals radius scaling of the non-polar atoms had been increased. The adjustment of the Van der Waals radius scaling can be used as an approximation of the enzymes flexibility, particularly when looking at an encapsulated active site.[154] Ligands that were significantly affected by these small changes were considered as having potential to be sensitive to differences in the active site between PDE3A and PDE3B.

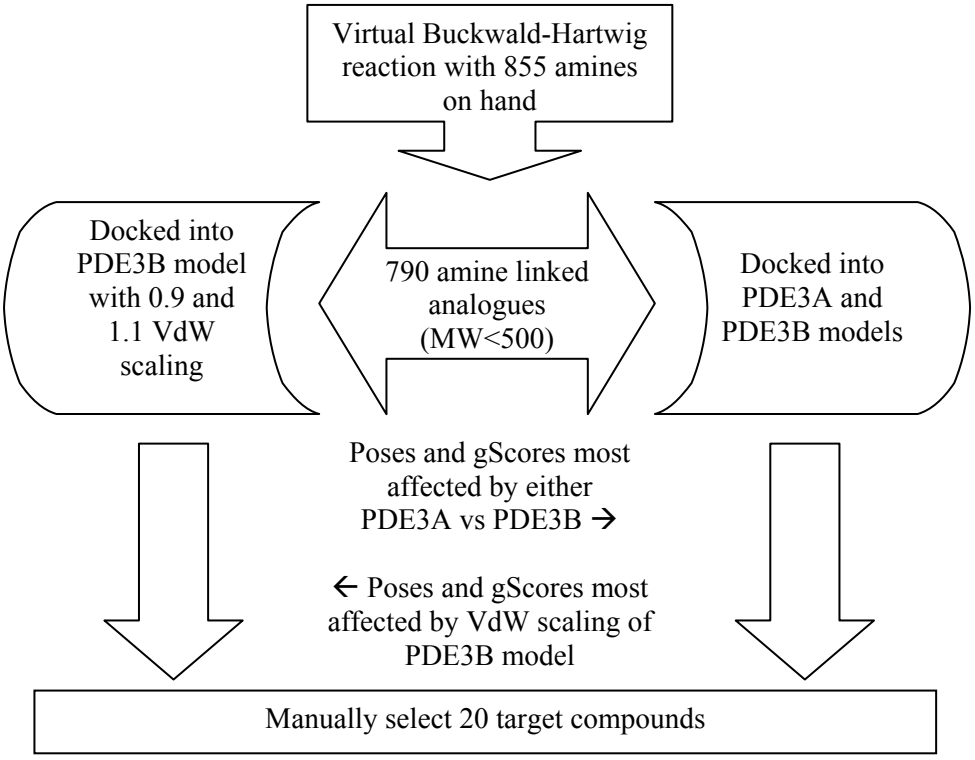

Figure 30 Virtual library synthesis and evaluation.

The ligands that were shortlisted by these two methods were then manually examined and a series of target compounds was selected. The Van der Waals scaling method more frequently gave differences in poses compared to the two isoform models, again this is because of the almost identical nature of the PDE3A and PDE3B models binding site.

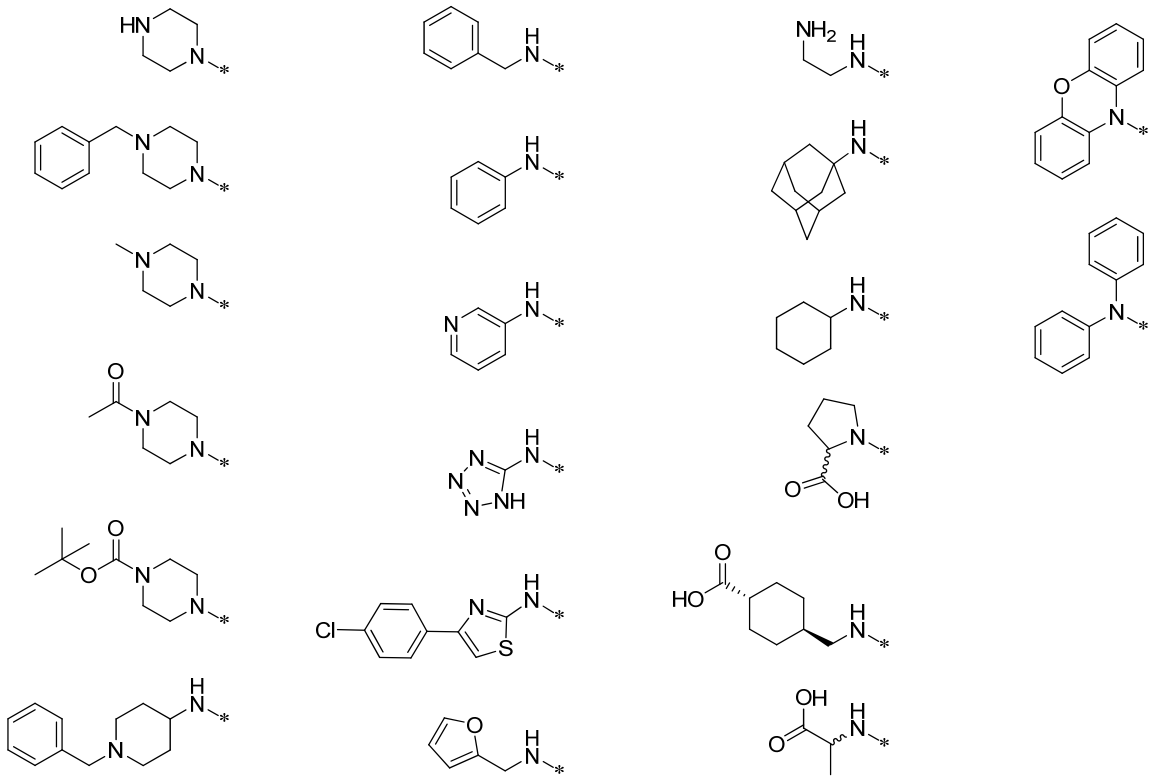

Figure 31 Target side chains chosen from virtual library.

Figure 31 shows an array of 20 amine linked side chains which were selected as synthetic targets from the virtual screen. Each of these analogues produced different binding modes in response to small changes in the binding site in at least one of the two regimes described above. In addition, each group was amenable to further elaboration, in a second generation library if required. The compounds that were selected included a number of substituted piperazines, a series of different aromatic rings with attached amines, and the remainder were a selection of conformationally diverse compounds.

As an example, in compound **66** the distal amine of the piperazine ring points toward the metal binding region and places the tertiary amine very close in space to a similar amine in the MERCK1 (**6**) crystal structure (Figure 32). The conformational restriction of piperazine was appealing as it dramatically

reduces the number of possible binding modes. Several derivatized piperazine rings were also chosen to evaluate what potential the piperazine ring had as a linker group.

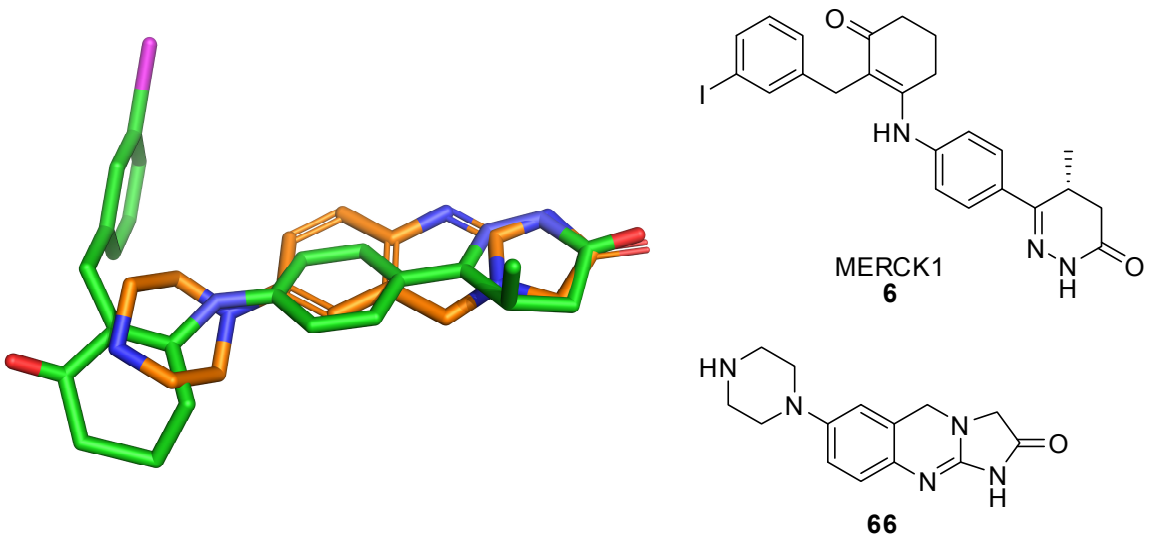

Figure 32 Overlay of 7-piperazine-IMQ and MERCK1.

When examining the predicted binding poses several aromatic substituents produced interesting results. In PDE3B, a benzylamino side chain extends toward the metal binding region of the binding site, and when the phenyl ring is replaced with a furan the same conformation is observed. In this pose the furan oxygen is positioned 2 Å from a metal bound water molecule, this would be advantageous over the benzyl group, however when the furanyl analogue is docked in PDE3A, the top pose places the furan ring in the opposite conformation pointing it toward the secondary binding pocket. The limited conformational space available to rigid substituents such as these suggested that they could be an effective way to probe the binding site.

Our earlier docking studies had suggested that reach to the outer parts of the binding pocket could be important for both potency and selectivity. We were looking for a scaffold that would allow access to different areas of the binding site, and those discussed above meet that requirement in different ways, those that didn't were examined no further. Ideally the scaffold would also contribute to binding affinity and or be itself inherently selective for either isoform. It was therefore necessary to synthesize and evaluate these analogues before further design could take place.

3.4 Conclusions

PDE3 inhibitors can possess a degree of isoform selectivity that is beyond the ability of structural biology to describe at present, and some aspects of ligand binding have not been accurately modelled in this docking study. One likely cause is the 44-amino acid loop region that is not included in the crystal structure, but has been implicated in ligand binding by mutagenesis studies. Modeling this loop would be a very computationally intensive process, and would not be likely to produce an accurate model. On the other hand, the docking study and in particular the detailed evaluation of the PDE3 binding site gave us a number of insights, and inspired ligand design in ways that would not have been accessible by traditional SAR approaches.

Chapter 4: Novel Imidazoquinazolinone PDE3 Inhibitors

A multitude of medicinal molecules with minute modifications can be manufactured by a mercurial modular methodology where a mishmash of moieties are merged with a master mold to maximize its morphological match for a macromolecular mark.

4.1 7-Aminoimidazoquinazolines

In the previous two Chapters, it has been shown that both the potency and isoform selectivity of IMQs are heavily influenced by the nature of the IMQ's side chain. In this Chapter, modern principles and techniques of design and synthesis were applied in order to discover novel IMQ analogues with improved potency against PDE3A or PDE3B. Despite the wealth of IMQ analogues synthesized through the 1980's, there are relatively few reported examples of IMQs with amine linked side chains. This may be because this period of intensive research pre-dated the development of facile cross-coupling reactions such as the Buchwald-Hartwig reaction. None of the reports included assessment of inhibition of PDE3A and PDE3B isoforms. Two different pathways were examined and compared. The first was analogous to that used in Chapter two and the majority of the IMQ literature; in which a derivatized precursor is prepared and then transformed into an IMQ over multiple steps. The second is a divergent synthetic route in which the completed IMQ scaffold is derivatized directly, yielding analogues in one step from a common intermediate. A series of novel and potent inhibitors of PDE3 isoforms were identified laying foundations for the pursuit of isoform selective inhibitors.

4.1.1 Reported Inhibitory Activity of 7-aminoIMQ Derivatives and Analogues

While 7-amino-IMQ (**71**) is described in the earliest IMQ patent (Beverung et al[124]) it was found to be significantly less active than the unsubstituted compound (**10**). On the other hand, Ishikawa et al[113] found that 7-dimethylamino or 6 membered heterocycles attached via an amine to the 7 position of IMQs (**67**) were only slightly (2 – 6 fold) less active than anagrelide (**2**). Moreover it was found that these substituents improved solubility. The 7-methylamino and 7-benzyl(methyl)amino analogues were much less active against PDE3A (30 – 32 fold less than anagrelide).[113, 159] IMQs with a fused ring which was attached to the 6- or 7- positions through an amino group (**68**) maintained their potency. Furthermore, the amino group

increased the potency when measured ex vivo after oral administration, which suggests improved oral bioavailability.[113, 114] In their study of the analogous imidazoquinolinone series, Meanwell et al included a range of N-linked aliphatic heterocycles (**69**), which generally led to a decrease in activity at PDE3A. A series of substituted 7-piperazinylimidazoquinolones were described and it was found that the inhibitory potency increased with larger N-substituents.

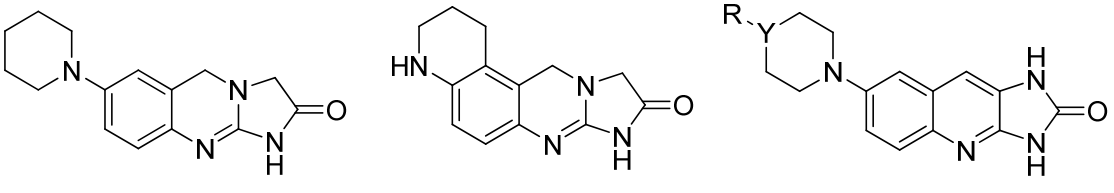

Figure 33 Examples of IMQs with amine linked side chains.

These literature reports indicated that there was a complex SAR around these amine linked analogues, which had only been touched upon lightly. There was an opportunity here to create novel ligands while exploring the SAR of both PDE3A and PDE3B.

4.1.2 Reported Synthetic Approaches

Beverung showed (Scheme 12) that treating IMQ (**10**) with 5% nitric acid in sulfuric acid yielded a 7-nitro-IMQ analogue (**70**) and that subsequent palladium catalyzed hydrogenation reduced the 7-nitro group (**70**) to 7-amino-IMQ (**71**). Further derivatization of this amino group was not reported, perhaps impeded by synthetic complications due to competing reactivity at other positions in the tricyclic core.

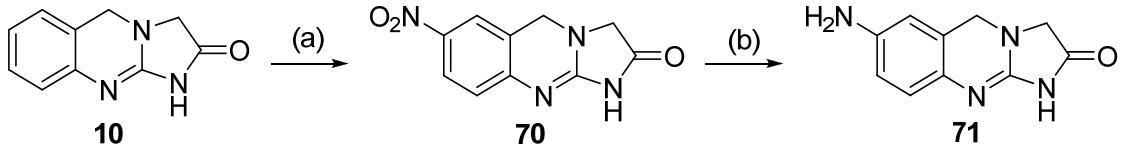

Scheme 12 Reported synthesis of 7-amino-IMQ (71).[112] Reagents and conditions: (a) HNO_3, H_2SO_4, ACN, 0 °C → RT, 3 h (b) Pd-C, H_2, HCl, EtOH, RT.

Ishikawa et al[113] developed and utilized a different synthetic scheme for preparing amino substituted IMQs (Scheme 13) based upon the elaboration of an amino substituted 2,4-dichloroquinazoline precursor as

described in Chapter 2 (Scheme 5). This method began by preparing a substituted 2-nitrobenzonitrile (**72**) by displacing a halogen with the desired alkyl amine (**73**). The nitro group is then reduced to a primary amine, and reacted with urea to give quinazoline-2,4-diones (**74**). Treatment with phosphoryl chloride gives 2,4-dichloroquinazoline (**75**), which is converted to the IMQ (**76**). However, several of the reported examples were not amenable to this synthetic strategy and were instead produced from a suitably substituted nitrobenzaldehyde as was used by Beverung et al, suggesting that Ishikawa et al's method is less robust.

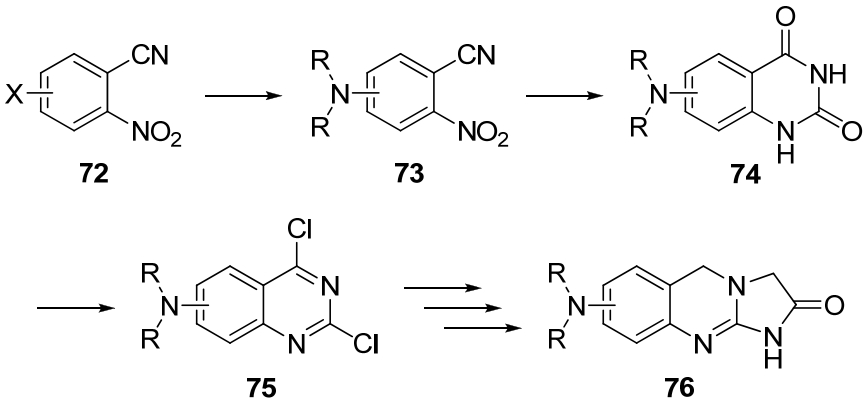

Scheme 13 Alternate synthesis of IMQs with amine linked side chains.[113]

Beyond the nitration reaction described in Scheme 12, there are only two reports concerning substitution onto a completed IMQ ring system (Scheme 14). Venuti et al reported that the reaction of 7-iodo-IMQ (**77**) with imidazole (**78**) would not proceed to **15**.[129] On the other hand, a C-C cross-coupling was successfully used to replace the iodo group of **77** with a pyridine ring to give **80**. That reaction used a zinc-chloride activated pyridine (**79**) and a palladium (0) triphenylphosphine catalyst complex facilitated the coupling.[160] This suggests that substituting directly onto a complete IMQ scaffold is possible, but not trivial. In the time since these attempts were reported a variety of reactions conditions have been discovered which may be better able to affect this transformation.

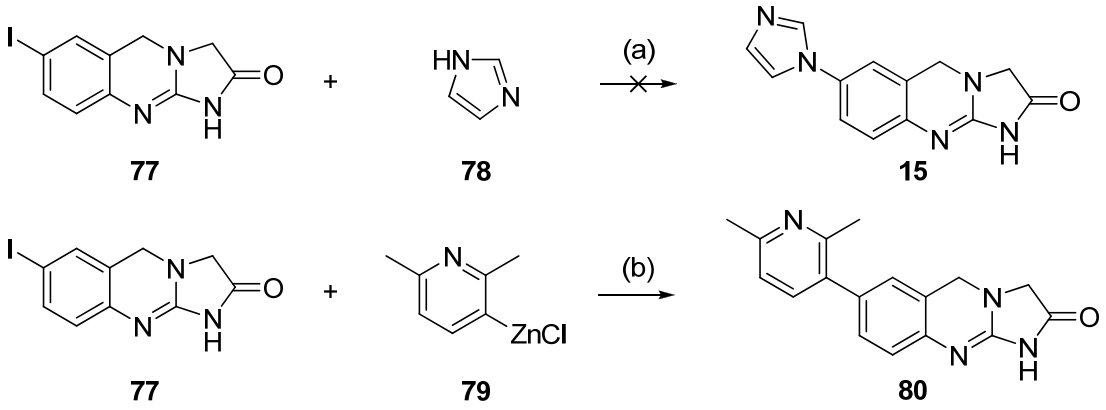

Scheme 14 Reported attempts to attach a side chain to a completed IMQ.[129] Reagents and conditions: (a) K_2CO_3, DMF (b) $Pd(PPh_3)_4$, THF.

4.2 Results and discussion

The literature reports described above, together with the results described in Chapters 2 and 3 led to the identification of an opportunity to generate new 7-aminoIMQ derivatives of significant potential as PDE3 inhibitors. While it was believed that adaptation of the synthetic route used in Chapter 2 was feasible, the syntheses of IMQ analogues have been hampered by the inability to introduce substituents to the scaffold as late as possible. The area of metal mediated cross coupling reactions has moved forward considerably since the majority of the work in this area was described and it was believed that success would constitute a significant step forward. Successful application of the Buchwald-Hartwig coupling reactions to substrates such as the 7-chloro- (**35**) or 7-bromo- (**36**) IMQ analogues described in Chapter 2 could achieve this. The relatively few reports of amine substituted IMQs means gaining rapid access to an almost completely novel chemical space.

4.2.1 Linear Synthesis of 7-piperazinyl-IMQ

In the first instance, the general approach detailed in Chapter two was used for the synthesis of 7-piperazinyl-IMQ (**66**) and is summarized in Scheme 15. The pivotal step was the introduction of the Boc-protected piperazine in the 2-nitrobenzaldehyde precursor (**84**).

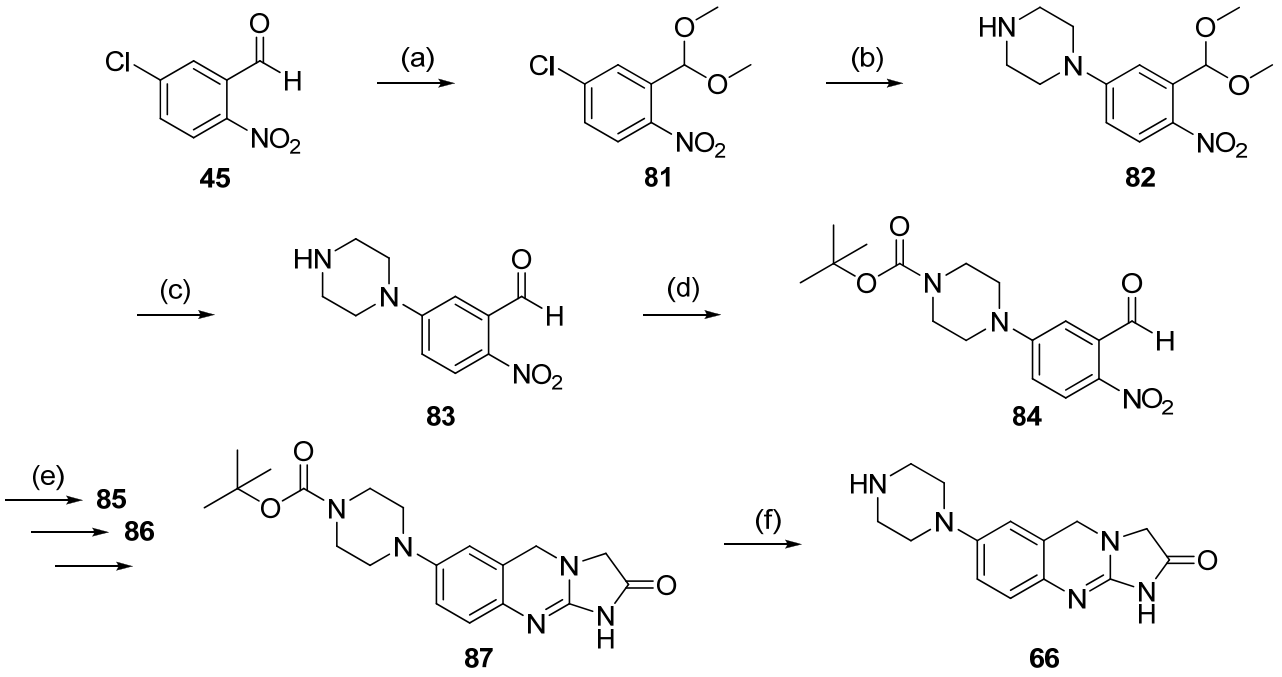

Scheme 15 Linear synthesis of 7-piperazinyl-IMQ. Reagents and conditions: (a) pTSA, MeOH, reflux, 18 h (b) piperazine, KI, DMF, 80 °C, 21 h (c) HCl, iPrOH, reflux, 2 h (d) Boc_2O, $NaHCO_3$, THF, H_2O, RT, 5 h (e - I) GlyOEt, $NaCNBH_3$, EtOH, RT, 4 h (e - II) 10% Pd-C, H_2, EtOH, RT, 16 h (e - III) CNBr, EtOH, RT, 16 h (e - IV) conc. NH_4OH, EtOH, RT, 1 h (f) TFA, RT, 16 h.

First, 5-chloro-2-nitrobenzaldehyde (**45**) was protected as its dimethyl acetal (**81**) by treatment with p-toluenesulfonic acid in methanol. The protected intermediate was obtained in 90% yield. The ^{1}H-NMR spectrum possessed a singlet at 3.4 ppm corresponding to the methyl ether protons and another singlet at 5.9 ppm for the methine proton.

The chloro group was then displaced by treatment with piperazine to give **82** in 32% yield. The ^{1}H-NMR spectrum showed two multiplets at 3.4 and 3.0 ppm corresponding to the piperazine methylene protons.

The aldehyde function was regenerated by refluxing (**82**) with HCl in isopropanol giving compound **83** in 91% yield with a corresponding aldehyde peak at 10.5 ppm. Lest it become alkylated in the subsequent reductive amination, the secondary amine of the piperazine was protected as the *tert*-butylcarbamate (**84**), obtained in 87% yield. The *tert*-butyl singlet appeared at the expected 1.5 ppm, mass spectrometry of this intermediate gave an M+15 base peak which was attributed to in-source aldolization reaction as reported by Wang et al.[161]

The construction of the core IMQ tricycle (**87**) was completed in three steps as with analogues described in Chapter 2; the reductive amination (**85**, 98%) and catalytic hydrogenation (**86**, 95%) went extremely efficiently, however the cyclization yielded only 10% of the desired **87**. The reduced yield of the cyclization step may have been due to an increase in solubility limiting the extent of precipitation; however an attempt to purify additional material from the mother liquor was unsuccessful.

Finally the amine was revealed by treatment with TFA in 42% yield of the desired compound (**66**). The resultant 25 mg of **66** showed the expected spectroscopic signals and was identical to the sample prepared by an independent method described later (Section 4.3.4).

That poor overall yield obtained from 3 g of starting 5-chloro-2-nitrobenzaldehyde (**45**) prevented the planned derivatization via amide coupling reactions. This process was laborious, requiring 8 steps to reach one analogue with poor yields. These results drove the need for a coupling reaction which would be a more efficient way to produce analogues.

4.3.2 Cross-Coupling Reactions of 7-bromo-IMQ

Two of the most widely used cross coupling reactions used in organic synthesis are the Suzuki reaction which generates aryl-aryl linkages and the Buchwald-Hartwig reaction in which an aryl halide is displaced by an amine. The reactions have in common the establishment of a catalytic cycle in which a transition metal, typically palladium undergoes three steps which can be generalized as follows: ***Oxidative addition***: whereby the palladium ligand complex inserts itself between the halogen and the aryl ring. ***Transmetalation***: involves the halogen being replaced by the coupling partner, typically a boronic acid in the Suzuki reaction or an amine in the Buchwald-Hartwig. A base is usually involved in this step to deprotonate the substrates and neutralize the generated halogen. ***Reductive elimination***: in which the palladium ligand complex is extricated from the coupling partners, regenerating the active catalytic species and leaving the two substrates coupled together.

In the first instance in this work, both reactions were attempted under what might be considered standard conditions, to ascertain the utility of cross-coupling reactions more generally to this project. Initially, 7-bromo-IMQ (**36**) was treated with phenyl boronic acid using a variety of Suzuki coupling conditions and the 7-phenyl-IMQ (**88**) was ultimately obtained albeit in poor yield. While a poor yield, it

provided the first indication of successful formation of the intermediate metal complex, required for both Suzuki and Buchwald additions. In further studies, it was found that the choice of base was important, with caesium carbonate giving improved yields over potassium carbonate or potassium t-butoxide; and that microwave heating was superior to the use of an oil bath. Crucial to the success of this reaction was the addition of a small amount of water without which the reaction would not proceed at all. Finally it was also noted that a large excess of phenyl boronic acid also improved the reaction outcome. In the last attempt, the product (**88**) was isolated in low yield (10%) however there is scope for further optimization of this reaction.

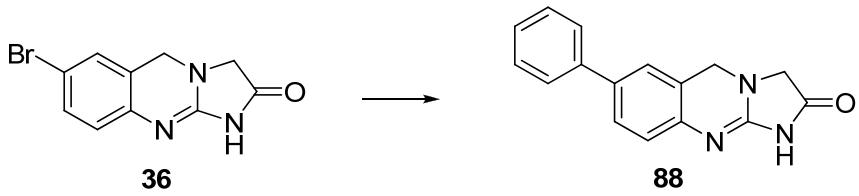

36 **88**

Scheme 16 Synthesis of 7-phenylIMQ. Reagents and Conditions: See Table 4.

Trial No.	Temperature	Time	Equiv. of boronic acid	% Water in DMF	Base	Catalyst (mol%)	Detected Product
1	Oil bath 80 °C	16 h	2.2	-	K_2CO_3 3 equiv.	$Pd(PPh_3)_4$ 2%	None
2	Microwave 100 °C	15 min	1.2	-	Cs_2CO_3 8 equiv.	$Pd(OAc)_2$ 18%	None
3	Microwave 100 °C	15 min	1.2	-	Cs_2CO_3 8 equiv.	$Pd(PPh_3)_4$ 3%	None
4	Microwave 140 °C	20 min	1.2	1%	Cs_2CO_3 8 equiv.	$Pd(OAc)_2$ 18%	Traces
5	Microwave 140 °C	20 min	4.5	-	Cs_2CO_3 16 equiv.	$Pd(OAc)_2$ 53%	None
6	Oil bath 80 °C	16 h	1.2	-	Cs_2CO_3 9 equiv.	$Pd(OAc)_2$ 18%	None
7	Microwave 140 °C	20 min	1.5	20%	tBuOK 35 equiv.	$Pd(OAc)_2$ 18%	None
8	Microwave 140 °C	20 min	4.8	20%	Cs_2CO_3 7 equiv.	$Pd(OAc)_2$ 18%	Significant
9	Microwave 140 °C	1 h	1.5	20%	Cs_2CO_3 6 equiv.	$Pd(OAc)_2$ 18%	Traces
10	Microwave 140 °C	20 min	5	20%	Cs_2CO_3 5 equiv.	$Pd(OAc)_2$ 12%	Significant (10% isolated)

Table 4 Optimization of Suzuki coupling conditions

The first attempt at the Buchwald-Hartwig reaction (Scheme 17) involved coupling aniline with the 7-bromo-IMQ (**36**). As above, trial and error was required to find successful conditions but it was found that the reaction would proceed to give **89** in moderate yield. The use of *t*-butanol as solvent seemed a pivotal

variation to the conditions. The coupling of aniline is generally recognized as one the most facile examples of a Buchwald- Hartwig reaction. Our synthetic objectives also called for the coupling of a variety of primary and secondary aliphatic amines, which are accepted to be more challenging coupling partners.

In summary, at this point there was sufficient evidence that if optimized the Buchwald-Hartwig method would be successful to justify pursuing a study of conditions that would yield useful amounts of a range of analogues. That study follows here.

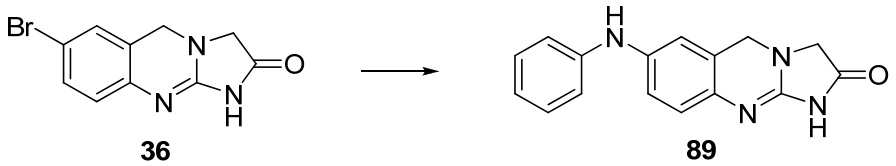

36 **89**

Scheme 17 Synthesis of 7-aminophenylIMQ via the Buchwald-Hartwig reaction. Reagents and conditions: See Table 5.

Temp / Time	Amine	Base	Palladium	Ligand	Solvent	Result
Oil Bath, 130 °C Overnight	Aniline	Cs_2CO_3	$Pd(OAc)_2$	BINAP	Toluene	Predominantly 7-bromo-IMQ starting material
Microwave 140 °C 20 mins	Aniline	Cs_2CO_3	$Pd(OAc)_2$	BINAP	DMF	Predominantly dehalogenated IMQ
Oil bath 90 °C Overnight	Aniline	tBuOK	$Pd(OAc)_2$	BINAP	tBuOH	Detected significant amount of product

Table 5 Initial evaluation of Buchwald-Hartwig reaction conditions.

4.3.3 Detailed Examination of Buchwald-Hartwig Conditions

The Buchwald-Hartwig reaction has been reported on many occasions for the substitution of an aryl halogen with a wide variety of amines. However optimizing this reaction can be difficult because it is governed by a number of inter-dependent variables. For example, the nature of the substrate will influence the suitability of the base, which may affect the choice of solvent, which in turn may affect the choice of

catalyst. To facilitate the synthesis of a focused library of amino substituted IMQs a reaction optimization regime focused on finding a set of conditions that would successfully and reliably couple a variety of amines. This process was informed by a number of recent publications on the subject.[162, 163]

The substrate: Firstly, the choice of 7-bromo-IMQ (**36**) was retained as the starting substrate. Although the Buchwald-Hartwig reaction can be used on a variety of halogens, the original discoveries used bromine substituents, and this is still the most compatible option. Thus 7-bromo-IMQ (**36**) became the focus of this investigation, and the first variable of the Buchwald-Hartwig reaction that was decided upon. 7-chloro-IMQ (**35**) was also available, but did not appear to offer a significant advantage. The 7-trifluoromethylsulfonyl-IMQ could not be prepared directly from the corresponding phenol (**38**).

The solvent: The most commonly reported solvents for the Buchwald-Hartwig reaction are dioxane and toluene, however 7-bromo-IMQ (**36**) was found to be insoluble in both of these. THF did not significantly improve solubility. DMF was a better solvent, but dramatically increased the rate of aryl halide reduction under the reaction conditions. *t*-Butanol was found to dissolve 7-bromo-IMQ (**36**), if a strong base was present.

Heating: Microwave heating offered no significant advantage over a conventional oil bath. However a sealed microwave vessel in conjunction with conventional heating was used as it allowed for long reaction times at elevated temperatures and pressures.

The base: The base with the greatest activity in Buchwald-Hartwig reactions is generally recognised to be sodium t-butoxide. Potassium t-butoxide is similarly effective and was used in several cases without detrimental effects. The main limitation in using these bases is their unfavourable side reactions with some functional groups. However our IMQ scaffold was not disrupted by the use of such a strong base, and no base sensitive coupling partners were incorporated. LHMDS was also trialled as it is reported to improve the reaction where protic functional groups such as phenols and amides are present, but without success.[162]

The catalyst complex: In order for the catalytic cycle to begin, a mono ligated palladium (0) complex is required. Three different types of palladium source are commonly used to prepare the catalyst complex. The most readily available is $Pd(OAc)_2$, however this must first be reduced to Pd(0) in order for it to form the catalytically active complex. This reduction can be achieved very simply if the amine coupling partner contains hydrogen atoms α to the nitrogen, which can undergo beta hydride elimination to reduce the

palladium. However when an aniline, which cannot reduce the palladium is to be coupled another reductant must be introduced. Other reported reductants include triethylamine and phenylboronic acid. A neater method is to use extra phosphine ligand to reduce the palladium. The introduction of water into the reaction expedites the reduction.[164]

Another commonly used palladium source is the air-stable Tris(dibenzylideneacetone)dipalladium(0) ($Pd_2(dba)_3$), this is more convenient as it doesn't require a reductant. However there is a slight disadvantage in that the dibenzylideneacetone (dba) can compete with the phosphine ligand for the palladium, which reduces the amount available to form the active catalyst complex.[165]

Recently several stable pre-catalysts have become commercially available. These pre-catalysts are composed of the active catalyst complex, trapped midway through the intramolecular cyclization of indoline. In the presence of a base, the cyclization is completed releasing indoline and the active catalyst complex as outlined in Scheme 18. Since the catalytic loading in these reactions is typically very low, only a very small amount of indoline is produced, which can be removed during the reaction work-up and purification.[166]

In this work we used all three palladium sources, and found $Pd_2(dba)_3$ to be the most useful. $Pd(OAc)_2$ was successfully used in some of the reactions reported here, however it was found to be inconsistent, and it was difficult to determine if and when the active catalytic species had formed. $Pd_2(dba)_3$ on the other hand was much more reliable. The pre-catalyst complex in Scheme 18 was used to prepare one analogue (**109**), however the ligand which we had found to be most useful was not available in this form.

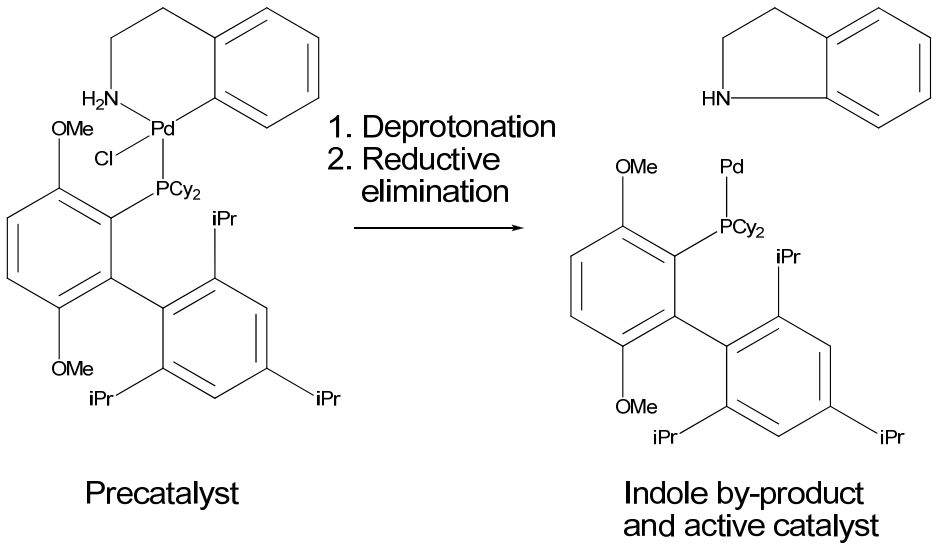

Scheme 18 Formation of an active catalyst complex from an air stable pre-catalyst.

The Ligand: Another variable with particularly a significant impact on the reaction outcome is the choice of ligand. This is particularly difficult to optimize as there are several aspects to each ligand that contribute to its applicability. Recent literature recommends that BrettPhos (**90**) and RuPhos (**91**) are the best ligands for coupling primary and secondary amines respectively.[162] However in this work it was found that the lesser known 1,1'-binaphthyl-2-yldi-*tert*-butylphosphine (TrixiePhos, **92**) was better able to couple both primary and secondary amines than either RuPhos (**91**) or BrettPhos (**90**). This could be due to the fact that TrixiePhos (**92**) possessed a di-*tert*-butyl substituted phosphine, whilst only the standard Di-cyclohexyl versions of RuPhos (**91**) and BrettPhos (**90**) were trialled. These bulky groups are important for facilitating the reductive elimination and oxidative addition steps of the catalytic cycle. It has also been reported that TrixiePhos (**92**) suppresses beta hydride elimination, which had been a problem in earlier trials.[167]

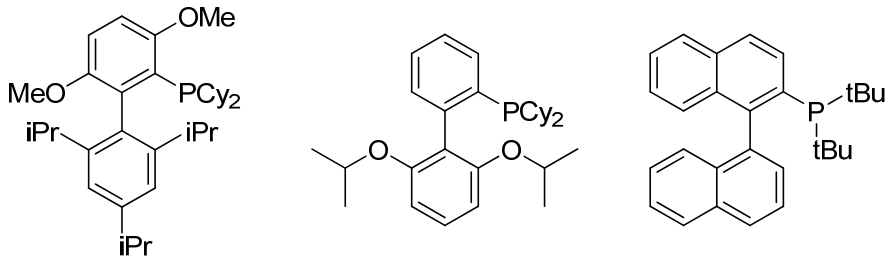

BrettPhos **90** RuPhos **91** TrixiePhos **92**

Figure 34 Buchwald-Hartwig reaction catalytic ligands.

The amine: We examined a variety of different amines in order to determine what could be coupled, as well as what effect different steric bulk, and electronic properties would have on the reaction yield. Ultimately, despite optimizing the other reaction conditions for a general procedure the most significant determinant on the yield was the type of amine being coupled. Primary and secondary aliphatic amines gave low yields or did not proceed at all. Anilines were coupled quite reliably and occasionally in good yields.

4.3.4 Optimization of Buchwald-Hartwig Conditions

The longer synthesis of 7-piperazine-IMQ (**66**) in Scheme 15 was found to be inefficient, it had been hoped that the Buchwald-Hartwig reaction would offer improved access to such compounds. As such the coupling of 7-bromo-IMQ (**36**) and piperazine was undertaken to determine the viability of this approach. It was found that the successful synthesis was dependent upon the use of TrixiePhos (**92**) as the ligand. Two

frequently used ligands, BINAP, and tris(o-tolyl)phosphine gave no product. The yield was improved by the use of potassium t-butoxide compared to caesium carbonate and it was also found that in this case the addition of water was detrimental to the reaction. While the yield was just 8%, the advantage of this route to multiple analogues from a common precursor was clearly apparent (Scheme 19).

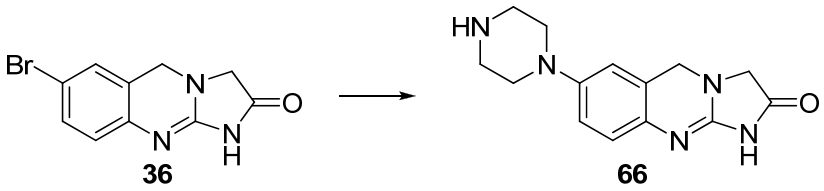

Scheme 19 Synthesis of 7-piperazineIMQ via the Buchwald Hartwig reaction. Reagents and conditions: See Table 6.

		Base / Solvent		
		Cs_2CO_3 / tBuOH	Cs_2CO_3 / tBuOH / H_2O	tBuOK / tBuOH
Ligand	BINAP	None	None	None
	$Pd(P(o\text{-}Tolyl)_3)_2$	None	None	None
	2-(di-t-butylphosphino)-1,1'-binaphthyl	0.6%	None	8%

Table 6 Yields from preliminary optimization of Buchwald-Hartwig reaction in the synthesis of 7-piperazine-IMQ. Conditions: $Pd_2(OAc)_2$, 110 °C (oil bath), 16 h.

While these conditions were adequate for the synthesis of a number of target analogues (Chapter 6, General Method E) further optimization was under taken during the synthesis of other targets. These trials led to the development of a more reliable set of conditions (General Method F). Some examples of those trials are given here.

First, in the synthesis of **93** (Scheme 20) the use of palladium acetate, which is soluble in *t*-butanol, with TrixiePhos (**92**) as ligand enabled modest success. While the use of $Pd_2(dba)_3$ using toluene failed as the 7-bromo-IMQ (**36**) was insoluble. It was later found that premixing the $Pd_2(dba)_3$ and ligand in toluene and the other reactants in t-butanol countered the solubility issues and the reaction became somewhat more reliable.[168]

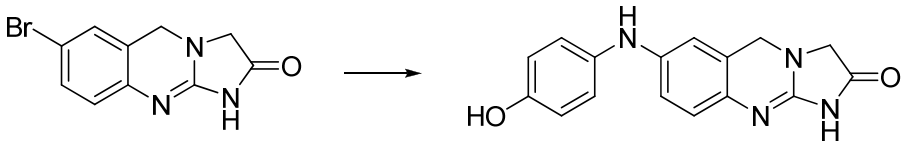

36 **93**

Scheme 20 Synthesis of 7-(4-hydroxyphenylamino)-IMQ via the Buchwald-Hartwig reaction. Reagents and conditions: See Table 7.

Temp / Time	Amine	Base	Palladium	Ligand	Solvent	Result
Oil bath, 110 °C Overnight	4-aminophenol	tBuONa	$Pd_2(dba)_3$	TrixiePhos	Toluene	None
Oil bath, 110 °C Overnight	4-aminophenol	tBuOK	$Pd(OAc)_2$	TrixiePhos	tBuOH	7% isolated

Table 7 Optimization of Buchwald-Hartwig reaction in the synthesis of 7-(4-hydroxyphenylamino)-IMQ.

TrixiePhos was also shown to be the most reliable ligand in the synthesis of **94**, giving a 15% isolated yield, clearly superior to RuPhos (**91**) and BrettPhos (**90**) (see Table 7).[162] Two attempts using the BrettPhos precatalyst (Scheme 18), in conjunction with the RuPhos ligand (**91**), which was reported to have a particularly broad substrate scope, also failed (Scheme 21).[163]

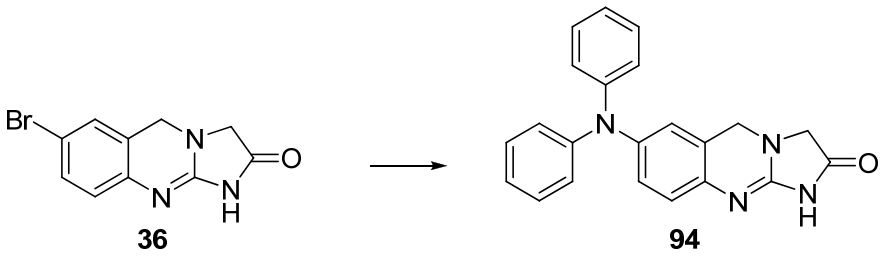

Scheme 21 Synthesis of 7-(diphenylamino)-IMQ via the Buchwald-Hartwig reaction. Reagents and conditions: See Table 8.

Temp / Time	Amine	Base	Palladium	Ligand	Solvent	Result
Oil bath 110 °C Overnight	diphenylamine	tBuONa	$Pd_2(dba)_3$	TrixiePhos	3 tBuOH : 1 Toluene	Significant 15% isolated
Oil bath, 110 °C 27 h	diphenylamine	tBuONa	$Pd_2(dba)_3$	RuPhos	6 tBuOH : 1 Toluene	Traces of product by LCMS
Oil bath, 70 °C 45 h	diphenylamine	LiHMDS	$Pd_2(dba)_3$	RuPhos	6 THF : 1 Toluene	None
Oil bath 110 °C Overnight	diphenylamine	Cs2CO3	BrettPhos precat	+ RuPhos	tBuOH	None
Oil bath 100 °C Overnight	diphenylamine	tBuONa	BrettPhos precat	+ RuPhos	THF	None

Table 8 Buchwald-Hartwig reaction conditions trialled in the synthesis of 7-(diphenylamino)-IMQ (94).

4.3.5 7-aminosubstituted-IMQ Analogues

Over two rounds of ligand design and synthesis 18 Buchwald-Hartwig derived amine linked analogues were produced. The Buchwald-Hartwig reactions used two sets of conditions, the first (General Method E) used palladium acetate and TrixiePhos in t-Butanol for the catalyst solution with potassium t-butoxide and t-butanol as the base and bulk solvent; the second set (General Method F) used $Pd_2(dba)_3$ and TrixiePhos in toluene for the catalyst solution with sodium t-butoxide and t-butanol as the base and bulk

solvent. Reactions were heated to 110°C in a sealed vessel for 16 hours. 7-(4-cyanophenyl)-amino-IMQ (**109**) was synthesized using a pre-catalyst complex, which was more convenient as there was no preparation of the catalyst complex required but considerably less economical and was limited in substrate scope.

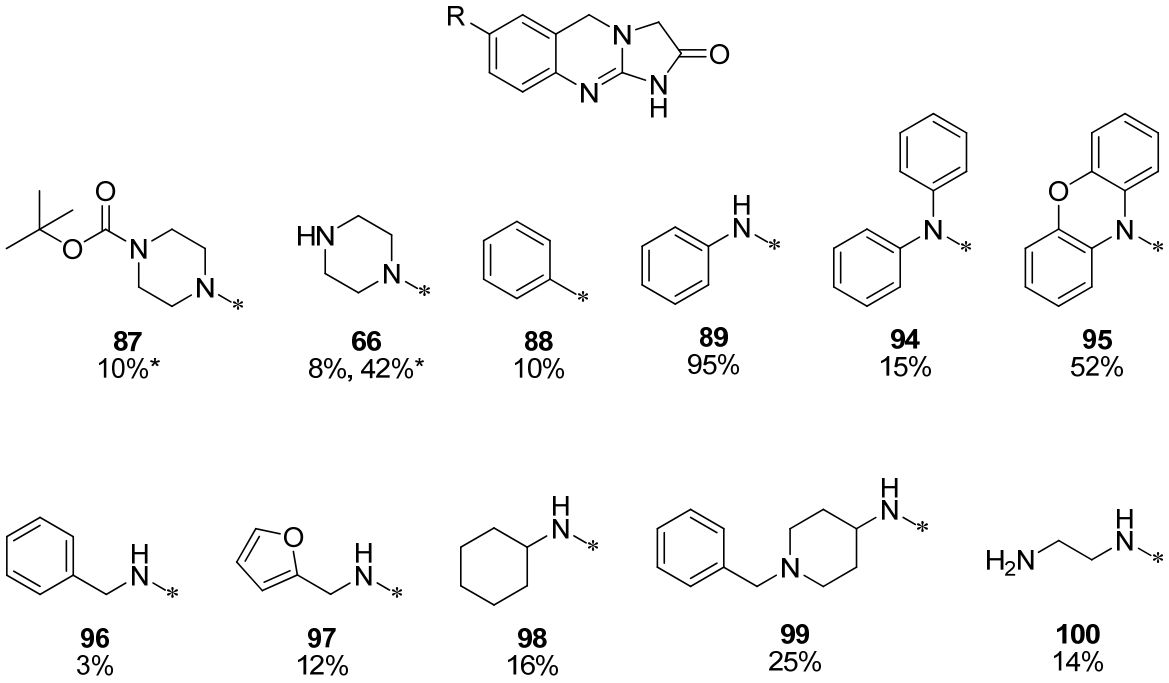

Scheme 22 Synthesized IMQs with a variety of amino linked side chains. *yields from linear synthesis.

Of those that were successfully coupled and assayed, the aniline analogue (**89**) was obtained with the highest yield; fortuitously this analogue was also the most active of the targeted compounds. In light of this, a series of analogues was produced by coupling substituted anilines to the IMQ core.

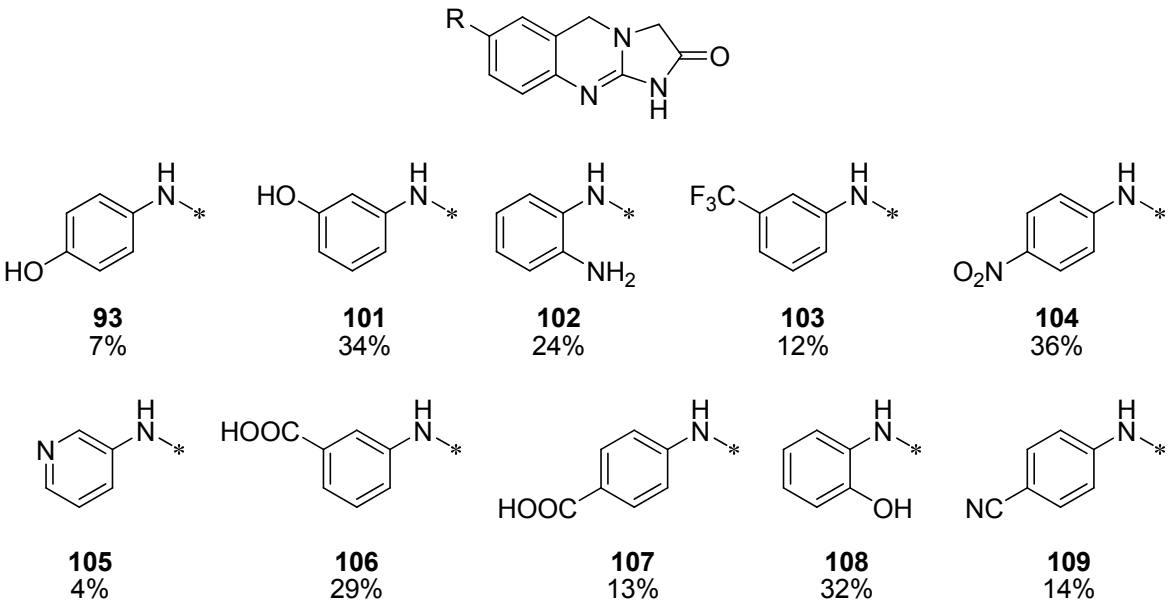

Scheme 23 Synthesized IMQs with substituted phenylamino side chains.

A contributing factor to these generally low yields was the difficulty encountered when isolating the desired compound, once the reaction mixture was neutralized the product would precipitate out along with other impurities (particularly starting material and the dehalogenated by-product). Chromatographic purification of the target compound was hampered by; their low solubility which required high loading volumes, their poor mobility through normal phase media, and in many cases poor resolution. In the unsubstituted aniline example (**89**) the reaction went almost to completion, eliminating these difficulties, unfortunately this approach could not be applied to other analogues. Two analogues, **96** and **105** were isolated in such low yield, that characterization by ^{13}C-NMR was not possible; resynthesis and characterization were considered contingent upon their level of inhibitory activity. Compounds **93**, **98** and **99** gave strong parent adducts in HPLC-ESI-single quadrupole MS, but a high resolution ion could not be obtained in ESI-TOF of the same sample.

Compounds were characterized by ^{1}H-NMR, ^{13}C-NMR and high resolution mass spectrometry. ^{13}C signals were predominantly obtained through HSQC and HMBC experiments. The combination of these techniques allowed for more sensitive signal detection and most of the unique carbon signals were detected for each analogue, despite their limited solubility.

The ^{1}H-NMR spectrum of 7-phenylamino-IMQ (**89**) was assigned as shown in Figure 35. As expected the aromatic signals of the IMQ core show strong ^{3}J coupling between 8-H and 9-H , and in this

and many other analogues there is some ^{4}J coupling between 6-H and 8-H. In this example the signals of 6-H and 9-H are superimposed to form multiplet D, while 8-H is represented by the double of doublets making up the right hand side of multiplet C. The secondary amine is seen further upfield than might have been expected, as a singlet at 8.07 ppm. The signals of the IMQ methylenes appear as expected, as do those of the phenyl ring although they did not exhibit any ^{4}J coupling.

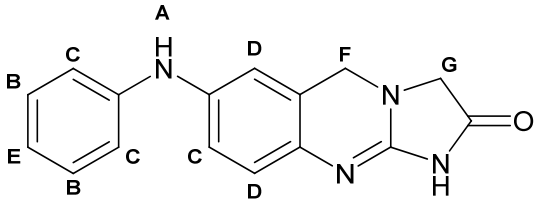

89

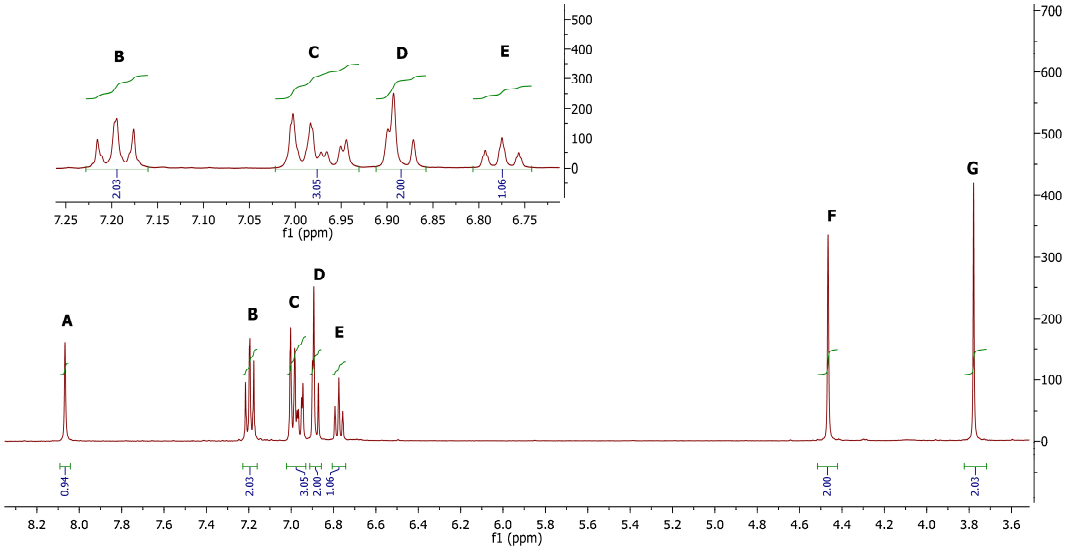

Figure 35 Assignment of 7-phenylamino-IMQ (89) ^{1}H-NMR spectrum in D_6-DMSO.

The ^{13}C spectrum of 7-phenylamino-IMQ (**89**) was obtained and assigned (Figure 36) through DEPT, HSQC and HMBC experiments. The HSQC (Figure 37) cross peaks allow for detection and assignment of each carbon with one or more protons directly attached. The HMBC (Figure 38) cross peaks show carbons two or more bonds from the corresponding proton(s). This can be seen where the methylene protons at 3.8 ppm give a signal for the carbonyl and guanidinyl tertiary carbons of the IMQ lactam ring, also showing that this signal corresponds to the lactam methylene rather than that of the central IMQ ring. Another clear example is where the secondary amine signal does not have a cross peak in the HSQC spectrum, but produces multiple cross peaks in the HMBC spectrum corresponding to the aromatic carbon atoms of the phenyl and IMQ rings.

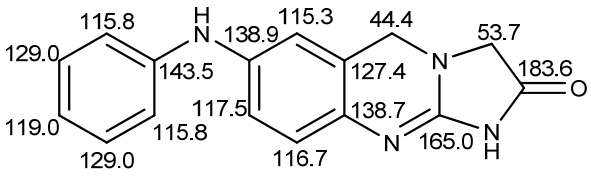

89

Figure 36 ^{13}C-NMR assignment of 7-phenylamino-IMQ (89) in D_6-DMSO.

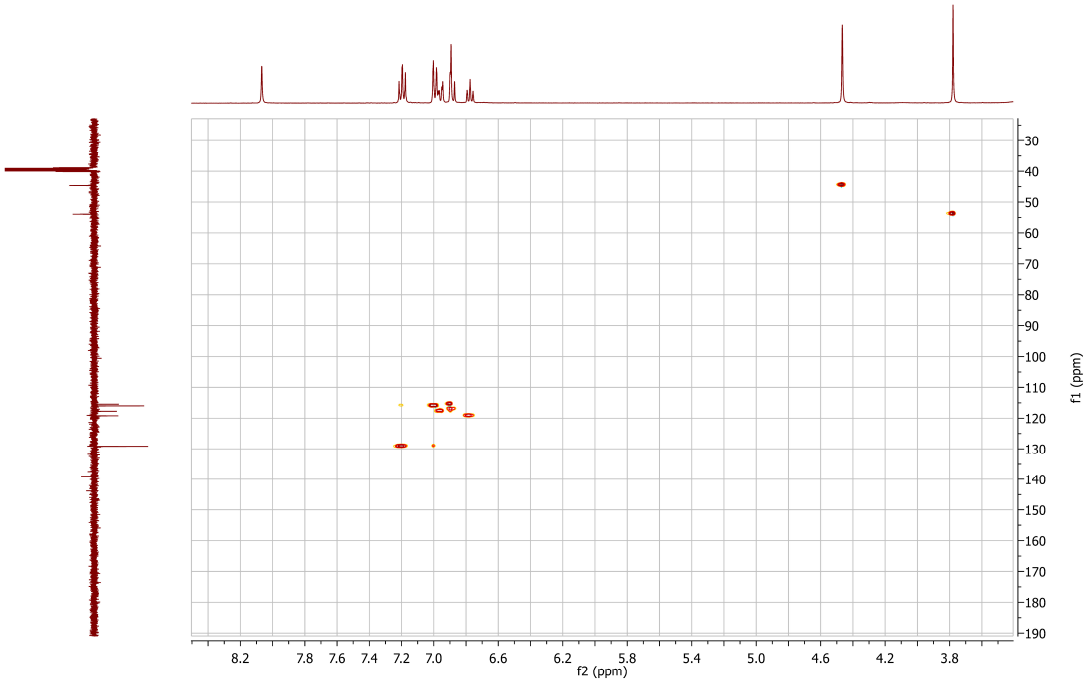

Figure 37 HSQC of 7-phenylamino-IMQ (89) in D_6-DMSO

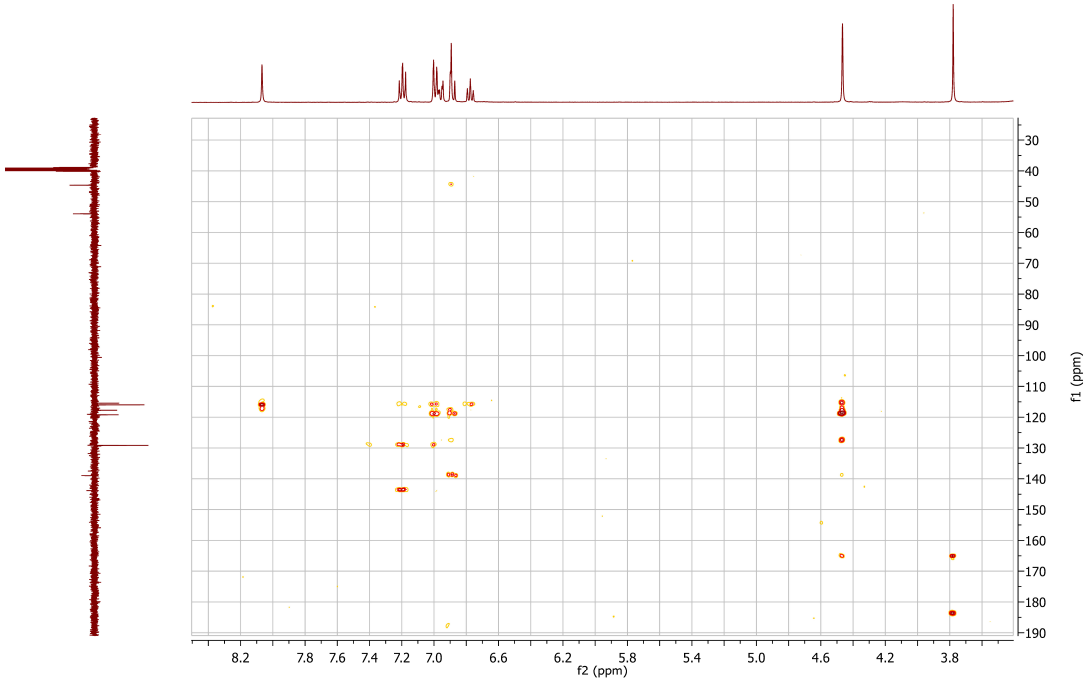

Figure 38 HMBC of 7-phenylamino-IMQ (89) in D_6-DMSO.

Of the analogues that were targeted for synthesis from the virtual screen discussed in Chapter three, there was a significant portion that were found to be completely intractable to the selected coupling conditions. It is worth noting that the reaction conditions used achieved our intended goal of being compatible with a wide range of amine coupling partners. The lack of success with certain coupling partners could perhaps be attributed to the presence of certain functional groups (i.e. carboxylic acids) or steric hindrance which kept them from effectively participating in the catalytic cycle. The amines that failed to give isolatable yields of product were:

- N-benzylpiperazine
- Adamantanamine
- N-methylpiperazine
- N-acetylpiperazine
- 1*H*-tetrazol-5-amine
- 4-(4-chlorophenyl)thiazole-2-amine
- (1r,4r)-4-(aminomethyl)cyclohexanecarboxylic acid
- 3-(phenylamino)phenol
- Proline
- Alanine
- 3-nitroaniline
- 3-ethynylaniline

4.4 Biochemical Assays

The results discussed in this Chapter were obtained from the PDE3A and PDE3B activity assays described in Chapter two. The assay results are presented in two sections, the first represents a screen of analogues with a diverse set of side chains and the second contains compounds that were produced with an understanding of the SAR gleaned from the first set. This represents the order in which the analogues were synthesized and evaluated with few exceptions. All compounds were screened at 500 nM with the exception of three analogues in the first round which were evaluated at 1000 nM. The results of this screen are summarized in Table 9.

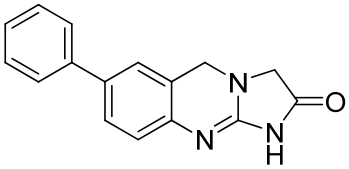

88

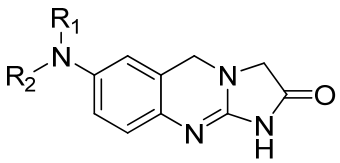

66, 87, 89, 94-100

#	R_1	R_2	[μM]	% Inhibition	
				3A	3B
66	Piperazine*	-	1	2	0
87	Boc-Piperazine*	-	1	59	32
88	-	-	0.5	80	44
89	Phenyl	H	0.5	76	46
94	Phenyl	Phenyl	0.5	4	-3
95	Phenoxazine	-	0.5	0	1
96	Benzyl	H	0.5	0	-4
97	Furanylmethyl	H	0.5	49	25
98	Cyclohexyl	H	0.5	8	2
99	1-benzylpiperidin-4-amine	H	0.5	-2	-4
100	Ethane-1,2-diamine	H	1	66	63

Table 9 Inhibitory activity of IMQs with structurally diverse side chains.

Four of the ten amine linked side chains that were screened in this round were found to be active, they were the analogues derived from Boc-piperazine (**87**), 1,2-diaminoethane (**100**), furan-2-ylmethanamine (**97**) and aniline (**89**). The 7-phenyl-IMQ (**88**) and 7-phenylamino-IMQ (**89**) were the most active analogues. The inactive compounds were those incorporating piperazine (**66**), 1-benzylpiperidin-4-amine (**99**), benzylamine (**96**), cyclohexylamine (**98**), phenoxazine (**95**) and diphenylamine (**94**). Further design and synthesis was informed by these results and led to a series of analogues derived from coupling substituted anilines. These substituted phenylamino- analogues were all screened at 500 nM, the results of which are summarized in Table 10.

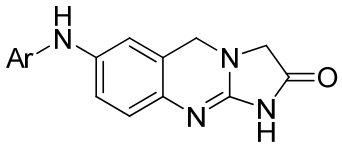

93, 101 - 109

#	Ar	[μM]	% Inhibition	
			3A	3B
93	4-hydroxyphenyl	0.5	77	46
101	3-hydroxyphenyl	0.5	87	69
102	2-aminophenyl	0.5	71	37
103	3-(trifluoromethyl)phenyl	0.5	95	77
104	4-nitrophenyl	0.5	97	83
105	pyridin-3-yl	0.5	76	50
106	3-carboxyphenyl	0.5	99	89
107	4-carboxyphenyl	0.5	92	68
108	2-hydroxyphenyl	0.5	58	28
109	4-cyanophenyl	0.5	94	78

Table 10 Inhibitory activity of IMQs with derivatized phenylamino side chains.

Four analogues bore substituents that did not significantly improve the analogues activity; those were the 4-hydroxy (**93**), 2-hydroxy (**108**), 2-amino (**102**), and pyridin-3-yl (**105**). The 3-hydroxy (**101**) substituent seems to offer a slight improvement in potency. The remaining five analogues bore substituents on the phenyl ring which increased their potency relative to the undecorated pendant ring; these substituents were 3-trifluoromethyl (**103**), 4-nitro (**104**), 4-cyano (**109**), 3-carboxy (**106**) and 4-carboxy (**107**) groups.

Dose response curves were obtained and IC_{50} values were determined for the 3-carboxy analogue (**106**, IC_{50} values of 43 nM at 3A and 88 nM at 3B), and the 4-carboxy analogue (**107**, IC_{50} values of 22 nM at PDE3A and 50 nM at PDE3B). This makes the 4-carboxy analogue (**107**) the most potent, novel compound identified in this study, it was found to be more potent that anagrelide (**2**, IC_{50} values of 35 nM at PDE3A, 100 nM at PDE3B), and equipotent with Cilostamide (**1**, IC_{50} values of 22 nM at 3A, 48 nM at 3B), which was used as a positive control in the assays. All of the amine linked analogues were more potent against PDE3A than PDE3B at the screened concentrations.

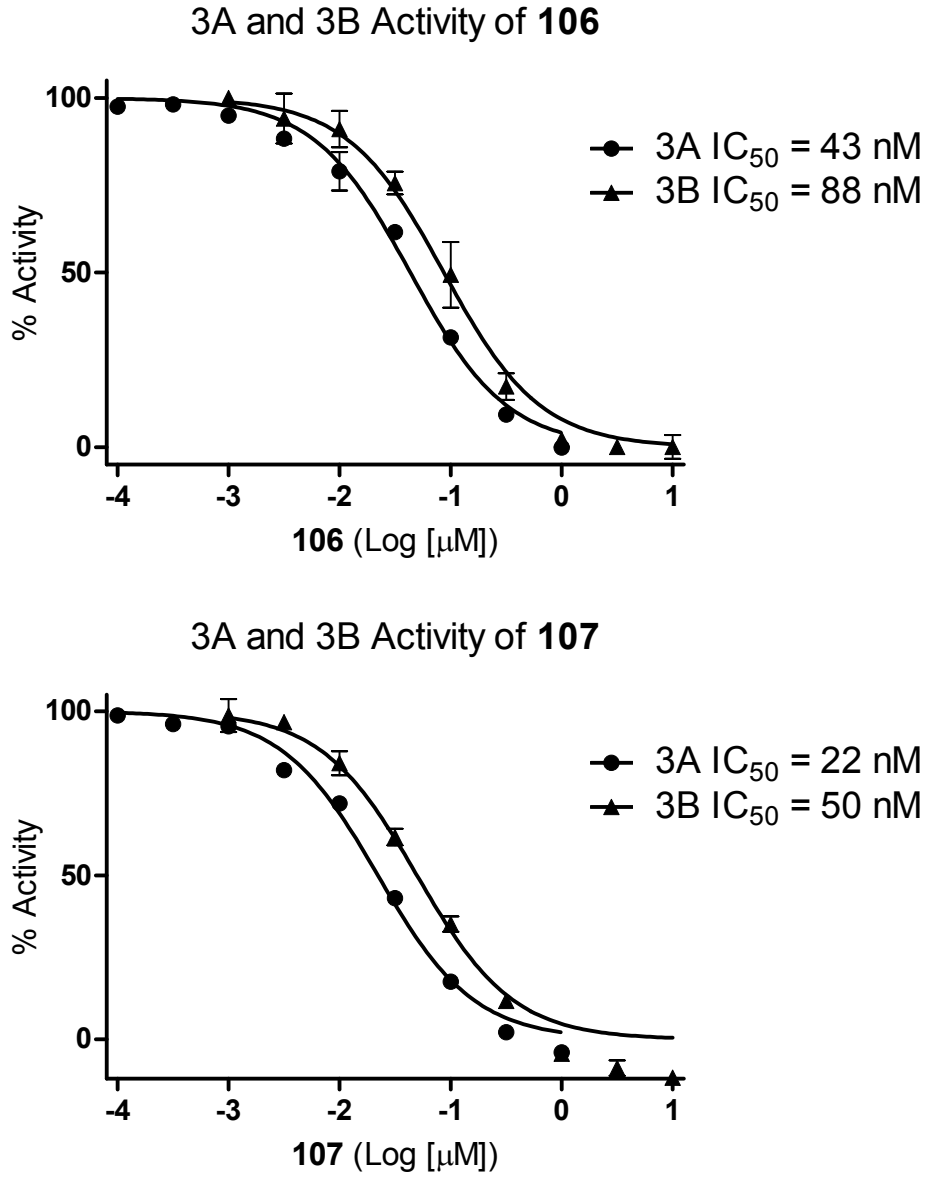

Figure 39 Dose response curves of 7-(3-carboxyphenylamino)-IMQ (106**) and 7-(4-carboxyphenylamino)-IMQ (**107**)**

4.5 Structure Activity Relationships

In order to develop a meaningful SAR from the assay data, we re-examined the virtual screening results for the assayed analogues. These were used to assess what areas of the binding site could be accessed by the ligand side chain and from that what interactions between the ligand and the active site could be taking place.

From the first screening assay we learnt about what kind of linkers or side chain scaffolds are tolerated by the PDE3 binding site. The results indicated that the 7-phenyl-IMQ (**88**) which was the produced via the Suzuki coupling reactions has similar potency its precursor 7-bromo-IMQ (**36**), the advantage of this analogue is that it offers particularly rigid scaffold which would be advantageous for further exploration of the binding site.

The screening assay revealed that the Boc protected piperazine analogue (**87**) retains appreciable activity. This could be due to either the bulky lipophilic Boc group, or the carbamate group having a favourable interaction with the active site. In either case it suggests potential for additional carbamate-, amide or urea-style derivatives that might be second generation analogues.

The diamino ethane analogue (**100**) features a flexible saturated amino linker, it does not lose nearly as much potency as **66** or **98** with saturated ring side chains, however it is not clear if this improvement is due to the reduced steric bulk, or the added flexibility, or both. In any case the linker itself does not appear to be adding to the analogues potency. Interestingly this is the only analogue that is equipotent between PDE3A and PDE3B.

A number of side chains consisting of different aromatic rings were also screened, these suggested that aromatic rings are favoured over unsaturated rings, but with some caveats. Interestingly the phenylamino-IMQ (**89**) is active, and the benzylamino-IMQ (**96**) is not. It is unclear why there is such significant loss of activity by addition of a methylene spacer in the benzyl analogue, when the same spacer is tolerated in the furanylmethylamino-IMQ (**97**). It seems unlikely that ring size would be the cause of this difference, as the larger cyclohexanamine (**98**) still shows some activity (albeit with a shorter link to the IMQ). The ability of the oxygen atom in the furan ring to accept hydrogen bonds is another possible explanation for the retained activity despite the added methylene. A wider variety of aromatic side chains would be needed to be evaluated in order to delineate this SAR.

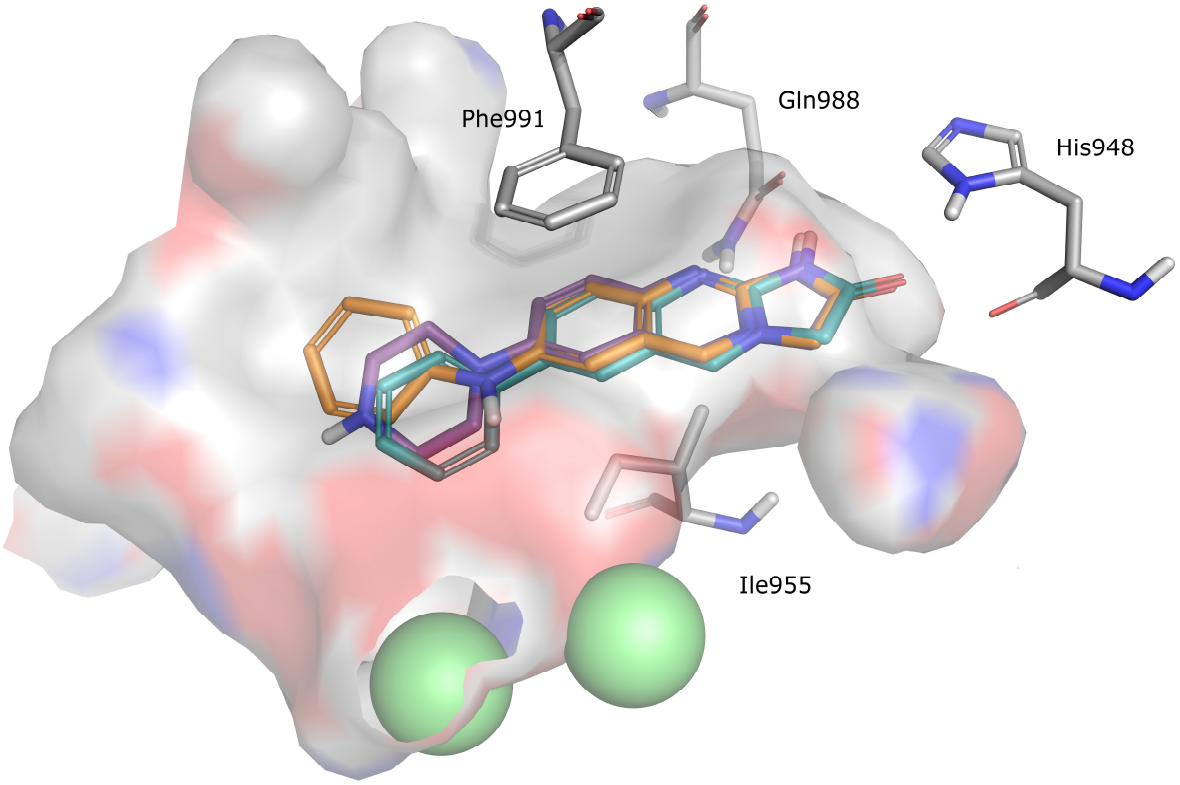

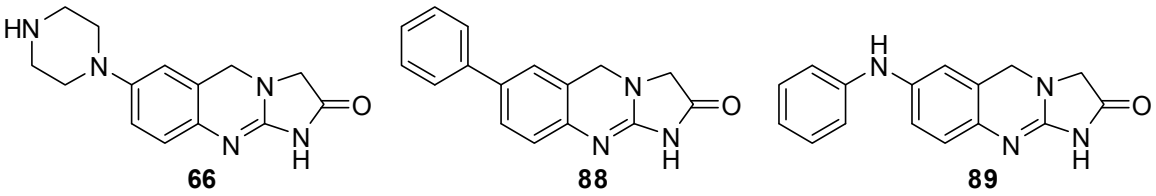

Figure 40 Overlay of conformationally restricted side chains 7-phenyl-IMQ (88**) in teal 7-piperazine-IMQ (**66**) in purple and 7-phenylamino-IMQ (**89**) in orange**

The complete loss in activity with the Di-phenylamino-IMQ (**94**) and phenoxazine-IMQ (**95**) indicates that they were both too sterically hindered to be active at either PDE3 isoform, this suggests that extended side chains are more useful than branched and/or bulky ones.

In the first round of amine linked analogues, the 7-phenylamino-IMQ (**89**) was the most active, fortuitously it was also synthesized in the highest yield and derivatized analogues of this scaffold could be accessed by coupling appropriately substituted anilines. A second series of analogues with functionalized phenyl rings was produced and evaluated, all of which were active at the screening concentration of 500 nM.

Looking at the effects on potency of different functional groups around the phenyl ring some trends start to appear. Very polar groups at the 3 and 4 positions of the aniline ring lead to greater improvements in potency. These included the 3-trifluoromethyl (**103**), 4-nitro (**104**) and 4-cyano (**109**) analogues, all of which nearly completely inhibited PDE3A at 500 nM. The 3- and 4-carboxy analogues (**106** and **107** respectively) were equally improved, and also have potential to be further derivatized. However, the presence of a carboxy group has significantly reduced related compounds ability to function in whole cell assays, presumably due to a lack of cell permeability.[132]

The only analogue which lost a meaningful amount of activity due to its derivatization was 2-hydroxyphenylamino-IMQ (**108**), the 1,2-diphenylamino-IMQ (**102**) lost a little activity from its substituent at the phenyl ring's 2 position. It could be that this position itself is unfavourable, perhaps due to conformational changes imparted by these substituents. Interestingly hydroxyl groups at both the 3- and 4-positions (**101** and **93** respectively) on the phenyl ring had improved activity, which supports the notion that the position rather than the nature of the 2-hydroxy group was to blame for the loss of activity in **108**.

Almost no change in activity was associated with a nitrogen atom being incorporated into the phenyl ring at the 3 position (**105**), or with a 4-hydroxy group (**93**). Comparing the 4-hydroxy (**93**) and 4-carboxy (**107**) analogues is interesting, it is not clear if the 4-carboxy fairs better due to its added size, acidity, or carbonyl function. Additional analogues derivatized at this position could explore these concepts further.

Finding five different favourable substitutions of this pendant ring from the ten that were tested is a fair ratio of success, this seems to indicate that there are a number of favourable interactions available in this region of the binding pocket. The more polar groups at the 3 and 4 positions seemed to convey the most potency, and the docking studies suggest that these may be positioned toward the metal binding region where a variety of hydrogen bonds would be possible (Figure 41).

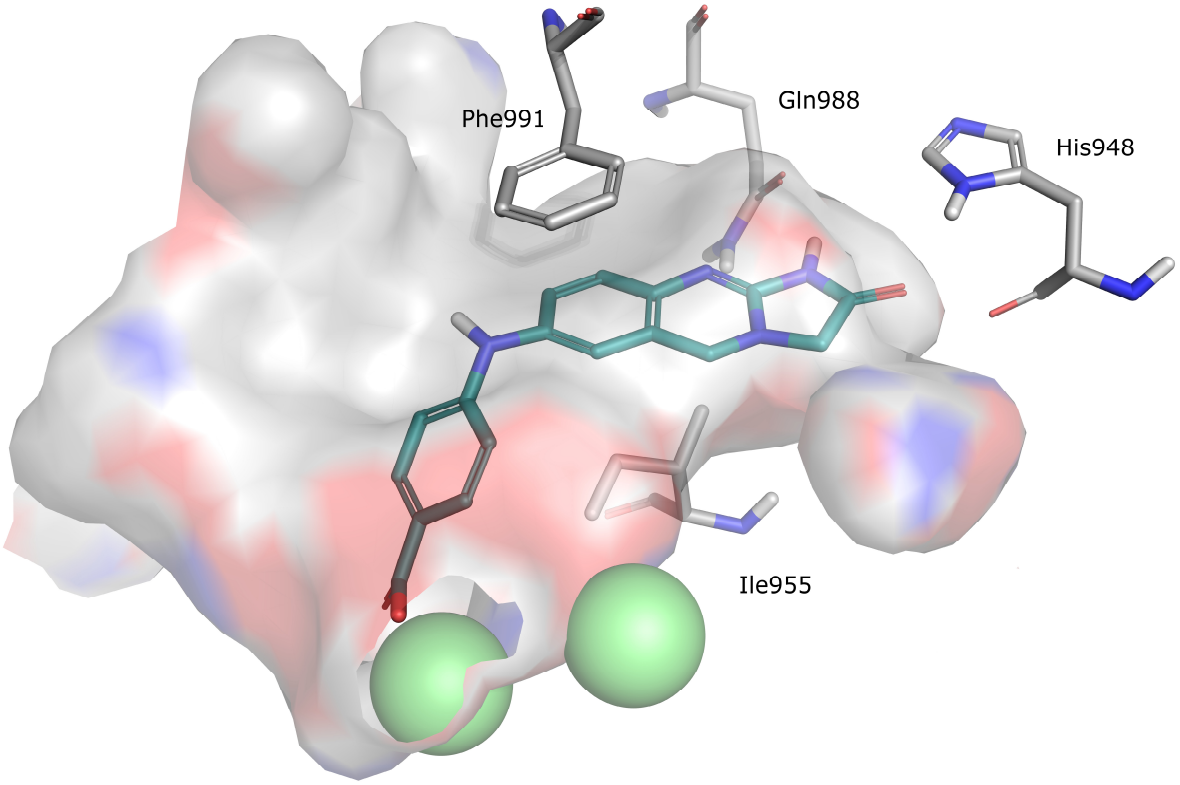

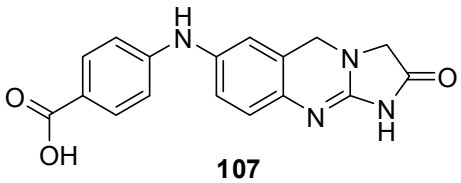

107

Figure 41 7-(4-carboxyphenylamino)-IMQ (107**) in the docked into the PDE3B binding site.**

All of the analogues were more potent at PDE3A than PDE3B to a similar extent that the unsubstituted IMQ scaffold (**10**) and IMQs with small substitutions at the 7 position were, this suggests that these amine linked side chains have very little effect on selectivity. This trend indicates that the binding mode of these compounds does not interact with any non-conserved areas of the binding site. This is not entirely surprising, as found in the previous Chapter, the compounds that are most selective usually have extended side chains. The advantage of this series are that it is novel, and has a more structured side chain which could lead to more selective interactions, and there is scope for further derivatization.

A number of novel potent compounds were uncovered in this series, with compound (**107**) having IC_{50} values of 22 nM at PDE3A and 50 nM at PDE3B. This was made possible by using a modular synthetic

scheme where the portion being varied is coupled to the scaffold at the end of the synthesis. When adding the side chain early in the synthesis the required labor to reach an analogue was much higher. Buchwald-Hartwig cross coupling reactions were effective as it allowed for evaluation of a wide variety of side chains and ultimately lead us to the aniline series. However the chemistry proved to be very challenging which ultimately limited the number of analogues that were produced.

4.6 Conclusions

The modular approach to IMQ analogue synthesis pioneered in this work has led to the discovery of a variety of novel potent PDE3 inhibitors. The advantage being that it gave us access to a wide variety of analogues, and reduced our investment in any of them. This was particularly well suited to this study where opportunities for informed design of analogues were limited, and the literature synthesis of those analogues quite laborious.

However, there were also several limitations that should not be over looked. While there proved to be a wide variety of achievable targets, there were perhaps just as many that remained firmly out of reach. It may be that a broader range of analogues would be available through the more labor intensive linear method. Additionally, the amount of optimization that was required limited the number of analogues that could be produced. Purification also proved to be a significant issue, one advantage of the linear approach is that it may allow for isolation of pure analogues via precipitation upon cyclization.

Of those novel potent analogues that were achieved in this work it is easy to imagine how they may be further elaborated upon. Such broad scope for functionalization and derivatization around the aniline ring of those potent analogues could very well allow for efficient exploration of the PDE3 binding site.

Chapter 5: Imidazolidin-4-ones

5.1 Outline

Lost and lonely imidazolidin-4-ones litter the literature, largely overlooked by lofty laboratories, left to languish until their lack of largeness landed them in the limelight, as the latest Lilliputian ligand.

In this chapter focus turns to an alternate class of compounds, the five membered lactam ring imidazolidin-4-ones (IMDs). This chemical class is largely unexplored but has some similarity to other PDE inhibitors. The IMD scaffold (**111**) can be found fused within the IMQ scaffold of anagrelide (**2**) and is an aza-analogue of the lactam found in Rolipram (**110**), which is a PDE4 inhibitor. To date few reports in the literature have used this scaffold in a medicinal chemistry context. A comprehensive review of the synthesis and applications of IMDs[169] was prepared by the author as part of this candidature and is included in Appendix B.

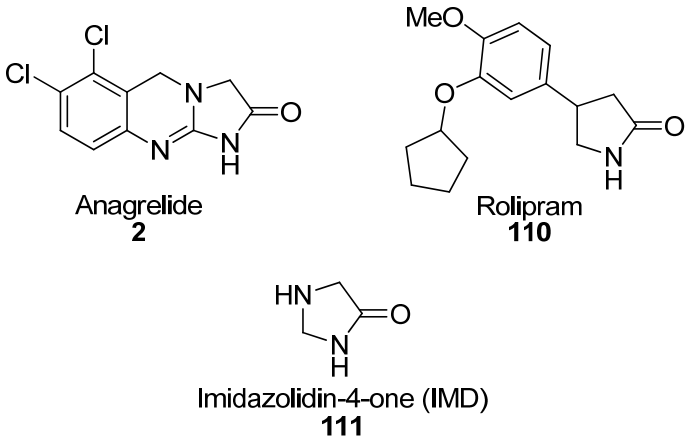

Figure 42 Imidazolidin-4-one, Anagrelide and Rolipram.

This underutilized chemical class might have potential in the development of novel PDE inhibitors but perhaps even more tellingly the potential of these compounds as leads in the technique of Fragment Based Drug Design (FBDD) for a broad array of targets was recognized.[170] IMDs represent a starting point for a FBDD due to their small size, potential for elaboration, and the broad regions of novel patent space around it. As such, this Chapter focuses on the synthesis and elaboration of IMDs.

5.1.1 Fragment Based Drug Design

Fragment-based Drug Design (FBDD) has emerged in recent years as a major strategic approach o the generation of new leads in drug discovery.[171] The principle is to search for very small (<300 MW) ligands of a drug target; these small fragment molecules can then be elaborated into lead like compounds. There are several advantages offered by FBDD compared to using larger lead-like ligands typically encountered in high throughput screening. Firstly a greater percentage of chemical space can be sampled with fewer compounds. Secondly fragment compounds tend to be more soluble. Finally the screening methods employed for a smaller range of compounds can be more robust or informative. These advantages combine to give a screening assay with more hits and less false positives. The limitations of this approach are that the fragments typically have low potency, may require specialized assay formats, and require extensive development.[172]

"Chemical space" is a representation of all the possible compounds that could be made. The number of potential compounds in a chemical space increases exponentially with the size of compounds being included. This means that fewer compounds are required to sample all constituent, shapes and sizes of small compounds than would be required to obtain an equally thorough sample of larger compounds. It has been suggested that the chemical space of lead like compounds is too large to be reliably sampled. Including only small compounds allows for the chemical space to be thoroughly sampled with a smaller library and in doing so the hit rate is significantly improved.[172, 173] Another advantage of screening fragments over lead-like compounds is that more elaborate ligands are less likely to fit into active sites in a chance fashion.

Early reports of fragment screening were performed using 2D NMR experiments to detect ligand binding to a target. Relative to other assay methods, 2D NMR is good for detecting the relatively weak binding of fragments. It also can provide insight into structure activity relationships (SAR) of a compound class and the binding mode of the fragment. Other methods which are sensitive enough to detect fragment binding range from techniques that give some structure-activity data (i.e. 2D NMR, X-ray crystallography) to those with increased throughput (i.e. Surface plasmon resonance[174], high concentration screening[175]). Combinations of these methods can be used so that hits can be identified in a high throughput assay, and further investigated through a second, more informative technique. This two phase approach is well suited to

FBDD where the more informative techniques are also more labor intensive however they are limited to targets amenable to NMR or crystallographic structural characterization. Without the structural data gleaned from these experiments it can be prohibitively difficult to elaborate a fragment into a lead compound.[176]

The design of a fragment library is critical to the success of a FBDD project. Each fragment can be evaluated by its compliance with the "Rule of 3", that is MW ≤ 300, H Bond donors ≤ 3, H bond acceptors ≤ 3, CLogP ≤ 3, and the number of rotatable bonds ≤ 3.[177] It is also vital that the fragment library is sufficiently diverse in order to thoroughly sample the available chemical space and that it consists of structures that can be developed into novel lead compounds.[178]

Another aspect to consider is masking the functionalities that are likely to be expanded upon when the fragment is grown. This reduces the occurrence of hits that are not amenable to derivatization, e.g. where key binding interaction is through the hydrogen of a secondary amine, and any attempt to substitute at that position abolishes activity.[173] This represents the difference between synthesis fragments and screening fragments. A screening fragment has already been substituted with a simple derivative, where as a synthesis fragment is ready to be derivatized to give rapid access to focused libraries.

5.1.2 Imidazolidin-4-ones as Fragments

Against this background, fragments based upon IMD (**111**) appeared be ideal for FBDD in a number of ways. First among them is their small size, the molecular weight of IMD (**111**) is just 86 Da. The unsubstituted ring contains two hydrogen bond donors and one acceptor, no rotatable bonds, and the CLogP is -1.3. These properties all qualify the 5 membered lactam as a viable synthesis fragment, and a wide variety of simply derivatized IMDs, for example the N-benzyl-imidazolidin-4-one (**112**) would qualify as screening fragments on this criterion.

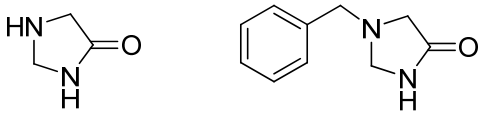

Synthesis fragment **111** Screening fragment **112**

Figure 43 Imidazolidin-4-ones as fragments.

Reviews of FBDD also stress the importance of only screening fragments that show potential for rapid elaboration.[171, 172, 176] IMDs allow for rapid synthesis of derivatized analogues, examples of which can be found in Appendix B. There are synthetic methods that allow for construction of the ring with substitutions at several positions, leaving the IMD sitting at the center of several larger branches acting as a diminutive scaffold. Alternatively, positioned at the end of a ligand, the heterocycle may contribute affinity through its distinct set of hydrogen bond donors and acceptors.

One suggested method to assess the likelihood of a fragment becoming a good drug is to determine if the same fragment occurs within other drugs that have made it to market.[179] The IMD motif (**111**) and the larger N-benzyl-IMD (**112**) are found within anagrelide (**2**). There are also parallels between the IMD template and the pyrrolidinone structure of the PDE4 inhibitor Rolipram (**110**). However, this investigation began with no evidence or presumption that such fragments would be active against PDEs. By using a FBDD approach the analogues that were developed were anticipated for use in many drug discovery areas beyond PDE inhibition.

5.1.3 Literature Syntheses of IMD and Derivatives

The IMD ring has appeared in relatively few medicinal chemistry projects, and areas of the surrounding chemical space have been explored only tentatively. A detailed account of syntheses and application of the IMD class was published recently,[169] and specific details are summarized here.

Pfeiffer et al[180] published the most recent synthesis of IMD which is outlined in Scheme 24. To begin, 2-(benzylamino)acetamide (**114**) was synthesized through a reductive amination between benzaldehyde and glycinamide (**113**). Treatment of (**114**) with excess formaldehyde gave the cyclized 1-benzyl-3-(hydroxymethyl)imidazolidin-4-one (**115**). The N-hydroxymethylene group of (**115**) was selectively decomposed at elevated temperature under high vacuum to give (**112**). Finally the benzyl group of (**112**) was removed by catalytic hydrogenation to reveal IMD (**111**).

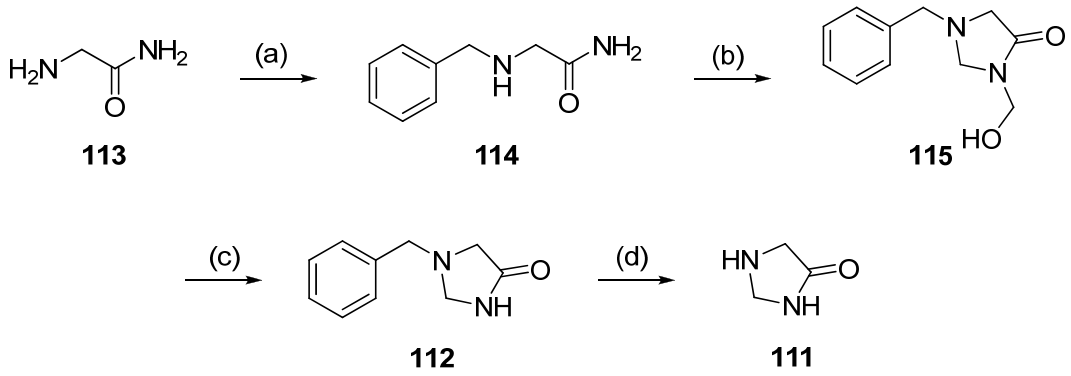

113 114 115 112 111

Scheme 24 Synthesis of imidazolidin-4-one reported by Pfieffer et al.[180] Reagents and conditions: (a) benzaldehyde, $NaBH_4$ (b) CH_2O, H_2O, reflux, 30 min (c) 15 Torr, 150 °C, 4 h (d) Pd-C, H_2, EtOH, RT, 4 h.

Scheme 25 shows an interesting alternate approach to synthesizing the ring system which was published by Suwinski et al[181] where 4-nitro-1-phenyl-1*H*-imidazole (**116**) was converted to 1-phenylimidazolidin-4-one oxime (**117**) by treatment with sodium borohydride and sodium methoxide in methanol. The oxime (**117**) was then oxidized to 1-phenylimidazolidin-4-one (**118**) by treatment with hydrogen peroxide and sodium hydroxide in methanol and water.

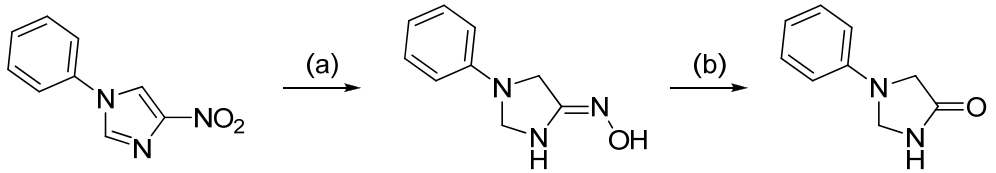

116 117 118

Scheme 25 Synthesis of 1-phenyl-IMD reported by Suwinski et al.[181] Reagents and conditions: (a) Na, $NaBH_4$, MeOH, RT, 24 h (b) H_2O_2, NaOH, MeOH, reflux, 8 h.

5.2 Results and Discussion

5.2.1 Synthesis of 4-Imidazolinone

This work commenced by recapitulation of the strategy of Pfeiffer et al.[180] The key intermediate, 2-(benzylamino)acetamide (**114**) was synthesized in 27% yield by alkylation of benzylamine with 2-chloroacetamide (**119**).[182] This reaction gave a lower yield of **114** than the reductive amination reported by

Pfieffer (70%). However the reduced yield of the approach used here was mitigated by the lower costs of reagents used.

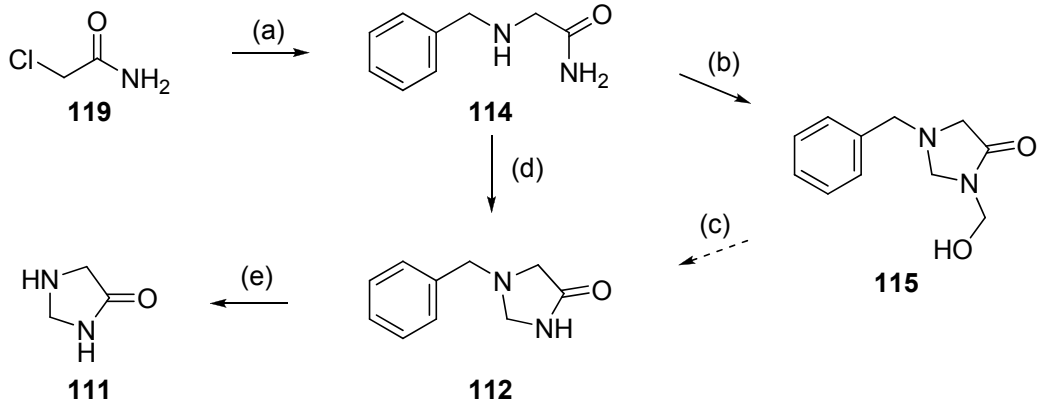

Scheme 26 Synthesis of IMD via cyclization. Reagents and conditions: (a) benzylamine, water, 90 °C, 20 mins (b) CH_2O, reflux, 30 mins (c) distil. (d) CH_2O, MeOH, reflux, 90 h (e) Pd-C, H_2, MeOH, RT, 120 h.

Cyclization to 1-benzyl-3-(hydroxymethyl)imidazolidin-4-one (**115**) was achieved in moderate yield (47%) by refluxing (**114**) in formaldehyde. However the controlled decomposition of the hydroxymethyl compound (**115**) to **112** could not be reproduced. A short path vacuum distillation apparatus was employed, but the material was converted to a complex mixture of degradation products which was obtained as a viscous black oil, possibly the product of a polymerization reaction.

Thankfully, it was found that it was possible to synthesize the desired 1-benzylimidazolidin-4-one (**112**) directly from (**114**). Instead of refluxing 2-(benzylamino)acetamide (**114**) in excess 40% formaldehyde solution for 30 mins, it was found that using formaldehyde as the limiting reagent, and refluxing for 90 h in methanol gave a modest yield (24%) of 1-benzylimidazolidin-4-one (**112**). Attempts to improve the yield by using a small excess of formaldehyde yielded a mixture of **112** and **115** that could not reliably be separated.

Under standard catalytic hydrogenolysis conditions, 1-benzylimidazolidin-4-one (**112**) was converted to the desired IMD (**111**) in good yield (92%). Recrystallization gave the product as hygroscopic needles and ^{1}H-NMR and ^{13}C-NMR signals matched literature values.[180] It should also be noted that IMD (**111**) is listed as a commercially available, although relatively expensive product. We attempted to purchase a 1g sample, however the supplier failed to provide this compound to us.

An alternative synthesis (Scheme 27) based on the work of Suwinski et al[181] (Scheme 25) was also investigated. Suwinski et al had reported the transformation of the phenyl substituted 4-nitro-1*H*-imidazole (**116**), whereas the benzylic precursor (**121**) would lead us to the corresponding imidazolidin-4-one **112.** The precursor **121** was prepared by alkylation of 4-nitro-1*H*-imidazole (**120**) using benzyl bromide in moderate yield (60%). The ^{1}H-NMR spectra shows two coupled doublets of the 4-nitroimidazole ring at 8.5 and 8 ppm and a methylene singlet at 5.4 ppm.

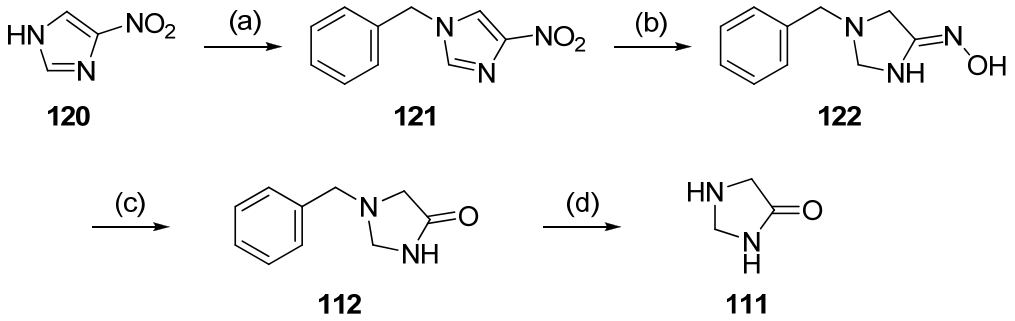

Scheme 27 Synthesis of IMD via reduction. Reagents and conditions: (a) Benzyl bromine, KOH, TBAB, water, toluene, 70 °C, 2 h (b) MeONa, $NaBH_4$, MeOH, RT, 5 h (c) NaOH, H_2O_2, MeOH, RT, 16 h (d) Pd-C, H_2, MeOH, RT, 120 h.

Reduction of (**121**) to the corresponding oxime (**122**) was achieved using a mixture of sodium methoxide and sodium borohydride. The yield of this transformation was 24%. The reduction of the imidazole ring is evident with the ^{1}H-NMR showing three methylene singlets at 3.9, 3.7, and 3.2 ppm. The low yield was attributed to the generation of an insoluble black oil. An alternate reducing agent sodium bis(2-methoxyethoxy)aluminiumhydride (Vitride) was examined however the yield was unchanged.

The isolated oxime (**122**) was hydrolyzed with sodium hydroxide and hydrogen peroxide in methanol to give 1-benzyl-IMD (**112**) in moderate yield (39%). Again in this hydrolysis decomposition products were significant. Catalytic hydrogenation of 1-benzyl-IMD (**112**) to reveal IMD (**111**) proceeded as before in quantitative yields.

The overall yields of the two approaches were very similar and disappointingly low. The cyclization route of Scheme 26 is more economical and uses milder conditions, but in both cases it seems that decomposition may be a limiting factor. Certainly, consideration could be given to changing the benzylic group which might in turn provide for more stability to the reaction conditions to facilitate improved yields.

5.2.2 Design of Substituted 4-Imidazolinones Fragment Scaffolds

With the IMD core (**111**) in hand, the next goal was to derivatize it to obtain a library of fragment-style compounds. The most immediate position on the ring for derivatization was the secondary amine. The amine stood out because of the number of different methods available to effect derivatization. Several of these were explored in attempts to make a small series of fragments composed of different scaffolds. Substituted 1-benzyl-IMD (**127**) and 1-phenyl-IMD (**126**) analogues were targeted as they most closely resembled the scaffolds of anagrelide (**2**) and rolipram (**110**) respectively. The 1-phenethyl-IMD analogue (**125**) was chosen to evaluate further expansion of linker length. Finally the 1-phenacetyl-IMD (**124**) and 1-benzoyl-IMD (**123**) were targeted as they were available through well established synthetic methods and offered some simple variation of functionality and flexibility. 1-Benzylimidazolidine-2,4-dione (**128**) was also incorporated as a being comparable to the IMQ structure of anagrelide.

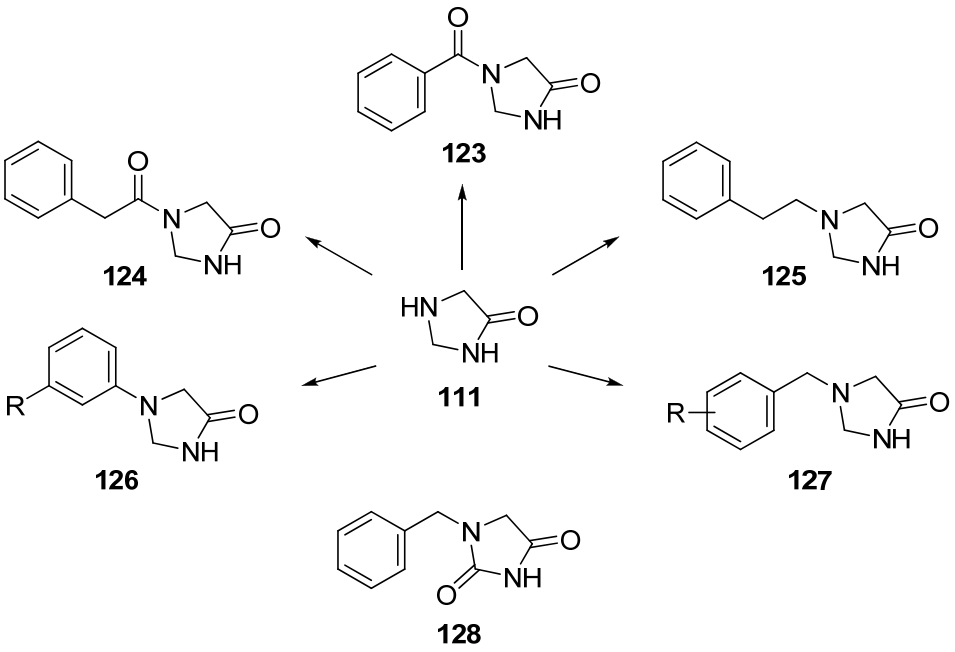

Figure 44 Targeted fragment scaffolds.

The analogues of **127** in this focused library incorporated a number of different functionalities around the phenyl ring. The specific targets were chosen with consideration of the Topliss decision tree (unsubstituted, 4-chloro, 4-methoxy, 4-methyl, and 3,4-dichloro), which is a system of selecting functional groups around a benzene ring to vary the hydrophobic, electronic and steric interactions of that ring, this allows for optimization while requiring relatively few analogues to be synthesized.[183]

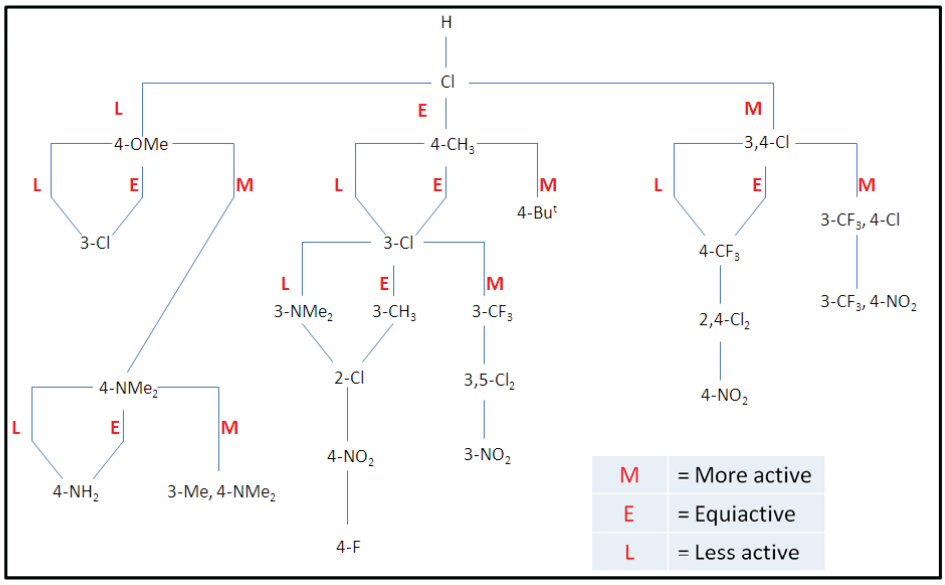

Figure 45 Topliss tree reproduced with permission from W. Nguyen[184]

Finally, an IMD (**129**) was targeted to allow comparison with the potent PDE3 inhibitor **43**. This synthesis could also serve as an example of how IMD fragments could be elaborated into higher affinity, 'lead-like' compounds.

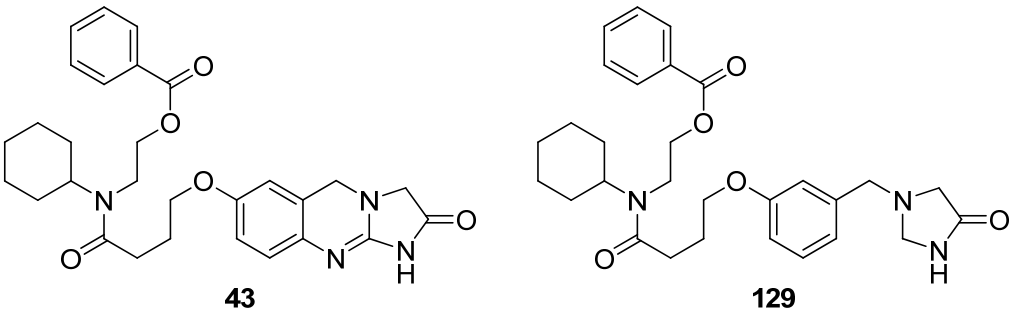

Figure 46 extended side chain analogues.

5.2.3 Synthesis of Imidazolidin-4-one Based Fragments

The synthesis of 1-benzoyl-IMD (**123**) by treatment of 4-benzoyl-5-thioxopyrrolidin-2-one with Raney Nickel was reported by Edward et al[185] in 1954 and Freter et al[186] in 1957 but has not reappeared in the literature since. Treatment of IMD (**111**) with benzoic anhydride also yielded 1-benzoyl-IMD (**123**) albeit in modest yield (27%). It was found to exist as tautomers by ^{1}H-NMR, with the two methylene peaks split at room temperature, the pairs at 4.88, 4.78 ppm and 3.98, 3.95 ppm. At 350°K these pairs of peaks coalesced to 4.84 ppm and 3.95 ppm respectively.

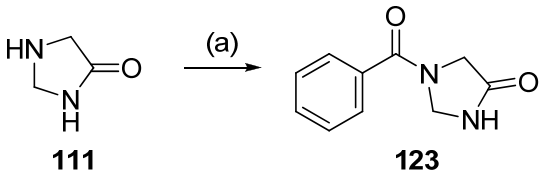

111 **123**

Scheme 28 Synthesis of 1-benzoyl-IMD (123**) Reagents and conditions: (a) Benzoic anhydride, Et_3N, DCM, RT, 2 d.**

The 1-phenylacetyl-IMD analogue (**124**) was also prepared by treatment of **111** with the activated ester phenylacetic acid in 60% yield. Like the 1-benzoyl-IMD (**123**), ^{1}H-NMR analysis showed split methylene peaks indicative of tautomers, however additional ^{1}H-NMR experiments at elevated temperatures did not show the peaks coalesce. The two sets of methylene signals were identified by their integration. The two larger (70%) methylene signals at 4.84, 4.1 ppm, and the smaller (30%) at 5.0, 3.94 ppm and two overlapping signals (100%) at 3.69 and 3.72 ppm, and the aromatic signals were all superimposed between 7.22 – 7.37 ppm. TLC and analytical HPLC indicated the compound was homogeneous. It remains unclear whether this reaction yields two positional isomers (**124** and **130**) or tautomers of **124** that do not interconvert rapidly at 350°K.

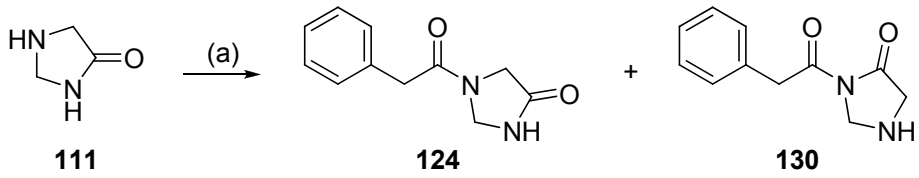

111 **124** **130**

Scheme 29 Synthesis of 1-(2-phenylacetyl)IMD (124**) and the unconfirmed isomer 3-(2-phenylacetyl)IMD (**130**) Reagents and conditions: (a) phenyl acetic acid, Et_3N, HCTU, DCM, RT, 16 h.**

The analogue 1-phenethyl-IMD (**125**) has also not been previously reported, although the structural motif was included as a part of single analogue in a patent of Plk1 inhibitors.[187] The synthesis of **125** was achieved by reaction of IMD (**111**) and (2-bromoethyl)benzene albeit in low yield (15%). No competing substitution at the amide nitrogen was observed but there was evidence of degradation products. As expected the compound produced two distinct methylene signals at 4.15 and 3.23 ppm, and two overlapping methylene multiplets between 2.75 to 2.88 ppm, and an aromatic multiplet between 7.15 and 7.31 ppm.

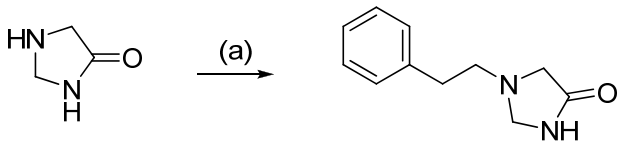

111 **125**

Scheme 30 Synthesis of 1-phenethyl-IMD (125**). Reagents and conditions: (a) (2-bromoethyl)benzene, Et_3N, ACN, reflux, 16 h.**

Direct arylation of the IMD ring (**111**) was achieved using the Chan-Lam coupling reaction with arylboronic acids using a copper (II) catalyst. Compounds with this structural motif have been reported by Suwinski et al[181] as outlined in Scheme 25, and in a patent where they were synthesized by alkylation of IMD (**111**) with 1-fluoro-4-nitrobenzenes.[188] Two analogues were synthesized this way and both were obtained in fairly low yields (**118,** R = H, 12%; **131**, R = OMe, 14%). Low yields are not uncommon with Chan-Lam coupling reactions, and there are a number of options for optimization that could be explored in future work.[189]

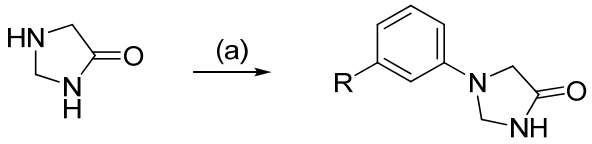

111 **118** R = H
131 R = OMe

Scheme 31 Synthesis of 1-aryl-IMDs (118 **and** 131**). Reagents and conditions: (a) $ArB(OH)_2$, $Cu(OAc)_2$, Et_3N, DCM, RT, 16 – 64 h.**

In the ^{1}H-NMR spectrum of the aryl derivatives, the IMD methylene signals were shifted downfield relative to alkyl substituted analogues, with peaks at 4.79 and 3.85 ppm in 1-phenyl-IMD (**118**). The corresponding 3-methoxyphenyl analogue (**131**) gave signals at 4.75 and 3.82 ppm respectively, while the protons of the methyl ether appeared at 3.77 ppm.

The one pot reductive alkylation of IMD (**111**) with benzaldehyde derivatives was the most successful method of derivatization by far. The unsubstituted analogue (**112**) was reported by Pfieffer, Suwinski and others, and just one analogue substituted-benzyl derivative has been described.[190] Following the two-step method of Abdel-Maguid,[191] **111** was treated with aromatic aldehydes to give derivatives (**127a - o**) in varying yields (6% - 94%).

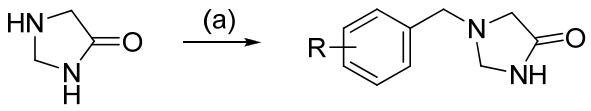

114 **127a - o**

Scheme 32 Synthesis of 1-benzylimidazolidin-4-one analogues (127a-o**). Reagents and conditions: (a) ArCHO, $NaBH(OAc)_3$, DCM, RT, 16 h.**

The reductive amination-based approach was used for the preparation of fifteen analogues with a range of substituents around the phenyl ring. The majority of the analogues were isolated in moderate to good yields (> ~50%). There were however several examples which were obtained in much lower yields (< 20%). These lower yields were possibly caused by the presence of charged functional groups, the added polarity of which made for more challenging chromatographic purification. In all cases the reaction was performed over molecular sieves in an attempt to remove adventitious water and drive the reaction forward.

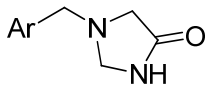

127a - o

127	Ar	Isolated % Yield
a	4-chlorophenyl	76
b	3,4-dimethoxyphenyl	83
c	3,4-dichlorophenyl	59
d	4-methylphenyl	57
e	4-methoxyphenyl	67
f	4-nitrophenyl	19
g	3-chlorophenyl	61
h	3-hydroxyphenyl	16
i	3-pyridinyl	94
j	4-(phenoxy)phenyl	81
k	4-(trifluoromethyl)phenyl	64
l	3-methylphenyl	47
m	3-(benzyloxy)phenyl	57
n	4-carboxyphenyl	8
o	4-hydroxyphenyl	6

Table 11 Substituted 1-benzyl-IMD analogues.

The synthesis of **128** (Scheme 33) was performed as reported by Kumar et al.[192] The synthesis began by treating benzylamine (**132**) with cyanogen bromide to produce a crude N-benzylcyanamide (**133**). Alkylation of the resulting secondary amine (**133**) with bromomethyl acetate gave intermediate (**134**). Finally the crude intermediate (**134**) was treated with sulfuric acid to give 1-benzylimidazolidine-2,4-dione (**128**) in moderate overall yield (20%).

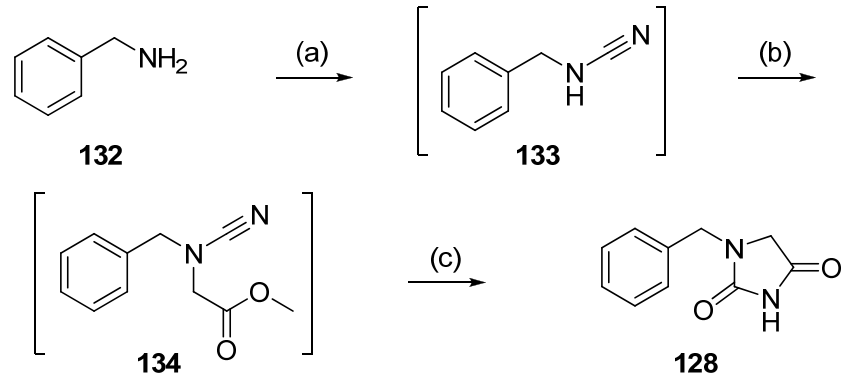

Scheme 33 Synthesis of 1-benzylimidazolidine-2,3-dione. Reagents and conditions: (a) CNBr, Et_2O, 0 °C, 2 h (b) NaH, $BrCH_2OAc$, THF, 0 °C, 2 h (c) 50% H_2SO_4, THF, 0 °C → RT, 150 mins.

The synthesis of the analogue **129** bearing the extended side chain was also successful (Scheme 31). In common with IMQ syntheses, (Chapter 2) a precursor ester **137** was prepared and elaboration to the desired material was achieved in a linear synthesis. First, alkylation of 3-hydroxy benzaldehyde (**135**) by ethyl-4-bromobutyrate gave ethyl 4-(3-formylphenoxy)butanoate (**136**) in quantitative yield. Reductive alkylation of **111** which proceeded as described above gave **137** in good yield (76%). Hydrolysis of the ester was accomplished with 2M NaOH in ethanol to give acid **138** (56%).

Finally, treatment of the HCTU-activated ester of **138** with **140** (prepared from **139**) gave a good yield (78%) of desired product **129**. The ^{1}H-NMR signals of compounds **137**, **138**, and **129** were concordant with the equivalent IMQ analogues **39**, **41** and **43** respectively. The IMDs of course showed a characteristic additional methylene peak at δ 4.1 ppm.

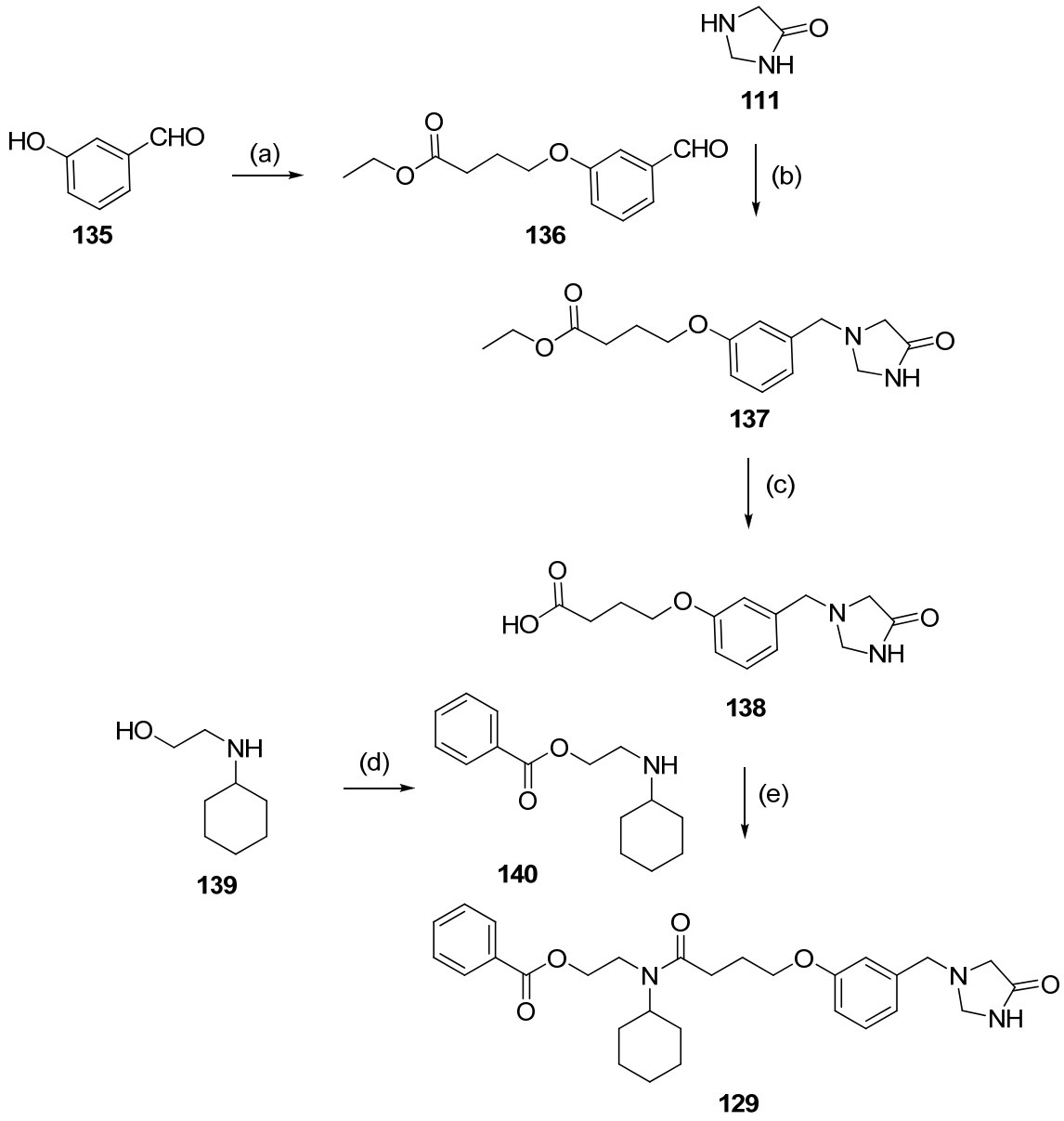

Scheme 34 Synthesis of IMDs with extended side chains. Reagent and conditions: (a) ethyl-4-bromobutyrate, K_2CO_3, DMF, 110 °C, 1 h (b) $NaBH(OAc)_3$, DCM, RT, 16 h (c) NaOH, EtOH, RT, 1 h (d) benzoic anhydride, toluene, RT, 3 d (e) HCTU, Et_3N, DCM, RT, 16 h.

In summary, the synthetic achievements described above show the versatility and potential of the IMD core for the synthesis of a diverse range of chemotypes – first it was shown that IMD can be subject to a variety of reactions yielding a range of product types. Second, a focused library of substituted 1-benzyl-IMDs was efficiently prepared via reductive amination. Third, an example of compound elaboration was shown generating an extended analogue of a known PDE3 inhibitor, demonstrating that the IMD core can be subject to further synthetic transformations.

5.4 Biochemical Assays Versus PDE3

While the majority of the synthesized compounds were not necessarily anticipated to inhibit PDE3, certainly it was of interest to see how certain compounds compared with the analogous PDE3 inhibitors, and if the new fragments showed any unexpected activity. The assay format was identical to that described in Chapter two. Compounds were screened at 10 μM and those showing some activity re-assayed at 30 μM. Emphatically, these compounds were poorly active as inhibitors of PDE3 isoforms with none showing IC_{50} values below 10 μM, and most showing negligible activity. Interestingly, the IMD analogues of the very potent IMQ-based PDE3 inhibitors (**137**, **138**, and **129**) gave virtually no inhibition showing how critical the planar tricyclic ring system is.

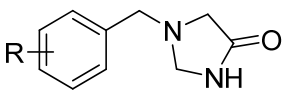

112, 127a - h, 127j - o 129, 137, 138

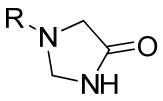

118, 123, 124, 125, 127i, 131

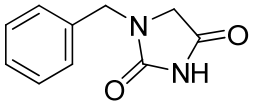

128

#	R	% Inhibition			
		10 μM		30 μM	
		3A	3B	3A	3B
112	H	4	-6		
118	Phenyl	-7	-4		
123	Benzoyl	-5	2		
124	2-phenylacetyl	-2	-3		
125	Ethylphenyl	4	-3		
127a	4-chloro	8	5		
127b	3,4-dimethoxy	-4	-1		
127c	3,4-dichloro	11	2		
127d	4-methyl	12	0	8	2
127e	4-methoxy	8	3		
127f	4-nitro	14	4	19	6
127g	3-chloro	0	-2		
127h	3-hydroxy	6	2		
127i	1-(pyridin-3-ylmethyl)	4	3		
127j	4-phenoxy	6	1		
127k	4-trifluoromethyl	9	2		
127l	3-methyl	13	6		
127m	3-benzyloxy	16	3	8	4
127o	4-hydroxy	17	5	11	8
128	-	15	4		
131	3-methoxy phenyl	-2	0		
137	Extended ester	7	-1		
138	Extended acid	8	0		
129	Lixazinone side chain	9	2		

Table 12 Percentage inhibition of PDE3A and PDE3B activity by 1-benzyl-IMD analogues.

Finally two analogues 1-(3,4-dimethoxybenzyl)-IMD (**127b**), and 1-(3-methoxyphenyl)-IMD (**131**) were assayed against PDE4B due to their similarity to the PDE4 inhibitor Rolipram (**110**), however they were inactive at the screened concentration of 10 μM.

5.6 Conclusion

This investigation is first to describe a class of N-substituted IMDs for use in fragment library screening. A number of challenges were successfully met. First, two alternate syntheses of IMD (**111**) were assessed, and both were successful but are still in need of improvement. In the cyclisation based approach (Scheme 26), this might be achieved by adaptation of the synthesis with reagents to facilitate cyclisation. In the imidazole pathway (Scheme 27), significant side reactions need to be suppressed.

Derivatization of the unsubstituted IMD ring (**111**) can be achieved through a variety of established chemistries. By synthesizing a focused compound library (Table 12) it was shown that a series of analogues can be synthesized from a common intermediate. Finally by incorporating an extended side chain into these analogues it was shown that elaboration into lead-like compounds could proceed without issue

While there was no observed dose dependant inhibition of PDE3 or PDE4 by these compounds, this in no way precludes there potential as compounds for use in fragment screening campaigns against other targets. Indeed a selection of the compounds discussed in this Chapter has been incorporated into on-going FBDD projects in our institute.

Chapter 6 Experimental

Computational Methods

Using Schrodinger's Maestro molecular modeling platform, the crystal structure (PDB ID: 1SO2) was converted to a molecular model via the protein preparation work flow. The three additional monomers were removed leaving only chain "A" and its associated waters and ligands. Appropriate bond orders were assigned, hydrogens were added, and metals were assigned charge and co-ordination states. There were several residues in the structure that had incomplete or missing side chains, (Leu659, Asp660, Leu661, Ile662, Lys687, Asn765, Gly797, Ser1053, and Arg1055d) these were filled in accordingly. Two detergent molecules and one additional metal ion (not in the active site) were deleted along with any waters within 5 Å of them. The orientations of the water molecules were sampled and the model was minimized to an RMSD of 0.3 Å.

In the Glide docking experiments the binding site was defined as all residues within a 20 Å centroid around the crystal structure's MERCK1 ligand. The ligands were pre-processed, apposite hydrogens were added to the structure, followed by minimization using the OPLS_2005 force field. Multiple models of each ligand were generated for different ionization ($5 \leq pH \leq 9$) and tautomeric states. High energy tautomeric states were retained.

In each docking experiment only the top scoring pose was retained for each ligand. The gScores are calculated by evaluating and combining a number of interactions between the ligand as follows: gScore = 0.05 * (Van der Waals energy term) + 0.015 * (Coulomb energy term) + (Lipophilic term) + (Hydrogen bonding term) + (Metal-binding term) + (Rewards and Penalties term) + (Rotatable bonds penalty term) + (Polar interactions term).

The virtual library was constructed using ChemAxon's JChem Reactor.[158] A structural index of available amines was generated using JChem for Excel.[193]

General Information

All chemical reagents acquired from Sigma-Aldrich, Fluka, Merck, Chem-Impex, Alfa Aesar, TCI-GR, Auspep and Accela ChemBio were used without further purification. Where indicated solvents were degassed by thoroughly purging with nitrogen prior to use. Analytical TLC was performed using Merck silica gel 60 F_{254}, 20 cm × 20 cm aluminium sheets. Flash chromatography was carried out using Scharlau silica gel 60, 0.06 - 0.20 mm (70-230 mesh ASTM). ^{1}H-NMR was recorded with either a 300 MHz Varian wide bore NMR spectrometer or a 400 MHz Bruker Ultrashield-Advance III NMR spectrometer. ^{13}C-NMR spectra were recorded with a 400 MHz Bruker Ultrashield-Advance III NMR spectrometer. Results were recorded as follows: chemical shift values are expressed as δ units acquired in either $CDCl_3$ (^{1}H 7.26 ppm, ^{13}C 77.16 ppm), D_2O (^{1}H 4.79), $(CD_3)_2SO$ (^{1}H 2.50 ppm, ^{13}C 39.52 ppm) or CD_3OD (^{1}H 3.31 ppm, ^{13}C 49.00 ppm) as references, multiplicity (s = singlet, d = doublet, t = triplet, q = quartet, m = multiplet, dd = doublet of doublets, dt = a doublet of triplets), coupling constants (*J*) in Hertz, and integration. Mass spectra were acquired in the positive and negative mode using an atmospheric pressure (ESI/APCI) ion source on either a Micromass Platform II/ESI/APCI single quadrupole mass spectrometer with sample management facilitated by an Agilent 1100 series HPLC system using MassLynx version 3.5 or an Agilent 6100 Series single quadrupole mass spectrometer with sample management facilitated by an Agilent 1200 series HPLC system using MassLynx version 3.5. High Resolution Mass Spectrometry analyses were collected on a Waters Micromass LCT Premier XE Orthogonal Acceleration Time-of-Flight Mass Spectrometer coupled to an Alliance 2795 Separation Module using MassLynx version 4.1 software. Preparative RP-HPLC was obtained on a Waters 600 HPLC system with UV detection at 254 nM. Gradient elution through a Phenomonex Luna C8 column (250 × 20 mm ID), 20-90% Buffer B (Buffer A: H_2O, 0.1% TFA; Buffer A: H_2O, 0.1% TFA; Buffer B: 80% CH_3CN, 0.1% TFA, 19.9% H_2O or Buffer B: 80% MeOH, 0.1% TFA, 19.9% H_2O) over 15 minutes at 10 ml/min. Melting point determination was performed uncorrected using a Mettler Toledo MP50 melting point apparatus. Microwave chemistry was performed using a Biotage Initiator Microwave Reactor. In cases where a compound has been reported previously, a reference is provided.

General Methods

General Method A: Reductive amination of amino acid esters and nitrobenzaldehydes

The selected amino acid alkyl ester hydrochloride (2.4 equiv.) and sodium acetate (2 equiv.) were warmed in ethanol (3 ml / mmol) and stirred overnight at RT. The mixture was filtered and the selected nitrobenzaldehyde (1 equiv.) was added to the filtrate. The solution was stirred at RT for 30 mins, sodium cyanoborohydride (0.6 equiv.) was added and stirring continued for 4 h. The mixture was concentrated under reduced pressure and taken up in ethyl acetate. The organic layer was washed with sat. $NaHCO_3$ thrice and brine once. The organic layer was then dried over sodium sulfate, filtered and concentrated under reduced pressure to give the desired product as an oil. If necessary the product was purified by column chromatography using 3/1 Hexane/Ethyl acetate as the eluent.

General Method B: Catalytic hydrogenation of aromatic nitro to amine

In a round bottom flask, the required alkyl 2-(2-nitrobenzylamino)acetate was dissolved in ethanol (5 ml / mmol) and 10% palladium on carbon (40 mg / mmol) was added. The flask was evacuated and blanketed with hydrogen three times, and stirred at room temperature for 16 h. The mixture was filtered through a pad of celite, and the filtrate was concentrated under reduced pressure. If necessary the product was purified by column chromatography using 3/1 Ethyl acetate/Hexane as the eluent.

General Method C: Cyclization with cyanogen bromide

In a round bottom flask, the appropriate alkyl 2-(2-aminobenzylamino)acetate (1 equiv) was dissolved in ethanol (10 ml / mmol), cyanogen bromide (1.1 equiv) was added and the reaction was stirred overnight at room temperature. Concentrated ammonia solution (1 ml / mmol) was added and stirring continued for 1 h. The product was collected by filtration and washed sparingly with ethanol and ether.

General Method D: Imidazoquinazolinone ester hydrolysis

The specified ethyl ester was dissolved in water (30 ml / mmol), ethanol (10 ml / mmol), and 2M sodium hydroxide solution (10 ml / mmol); and stirred at room temperature for 1 hour. The reaction mixture was

neutralized with 1M hydrochloric acid. The precipitate was collected by filtration and washed sparingly with ethanol and ether to give the desired product.

General Method E: Buchwald-Hartwig in t-butanol with potassium t-butoxide

Palladium (II) acetate (0.02 equiv.) and 2-(di-t-butylphosphino)-1,1'-binaphthyl (0.04 equiv.) were added to an oven dried round-bottomed flask equipped with a magnetic stirrer bar. The flask was sealed, and evacuated. Degassed t-butanol (1 ml) was added by injection. The flask was evacuated and refilled with nitrogen twice. The mixture was stirred at room temperature for 30 minutes to give a catalyst solution. The appropriate amine (if solid) (2 equiv.), 7-bromo-IMQ (**36**) (50 mg, 0.19 mmol), and potassium t-butoxide (5 equiv.) were added to an oven dried microwave vial equipped with a magnetic stirrer bar. The vial was sealed, evacuated and refilled with nitrogen. Degassed t-butanol (10 ml) was added by injection followed by the appropriate amine (if liquid). The mixture was sonicated to give a homogeneous mixture. The catalyst solution was injected and the vial was evacuated and refilled with nitrogen twice. The reaction was stirred at 110 °C for 16 hours in an oil bath. The mixture was vacuum filtered and the crude product was obtained from either the filtrate or filtrand. The crude product was purified by flash column chromatography ($CHCl_3$ → 5% MeOH). The product was further purified by preparatory HPLC (H_2O → 80% ACN) if deemed necessary.

General Method F: Buchwald-Hartwig in t-butanol and toluene with sodium t-butoxide

Tris(dibenzylideneacetone)dipalladium(0) (0.01 equiv.) and 2-(di-t-butylphosphino)-1,1'-binaphthyl (0.02 equiv.) were added to an oven dried round-bottomed flask equipped with a magnetic stirrer bar. The flask was sealed, and evacuated. Degassed toluene (1 ml) was added by injection. The flask was evacuated and refilled with nitrogen twice. The mixture was stirred at room temperature for 30 minutes to give a catalyst solution. Amine (if solid) (1.5 equiv.), 7-bromo-IMQ (**36**) (50 mg, 0.19 mmol), and sodium t-butoxide (1.5 equiv.) were added to an oven dried microwave vial equipped with a magnetic stirrer bar. The vial was sealed, evacuated and refilled with nitrogen. Degassed t-butanol (10 ml) was added by injection followed by the amine (if liquid). The mixture was sonicated to give a homogeneous mixture. The catalyst solution was injected and the vial was evacuated and refilled with nitrogen twice. The reaction was stirred at 110 °C for

16 hours in an oil bath. The mixture was vacuum filtered and the crude product was obtained from either the filtrate or filtrand. The crude product was purified by flash column chromatography ($CHCl_3$ → 5% MeOH). The product was further purified by preparatory HPLC (H_2O → 80% ACN) if deemed necessary.

General Method G: Chan-Lam couplings

Imidazolidin-4-one (50 mg, 0.58 mmol), aryl boronic acid (2 equiv.), copper (II) acetate (1.5 equiv.) and triethylamine (2 equiv.) were added to an RBF (250 ml) charged with DCM (20 ml) over activated molecular sieves. The reaction vessel was stoppered and stirred for 16 – 64 h at room temperature. The mixture was diluted with methanol (50 ml), filtered through celite, and washed through with additional methanol (10 ml). The filtrate was concentrated under reduced pressure. The resulting oil was taken up in ethyl acetate and washed twice with concentrated ammonia solution. The organic layer was dried over magnesium sulfate, filtered, and concentrated under reduced pressure. The crude product was purified by column chromatography using THF (5-10%) in DCM as the eluent.

General Method H: Reductive Amination of imidazolidin-4-one and aromatic aldehydes

Imidazolidin-4-one (**111**) (1 equiv) was dissolved in DCM (3 ml) over activated molecular sieves. The appropriate aldehyde (1.5 equiv) was added and the mixture was stirred for 20 mins at RT. Sodium triacetoxyborohydride (2 equiv) was added and the reaction was stirred for 16 h. The mixture was diluted with methanol and filtered through a pad of celite. The celite was washed through with additional methanol. The filtrate was concentrated under reduced pressure. The resulting residue was purified by column chromatography using 5% methanol in chloroform.

Chapter Two Compounds

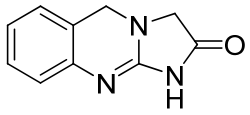

3,5-dihydroimidazo[2,1-b]quinazolin-2(1H)-one (**10**) [124]

Ethyl 2-(2-aminobenzylamino)acetate (**20**) (1.77 g, 8.49 mmol) was reacted according to General Method C, to give a tan solid (943 mg, 59%). ^{1}H-NMR (400 MHz, CDCl3) δ 7.30 (t, J = 7.7 Hz, 1H), 7.21 (t, J = 7.6 Hz, 1H), 7.11 (d, J = 7.6 Hz, 1H), 7.07 (d, J = 7.9 Hz, 1H), 4.74 (s, 2H), 4.19 (s, 2H). ^{13}C-NMR (101 MHz, CDCl3) δ 168.46, 153.76, 129.9, 127.12, 126.92, 117.97, 116.59, 115.85, 51.63, 44.92. ESI-HRMS, Found 188.0821 $[M+H]^+$ $C_{10}H_9N_3O$ requires 188.0824 $[M+H]^+$.

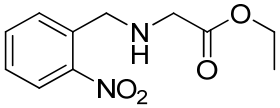

ethyl 2-(2-nitrobenzylamino)acetate (**19**) [124]

Glycine ethyl ester hydrochloride (5.31 g, 38.1 mmol) and 2-nitrobenzaldehyde (2.4 g, 15.8 mmol) were reacted according to General Method A to give a yellow oil (2.1 g, 93%). ^{1}H NMR (400 MHz, $CDCl_3$) δ 7.94 (dd, *J* = 8.1, 1.2 Hz, 1H), 7.62 (dd, *J* = 7.7, 1.2 Hz, 1H), 7.57 (td, *J* = 7.5, 1.3 Hz, 1H), 7.40 (td, *J* = 7.6, 1.2 Hz, 1H), 4.16 (q, *J* = 7.1 Hz, 2H), 3.41 (s, 2H), 2.02 (s, 2H), 1.24 (t, *J* = 7.1 Hz, 3H). ^{13}C-NMR (101 MHz, CDCl3) δ 172.29, 149.20, 135.19, 133.33, 131.09, 128.22, 124.94, 60.99, 50.59, 50.30, 14.32. ESI-MS, *m/z* 239.1, 100% $[M+H]^+$.

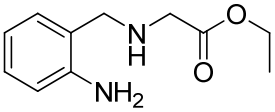

ethyl 2-(2-aminobenzylamino)acetate (**20**) [124]

Ethyl 2-(2-nitrobenzylamino)acetate (**19**) (2.1 g, 8.8 mmol) was reacted according to General Method B to give a dark yellow oil (1.77 g, 96%). ^{1}H-NMR (400 MHz, CDCl3) δ 7.09 (td, J = 7.7, 1.6 Hz, 1H), 7.01 (dd, J = 7.9, 1.5 Hz, 1H), 6.70 – 6.64 (m, 2H), 4.20 (q, J = 7.1 Hz, 2H), 3.79 (s, 2H), 3.39 (s, J = 2.5 Hz, 2H), 1.28

(t, J = 7.1 Hz, 3H). ^{13}C-NMR (101 MHz, CDCl3) δ 172.72, 146.89, 130.31, 128.77, 123.22, 117.84, 115.83, 77.16, 60.94, 52.17, 49.85, 14.36. ESI-MS, *m/z* 209.1, 60% $[M+H]^+$.

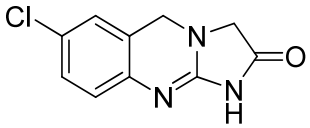

7-chloro-3,5-dihydroimidazo[2,1-b]quinazolin-2(1H)-one (**35**) [129]

Ethyl 2-(2-amino-5-chlorobenzylamino)acetate (**47**) (1.32g, 5.46 mmol) was reacted according to General Method C to give an off white solid (457 mg, 38%). ^{1}H-NMR (400 MHz, DMSO) δ 7.31 – 7.26 (m, 2H), 6.95 (d, J = 8.7 Hz, 1H), 4.51 (s, 2H), 3.82 (s, 2H). ^{13}C-NMR (101 MHz, DMSO) δ 183.19, 165.18, 135.06, 127.88, 126.41, 120.62, 117.95, 53.54, 43.92. ESI-HRMS, Found 222.0435 $[M+H]^+$ $C_{10}H_8ClN_3O$ requires 222.0429 $[M+H]^+$.

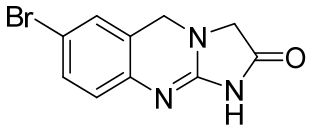

7-bromo-3,5-dihydroimidazo[2,1-b]quinazolin-2(1H)-one (**36**) [124]

Ethyl 2-(2-amino-5-bromobenzylamino)acetate (**55**) (320 mg, 1.1 mmol) was reacted according to General Method C to give a tan solid (234 mg, 79%). ^{1}H-NMR (300 MHz, DMSO) δ 7.60 – 7.49 (m, 2H), 7.11 (d, J = 8.4 Hz, 1H), 4.69 (s, 2H), 4.26 (s, 2H). ^{13}C-NMR (101 MHz, DMSO) δ 183.53, 165.72, 131.45, 130.46, 129.87, 121.16, 119.14, 54.13, 44.5. ESI-HRMS, Found 265.9930 $[M+H]^+$ $C_{10}H_8BrN_3O$ requires 265.9923 $[M+H]^+$.

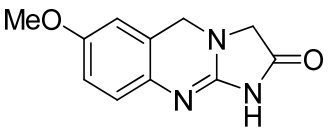

7-methoxy-3,5-dihydroimidazo[2,1-b]quinazolin-2(1H)-one (**37**) [127]

Ethyl 2-(2-amino-5-methoxybenzylamino)acetate (**51**) (203 mg, 0.85 mmol) was reacted according to General Method C to give a tan solid (24 mg, 13%). ^{1}H-NMR (400 MHz, DMSO) δ 6.91 (d, *J* = 8.7 Hz, 1H), 6.83

(dd, *J* = 8.7, 2.8 Hz, 1H), 6.79 (d, *J* = 2.6 Hz, 1H), 4.48 (s, 2H), 3.79 (s, 2H), 3.72 (s, 3H). ^{13}C-NMR (101 MHz, DMSO) δ 184.11, 155.24, 119.41, 116.89, 113.77, 111.57, 55.34, 53.89, 44.64. ESI-HRMS, Found 218.0927 $[M+H]^+$ $C_{11}H_{11}N_3O_2$ requires 218.0924 $[M+H]^+$.

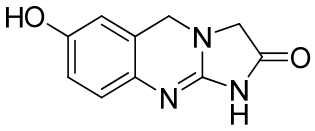

7-hydroxy-3,5-dihydroimidazo[2,1-b]quinazolin-2(1H)-one (**38**) [129]

7-methoxy-3,5-dihydroimidazo[2,1-b]quinazolin-2(1H)-one (**37**) (109 mg, 0.5 mmol) was added to 47% HBr solution (15 ml), the solution was stirred at 110 °C for 1 h. The solution was poured into a beaker of saturated $NaHCO_3$ solution (200 ml). The product was collected by filtration and washed sparingly with ethanol and ether to give a light brown powder (93 mg, 92%). ^{1}H-NMR (400 MHz, DMSO) δ 9.31 (s, 1H), 6.80 (d, J = 8.6 Hz, 1H), 6.64 (dd, J = 8.5, 2.6 Hz, 1H), 6.57 (d, J = 2.5 Hz, 1H), 4.43 (s, 2H), 3.76 (s, 2H). ^{13}C-NMR (101 MHz, DMSO) δ 185.54, 165.28, 154.09, 126.24, 120.42, 117.55, 115.43, 113.40, 54.22, 44.73. ESI-HRMS, Found 204.0793 $[M+H]^+$ $C_{10}H_9N_3O_2$ requires 204.0768 $[M+H]^+$.

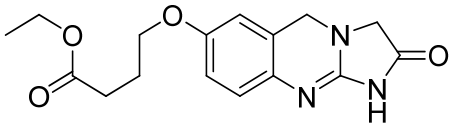

ethyl 4-(2-oxo-1,2,3,5-tetrahydroimidazo[2,1-b]quinazolin-7-yloxy)butanoate (**39**) [111]

ethyl 4-(4-amino-3-((2-methoxy-2-oxoethylamino)methyl)phenoxy)butanoate (**60**) (3.33 g, 9.85 mmol) was reacted according to General Method C to give a tan solid (1.61 g, 57%). ^{1}H-NMR (400 MHz, DMSO) δ 6.90 (d, J = 8.6 Hz, 1H), 6.82 (dd, J = 8.6, 2.8 Hz, 1H), 6.78 (d, J = 2.6 Hz, 1H), 4.47 (s, 2H), 4.07 (q, J = 7.1 Hz, 2H), 3.94 (t, J = 6.3 Hz, 2H), 3.79 (s, 2H), 2.44 (t, J = 7.3 Hz, 2H), 1.94 (p, J = 6.7 Hz, 2H), 1.18 (t, J = 7.1 Hz, 3H). ^{13}C-NMR (101 MHz, DMSO) δ 184.04, 172.85, 165.47, 154.68, 128.31, 119.6, 116.95, 114.32, 112.28, 66.54, 59.59, 53.63, 44.34, 29.78, 23.87, 13.76. ESI-HRMS, Found 318.1455 $[M+H]^+$, 340.1267 $[M+Na]^+$ $C_{16}H_{19}N_3O_4$ requires 318.1454 $[M+H]^+$, 340.1273 $[M+Na]^+$

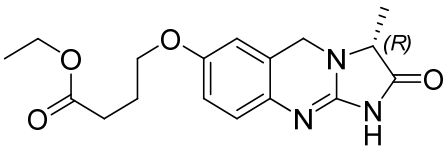

(R)-ethyl 4-(3-methyl-2-oxo-1,2,3,5-tetrahydroimidazo[2,1-b]quinazolin-7-yloxy)butanoate (**40**)

(R)-ethyl 4-(4-amino-3-((1-methoxy-1-oxopropan-2-ylamino)methyl)phenoxy)butanoate (**61**) (323 mg, 0.91 mmol) was reacted according to General Method C to give a tan solid (52 mg, 17%). ^{1}H-NMR (400 MHz, DMSO) δ 6.95 (d, *J* = 8.7 Hz, 1H), 6.84 (dd, *J* = 8.7, 2.7 Hz, 1H), 6.79 (d, *J* = 2.6 Hz, 1H), 4.56 (d, *J* = 14.2 Hz, 1H), 4.43 (d, *J* = 14.1 Hz, 1H), 4.06 (q, *J* = 7.1 Hz, 2H), 3.98 – 3.88 (m, 3H), 2.44 (t, *J* = 7.3 Hz, 2H), 1.98 – 1.90 (m, 2H), 1.30 (d, *J* = 7.1 Hz, 3H), 1.18 (t, *J* = 7.1 Hz, 3H). ^{13}C-NMR (101 MHz, DMSO) δ 184.26, 172.55, 154.82, 127.27, 119.21, 117.28, 114.43, 112.48, 66.54, 59.57, 58.72, 42.57, 29.80, 23.85, 13.84, 13.30. ESI-HRMS, Found 332.1605 $[M+H]^+$, 354.1426 $[M+Na]^+$ $C_{17}H_{21}N_3O_4$ requires 332.1610 $[M+H]^+$, 354.1430 $[M+Na]^+$

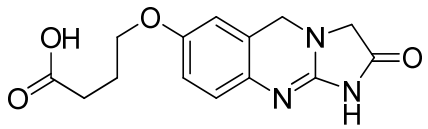

4-(2-oxo-1,2,3,5-tetrahydroimidazo[2,1-b]quinazolin-7-yloxy)butanoic acid (**41**) [111]

ethyl 4-(2-oxo-1,2,3,5-tetrahydroimidazo[2,1-b]quinazolin-7-yloxy)butanoate (**39**) (1.55 g, 4.89 mmol) was reacted according to General Method D to give a tan solid (1.39 g, 98%). ^{1}H-NMR (400 MHz, DMSO) δ 6.89 (d, *J* = 8.6 Hz, 1H), 6.81 (dd, *J* = 8.6, 2.7 Hz, 1H), 6.78 (d, *J* = 2.5 Hz, 1H), 4.47 (s, 2H), 3.90 (t, *J* = 6.8 Hz, 2H), 3.78 (s, 2H), 2.02 (t, *J* = 7.0 Hz, 2H), 1.88 – 1.77 (m, 2H). ^{13}C-NMR (101 MHz, DMSO) δ 184.39, 174.40, 165.99, 119.62, 117.66, 114.93, 112.87, 68.21, 54.27, 44.99, 33.14, 25.84. ESI-HRMS, Found 288.0986 $[M-H]^-$, 312.0956 $[M+Na]^+$ $C_{14}H_{15}N_3O_4$ requires 288.0984 $[M-H]^-$, 312.0960 $[M+Na]^+$.

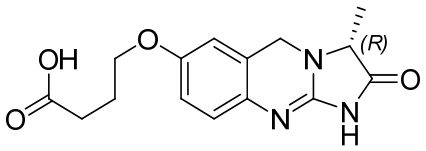

(R)-4-(3-methyl-2-oxo-1,2,3,5-tetrahydroimidazo[2,1-b]quinazolin-7-yloxy)butanoic acid (**42**)

(R)-ethyl 4-(3-methyl-2-oxo-1,2,3,5-tetrahydroimidazo[2,1-b]quinazolin-7-yloxy)butanoate (**40**) (41 mg, 0.12 mmol) was reacted according to General Method D to give an off white solid (24 mg, 65%). ^{1}H-NMR (400 MHz, DMSO) δ 6.89 (d, *J* = 8.7 Hz, 1H), 6.82 (dd, *J* = 8.7, 2.6 Hz, 1H), 6.79 (d, *J* = 2.6 Hz, 1H), 4.51 (d, *J* = 14.2 Hz, 1H), 4.40 (d, *J* = 14.0 Hz, 1H), 3.93 (t, *J* = 6.4 Hz, 2H), 3.79 (q, *J* = 7.1 Hz, 1H), 2.36 (t, *J* = 7.3 Hz, 2H), 1.95 – 1.86 (m, 2H), 1.26 (d, *J* = 7.0 Hz, 3H). ^{13}C-NMR (101 MHz, DMSO) δ 174.09, 115.89, 114.31, 112.46, 66.60, 58.78, 42.64, 39.52, 29.67, 24.02, 13.56. ESI-HRMS, Found 302.1145 $[M-H]^-$, 304.1291 $[M+H]^+$, 326.1109 $[M+Na]^+$ $C_{15}H_{17}N_3O_4$ requires 302.1141 $[M-H]^-$, 304.1297 $[M+H]^+$, 326.1117 $[M+Na]^+$.

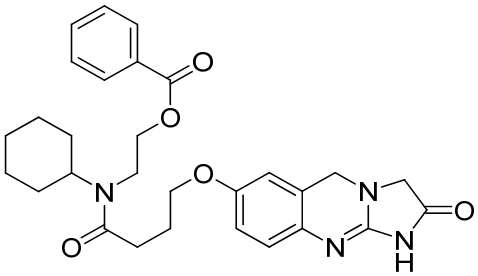

2-(N-cyclohexyl-4-(2-oxo-1,2,3,5-tetrahydroimidazo[2,1-b]quinazolin-7-yloxy)butanamido)ethyl benzoate (**43**) [111]

4-(2-oxo-1,2,3,5-tetrahydroimidazo[2,1-b]quinazolin-7-yloxy)butanoic acid (**41**) (55 mg, 0.19 mmol) and HBTU (90 mg, 0.21 mmol) were stirred in DMF (8 ml) for 20 mins at room temperature. Triethylamine (32 µl, 0.23 mmol) and *2-(cyclohexylamino)ethyl benzoate* (**140**) (52 mg, 0.21 mmol) were added and the reaction was stirred overnight at room temperature. The mixture was concentrated under reduced pressure, taken up in ethyl acetate (100 ml), washed with saturated $NaHCO_3$ solution (2 × 50 ml) and brine (50 ml). The organic layer was dried over sodium sulfate, filtered and concentrated under reduced pressure. The resulting residue was purified by flash column chromatography using 19/1 CHCl3/MeOH as eluent to give a yellow oil (12 mg, 12%). ^{1}H-NMR (400 MHz, $CDCl_3$) δ 7.95 (d, *J* = 8.4 Hz, 2H), 7.55 – 7.44 (m, 1H), 7.41 –

7.20 (m, 4H), 6.75 – 6.62 (m, 1H), 6.51 – 6.41 (m, 1H), 4.52 – 4.39 (m, 2H), 4.34 (t, *J* = 6.7 Hz, 2H), 3.95 – 3.77 (m, 4H), 3.58 – 3.48 (m, 3H), 2.58 – 2.45 (m, 2H), 2.09 – 1.99 (m, 2H), 1.80 – 1.55 (m, 5H), 1.47 – 1.16 (m, 5H). ^{13}C-NMR (101 MHz, DMSO) δ 172.34, 170.71, 166.07, 133.02, 129.6, 128.43, 126.02, 118.81, 114.95, 111.95, 67.19, 62.58, 56.71, 53.20, 45.11, 40.36, 31.40, 29.51, 25.57, 25, 24.67. ESI-HRMS, Found 519.2614 $[M+H]^+$ $C_{29}H_{34}N_4O_5$ requires 519.2602 $[M+H]^+$.

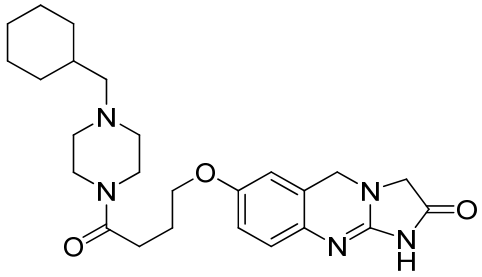

7-(4-(4-(cyclohexylmethyl)piperazin-1-yl)-4-oxobutoxy)-3,5-dihydroimidazo[2,1-b]quinazolin-2(1H)-one (**44**) [132]

4-(2-oxo-1,2,3,5-tetrahydroimidazo[2,1-b]quinazolin-7-yloxy)butanoic acid (**41**) (116 mg, 0.4 mmol) and triethylamine (134 µl, 1 mmol) were dissolved in THF (6 ml), 1-ethyl-3-(3-dimethylaminopropyl) carbodiimide hydrochloride (158 mg, 0.8 mmol) was added and the mixture was stirred for 10 minutes at room temperature. 1-(cyclohexylmethyl)piperazine (131 µl, 0.7 mmol) was added and stirring continued for 24 hours. The reaction mixture was concentrated under reduced pressure, taken up in DCM (20 ml), and washed with water (3 × 20 ml). The organic layer was concentrated under reduced pressure, and the residue purified by preparatory RP-HPLC. Purified product was freeze dried to give a pale yellow solid (11 mg, 6%). Insufficient material remained for ^{13}C-NMR after the majority was used in activity assays. ^{1}H-NMR (300MHz, $CDCl_3$): 7.5 (d, *J* = 8.4 Hz, 1H), 6.78 (d, *J* = 7.8 Hz, 1H), 6.48 (s, 1H), 4.47 (s, 2H), 3.95 (t, *J* = 5.4 Hz, 2H), 3.83 (s, 2H), 3.61 (bs, 2H), 3.47 (bs, 2H), 2.5 (t, 2H), 2.36 (bs, 4H), 2.1 (m, 4H), 1.73 (m, 4H), 1.47 (m, 1H), 1.24 (m, 4H), 0.88 (m, 2H). ESI-HRMS, Found 454.2825 $[M+H]^+$ $C_{25}H_{35}N_5O_3$ requires 454.2813 $[M+H]^+$.

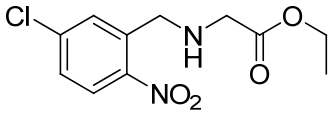

ethyl 2-(5-chloro-2-nitrobenzylamino)acetate (**46**) [194]

Glycine ethyl ester hydrochloride (1.8 g, 12.9 mmol) and 5-chloro-2-nitrobenzaldehyde (1.02 g, 5.39 mmol) were reacted according to General Method A to give a dark yellow oil (1.43 g, 95%). ^{1}H-NMR (300MHz, CDCl3) δ 7.95 (d, J = 8.7 Hz, 1H), 7.73 (d, J = 2.4 Hz, 1H), 7.38 (dd, J = 8.7, 2.4 Hz, 1H), 4.20 (q, J = 7.2 Hz, 2H), 4.12 (s, 2H), 3.44 (s, 2H), 1.28 (t, J = 7.2 Hz, 1H). ESI-MS, *m/z* 273.2, 100% $[M+H]^{+}$.

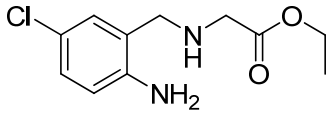

ethyl 2-(2-amino-5-chlorobenzylamino)acetate (**47**) [194]

ethyl 2-(5-chloro-2-nitrobenzylamino)acetate (**46**) (1.42 g, 5.24 mmol) was reacted according to General Method B to give a brown oil (1.25 g, 98%). ^{1}H-NMR (300 MHz, $CDCl_3$) δ 7.04 (dd, *J* = 8.2, 2.2 Hz, 1H), 7.00 (d, *J* = 2.1 Hz, 1H), 6.57 (d, *J* = 8.4 Hz, 1H), 4.21 (q, *J* = 6.9 Hz, 2H), 3.75 (s, 2H), 3.38 (s, 2H), 1.29 (t, *J* = 6.9 Hz, 3H). ESI-MS, *m/z* 243.2, 50% $[M+H]^{+}$.

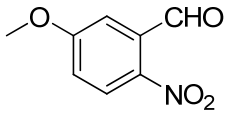

5-methoxy-2-nitrobenzaldehyde (**49**) [195]

5-hydroxy-2-nitrobenzaldehyde (2 g, 12 mmol) and Cs_2Co_3 (3.9 g, 12 mmol) were dissolved in DMF (15 ml) and cooled to 0 °C. Methyl iodide (1.7 g, 12 mmol) was added dropwise and the reaction was stirred at RT for 3 d. The mixture was poured into saturated $NaHCO_3$ solution (250 ml) and extracted with ethyl acetate (7 × 50 ml). The combined organic extracts were dried over sodium sulfate, filtered and concentrated under reduced pressure to give a yellow solid (2.08 g, 96%). ^{1}H-NMR (400 MHz, CDCl3) δ 10.48 (s, 1H), 8.16 (d, J = 9.1 Hz, 1H), 7.33 (d, J = 2.9 Hz, 1H), 7.16 (dd, J = 9.1, 2.9 Hz, 1H), 3.96 (s, 3H). ^{13}C-NMR (101 MHz, CDCl3) δ 188.64, 163.94, 142.12, 134.17, 127.24, 118.56, 113.05, 56.04. ESI-MS, *m/z* 180.2, 50% $[M-H]^{-}$.

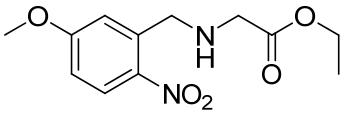

ethyl 2-(5-methoxy-2-nitrobenzylamino)acetate (**50**) [124]

Glycine ethyl ester hydrochloride (407 mg, 2.92 mmol) and *5-methoxy-2-nitrobenzaldehyde* (**49**) (220 mg, 1.22 mmol) were reacted according to General Method A to give a yellow oil (286 mg, 88%). ^{1}H-NMR (300 MHz, CDCl3) δ 8.10 (d, J = 9.1 Hz, 1H), 7.18 (d, J = 2.6 Hz, 1H), 6.86 (dd, J = 9.1, 2.7 Hz, 1H), 4.24 – 4.12 (m, 4H), 3.90 (s, 3H), 3.48 (s, 2H), 1.27 (t, J = 7.1 Hz, 3H). ESI-MS, *m/z* 269.4, 100% $[M+H]^{+}$.

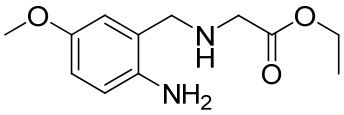

ethyl 2-(2-amino-5-methoxybenzylamino)acetate (**51**) [124]

ethyl 2-(5-methoxy-2-nitrobenzylamino)acetate (**50**) (275 mg, 1.02 mmol) was reacted according to General Method B to give a dark yellow oil (216 mg, 89%). ^{1}H-NMR (300 MHz, CDCl3) δ 6.70 (dd, J = 8.4, 2.8 Hz, 1H), 6.66 (d, J = 2.7 Hz, 1H), 6.63 (d, J = 8.4 Hz, 1H), 4.21 (q, J = 7.1 Hz, 2H), 3.79 (s, 2H), 3.74 (s, 3H), 3.42 (s, 2H), 1.29 (t, J = 7.1 Hz, 3H). ESI-MS, *m/z* 239.4, 100% $[M+H]^{+}$.

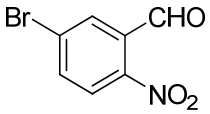

5-bromo-2-nitrobenzaldehyde (**53**) [196]

3-bromobenzaldehyde (3 g, 16.2 mmol) was added over 10 minutes to a mixture of fuming nitric acid (1.6 ml) and sulfuric acid (19.5 ml) at 0 °C and stirred for 3 h. The reaction mixture was poured onto ice (60 g) and the precipitate was collected by filtration. The precipitate was dissolved in methanol (10 ml), dried over sodium sulfate and filtered. The filtrate was stripped of solvent and the resulting residue was recrystallised from hot hexane to give yellow needle like crystals (2.47 g; 66%). Mp: 69-71.5°C (lit. 63-66).[196] ^{1}H-NMR (400 MHz, CDCl3) δ 10.42 (s, 1H), 8.07 (d, J = 2.2 Hz, 1H), 8.03 (d, J = 8.6 Hz, 1H), 7.89 (dd, J = 8.6, 2.2 Hz, 1H). ^{13}C-NMR (101 MHz, CDCl3) δ 186.75, 148.03, 136.36, 132.59, 132.40, 129.49, 126.17. ESI-MS, *m/z* 228.2, 230.2, 90% $[M-H]^{-}$.

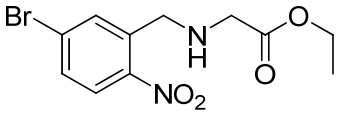

ethyl 2-(5-bromo-2-nitrobenzylamino)acetate (**54**)

Glycine ethyl ester hydrochloride (4.88 g, 34.9 mmol) and *5-bromo-2-nitrobenzaldehyde* (**53**) (3.09 g, 13.43 mmol) were reacted according to General Method A to give a yellow oil (2.73 g, 64%). ^{1}H-NMR (300 MHz, CDCl3) δ 7.95 (d, J = 2.2 Hz, 1H), 7.92 (d, J = 8.7 Hz, 1H), 7.61 (dd, J = 8.6, 2.2 Hz, 1H), 4.25 (q, J = 7.1 Hz, 2H), 4.16 (s, 2H), 3.49 (s, 2H), 1.34 (t, J = 7.1 Hz, 3H). ESI-MS, *m/z* 317.3, 319.3, 100% $[M+H]^{+}$.

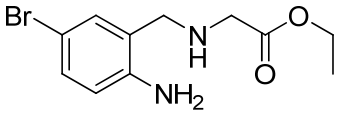

ethyl 2-(2-amino-5-bromobenzylamino)acetate (**55**)

In a round bottom flask *ethyl 2-(5-bromo-2-nitrobenzylamino)acetate* (**54**) (375 mg, 1.28 mmol) was dissolved in a mixture of ethanol (30 ml), water (8 ml) and 1M HCl (4 ml). Iron powder (340 mg, 6.09 mmol) was added and the mixture was stirred at 45 °C for 2 h. The mixture was filtered through celite and the filtrate was neutralized with 1M NaOH. The solution was extracted with DCM (3 × 50 ml); the combined organic layers were dried over sodium sulfate and filtered. The filtrate was concentrated under reduced pressure and the resulting residue was purified by flash column chromatography using 9/1 EtOAc/MeOH as the eluent. The product was isolated as a brown oil (178 mg, 52%). ^{1}H-NMR (300 MHz, CDCl3) δ 7.23 (dd, J = 8.4, 2.3 Hz, 1H), 7.18 (d, J = 2.2 Hz, 1H), 6.59 (d, J = 8.3 Hz, 1H), 4.26 (q, J = 7.1 Hz, 2H), 3.80 (s, 2H), 3.43 (s, 2H), 1.35 (t, J = 7.2 Hz, 3H). ESI-MS, *m/z* 283, 285, 100% $[M-4]^{+}$.

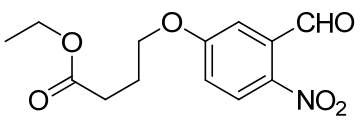

ethyl 4-(3-formyl-4-nitrophenoxy)butanoate (**57**) [127]

5-Hydroxy-2-nitrobenzaldehyde (465 mg, 2.78 mmol) ethyl-4-bromobutyrate (511 µL, 3.54 mmol) and potassium carbonate (501 mg, 3.63 mmol) were dissolved in DMF (5 ml) and stirred at 100 °C for 1 h. The reaction mixture was concentrated under reduced pressure and the residue was taken up in EtOAc (50 ml).

The organic layer was washed with saturated $NaHCO_3$ (3 × 20 ml) and brine (2 × 20 ml) then dried over sodium sulfate and filtered. The filtrate was concentrated under reduced pressure to give a yellow oil (765 mg, 98%). ^{1}H-NMR (300 MHz, $CDCl_3$) δ 10.51 (s, 1H), 8.20 (d, *J* = 9.1 Hz, 1H), 7.35 (d, *J* = 2.8 Hz, 1H), 7.19 (dd, *J* = 9.1, 2.8 Hz, 1H), 4.25 – 4.11 (m, 4H), 2.57 (t, *J* = 7.2 Hz, 2H), 2.21 (p, *J* = 6.6 Hz, 2H), 1.31 (t, *J* = 7.1 Hz, 3H). ESI-MS, *m/z* 282.2, 80% $[M+H]^+$.

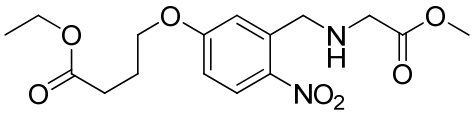

ethyl 4-(3-((2-methoxy-2-oxoethylamino)methyl)-4-nitrophenoxy)butanoate (**58**)

Glycine methyl ester hydrochloride (245 mg, 1.95 mmol) and *ethyl 4-(3-formyl-4-nitrophenoxy)butanoate* (**57**) (124 mg, 0.48 mmol) were reacted according to General Method A to give a yellow oil (84 mg, 49%). ^{1}H-NMR (300MHz, CDCl3) δ 8.09 (d, J = 9.3 Hz, 1H), 7.19 (d, J = 2.4 Hz, 1H), 6.86 (dd, J = 2.4, 9.3 Hz, 1H), 4.15 (m, 4H), 3.74 (s, 3H), 3.5 (s, 2H), 2.52 (t, J = 7.2 Hz, 2H), 2.34 (bs, 1H), 2.15 (m, J = 6.6 Hz, 2H), 1.27 (t, J = 7.2 Hz, 3H). ESI-MS, *m/z* 355.3, 100% $[M+H]^+$.

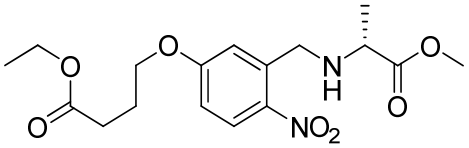

(R)-ethyl 4-(3-((1-methoxy-1-oxopropan-2-ylamino)methyl)-4-nitrophenoxy)butanoate (**59**)

D-alanine methyl ester hydrochloride (360 mg, 2.87 mmol) and *ethyl 4-(3-formyl-4-nitrophenoxy)butanoate* (340 mg, 1.2 mmol) were reacted according to General Method A to give a brown oil (411 mg, 93%). ^{1}H-NMR (300MHz, CDCl3) δ 8.07 (d, J = 9 Hz, 1H), 7.17 (d, J = 2.1 Hz, 1H), 6.84 (dd, J = 9, 2.4 Hz, 1H), 4.15 (m, 6H), 3.72 (s, 3H), 3.4 (m, 1H), 2.53 (t, J = 7.2 Hz, 2H), 2.15 (p, J = 6.6 Hz, 2H), 1.35 (d, J = 6.9 Hz, 3H), 1.28 (t, J = 7.2 Hz, 3H). ESI-MS, *m/z* 369.4, 70% $[M+H]^+$.

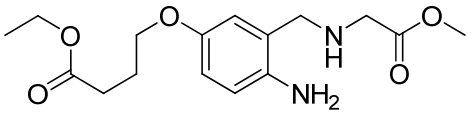

ethyl 4-(4-amino-3-((2-methoxy-2-oxoethylamino)methyl)phenoxy)butanoate (**60**)

ethyl 4-(3-((2-methoxy-2-oxoethylamino)methyl)-4-nitrophenoxy)butanoate (**58**) (84 mg, 0.24 mmol) was reacted according to General Method B to give a brown oil (64 mg, 69%). ^{1}H-NMR (300MHz, $CDCl_3$) δ 6.64 (m, 3H), 4.14 (q, *J* = 7.2 Hz, 2H), 3.92 (t, *J* = 6 Hz, 2H), 3.78 (s, 2H), 3.74 (s, 3H), 3.42 (s, 2H), 2.49 (t, *J* = 7.2 Hz, 2H), 2.06 (p, *J* = 6.6 Hz, 2H), 1.26 (t, *J* = 7.2 Hz, 3H). ESI-MS, *m/z* 325.2, 40% $[M+H]^+$.

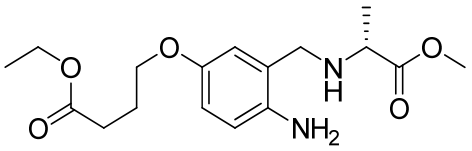

(R)-ethyl 4-(4-amino-3-((1-methoxy-1-oxopropan-2-ylamino)methyl)phenoxy)butanoate (**61**)

(R)-ethyl 4-(3-((1-methoxy-1-oxopropan-2-ylamino)methyl)-4-nitrophenoxy)butanoate (**59**) (411 mg, 1.12 mmol) was reacted according to General Method B to give a brown oil (323 mg, 72%). ^{1}H-NMR (300MHz, $CDCl_3$) δ 6.63 (m, 3H), 4.17 (m, 4H), 3.92 (t, *J* = 6.4 Hz, 2H), 3.76 (s, 3H), 3.38 (m, 1H), 2.5 (t, *J* = 7.2 Hz, 2H), 2.06 (p, *J* = 6.7 Hz, 2H), 1.28 (m, 6H). ESI-MS, *m/z* 339.3, 20% $[M+H]^+$.

Chapter Four Compounds

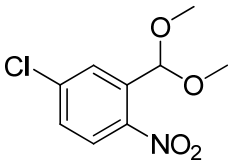

4-chloro-2-(dimethoxymethyl)-1-nitrobenzene (**81**) [195]

5-Chloro-2-nitrobenzaldehyde (3 g, 16.17 mmol) and p-toluenesulfonic acid monohydrate (0.87 g, 0.46 mmol) were dissolved in methanol (30 ml) with molecular sieves and refluxed overnight. The mixture was filtered through celite to remove partially crushed molecular sieves. The filtrate was concentrated under reduced pressure and the residue was taken up in saturated $NaHCO_3$ solution (250 ml) and extracted with ether (3 × 100 ml). The combined organic layers were dried over sodium sulfate, filtered and concentrated under reduced pressure to give a light yellow oil (3.36 g, 90%). ^{1}H-NMR (400 MHz, CDCl3) δ 7.82 (d, J =

8.6 Hz, 1H), 7.80 (d, J = 2.4 Hz, 1H), 7.45 (dd, J = 8.6, 2.3 Hz, 1H), 5.93 (s, 1H), 3.42 (s, 6H). ^{13}C-NMR (101 MHz, CDCl3) δ 147.01, 139.15, 134.89, 129.38, 128.53, 125.82, 99.34, 54.75. ESI-MS, *m/z* 200.0, 100% $[M\text{-}CH_3O]^{+}$.

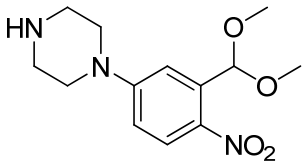

1-(3-(dimethoxymethyl)-4-nitrophenyl)piperazine (**82**)

Piperazine (4.1 g, 47.62 mmol) and potassium iodide (1.58 g, 9.52) were dissolved in DMF (50 ml) and heated to 90 °C with stirring. A solution of *4-chloro-2-(dimethoxymethyl)-1-nitrobenzene* (**81**) (2.2 g, 9.52 mmol) in DMF (20 ml) was added dropwise over 20 mins, and stirring continued at 90 °C for 4 h. The reaction mixture was concentrated under reduced pressure then partitioned between DCM (100 ml) and 1M NaOH (250 ml). The aqueous layer was extracted with DCM (2 × 100 ml), the combined organic layers were washed with brine (50 ml) then dried over sodium sulfate and filtered. The filtrate was concentrated under reduced pressure and purified by flash column chromatography using 189/10/1 $CHCl_3$/MeOH/NH_4OH as eluent. The product was obtained as an orange oil (0.84 g, 32%). ^{1}H-NMR (400 MHz, CDCl3) δ 8.03 (d, J = 9.2 Hz, 1H), 7.21 (d, J = 2.9 Hz, 1H), 6.78 (dd, J = 9.3, 3.0 Hz, 1H), 6.08 (s, 1H), 3.47 (s, 6H), 3.43 – 3.38 (m, 4H), 3.06 – 3.00 (m, 4H). ^{13}C-NMR (101 MHz, CDCl3) δ 154.22, 138.15, 135.98, 127.88, 112.52, 111.62, 100.90, 55.46, 48.02, 45.66. ESI-MS, *m/z* 282.4, 100% $[M+H]^{+}$.

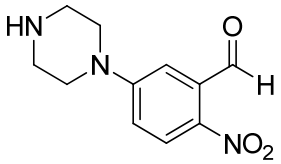

2-nitro-5-(piperazin-1-yl)benzaldehyde (**83**) [195]

1-(3-(dimethoxymethyl)-4-nitrophenyl)piperazine (**82**) (0.85 g, 3.02 mmol) was dissolved in iospropanol (15 ml) and 1M HCl (15 ml) and the solution was refluxed for 2 h. After cooling, saturated $NaHCO_3$ solution (50 ml) was added to quench the reaction. The reaction mixture was extracted with DCM (3 × 50 ml) and the combined organic layers were washed with brine (50 ml). The organic layer was dried over sodium sulfate,

filtered and concentrated under reduced pressure to give an orange solid (0.65 g, 91%). ^{1}H-NMR (300 MHz, CDCl3) δ 10.53 (s, 1H), 8.11 (d, J = 9.0 Hz, 1H), 7.15 (d, J = 3.2 Hz, 1H), 6.95 (dd, J = 9.3, 2.9 Hz, 1H), 3.47 (t, J = 5.2 Hz, 4H), 3.05 (t, J = 5.1 Hz, 4H). ^{13}C-NMR (101 MHz, CDCl3) δ 190.13, 173.42, 158.72, 151.18, 127.74, 115.36, 112.61, 47.99, 45.73. ESI-MS, *m/z* 236.1, 100% $[M+H]^{+}$.

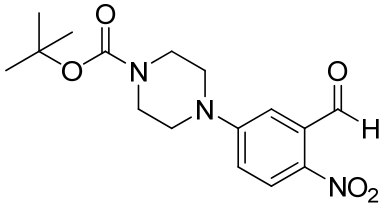

tert-butyl 4-(3-formyl-4-nitrophenyl)piperazine-1-carboxylate (**84**)

2-nitro-5-(piperazin-1-yl)benzaldehyde (0.95 g, 4.03 mmol) and $NaHCO_3$ (0.68 g, 8.05 mmol) were dissolved in THF (30 ml) and water (1 ml). While stirring at room temperature under nitrogen, a solution of Di-*tert*-butyl dicarbonate (1.76 g, 8.05 mmol) in THF (30 ml) was added dropwise over 2 h. Stirring continued at RT for an additional 3 h. The reaction was diluted with ethyl acetate (200 ml) and washed with saturated $NaHCO_3$ solution (2 × 50 ml) and brine (50 ml). The organic layer was collected, dried over sodium sulfate, filtered and concentrated under reduced pressure. The residue was purified by column chromatography using 1/3 EtOAc/Hex to give an orange solid (1.18 g, 87%). ^{1}H-NMR (400 MHz, CDCl3) δ 10.55 (s, 1H), 8.15 (d, J = 9.3 Hz, 1H), 7.16 (d, J = 3.0 Hz, 1H), 6.97 (dd, J = 9.3, 3.0 Hz, 1H), 3.67 – 3.59 (m, 4H), 3.53 – 3.47 (m, 4H), 1.51 (s, 9H). ^{13}C-NMR (101 MHz, CDCl3) δ 189.75, 153.84, 138.64, 134.75, 127.60, 115.43, 112.60, 46.67, 28.38. ESI-MS, *m/z* 336.3, 20% $[M+H]^{+}$ 350.3, 100% $[M+15]^{+}$.[161]

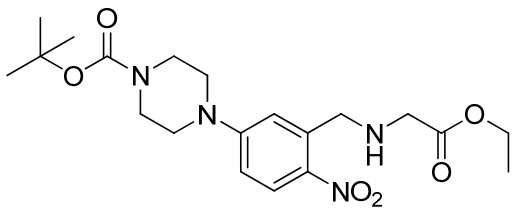

tert-butyl 4-(3-((2-ethoxy-2-oxoethylamino)methyl)-4-nitrophenyl)piperazine-1-carboxylate (**85**)

Glycine ethyl ester hydrochloride (1.26 g, 9.06 mmol) and *tert-butyl 4-(3-formyl-4-nitrophenyl)piperazine-1-carboxylate* (**84**) (1.15 g, 3.43 mmol) were reacted according to General Method A to give a yellow oil (1.48

g, 98%). ^{1}H-NMR (400 MHz, $CDCl_3$) δ 8.12 (d, *J* = 9.3 Hz, 1H), 7.12 (d, *J* = 2.8 Hz, 1H), 6.76 (dd, *J* = 9.3, 2.8 Hz, 1H), 4.26 – 4.18 (m, 4H), 3.63 – 3.59 (m, 6H), 3.48 – 3.44 (m, 4H), 1.50 (s, 9H), 1.29 (t, *J* = 7.1 Hz, 3H). ^{13}C-NMR (101 MHz, $CDCl_3$) δ 170.80, 154.55, 153.89, 138.45, 136.13, 128.34, 115.51, 112.12, 80.37, 61.37, 51.22, 49.84, 46.78, 28.39, 14.16. ESI-MS, *m/z* 423.4, 100% $[M+H]^+$.

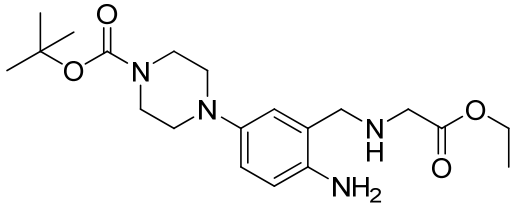

tert-butyl 4-(4-amino-3-((2-ethoxy-2-oxoethylamino)methyl)phenyl)piperazine-1-carboxylate (**86**)

tert-butyl 4-(3-((2-ethoxy-2-oxoethylamino)methyl)-4-nitrophenyl)piperazine-1-carboxylate (**85**) (1.43 g, 3.4 mmol) was reacted according to General Method B to give a brown oil (1.27 g, 95%). ^{1}H-NMR (300 MHz, $CDCl_3$) δ 8.09 (d, *J* = 9.3 Hz, 1H), 7.03 (d, *J* = 2.7 Hz, 1H), 6.72 (dd, *J* = 9.3, 2.8 Hz, 1H), 4.23 – 4.13 (m, 4H), 3.62 – 3.56 (m, 4H), 3.47 (s, 2H), 3.45 – 3.39 (m, 4H), 1.49 (s, 9H), 1.23 (t, *J* = 7.0 Hz, 3H). ^{13}C-NMR (101 MHz, $CDCl_3$) δ 173.65, 157.86, 130.65, 122.71, 118.77, 118.03, 117.1, 79.94, 58.09, 51.78, 50.54, 50.27, 44.48, 28.36, 18.04. ESI-MS, *m/z* 393.5, 100% $[M+H]^+$.

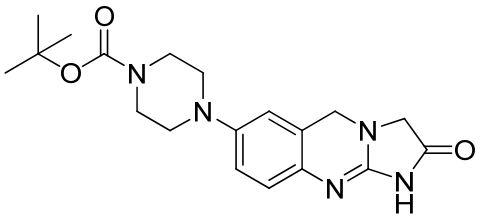

tert-butyl 4-(2-oxo-1,2,3,5-tetrahydroimidazo[2,1-b]quinazolin-7-yl)piperazine-1-carboxylate (**87**)

tert-butyl 4-(4-amino-3-((2-ethoxy-2-oxoethylamino)methyl)phenyl)piperazine-1-carboxylate (**86**) (1.25 g, 3.18 mmol) was reacted according to General Method C to give a yellow solid (134 mg, 11%). ^{1}H-NMR (300 MHz, MeOD) δ 7.09 (d, J = 8.8 Hz, 1H), 7.03 (dd, J = 8.9, 2.6 Hz, 1H), 6.91 (d, J = 2.3 Hz, 1H), 4.72 (s, 2H), 4.22 (s, 2H), 3.47 – 3.33 (m, 8H), 1.30 (s, 9H). ^{13}C-NMR (101 MHz, DMSO) δ 183.54, 163.21, 157.87, 148.12, 126.03, 117.77, 117.32, 114.62, 80.3, 53.8, 49.41, 45.1, 43.12, 27.9. ESI-HRMS, Found 371.2040 $[M+H]^+$ $C_{19}H_{25}N_5O_3$ requires 372.2030 $[M+H]^+$.

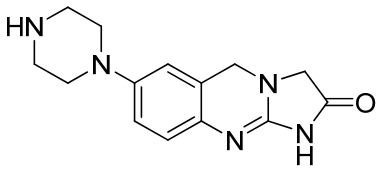

7-(piperazin-1-yl)-3,5-dihydroimidazo[2,1-b]quinazolin-2(1H)-one (**66**)

Method A

tert-butyl 4-(2-oxo-1,2,3,5-tetrahydroimidazo[2,1-b]quinazolin-7-yl)piperazine-1-carboxylate (**87**) (81 mg, 0.22 mmol) was stirred in TFA (2 ml) overnight, the reaction was quenched with saturated $NaHCO_3$ solution (5 ml). The precipitate was collected by filtration and washed sparingly with ethanol and ether to give a tan powder (25 mg, 42%)

Method B

To prepare a catalyst solution Palladium (II) acetate (4.2 mg, .02 mmol) and 1,1'-binaphthyl-2-di-t-butylphosphine (27 mg, 0.09 mmol) were stirred in degassed t-BuOH (10 ml) for 30 mins at RT. Piperazine (486 mg, 5.64 mmol), *7-bromo-3,5-dihydroimidazo[2,1-b]quinazolin-2(1H)-one* (**36**) (500 mg, 1.88 mmol) and potassium t-butoxide were sealed in a an oven dried microwave vessel. The vessel was evacuated, then charged with t-BuOH (10 ml), and the catalyst solution (10 ml). The vessel was evacuated and blanketed with nitrogen three times, then stirred over an oil bath at 90 °C for 16 h. The solution was neutralized with sat. $NaHCO_3$ and the crude product was collected by vacuum filtration and then purified by reverse phase chromatography to give a brown solid (42 mg, 8%). ^{1}H-NMR (400 MHz, D2O) δ 6.98 (dd, J = 8.8, 2.3 Hz, 1H), 6.94 (d, J = 8.7 Hz, 1H), 6.87 (d, J = 1.9 Hz, 1H), 4.54 (s, 2H), 3.96 (s, 2H), 3.12 (dd, J = 6.4, 3.1 Hz, 4H), 3.04 (dd, J = 6.4, 3.2 Hz, 4H). ^{13}C-NMR (101 MHz, DMSO) δ 158.54, 147.41, 125.79, 118.65, 117.52, 116.78, 114.47, 53.11, 45.83, 44.48, 42.86. ESI-HRMS, Found 272.1515 $[M+H]^+$ $C_{14}H_{17}N_5O$ requires 272.1506 $[M+H]^+$.

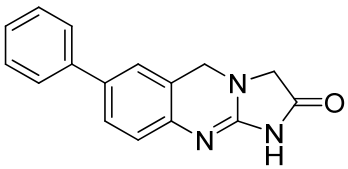

7-phenyl-3,5-dihydroimidazo[2,1-b]quinazolin-2(1H)-one (**88**)

7-bromo-3,5-dihydroimidazo[2,1-b]quinazolin-2(1H)-one (**36**) (0.02 g, 0.08 mmol), phenyl boronic acid (0.046 g, 0.38 mmol), palladium (II) acetate (0.002 g, 0.01 mmol) and caesium carbonate (0.123 g, 0.38 mmol) were added to an oven dried microwave vessel. The vessel was sealed; DMF (4 ml) and water (1 ml) were added by injection. The vessel was evacuated and refilled with nitrogen twice. The reaction was heated in a microwave reactor at 140 °C for 20 mins. The reaction mixture was filtered through celite, then diluted with water (10 ml) and acetonitrile (5 ml). The mixture was frozen and lyophilized. The residue was purified by preparatory HPLC. The product was isolated as a tan powder (2 mg, 10%). ^{1}H-NMR (400 MHz, DMSO) δ 7.66 – 7.62 (m, 2H), 7.58 (dd, J = 8.3, 2.1 Hz, 1H), 7.54 (d, J = 1.7 Hz, 1H), 7.48 – 7.42 (m, 2H), 7.37 – 7.32 (m, 1H), 7.08 (d, J = 8.3 Hz, 1H), 4.62 (s, 2H), 3.92 (s, 2H). ^{13}C-NMR (101 MHz, DMSO) δ 129.29, 127.69, 127.3, 126.66, 125.42, 119.05, 117.36, 53.96, 44.74. ESI-HRMS, Found 264.1141 $[M+H]^+$ $C_{16}H_{13}N_3O$ requires 264.1131 $[M+H]^+$.

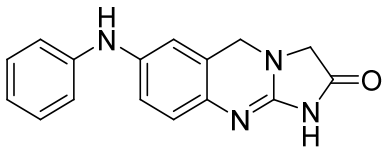

7-(phenylamino)-3,5-dihydroimidazo[2,1-b]quinazolin-2(1H)-one (**89**)

Prepared according to General Method E to give a brown solid (99 mg, 95%). ^{1}H-NMR (400 MHz, DMSO) δ 8.08 (s, 1H), 7.19 (t, J = 7.7 Hz, 2H), 7.11 – 6.86 (m, 5H), 6.77 (t, J = 7.2 Hz, 1H), 4.47 (s, 2H), 3.78 (s, 2H). ^{13}C-NMR (101 MHz, DMSO) δ 183.87, 165.23, 143.78, 138.98, 129.14, 127.59, 119.20, 119.00, 117.71, 117.00, 115.96, 115.38, 53.91, 44.62. ESI-HRMS, Found 279.1253 $[M+H]^+$ $C_{16}H_{14}N_4O$ requires 279.1240 $[M+H]^+$.

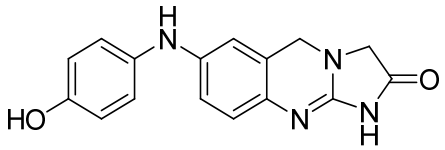

7-(3-hydroxyphenylamino)-3,5-dihydroimidazo[2,1-b]quinazolin-2(1H)-one (**93**)

Prepared according to General Method E to give a brown solid (4 mg, 7%). ^{1}H-NMR (400 MHz, DMSO) δ 7.60 (s, 1H), 6.88 (d, J = 8.7 Hz, 2H), 6.80 (d, J = 8.6 Hz, 1H), 6.75 (dd, J = 8.5, 2.2 Hz, 1H), 6.68 (d, J = 8.7 Hz, 3H), 4.41 (s, 2H), 3.75 (s, 2H). ^{13}C-NMR (101 MHz, DMSO) δ 184.04, 133.12, 130.97, 121.26, 117.22, 116.22, 115.41, 112.77, 54.26, 44.98. ESI-MS, *m/z* 295.2, 100% $[M+H]^{+}$.

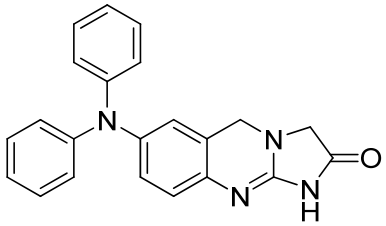

7-(diphenylamino)-3,5-dihydroimidazo[2,1-b]quinazolin-2(1H)-one (**94**)

Prepared according to General Method F to give a brown solid (10 mg, 15%). ^{1}H-NMR (400 MHz, 4:1 CDCl3/MeOD) δ 7.21 – 7.14 (m, 4H), 6.99 – 6.94 (m, 6H), 6.92 (dd, J = 6.9, 1.7 Hz, 1H), 6.87 (d, J = 8.6 Hz, 1H), 6.75 (d, J = 2.2 Hz, 1H), 4.43 (s, 2H), 3.83 (s, 2H). ^{13}C-NMR (101 MHz, 4:1 CDCl3/MeOD) δ 183.95, 157.69, 146.55, 143.77, 128.45, 127.48, 123.83, 123.12, 122.15, 120.97, 117.11, 116.68, 53.22, 44.19. ESI-HRMS, Found 355.1561 $[M+H]^{+}$ $C_{22}H_{18}N_4O$ requires 355.1553 $[M+H]^{+}$.

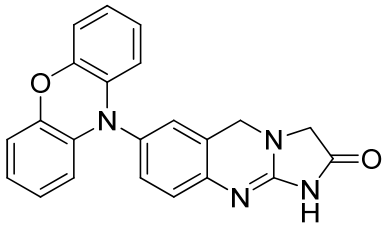

7-(10H-phenoxazin-10-yl)-3,5-dihydroimidazo[2,1-b]quinazolin-2(1H)-one (**95**)

Prepared according to General Method F to give a dark green solid (36 mg, 52%). ^{1}H-NMR (400 MHz, DMSO) δ 7.30 – 7.18 (m, 4H), 6.74 – 6.71 (m, 2H), 6.68 – 6.65 (m, 3H), 5.95 – 5.89 (m, 2H), 4.57 (s, 2H), 3.85 (s, 2H). ^{13}C-NMR (101 MHz, DMSO) δ 143.09, 133.92, 132.91, 130.46, 129.61, 128.78, 123.68,

121.41, 115.22, 113.22, 53.79, 44.36. ESI-HRMS, Found 369.1357 $[M+H]^+$ $C_{22}H_{16}N_4O_2$ requires 369.1346 $[M+H]^+$.

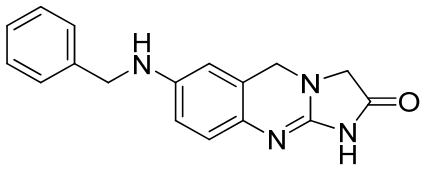

7-(benzylamino)-3,5-dihydroimidazo[2,1-b]quinazolin-2(1H)-one (**96**)

Prepared according to General Method F to give a tan solid (1.5 mg, 3%). ^{1}H-NMR (400 MHz, DMSO) δ 7.36 – 7.19 (m, 5H), 6.72 (d, J = 8.6 Hz, 1H), 6.49 (dd, J = 8.5, 2.5 Hz, 1H), 6.39 (d, J = 2.2 Hz, 1H), 6.15 (t, J = 6.0 Hz, 1H), 4.36 (s, 2H), 4.23 (d, J = 6.1 Hz, 2H), 3.73 (s, 2H). ^{13}C-NMR was not obtained due to insufficient material ESI-HRMS, Found 293.1399 $[M+H]^+$ $C_{17}H_{16}N_4O$ requires 293.1397 $[M+H]^+$.

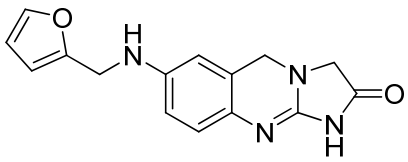

7-(furan-2-ylmethylamino)-3,5-dihydroimidazo[2,1-b]quinazolin-2(1H)-one (**97**)

Prepared according to General Method F to give a brown solid (6 mg, 12%). ^{1}H-NMR (400 MHz, DMSO) δ 7.56 (dd, J = 1.8, 0.8 Hz, 1H), 6.87 (d, J = 8.7 Hz, 1H), 6.60 (dd, J = 8.6, 2.5 Hz, 1H), 6.48 (d, J = 2.5 Hz, 1H), 6.38 (dd, J = 3.2, 1.8 Hz, 1H), 6.29 (dd, J = 3.2, 0.7 Hz, 1H), 4.51 (s, 2H), 4.23 (s, 2H), 4.06 (s, J = 5.3 Hz, 2H). ^{13}C-NMR (101 MHz, DMSO) δ 174.26, 156.76, 153.34, 146.59, 142.64, 121.69, 118.21, 113.02, 110.73, 109.93, 107.39, 53.04, 44.87, 40.06. ESI-HRMS, Found 283.1195 $[M+H]^+$ $C_{15}H_{14}N_4O$ requires 283.1190 $[M+H]^+$.

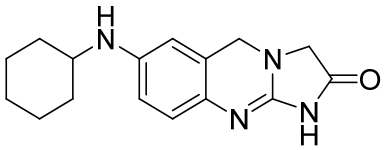

7-(cyclohexylamino)-3,5-dihydroimidazo[2,1-b]quinazolin-2(1H)-one (**98**)

Prepared according to General Method F to give a tan solid (8 mg, 16%). ^{1}H-NMR (400 MHz, DMSO) δ 7.92 (s, 1H), 6.91 (d, J = 8.7 Hz, 1H), 6.61 (d, J = 8.4 Hz, 1H), 6.49 (s, 1H), 4.54 (s, 2H), 4.15 – 4.08 (m, 2H), 3.23 – 3.07 (m, 1H), 1.92 – 1.85 (m, 2H), 1.74 – 1.68 (m, 2H), 1.62 – 1.56 (m, 2H), 1.36 – 1.25 (m, 2H), 1.20 – 1.11 (m, 2H). ^{13}C-NMR (101 MHz, MeOD) δ 152.14, 117.89, 116.80, 115.82, 87.71, 44.19, 30.99, 29.41, 28.73, 24.55, 24.17, 23.85, 23.67. ESI-MS, *m/z* 285.1, 100% $[M+H]^{+}$.

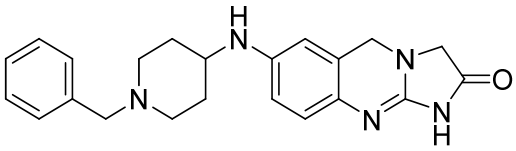

7-(1-benzylpiperidin-4-ylamino)-3,5-dihydroimidazo[2,1-b]quinazolin-2(1H)-one (**99**)

Prepared according to General Method F to give a tan solid (17 mg, 25%). ^{1}H-NMR (400 MHz, DMSO) δ 7.54 – 7.46 (m, 5H), 6.90 (d, J = 8.7 Hz, 1H), 6.58 (d, J = 8.9 Hz, 1H), 6.45 (s, 1H), 4.54 (s, 2H), 4.32 (s, 2H), 4.16 (s, 2H), 3.42 (d, J = 11.3 Hz, 2H), 3.24 (s, 1H), 3.02 (bs, 2H), 2.11 (d, J = 12.7 Hz, 2H), 1.58 (d, J = 12.1 Hz, 2H). ^{13}C-NMR (101 MHz, DMSO) δ 145.34, 131.39, 129.55, 128.81, 118.35, 118.13, 118.00, 112.70, 109.59, 58.84, 52.44, 50.66, 46.88, 44.52, 28.81. ESI-MS, *m/z* 376.2, 100% $[M+H]^{+}$.

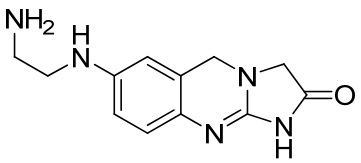

7-(2-aminoethylamino)-3,5-dihydroimidazo[2,1-b]quinazolin-2(1H)-one (**100**)

Prepared according to General Method E to give a brown solid (13 mg, 14%). ^{1}H-NMR (400 MHz, DMSO) δ 6.79 (d, J = 8.6 Hz, 1H), 6.50 (dd, J = 8.5, 2.0 Hz, 1H), 6.37 (d, J = 12.6 Hz, 1H), 4.40 (s, J = 10.6 Hz, 2H), 3.76 (s, J = 10.6 Hz, 2H), 3.13 (t, J = 6.0 Hz, 2H), 2.85 (t, J = 5.1 Hz, 2H). ^{13}C-NMR (101 MHz, DMSO) δ

183.99, 165.11, 144.98, 124.18, 118.90, 116.98, 112.35, 109.50, 54.01, 44.81, 43.14, 22.15. ESI-HRMS, Found 246.1360 $[M+H]^+$ $C_{12}H_{15}N_5O$ requires 246.1247 $[M+H]^+$.

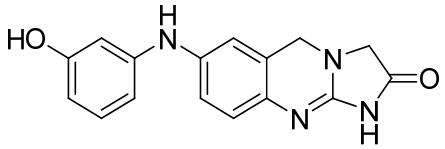

7-(3-hydroxyphenylamino)-3,5-dihydroimidazo[2,1-b]quinazolin-2(1H)-one (**101**)

Prepared according to General Method E to give a brown solid (19 mg, 34%). ^{1}H-NMR (400 MHz, DMSO) δ 7.96 (s, 1H), 6.98 – 6.90 (m, 2H), 6.86 (d, J = 8.5 Hz, 2H), 6.45 (d, J = 2.0 Hz, 1H), 6.41 (d, J = 8.0 Hz, 1H), 6.19 (dd, J = 7.9, 1.6 Hz, 1H), 4.43 (s, 2H), 3.73 (s, 2H). ^{13}C-NMR (101 MHz, DMSO) δ 158.23, 145.18, 138.59, 129.66, 119.25, 118.06, 115.78, 106.86, 106.47, 102.66, 54.14, 44.98. ESI-HRMS, Found 295.1193 $[M+H]^+$ $C_{16}H_{14}N_4O_2$ requires 295.1190 $[M+H]^+$.

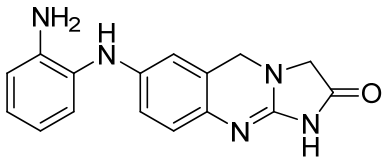

7-(2-aminophenylamino)-3,5-dihydroimidazo[2,1-b]quinazolin-2(1H)-one (**102**)

Prepared according to General Method E to give a dark red solid (13 mg, 24%). ^{1}H-NMR (400 MHz, DMSO) δ 7.00 (dd, J = 7.8, 1.3 Hz, 1H), 6.94 (d, J = 8.6 Hz, 1H), 6.90 – 6.84 (m, 1H), 6.82 – 6.77 (m, 1H), 6.68 (dd, J = 8.6, 2.2 Hz, 1H), 6.65 – 6.58 (m, 1H), 6.55 (d, J = 2.1 Hz, 1H), 4.53 (s, 2H), 4.08 (s, 2H). ^{13}C-NMR (101 MHz, DMSO) δ 124.34, 123.15, 118.35, 117.78, 116.13, 114.85, 112.05, 52.70, 44.51. ESI-HRMS, Found 294.1353 $[M+H]^+$ $C_{16}H_{15}N_5O$ requires 294.1349 $[M+H]^+$.

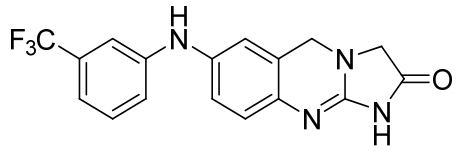

7-(3-(trifluoromethyl)phenylamino)-3,5-dihydroimidazo[2,1-b]quinazolin-2(1H)-one (**103**)

Prepared according to General Method E to give a grey solid (8 mg, 12%). ^{1}H-NMR (400 MHz, DMSO) δ 8.43 (s, 1H), 7.39 (t, J = 7.8 Hz, 1H), 7.23 (d, J = 7.9 Hz, 1H), 7.17 (s, 1H), 7.07 – 6.92 (m, 4H), 4.50 (s, 2H), 3.80 (s, 2H). ^{13}C-NMR (101 MHz, DMSO) δ 145.17, 137.34, 130.27, 119.44, 119.29, 118.15, 117.35, 114.60, 110.94, 53.89, 44.57. ESI-HRMS, Found 347.1116 $[M+H]^+$ $C_{17}H_{13}F_3N_4O$ requires 347.1114 $[M+H]^+$.

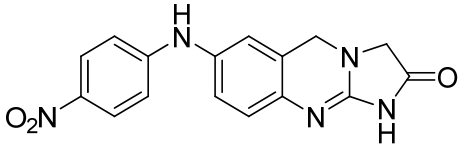

7-(4-nitrophenylamino)-3,5-dihydroimidazo[2,1-b]quinazolin-2(1H)-one (**104**)

Prepared according to General Method E to give a yellow solid (22 mg, 36%). ^{1}H-NMR (400 MHz, DMSO) δ 9.58 (s, 1H), 8.13 – 8.05 (m, 2H), 7.29 (d, J = 8.6 Hz, 1H), 7.22 (dd, J = 8.6, 2.3 Hz, 1H), 7.18 (d, J = 2.1 Hz, 1H), 7.12 – 7.07 (m, 2H), 4.68 (s, 2H), 4.24 (s, 2H). ^{13}C-NMR (101 MHz, DMSO) δ 171.93, 153.59, 150.38, 138.10, 137.70, 126.70, 126.06, 121.12, 118.74, 118.72, 118.33, 113.57, 52.41, 44.32. ESI-HRMS, Found 324.1095 $[M+H]^+$ $C_{16}H_{13}N_5O_3$ requires 324.1091 $[M+H]^+$.

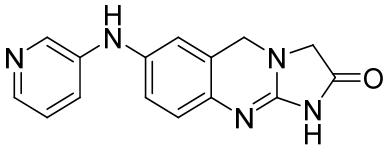

7-(pyridin-3-ylamino)-3,5-dihydroimidazo[2,1-b]quinazolin-2(1H)-one (**105**)

Prepared according to General Method F to give a brown solid (2 mg, 4%). ^{1}H-NMR (400 MHz, MeOD) δ 8.26 (d, J = 2.5 Hz, 1H), 7.99 (dd, J = 4.7, 1.3 Hz, 1H), 7.52 (ddd, J = 8.4, 2.8, 1.4 Hz, 1H), 7.28 (ddd, J = 8.4, 4.8, 0.6 Hz, 1H), 7.08 (dd, J = 8.7, 2.3 Hz, 1H), 7.03 – 6.96 (m, 2H), 4.63 (s, 2H), 4.00 (d, J = 8.2 Hz, 2H). ^{13}C-NMR was not obtained due to insufficient material. ESI-HRMS, Found 280.1198 $[M+H]^+$ $C_{15}H_{13}N_5O$ requires 280.1193 $[M+H]^+$.

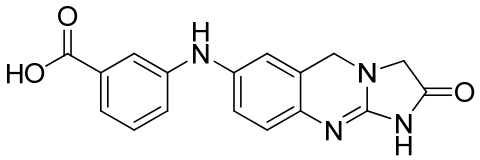

3-(2-oxo-1,2,3,5-tetrahydroimidazo[2,1-b]quinazolin-7-ylamino)benzoic acid (**106**)

Prepared according to General Method F to give a dark solid (18 mg, 29%). ^{1}H-NMR (400 MHz, DMSO) δ 8.02 (s, 1H), 7.61 (s, 1H), 7.34 (d, J = 7.5 Hz, 1H), 7.11 (t, J = 7.6 Hz, 1H), 6.99 – 6.84 (m, 3H), 4.46 (s, 2H), 3.78 (s, 2H). ^{13}C-NMR (101 MHz, DMSO) δ 169.88, 142.73, 141.30, 139.68, 127.73, 120.70, 118.93, 117.64, 117.12, 116.97, 116.77, 114.87, 53.94, 44.67. ESI-HRMS, Found 323.1147 $[M+H]^+$ $C_{17}H_{14}N_4O_3$ requires 323.1139 $[M+H]^+$.

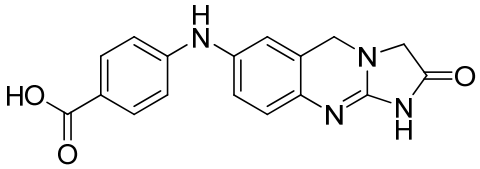

4-(2-oxo-1,2,3,5-tetrahydroimidazo[2,1-b]quinazolin-7-ylamino)benzoic acid (**107**)

Prepared according to General Method F to give a brown solid (8 mg, 13%). ^{1}H-NMR (400 MHz, DMSO) δ 8.61 (s, 1H), 7.75 (d, J = 8.4 Hz, 2H), 7.09 – 6.91 (m, 5H), 4.50 (s, 2H), 3.80 (s, 2H). ^{13}C-NMR (101 MHz, DMSO) δ 167.17, 148.43, 136.82, 131.14, 120.14, 119.18, 118.03, 117.09, 113.46, 53.89, 44.54. ESI-HRMS, Found 323.1133 $[M+H]^+$ $C_{17}H_{14}N_4O_3$ requires 323.1139 $[M+H]^+$.

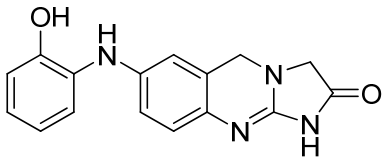

7-(2-hydroxyphenylamino)-3,5-dihydroimidazo[2,1-b]quinazolin-2(1H)-one (**108**)

Prepared according to General Method F to give a brown solid (18 mg, 32%). ^{1}H-NMR (400 MHz, DMSO) δ 9.49 (s, 1H), 7.34 (s, 1H), 7.12 (dd, J = 7.7, 1.7 Hz, 1H), 6.96 (d, J = 8.7 Hz, 1H), 6.92 (dd, J = 8.7, 2.4 Hz, 1H), 6.86 (dd, J = 7.8, 1.6 Hz, 1H), 6.83 – 6.76 (m, 2H), 6.73 (td, J = 7.5, 1.6 Hz, 1H), 4.55 (s, 2H), 4.08 (s, J = 7.6 Hz, 2H). ^{13}C-NMR (101 MHz, DMSO) δ 148.25, 142.04, 130.17, 121.83, 119.18, 118.81, 118.24,

117.59, 116.17, 115.47, 113.44, 52.76, 44.52. ESI-HRMS, Found 295.1198 $[M+H]^+$ $C_{16}H_{14}N_4O_2$ requires 295.1190 $[M+H]^+$.

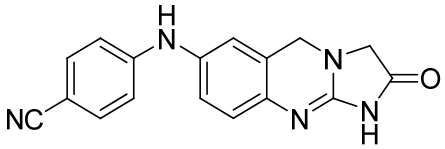

4-(2-oxo-1,2,3,5-tetrahydroimidazo[2,1-b]quinazolin-7-ylamino)benzonitrile (**109**)

Chloro[2-(dicyclohexylphosphino)-3,6-dimethoxy-2'-4'-6'-tri-i-propyl-1,1'-biphenyl][2-(2-aminoethyl)phenyl]palladium(II) (0.003 g, 0.004 mmol), 4-aminobenzonitrile (0.033 g, 0.28 mmol), 7-bromoimidazoquinazolinone (0.05 g, 0.19 mmol) and sodium t-butoxide (0.047 g, 0.28 mmol) were added to an oven dried microwave vial equipped with a magnetic stirrer bar. The vial was sealed, evacuated and refilled with nitrogen. Degassed t-butanol (10 ml) was added by injection. The mixture was sonicated to give a homogeneous mixture. The vial was evacuated and refilled with nitrogen twice. The reaction was stirred at 110 °C for 16 hours in an oil bath. The mixture was purified by flash column chromatography ($CHCl_3$ → 5% MeOH) to give a tan powder (8 mg, 14%). ^{1}H-NMR (400 MHz, DMSO) δ 7.61 – 7.51 (m, 2H), 7.20 – 7.01 (m, 5H), 4.67 (s, 2H), 4.24 (s, 2H). ^{13}C-NMR (101 MHz, DMSO) δ 171.02, 147.74, 138.61, 133.54, 125.49, 120.12, 119.23, 118.23, 117.63, 114.75, 99.69, 52.23, 44.29. ESI-HRMS, Found 304.1206 $[M+H]^+$ $C_{17}H_{13}N_5O$ requires 304.1193 $[M+H]^+$.

Chapter Five Compounds

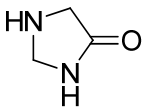

imidazolidin-4-one (**111**) [180]

1-benzylimidazolidin-4-one (**112**) (2.3 g, 13.07 mmol) was dissolved in methanol and 10% Pd-C (214 mg) was added. The flask was evacuated and charged with hydrogen twice. The reaction was stirred at RT for 120 h under a hydrogen balloon. The reaction mixture was diluted with methanol and filtered through a pad of celite. The filtrate was concentrated under reduced pressure to give a yellow oil. The crude product was

then purified by flash column chromatography using 10% methanol in chloroform as the eluent. The product was isolated as yellow hygroscopic needles (1 g, 92%). ^{1}H-NMR (400 MHz, MeOD) δ 4.39 (t, J = 0.9 Hz, 2H), 3.32 (t, J = 0.9 Hz, 2H). ^{13}C-NMR (101 MHz, MeOD) δ 179.49, 61.53, 49.17. ^{1}H-NMR (400 MHz, D_6-DMSO) δ 4.16 (s, 2H), 3.04 (s, 2H). ^{13}C-NMR (101 MHz, D_6-DMSO) δ 177.2, 60.52, 48.61. $[M+H]^+$ 87, 100%.

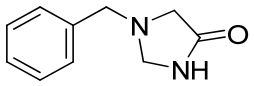

1-benzylimidazolidin-4-one (**112**) [180, 181]

Method A

1-benzylimidazolidin-4-one oxime (**122**) (3.15 g, 16.5 mmol) was dissolved in methanol (200 ml), then sodium hydroxide (6.6 g, 165 mmol) and 30% hydrogen peroxide (165 mmol, 16.8 ml) were added. The reaction was stirred for 16 h at RT. The precipitate was removed by filtration. The filtrate was diluted with water (50 ml) and stripped of methanol under reduced pressure. The remaining solution was extracted with DCM (3 × 75 ml). The combined organic extracts were dried over sodium sulfate and filtered. The filtrate was concentrated under reduced pressure. The resulting residue was purified by column chromatography using 5% methanol in chloroform as the eluent. The product was isolated as a yellow solid (1.12 g, 39%).

Method B

2-(benzylamino)acetamide (**114**) (5 g, 30.4 mmol) was dissolved in methanol (250 ml) and 37% (w/v) formaldehyde solution (1.8 ml, 24.4 mmol) was added. The reaction was stirred at reflux for 90 h under a nitrogen balloon. The reaction mixture was concentrated under reduced pressure and taken up in ether (200 ml). Some insoluble residue was removed by decantation. The ether layer was concentrated under reduced pressure. The residue was purified by column chromatography using 5% methanol in ethyl acetate as the eluent. The product was isolated as a white crystalline solid (1.01 g, 24%). ^{1}H-NMR (400 MHz, MeOD) δ 7.33 – 7.10 (m, 5H), 4.00 (t, J = 1.2 Hz, 2H), 3.66 (s, 2H), 3.08 (t, J = 1.2 Hz, 2H). ^{13}C-NMR (101 MHz, MeOD) δ 176.66, 138.62, 129.91, 129.63, 128.70, 66.73, 59.55, 56.02. ESI-HRMS, Found 177.1026 $[M+H]^+$ $C_{10}H_{12}N_2O$ requires 177.1022 $[M+H]^+$.

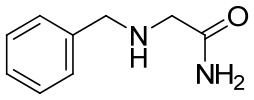

2-(benzylamino)acetamide (**114**) [182]

2-chloroacetamide (10 g, 106 mmol) was dissolved in water (100 ml), benzylamine (23 ml, 213 mmol) was added and the mixture was stirred for 20 mins at 90 °C. The mixture was allowed to cool, then washed with ether (3 × 20 ml) to remove excess benzylamine. The product was extracted from the aqueous layer with ethyl acetate (3 × 50 ml). The combined organic extracts were dried over magnesium sulfate and filtered. The filtrate was concentrated under reduced pressure and the residue was digested with ether. The product was collected by filtration as a white powder (4.7 g, 27%). ^{1}H-NMR (400 MHz, MeOD) δ 7.45 – 7.21 (m, 5H), 3.76 (s, 2H), 3.25 (s, 2H). ^{13}C-NMR (101 MHz, MeOD) δ 176.81, 140.57, 129.54, 129.50, 128.30, 54.21, 51.58. $[M+H]^+$ 165.2, 100%.

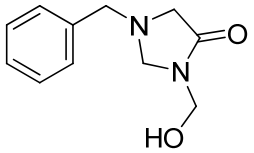

1-benzyl-3-(hydroxymethyl)imidazolidin-4-one (**115**) [180]

2-(benzylamino)acetamide (**114**) (1.13 g, 6.87 mmol) was refluxed in 37% formaldehyde solution (6 ml) for 30 mins. The mixture was diluted with water (100 ml) and extracted with DCM (3 × 100 ml). The organic extracts were combined and dried over sodium sulfate. The mixture was filtered and the filtrate was concentrated under reduced pressure. The resulting residue was purified by column chromatography using 10% methanol in ethyl acetate. The product was isolated as a clear oil (0.66 g, 47%). ^{1}H-NMR (300 MHz, CDCl3) δ 7.44 – 7.32 (m, 5H), 4.85 (s, 2H), 4.32 (s, 2H), 3.82 (s, 2H), 3.38 (s, 2H). ^{13}C-NMR (101 MHz, MeOD) δ 172.13, 136.96, 128.73, 128.69, 127.78, 68.59, 65.05, 58.8, 56.08. $[M-CH_3O]$+ 177.1, 100%, $[M+H]^+$ 207.1, 85%.

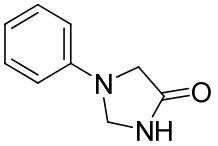

1-phenylimidazolidin-4-one (**118**) [181]

Prepared according to General Method G, stirred for 16 h to give an off white solid (22 mg, 12%). ^{1}H-NMR (400 MHz, MeOD) δ 7.29 – 7.24 (m, 2H), 6.82 – 6.76 (m, 1H), 6.63 – 6.57 (m, 2H), 4.79 (t, J = 2.0 Hz, 2H), 3.85 (t, J = 2.0 Hz, 2H). ^{13}C-NMR (101 MHz, MeOD) δ 130.39, 119.09, 112.80, 62.58, 50.55. ESI-HRMS, Found 163.0874 $[M+H]^+$ $C_9H_{10}N_2O_1$ requires 163.0866 $[M+H]^+$.

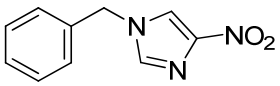

1-benzyl-4-nitro-1H-imidazole (**121**) [197]

4-nitroimidazole (18 g, 160 mmol) and benzyl bromide (19 ml, 160 mmol) were added to a RBF charged with toluene (320 ml). A solution of potassium hydroxide (48 g, 857 mmol) and tetrabutylammonium bromide (1 g, 3 mmol) in water (240 ml) was added. The mixture was stirred at 70 °C for 2 h. The aqueous layer was discarded; and the remaining organic layer was concentrated under reduced pressure. The residue was triturated with water, slowly forming a solid over 16 h. The solid was isolated by filtration then taken up in ethanol and dried over sodium sulfate. The mixture was filtered and concentrated under vacuum. The residue was recrystallized from hot ethanol / ether to give orange crystals (19.5 g, 60%). ^{1}H-NMR (400 MHz, DMSO) δ 8.54 (d, J = 1.5 Hz, 1H), 8.05 (d, J = 1.4 Hz, 1H), 7.48 – 7.33 (m, 5H), 5.36 (s, 2H). ^{13}C-NMR (101 MHz, MeOD) δ 148.90, 138.24, 136.75, 130.26, 129.83, 129.12, 121.47, 52.76. $[M+H]^+$ 204.2, 100%.

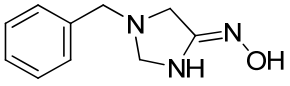

1-benzylimidazolidin-4-one oxime (**122**) [181]

Sodium metal (1.62 g, 70 mmol) was gradually added to a RBF charged with methanol (75 ml) whilst stirring. Once the sodium had completely dissolved, *1-benzyl-4-nitro-1H-imidazole* (**121**) (0.55 g, 2.7 mmol)

and sodium borohydride (0.81 g, 21.5 mmol) were added. The reaction was stirred for 5 h at RT under a nitrogen balloon, gas was vented as needed. The flask was cooled in an ice bath, and the reaction was neutralized by addition of conc. HCl (6 ml). The mixture was concentrated under reduced pressure then poured onto ice (~200 ml). The solution was extracted with DCM (3 × 75 ml). The organic extracts were combined and dried over sodium sulfate. The mixture was filtered and the filtrate was concentrated under reduced pressure. The resulting residue was purified by column chromatography using 5% methanol in DCM as the eluent. The product was isolated as a pale yellow solid (0.12 g, 24%). ^{1}H-NMR (400 MHz, DMSO) δ 8.79 (s, 1H), 7.46 – 7.16 (m, 5H), 3.87 (s, 2H), 3.66 (s, 2H), 3.17 (s, 2H). ^{13}C-NMR (101 MHz, DMSO) δ 153.37, 138.30, 128.39, 128.27, 127.06, 67.35, 57.46, 52.60. $[M+H]^+$ 192.2, 100%.

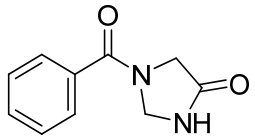

1-benzoylimidazolidin-4-one (**123**) [185]

Imidazolidin-4-one (**111**) (50 mg, 0.58 mmol), triethylamine (122 µl, 0.87 mmol), and benzoic anhydride (145 mg, 0.64 mmol) were stirred in DCM (15 ml) over activated molecular sieves at RT for 2 d. The reaction was diluted with methanol and filtered through celite. The filtrate was concentrated under reduced pressure to give a white solid. The crude product was purified by column chromatography using 5% methanol in chloroform as the eluent. The product was then recrystallized from hot DCM and hexane as small white needles (29 mg, 27%). ^{1}H-NMR (400 MHz, DMSO, 350 °K) δ 8.38 (s, 1H), 7.62 – 7.42 (m, 4H), 4.84 (s, 2H), 3.95 (s, 2H). ^{13}C-NMR (101 MHz, CDCl3) δ 171.59, 169.55, 134.62, 131.28, 128.88, 127.30, 59.18, 49.97. ESI-HRMS, Found 191.0824 $[M+H]^+$ $C_{10}H_{10}N_2O_2$ requires 191.0815 $[M+H]^+$.

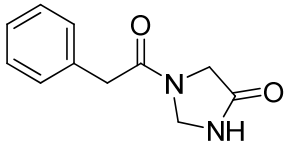

1-(2-phenylacetyl)imidazolidin-4-one (**124**)

Phenyl acetic acid (79 mg, 0.58 mmol), triethylamine (97 µL, 0.7 mmol), and HCTU (241 mg, 0.58 mmol) were stirred in DCM (10 ml) over activated molecular sieves for 30 mins at RT. *Imidazolidin-4-one* (**111**) (50 mg, 0.58 mmol) was dissolved in DCM (4 ml) over activated molecular sieves, and the activated ester solution was added. The reaction was stirred at RT for 16 h. The reaction was diluted with methanol (3 ml) and filtered through celite. The filtrate was concentrated under reduced pressure and the resulting residue purified by flash chromatography to give a pale yellow solid (72 mg, 60%). ^{1}H-NMR (400 MHz, MeOD) Component A (70%) δ 7.37 – 7.22 (m, 5H), 4.84 (t, J = 1.1 Hz, 2H), 4.10 (t, J = 0.9 Hz, 2H), 3.72 (s, 2H). Component B (30%) δ 7.37 – 7.22 (m, 5H), 5.00 (t, J = 1.1 Hz, 2H), 3.94 (t, J = 1.2 Hz, 2H), 3.69 (s, 2H). ^{13}C-NMR (101 MHz, MeOD) Component A δ 169.91, 168.62, 134.82, 129.51, 128.25, 126.52, 58.38, 47.46, 40.38. Component B δ 169.67, 168.14, 134.82, 129.47, 128.25, 126.52, 58.69, 46.67, 39.21. $[M+H]^+$ 205.1, 100%. ESI-HRMS, Found 205.0967 $[M+H]^+$ $C_{11}H_{12}N_2O_2$ requires 205.0972 $[M+H]^+$.

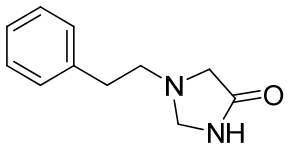

1-phenethylimidazolidin-4-one (**125**)

Imidazolidin-4-one (**111**) (47 mg, 0.55 mmol), triethylamine (122 µl, 0.87 mmol), and (2-bromoethyl)benzene (87 µl, 0.64 mmol) were dissolved in acetonitrile (10 ml) over activated molecular sieves. The mixture was stirred at RT for 10 mins, then slowly heated to reflux, and stirred for 16 h. The reaction was diluted with methanol and filtered through celite. The filtrate was concentrated under vacuum to give an oil with some solids present. The crude mixture was purified by column chromatography using 5% methanol in chloroform as the eluent. The product was isolated as a white solid (17 mg, 15%). ^{1}H-NMR (400 MHz, MeOD) δ 7.31 – 7.15 (m, 5H), 4.15 (t, J = 1.2 Hz, 2H), 3.23 (t, J = 1.2 Hz, 2H), 2.88 – 2.82 (m, 2H),

2.82 – 2.75 (m, 2H). ^{13}C-NMR (101 MHz, MeOD) δ 183.67, 140.84, 129.70, 129.49, 127.32, 67.03, 57.36, 56.15, 35.59. ESI-HRMS, Found 191.1186 $[M+H]^+$ $C_{11}H_{14}N_2O$ requires 191.1179 $[M+H]^+$.

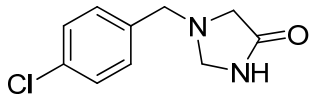

1-(4-chlorobenzyl)imidazolidin-4-one (**127a**)

Imidazolidin-4-one (**111**) (30 mg, 0.35 mmol), and 4-chlorobenzaldehyde were reacted according to General Method H. Yield (56 mg, 76%). ^{1}H-NMR (400 MHz, MeOD) δ 7.37 – 7.30 (m, 4H), 4.11 (t, J = 1.2 Hz, 2H), 3.75 (s, 2H), 3.18 (t, J = 1.2 Hz, 2H). ^{13}C-NMR (101 MHz, MeOD) δ 176.57, 137.62, 134.40, 131.40, 129.70, 66.73, 58.70, 55.96. ESI-HRMS, Found 211.0641 $[M+H]^+$ $C_{10}H_{11}ClN_2O$ requires 211.0633 $[M+H]^+$.

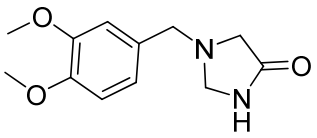

1-(3,4-dimethoxybenzyl)imidazolidin-4-one (**127b**)

Imidazolidin-4-one (**111**) (30 mg, 0.35 mmol), and 3,4-dimethoxybenzaldehyde were reacted according to General Method H. Yield (68 mg, 83%). ^{1}H-NMR (400 MHz, MeOD) δ 6.99 (d, J = 1.6 Hz, 1H), 6.93 – 6.86 (m, 2H), 4.10 (t, J = 1.2 Hz, 2H), 3.83 (s, 3H), 3.82 (s, 3H), 3.71 (s, 2H), 3.19 (t, J = 1.2 Hz, 2H). ^{13}C-NMR (101 MHz, MeOD) δ 176.65, 150.66, 150.12, 131.31, 122.45, 113.66, 112.86, 66.61, 59.27, 56.50, 56.44, 55.94. ESI-HRMS, Found 237.1236 $[M+H]^+$ $C_{12}H_{16}N_2O_3$ requires 237.1234 $[M+H]^+$.

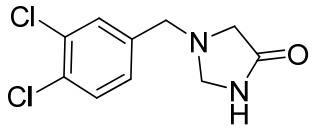

1-(3,4-dichlorobenzyl)imidazolidin-4-one (**127c**)

Imidazolidin-4-one (**111**) (30 mg, 0.35 mmol), and 3,4-dichlorobenzaldehyde were reacted according to General Method H. Yield (50 mg, 59%). ^{1}H-NMR (400 MHz, MeOD) δ 7.54 (d, J = 1.9 Hz, 1H), 7.48 (d, J = 8.2 Hz, 1H), 7.30 (dd, J = 8.2, 2.0 Hz, 1H), 4.13 (t, J = 1.3 Hz, 2H), 3.76 (s, 2H), 3.20 (t, J = 1.3 Hz, 2H).

^{13}C-NMR (101 MHz, MeOD) δ 176.50, 139.94, 133.46, 132.34, 131.70, 131.68, 129.52, 66.76, 58.20, 55.93. ESI-HRMS, Found 245.0255 $[M+H]^+$ $C_{10}H_{10}Cl_2N_2O$ requires 245.0243 $[M+H]^+$.

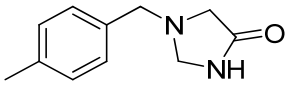

1-(4-methylbenzyl)imidazolidin-4-one (**127d**)

Imidazolidin-4-one (**111**) (30 mg, 0.35 mmol), and 4-methylbenzaldehyde were reacted according to General Method H. Yield (38 mg, 57%). ^{1}H-NMR (400 MHz, MeOD) δ 7.25 (d, J = 8.0 Hz, 2H), 7.17 (d, J = 7.8 Hz, 2H), 4.11 (t, J = 1.2 Hz, 2H), 3.74 (s, 2H), 3.19 (t, J = 1.2 Hz, 2H), 2.34 (s, 3H). ^{13}C-NMR (101 MHz, MeOD) δ 176.65, 138.50, 135.43, 130.22, 129.91, 66.65, 59.27, 55.97, 21.17. ESI-HRMS, Found 191.1173 [M+H]+ $C_{11}H_{14}N_2O$ requires 191.1179 [M+H]+.

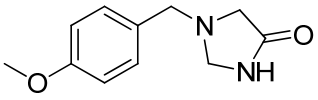

1-(4-methoxybenzyl)imidazolidin-4-one (**127e**)

Imidazolidin-4-one (**111**) (30 mg, 0.35 mmol), and 4-methoxybenzaldehyde were reacted according to General Method H. Yield (48 mg, 67%). ^{1}H-NMR (400 MHz, MeOD) δ 7.34 – 7.21 (m, 2H), 6.97 – 6.83 (m, 2H), 4.10 (t, J = 1.2 Hz, 2H), 3.80 (s, 3H), 3.71 (s, 2H), 3.18 (t, J = 1.2 Hz, 2H). ^{13}C-NMR (101 MHz, MeOD) δ 176.66, 160.75, 131.16, 130.44, 114.98, 66.59, 58.91, 55.92, 55.71. ESI-HRMS, Found 207.1125 $[M+H]^+$ $C_{11}H_{14}N_2O_2$ requires 207.1128 $[M+H]^+$.

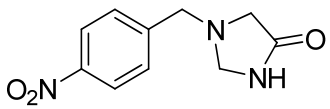

1-(4-nitrobenzyl)imidazolidin-4-one (**127f**)

Imidazolidin-4-one (**111**) (32 mg, 0.37 mmol), and 4-nitrobenzaldehyde were reacted according to General Method H. Yield (16 mg, 19%). ^{1}H-NMR (400 MHz, MeOD) δ 8.16 – 8.10 (m, 2H), 7.51 – 7.45 (m, 2H), 4.10 (t, J = 1.2 Hz, 2H), 3.82 (s, 2H), 3.18 (t, J = 1.2 Hz, 2H). ^{13}C-NMR (101 MHz, MeOD) δ 176.21,

148.83, 146.41, 130.50, 125.19, 67.14, 59.41, 56.38. ESI-HRMS, Found 222.0867 $[M+H]^+$ $C_{10}H_{11}N_3O_3$ requires 222.0873 $[M+H]^+$.

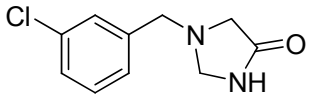

1-(3-chlorobenzyl)imidazolidin-4-one (**127g**)

Imidazolidin-4-one (**111**) (36 mg, 0.42 mmol), and 3-chlorobenzaldehyde were reacted according to General Method H. Yield (54 mg, 61%). ^{1}H-NMR (400 MHz, MeOD) δ 7.44 – 7.39 (m, 1H), 7.37 – 7.27 (m, 3H), 4.14 (t, J = 1.2 Hz, 2H), 3.78 (s, 2H), 3.21 (t, J = 1.2 Hz, 2H). ^{13}C-NMR (101 MHz, MeOD) δ 176.56, 141.30, 135.50, 131.15, 129.75, 128.73, 128.14, 66.76, 58.87, 55.97. ESI-HRMS, Found 211.0643 $[M+H]^+$ $C_{10}H_{11}ClN_2O$ requires 211.0633 $[M+H]^+$.

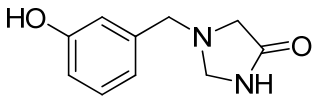

1-(3-hydroxybenzyl)imidazolidin-4-one (**127h**)

Imidazolidin-4-one (**111**) (30 mg, 0.35 mmol), and 3-hydroxybenzaldehyde were reacted according to General Method H. Yield (11 mg, 16%). ^{1}H-NMR (400 MHz, MeOD) δ 7.16 (t, J = 8.0 Hz, 1H), 6.85 – 6.80 (m, 2H), 6.72 (ddd, J = 8.1, 2.4, 1.0 Hz, 1H), 4.12 (t, J = 1.2 Hz, 2H), 3.71 (s, 2H), 3.20 (t, J = 1.2 Hz, 2H). ^{13}C-NMR (101 MHz, MeOD) δ 176.71, 158.79, 140.03, 130.61, 120.96, 116.62, 115.60, 66.70, 59.52, 56.02. ESI-HRMS, Found 193.0967 [M+H]+ $C_{10}H_{12}N_2O_2$ requires 193.0972 [M+H]+.

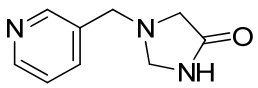

1-(pyridin-3-ylmethyl)imidazolidin-4-one (**127i**)

Imidazolidin-4-one (**111**) (30 mg, 0.35 mmol), and nicotinaldehyde were reacted according to General Method H. Yield (58 mg, 94%). ^{1}H-NMR (400 MHz, MeOD) δ 8.56 (d, J = 1.6 Hz, 1H), 8.49 (dd, J = 4.9, 1.6 Hz, 1H), 7.89 (ddd, J = 7.9, 2.2, 1.7 Hz, 1H), 7.45 (ddd, J = 7.8, 4.9, 0.7 Hz, 1H), 4.17 (t, J = 1.2 Hz, 2H), 3.86 (s, 2H), 3.23 (t, J = 1.2 Hz, 2H). ^{13}C-NMR (101 MHz, MeOD) δ 176.44, 150.35, 149.31, 138.73,

135.53, 125.36, 66.80, 56.54, 55.93.ESI-HRMS, Found 178.0983 [M+H]+ $C_9H_{11}N_3O$ requires 178.0975 [M+H]+.

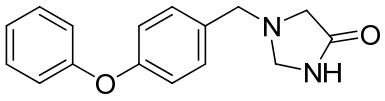

1-(4-phenoxybenzyl)imidazolidin-4-one (**127j**)

Imidazolidin-4-one (**111**) (30 mg, 0.35 mmol), and 4-phenoxybenzaldehyde were reacted according to General Method H. Yield (76 mg, 81%). ^{1}H-NMR (400 MHz, MeOD) δ 7.39 – 7.33 (m, 4H), 7.15 – 7.09 (m, 1H), 7.02 – 6.94 (m, 4H), 4.14 (t, J = 1.2 Hz, 2H), 3.77 (s, 2H), 3.21 (t, J = 1.2 Hz, 2H). ^{13}C-NMR (101 MHz, MeOD) δ 176.65, 158.61, 158.34, 133.50, 131.42, 130.92, 124.51, 119.97, 119.77, 66.68, 58.85, 55.96. ESI-HRMS, Found 269.1294 $[M+H]^+$ $C_{16}H_{16}N_2O_2$ requires 269.1285 $[M+H]^+$.

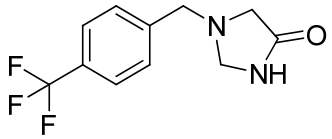

1-(4-(trifluoromethyl)benzyl)imidazolidin-4-one (**127k**)

Imidazolidin-4-one (**111**) (30 mg, 0.35 mmol), and 4-(trifluoromethyl)benzaldehyde were reacted according to General Method H. Yield (55 mg, 64%). ^{1}H-NMR (400 MHz, MeOD) δ 7.66 (d, J = 8.2 Hz, 2H), 7.59 (d, J = 8.0 Hz, 2H), 4.16 (t, J = 1.3 Hz, 2H), 3.89 (s, 2H), 3.23 (t, J = 1.3 Hz, 2H). ^{13}C-NMR (101 MHz, MeOD) δ 176.55, 143.59, 130.95, 130.63, 130.29, 127.07, 126.47 (q, J = 3.8 Hz), 124.37, 66.84, 58.92, 56.01. ESI-HRMS, Found 245.0908 $[M+H]^+$ $C_{11}H_{11}F_3N_2O$ requires 245.0896 $[M+H]^+$.

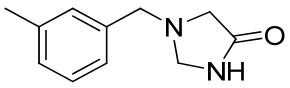

1-(3-methylbenzyl)imidazolidin-4-one (**127l**)

Imidazolidin-4-one (**111**) (30 mg, 0.35 mmol), and 3-methylbenzaldehyde were reacted according to General Method H. Yield (31 mg, 47%). ^{1}H-NMR (400 MHz, MeOD) δ 7.23 (t, J = 7.5 Hz, 1H), 7.19 (s, 1H), 7.15 (d, J = 7.6 Hz, 1H), 7.11 (d, J = 7.5 Hz, 1H), 4.12 (t, J = 1.2 Hz, 2H), 3.75 (s, 2H), 3.20 (t, J = 1.2 Hz, 2H),

2.35 (s, 3H). ^{13}C-NMR (101 MHz, MeOD) δ 176.67, 139.39, 138.46, 130.57, 129.52, 129.36, 126.98, 66.71, 59.56, 56.01, 21.43. ESI-HRMS, Found 191.1172 $[M+H]^+$ $C_{11}H_{14}N_2O$ requires 191.1179 $[M+H]^+$.

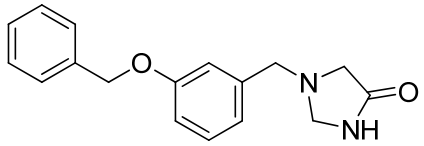

1-(3-(benzyloxy)benzyl)imidazolidin-4-one (**127m**)

Imidazolidin-4-one (**111**) (30 mg, 0.35 mmol), and 3-(benzyloxy)benzaldehyde were reacted according to General Method H. Yield (56 mg, 57%). ^{1}H-NMR (400 MHz, MeOD) δ 7.46 – 7.20 (m, 6H), 7.02 (t, J = 2.0 Hz, 1H), 6.97 – 6.89 (m, 2H), 5.08 (s, 2H), 4.08 (t, J = 1.2 Hz, 2H), 3.73 (s, 2H), 3.17 (t, J = 1.2 Hz, 2H). ^{13}C-NMR (101 MHz, MeOD) δ 176.65, 160.47, 140.19, 138.73, 130.67, 129.53, 128.91, 128.62, 122.36, 116.31, 115.35, 70.96, 66.69, 59.46, 56.00. ESI-HRMS, Found 283.1451 $[M+H]^+$ $C_{17}H_{18}N_2O_2$ requires 283.1441 $[M+H]^+$.

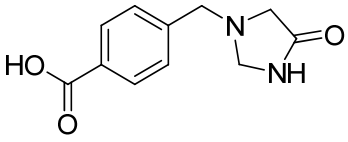

4-((4-oxoimidazolidin-1-yl)methyl)benzoic acid (**127n**)

Imidazolidin-4-one (**111**) (30 mg, 0.35 mmol), and 4-formylbenzoicacid were reacted according to General Method H. Yield (6 mg, 8%). ^{1}H-NMR (400 MHz, MeOD) δ 8.00 (d, J = 8.4 Hz, 2H), 7.48 (d, J = 8.5 Hz, 2H), 4.14 (t, J = 1.2 Hz, 2H), 3.86 (s, 2H), 3.22 (t, J = 1.2 Hz, 2H). ^{13}C-NMR (101 MHz, MeOD) δ 176.57, 169.65, 144.20, 131.04, 129.75, 66.82, 59.13, 56.02. ESI-HRMS, Found 219.0769 $[M-H]^-$ $C_{11}H_{12}N_2O_3$ requires 219.0775 $[M-H]^-$.

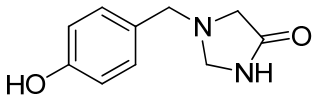

1-(4-hydroxybenzyl)imidazolidin-4-one (**127o**)

Imidazolidin-4-one (**111**) (30 mg, 0.35 mmol), and 4-hydroxybenzaldehyde were reacted according to General Method H. Yield (6 mg, 6%). ^{1}H-NMR (400 MHz, MeOD) δ 7.18 (d, J = 8.6 Hz, 2H), 6.77 (d, J = 8.6 Hz, 2H), 4.10 (t, J = 1.2 Hz, 2H), 3.69 (s, 2H), 3.19 (t, J = 1.2 Hz, 2H). ^{13}C-NMR (101 MHz, MeOD) δ 176.69, 158.16, 131.23, 129.11, 116.29, 66.53, 59.01, 55.89. ESI-HRMS, Found 193.0974 $[M+H]^+$ $C_{10}H_{12}N_2O_2$ requires 193.0972 $[M+H]^+$.

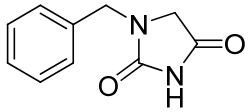

1-benzylimidazolidine-2,4-dione (**128**) [192]

A solution of benzylamine (638 mg, 5.95 mmol) in ether (15 ml) was added dropwise to a mixture of cyanogen bromide (504 mg, 4.75 mmol) in ether (15 ml) and the reaction was stirred at 0 °C for 1 h. The mixture was filtered to remove any precipitate, and the filtrate was washed with water (2 × 50 ml). The organic layer was collected, dried over sodium sulfate, filtered and concentrated under vacuum. The crude intermediate was partially purified by flash column chromatography to give **133** as a yellow oil (240 mg, 38%). The cyanamide intermediate (199 mg, 1.51 mmol) was dissolved in THF (8 ml) cooled to 0 °C followed by addition of sodium hydride (78 mg, 1.95 mmol) and stirred for 1 h. Methyl bromoacetate (231 mg, 1.51 mmol) was added and the reaction was stirred at 0 °C for a further 2 h. The reaction mixture was filtered to remove any precipitate; then diluted with DCM (20 ml), and washed with water (2 × 20 ml). The organic layer was collected and dried over sodium sulfate. The mixture was filtered and concentrated under vacuum to give the crude intermediate (**134**) as a clear oil (185 mg, 60%). Crude methyl 2-(N-benzylcyanamido)acetate (142 mg, 0.69 mmol) was taken up in THF (2 ml) and cooled to 0 °C. Concentrated sulfuric acid (2 ml) was added dropwise and the reaction was stirred for 30 mins at 0 °C and a further 2 h at room temperature. The reaction mixture was poured onto ice, and neutralized with sat. $NaHCO_3$ solution and extracted with DCM (2 × 10 ml). The extracts were combined, dried over sodium

sulfate, filtered and concentrated under vacuum. The residue was purified by flash column chromatography using 25% ethyl acetate in hexane to give a off white solid (27 mg, 20%). ^{1}H-NMR (400 MHz, MeOD) δ 7.31 – 7.12 (m, 5H), 4.41 (s, 2H), 3.71 (s, 2H). ^{13}C-NMR (101 MHz, MeOD) δ 173.58, 159.16, 137.48, 129.97, 129.05, 128.99, 51.49, 46.98. ESI-HRMS, Found 191.0823 $[M+H]^{+}$ $C_{10}H_{10}N_2O_2$ requires 191.0815 $[M+H]^{+}$.

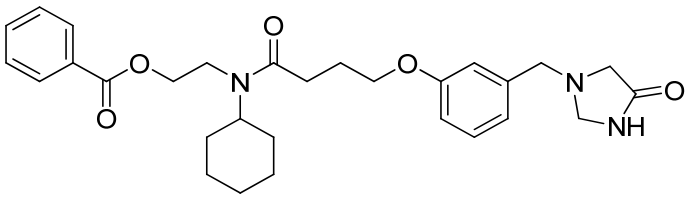

2-(N-cyclohexyl-4-(3-((4-oxoimidazolidin-1-yl)methyl)phenoxy)butanamido)ethyl benzoate (**129**)

4-(3-((4-oxoimidazolidin-1-yl)methyl)phenoxy)butanoic acid (**138**) (316 mg, 0.11 mmol), HCTU (53 mg, 0.13 mmol), and triethylamine (20 µl, 0.14 mmol) were stirred in DCM (5 ml) over activated molecular sieves for 30 mins at RT. *2-(cyclohexylamino)ethyl benzoate* (**140**) (31 mg, 0.13 mmol) was added and stirring continued for 16 h at RT. The mixture was diluted with methanol and filtered through a pad of celite. The filtrate was concentrated under reduced pressure. The resulting residue was purified by column chromatography using 5% methanol in chloroform as the eluent. The product was isolated as a yellow oil (45 mg, 78%). ^{1}H-NMR (400 MHz, DMSO, 350 °K) δ 8.01 – 7.94 (m, 2H), 7.87 (s, 1H), 7.68 – 7.60 (m, 1H), 7.55 – 7.47 (m, 2H), 7.21 (t, J = 8.0 Hz, 1H), 6.92 – 6.86 (m, 2H), 6.81 (d, J = 8.0 Hz, 1H), 4.35 (t, J = 5.1 Hz, 2H), 4.05 – 3.96 (m, 4H), 3.68 (s, 2H), 3.60 (bs, 2H), 3.03 (s, 2H), 2.54 (t, J = 7.1 Hz, 2H), 1.98 (p, J = 6.8 Hz, 2H), 1.79 – 1.49 (m, 7H), 1.37 – 1.25 (m, 2H), 1.16 – 1.07 (m, 1H). ^{13}C-NMR (101 MHz, MeOD) δ 173.37, 172.02, 165.76, 158.82, 139.64, 133.24, 129.40, 129.27, 129.05, 128.64, 120.40, 114.11, 113.07, 66.45, 64.86, 62.55, 57.71, 55.72, 54.58, 41.76, 30.98, 29.76, 28.78, 25.19, 24.50. ESI-HRMS, Found 508.2829 [M+H]+ $C_{29}H_{37}N_3O_5$ requires 508.2806 [M+H]+.

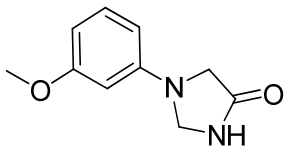

1-(3-methoxyphenyl)imidazolidin-4-one (**131**)

Prepared according to General Method G, stirred for 64 h. Yield (16 mg, 14%). ^{1}H-NMR (400 MHz, MeOD) δ 7.15 (t, J = 8.2 Hz, 1H), 6.36 (dd, J = 8.2, 1.8 Hz, 1H), 6.12 (dd, J = 8.1, 1.7 Hz, 1H), 6.04 (t, J = 2.3 Hz, 1H), 4.75 (t, J = 2.0 Hz, 2H), 3.82 (t, J = 2.0 Hz, 2H), 3.77 (s, 3H). ^{13}C-NMR (101 MHz, MeOD) δ 174.38, 162.30, 147.89, 131.62, 105.84, 104.51, 99.34, 62.67, 56.25, 50.81. ESI-HRMS, Found 193.0975 $[M+H]^+$ $C_{10}H_{12}N_2O_2$ requires 193.0972 $[M+H]^+$.

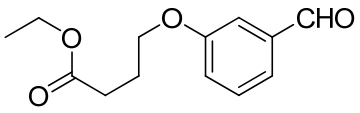

ethyl 4-(3-formylphenoxy)butanoate (**136**) [198]

3-hydroxybenzaldehyde (270 mg, 2.21 mmol), potassium carbonate (320 mg, 2.32 mmol), and ethyl-4-bromobutyrate (344 µl, 2.4 mmol) were dissolved in DMF (5 ml). The RBF was evacuated and charged with nitrogen. The reaction was stirred at 110 °C for 1 h. Water (50 ml) was added, the mixture was frozen and lyophilized. The resulting residue was taken up in ethyl acetate (100 ml) and washed with sat. $NaHCO_3$ (3 × 50 ml) and brine (2 × 50 ml). The organic layer was collected and dried over sodium sulfate. The mixture was filtered and concentrated to give a clear oil. The crude product was purified by column chromatography using chloroform as the eluent to give a clear oil (504 mg, 96%). ^{1}H-NMR (400 MHz, CDCl3) δ 9.96 (s, 1H), 7.45 – 7.40 (m, 2H), 7.38 – 7.34 (m, 1H), 7.16 (dt, J = 6.7, 2.6 Hz, 1H), 4.15 (q, J = 7.1 Hz, 2H), 4.07 (t, J = 6.2 Hz, 2H), 2.52 (t, J = 7.3 Hz, 2H), 2.13 (m, 2H), 1.25 (t, J = 7.1 Hz, 3H). ^{13}C-NMR (101 MHz, CDCl3) δ 192.08, 173.05, 159.42, 137.81, 130.05, 123.48, 121.85, 112.85, 67.06, 60.49, 30.73, 24.52, 14.22. ESI-MS, *m/z* 237.2, 12% $[M+H]^+$, 191.2, 100% $[M-C_2H_5O]^+$.

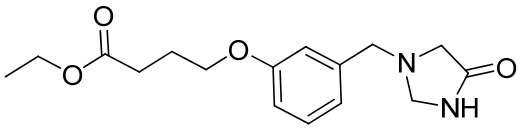

ethyl 4-(3-((4-oxoimidazolidin-1-yl)methyl)phenoxy)butanoate (**137**)

Imidazolidin-4-one (**111**) (30 mg, 0.35 mmol), was reacted with *ethyl 4-(3-formylphenoxy)butanoate* (**136**) according to General Method H. Yield (274 mg, 76%). ^{1}H-NMR (400 MHz, MeOD) δ 7.25 (t, J = 8.0 Hz, 1H), 6.94 (d, J = 7.1 Hz, 2H), 6.85 (ddd, J = 8.1, 2.3, 1.1 Hz, 1H), 4.19 – 4.10 (m, 4H), 4.03 (t, J = 6.2 Hz, 2H), 3.76 (s, 2H), 3.21 (t, J = 1.2 Hz, 2H), 2.52 (t, J = 7.3 Hz, 2H), 2.12 – 2.03 (m, 2H), 1.26 (t, J = 7.1 Hz, 3H). ^{13}C-NMR (101 MHz, MeOD) δ 176.66, 175.08, 160.64, 140.19, 130.63, 122.18, 115.86, 114.86, 67.94, 66.72, 61.57, 59.51, 56.02, 31.76, 25.87, 14.54. ESI-HRMS, Found 307.1639 $[M+H]^+$ $C_{16}H_{22}N_2O_4$ requires 307.1652 $[M+H]^+$.

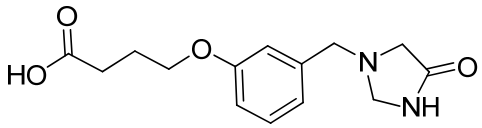

4-(3-((4-oxoimidazolidin-1-yl)methyl)phenoxy)butanoic acid (**138**)

Ethyl 4-(3-((4-oxoimidazolidin-1-yl)methyl)phenoxy)butanoate (**137**) (241 mg, 0.79 mmol) was taken up in ethanol (5 ml) and 2M NaOH (5 ml). The reaction was stirred at RT for 1 h. The reaction was neutralized by addition of glacial acetic acid. Ethanol was removed under reduced pressure. The aqueous mixture was extracted with DCM (5 × 10 ml). The organic extracts were combined and dried over sodium sulfate. The mixture was filtered and concentrated under reduced pressure. The resulting oil was purified by column chromatography using 10% methanol in chloroform as the eluent. The product was isolated as a white solid (122 mg, 56%). ^{1}H-NMR (400 MHz, MeOD) δ 7.23 (t, J = 7.9 Hz, 1H), 6.93 (dd, J = 7.5, 4.8 Hz, 2H), 6.87 – 6.82 (m, 1H), 4.11 (t, J = 1.2 Hz, 2H), 4.02 (t, J = 6.2 Hz, 2H), 3.74 (s, 2H), 3.20 (t, J = 1.2 Hz, 2H), 2.48 (t, J = 7.3 Hz, 2H), 2.10 – 2.01 (m, 2H). ^{13}C-NMR (101 MHz, MeOD) δ 177.13, 176.67, 160.68, 140.13, 130.62, 122.17, 115.91, 114.88, 68.00, 66.71, 59.52, 56.01, 31.52, 25.92. ESI-HRMS, Found 279.1353 $[M+H]^+$ $C_{14}H_{18}N_2O_4$ requires 279.1353 $[M+H]^+$.

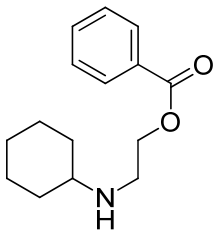

2-(cyclohexylamino)ethyl benzoate (**140**) [199]

N-cyclohexylethanolamine (1 g, 6.98 mmol) was dissolved in toluene (100 ml) and cooled to 0 °C. Benzoic anhydride (1.58 g, 6.98 mmol) was added and the reaction was stirred for 3 d at room temperature. The reaction was quenched with saturated $NaHCO_3$ solution (100 ml). The organic layer was extracted and washed with saturated $NaHCO_3$ solution (2 × 50 ml) and brine (2 × 50 ml), then dried over sodium sulfate and filtered. The filtrate was concentrated under reduced pressure. The resulting oil was purified by column chromatography using 5% methanol in chloroform as eluent to give a pale yellow oil (1.12 g, 65%). ^{1}H-NMR (400 MHz, CDCl3) δ 8.07 – 8.03 (m, 2H), 7.59 – 7.54 (m, 1H), 7.45 (tt, J = 6.8, 1.2 Hz, 2H), 4.43 (t, J = 5.6 Hz, 2H), 3.03 (t, J = 5.6 Hz, 2H), 2.51 (tt, J = 10.4, 3.8 Hz, 1H), 1.95 – 1.60 (m, 5H), 1.34 – 1.04 (m, 5H). ^{13}C-NMR (101 MHz, CDCl3) δ 166.62, 133.04, 130.33, 129.67, 128.46, 65.17, 56.55, 45.38, 33.73, 26.21, 25.11. ESI-MS, *m/z* 248.2.3, 100% $[M+H]^+$.

References

1. Manganiello, V. C.; Degerman, E. Cyclic nucleotide phosphodiesterases (PDEs): diverse regulators of cyclic nucleotide signals and inviting molecular targets for novel therapeutic agents. *Thrombosis and haemostasis* 1999, 82, 407-11.

2. Manganiello, V. C.; Degerman, E.; Editors-in-Chief: William, J. L.; Lane, M. D. Cyclic Nucleotide Phosphodiesterases. In *Encyclopedia of Biological Chemistry*, Elsevier: New York, 2004; pp 501-505.

3. Conti, M.; Jin, S. L. C.; Kivie, M. The Molecular Biology of Cyclic Nucleotide Phosphodiesterases. In *Progress in nucleic acid research and molecular biology*, Academic Press: 1999; Vol. Volume 63, pp 1-38.

4. Shakur, Y.; Holst, L. S.; Landstrom, T. R.; Movsesian, M.; Degerman, E.; Manganiello, V. Regulation and function of the cyclic nucleotide phosphodiesterase (PDE3) gene family. In *Progress in nucleic acid research and molecular biology*, Academic Press Inc: San Diego, 2001; Vol. 66, pp 241-277.

5. Movsesian, M. A.; Smith, C. J. In *Role of cyclic nucleotide phosphodiesterases in heart failure and hypertension*, 2007; CRC Press LLC: 2007; pp 485-500.

6. Manganiello, V. C.; Murata, T.; Taira, M.; Belfrage, P.; Degerman, E. Diversity in Cyclic Nucleotide Phosphodiesterase Isoenzyme Families. *Archives of Biochemistry and Biophysics* 1995, 322, 1-13.

7. Conti, M.; Nemoz, G.; Sette, C.; Vicini, E. Recent Progress in Understanding the Hormonal Regulation of Phosphodiesterases. *Endocrine Reviews* 1995, 16, 370-389.

8. Beavo, J. A. Cyclic nucleotide phosphodiesterases: functional implications of multiple isoforms. *Physiological Reviews* 1995, 75, 725-748.

9. Maurice, D. H.; Haslam, R. J. Molecular basis of the synergistic inhibition of platelet function by nitrovasodilators and activators of adenylate cyclase: inhibition of cyclic AMP breakdown by cyclic GMP. *Molecular Pharmacology* 1990, 37, 671-681.

10. Kirstein, M.; Rivet-Bastide, M.; Hatem, S.; Bernardeau, A.; Mercadier, J.-J.; Fischmeister, R. Nitric oxide regulates the calcium current in isolated human atrial myocytes. *The Journal of Clinical Investigation* 1995, 95, 794-802.

11. Meacci, E.; Taira, M.; Moos, M., Jr.; Smith, C. J.; Movsesian, M. A.; Degerman, E.; Belfrage, P.; Manganiello, V. Molecular cloning and expression of human myocardial cGMP-inhibited cAMP phosphodiesterase. *Proceedings of the National Academy of Sciences of the United States of America* 1992, 89, 3721-5.

12. Taira, M.; Hockman, S. C.; Calvo, J. C.; Belfrage, P.; Manganiello, V. C. Molecular cloning of the rat adipocyte hormone-sensitive cyclic GMP-inhibited cyclic nucleotide phosphodiesterase. *Journal of Biological Chemistry* 1993, 268, 18573-18579.

13. Löbbert, R. W.; Winterpacht, A.; Seipel, B.; Zabel, B. U. Molecular Cloning and Chromosomal Assignment of the Human Homologue of the Rat cGMP-Inhibited Phosphodiesterase 1 (PDE3A)--A Gene Involved in Fat Metabolism Located at 11p15.1. *Genomics* 1996, 37, 211-218.

14. Miki, T.; Taira, M.; Hockman, S.; Shimada, F.; Lieman, J.; Napolitano, M.; Ward, D.; Taira, M.; Makino, H.; Manganiello, V. C. Characterization of the cDNA and Gene Encoding Human PDE3B, the cGIP1 Isoform of the Human Cyclic GMP-Inhibited Cyclic Nucleotide Phosphodiesterase Family. *Genomics* 1996, 36, 476-485.

15. Degerman, E.; Manganiello, V. Phosphodiesterase 3B: An Important Regulator of Energy Homeostasis. In *Cyclic Nucleotide Phosphodiesterases in Health and Disease*, CRC Press: 2006.

16. Klannemark, M. I. A.; Orho-Melander, M.; Aberg, M.; Groop, L. Association Between the Phosphodiesterase 3B Gene and Features of the Metabolic Syndrome. (abstract). *Diabetes* 1999, 48, SA408.

17. Osawa, H.; Niiya, T.; Onuma, H.; Murakami, A.; Ochi, M.; Nishimiya, T.; Ogura, T.; Kato, K.; Shimizu, I.; Fujii, Y.; Ohashi, J.; Yamada, K.; Liang, S.-J.; Manganiello, V. C.; Fujita-Yamaguchi, Y.; Makino, H. Systematic search for single nucleotide polymorphisms in the 5â€² flanking region of the human phosphodiesterase 3B gene: absence of evidence for major effects of identified polymorphisms on susceptibility to Japanese type 2 diabetes. *Molecular Genetics and Metabolism* 2003, 79, 43-51.

18. Omburo, G. A.; Brickus, T.; Ghazaleh, F. A.; Colman, R. W. Divalent metal cation requirement and possible classification of cGMP-inhibited phosphodiesterase as a metallohydrolase. *Arch. Biochem. Biophys.* 1995, 323, 1-5.

19. Charbonneau, H.; Beier, N.; Walsh, K. A.; Beavo, J. A. Identification of a conserved domain among cyclic nucleotide phosphodiesterases from diverse species. *Proceedings of the National Academy of Sciences of the United States of America* 1986, 83, 9308-9312.

20. Leroy, M.-J.; Degerman, E.; Taira, M.; Murata, T.; Wang, L. H.; Movsesian, M. A.; Meacci, E.; Manganiello, V. C. Characterization of Two Recombinant PDE3 (cGMP-Inhibited Cyclic Nucleotide Phosphodiesterase) Isoforms, RcGIP1 and HcGIP2, Expressed in NIH 3006 Murine Fibroblasts and Sf9 Insect Cells *Biochemistry* 1996, 35, 10194-10202.

21. Varnerin, J. P.; Chung, C. C.; Patel, S. B.; Scapin, G.; Parmee, E. R.; Morin, N. R.; MacNeil, D. J.; Cully, D. F.; Van der Ploeg, L. H. T.; Tota, M. R. Expression, refolding, and purification of recombinant human phosphodiesterase 3B: definition of the N-terminus of the catalytic core. *Protein Expression and Purification* 2004, 35, 225-236.

22. He, R.; Komas, N.; Ekholm, D.; Murata, T.; Taira, M.; Hockman, S.; Degerman, E.; Manganiello, V. C. Expression and characterization of deletion recombinants of two cGMP-inhibited cyclic nucleotide phosphodiesterases (PDE-3). *Cell Biochemistry and Biophysics* 1998, 29, 89-111.

23. Kenan, Y.; Murata, T.; Shakur, Y.; Degerman, E.; Manganiello, V. C. Functions of the N-terminal region of cyclic nucleotide phosphodiesterase 3 (PDE 3) isoforms. *The Journal of Biological Chemistry* 2000, 275, 12331-8.

24. Tang, K. M.; Jang, E. K.; Haslam, R. J. Expression and mutagenesis of the catalytic domain of cGMP-inhibited phosphodiesterase (PDE3) cloned from human platelets. *The Biochemical journal* 1997, 323, 217-224.

25. Reinhardt, R. R.; Chin, E.; Zhou, J.; Taira, M.; Murata, T.; Manganiello, V. C.; Bondy, C. A. Distinctive anatomical patterns of gene expression for cGMP-inhibited cyclic nucleotide phosphodiesterases. *Journal of Clinical Investigation* 1995, 95, 1528-38.

26. Zhao, A. Z.; Zhao, H.; Teague, J.; Fujimoto, W.; Beavo, J. A. Attenuation of insulin secretion by insulin-like growth factor 1 is mediated through activation of phosphodiesterase 3B. *Proceedings of the National Academy of Sciences* 1997, 94, 3223-3228.

27. Reinhardt, R. R.; Bondy, C. A. Differential cellular pattern of gene expression for two distinct cGMP-inhibited cyclic nucleotide phosphodiesterases in developing and mature rat brain. *Neuroscience* 1996, 72, 567-578.

28. Degerman, E.; Moos, M., Jr.; Rascon, A.; Vasta, V.; Meacci, E.; Smith, C. J.; Lindgren, S.; Andersson, K. E.; Belfrage, P.; Manganiello, V. Single-step affinity purification, partial structure and properties of human platelet cGMP inhibited cAMP phosphodiesterase. *Biochimica et biophysica acta* 1994, 1205, 189-98.

29. Schudt, C.; Gantner, F.; Tenors, H.; Hatzelmann, A. Therapeutic Potential of Selective PDE Inhibitors in Asthma. *Pulmonary Pharmacology & Therapeutics* 1999, 12, 123-129.

30. Sun, B.; Li, H.; Shakur, Y.; Hensley, J.; Hockman, S.; Kambayashi, J.; Manganiello, V. C.; Liu, Y. Role of phosphodiesterase type 3A and 3B in regulating platelet and cardiac function using subtype-selective knockout mice. *Cellular Signalling* 2007, 19, 1765-1771.

31. Choi, Y. H.; Park, S.; Hockman, S.; Zmuda-Trzebiatowska, E. Alterations in regulation of energy homeostasis in cyclic nucleotide phosphodiesterase 3B-null mice. *Journal of Clinical Investigation* 2006, 116, 3240-51.

32. Chini, C. C. S.; Grande, J. P.; Chini, E. N.; Dousa, T. P. Compartmentalization of cAMP Signaling in Mesangial Cells by Phosphodiesterase Isozymes PDE3 and PDE4 Regulation of Superoxidation and Mitogenesis. *Journal of Biological Chemistry* 1997, 272, 9854-9859.

33. Kono, T.; Robinson, F. W.; Sarver, J. A. Insulin-sensitive phosphodiesterase. Its localization, hormonal stimulation, and oxidative stabilization. *Journal of Biological Chemistry* 1975, 250, 7826-7835.

34. Grant, P. G.; Coleman, R. W. Purification and Characeterisation of a Human Platelet Cyclic Nucleotide Phosphodiesterase. *Biochemistry* 1984, 23, 1801-1807.

35. Liu, H.; Maurice, D. H. Expression of cyclic GMP-inhibited phosphodiesterases 3A and 3B (PDE3A and PDE3B) in rat tissues: Differential subcellular localization and regulated expression by cyclic AMP. *British Journal of Pharmacology* 1998, 125, 1501-1510.

36. Shakur, Y.; Takeda, K.; Kenan, Y.; Yu, Z.-X.; Rena, G.; Brandt, D.; Houslay, M. D.; Degerman, E.; Ferrans, V. J.; Manganiello, V. C. Membrane Localization of Cyclic Nucleotide Phosphodiesterase 3 (PDE3). *Journal of Biological Chemistry* 2000, 275, 38749-38761.

37. Hambleton, R.; Krall, J.; Tikishvili, E.; Honeggar, M.; Ahmad, F.; Manganiello, V. C.; Movsesian, M. A. Isoforms of Cyclic Nucleotide Phosphodiesterase PDE3 and Their Contribution to cAMP Hydrolytic Activity in Subcellular Fractions of Human Myocardium. *Journal of Biological Chemistry* 2005, 280, 39168-39174.

38. Choi, Y. H.; Ekholm, D.; Krall, J.; Ahmad, F.; Degerman, E.; Manganiello, V. C.; Movsesian, M. A. Identification of a novel isoform of the cyclic-nucleotide phosphodiesterase PDE3A expressed in vascular smooth-muscle myocytes. *The Biochemical journal* 2001, 353, 41-50.

39. Smith, C. J.; Krall, J.; Manganiello, V. C.; Movsesian, M. A. Cytosolic and Sarcoplasmic Reticulum-Associated Low Km, cGMP-Inhibited cAMP Phosphodiesterase in Mammalian Myocardium. *Biochemical and Biophysical Research Communications* 1993, 190, 516-521.

40. Wechsler, J.; Choi, Y.-H.; Krall, J.; Ahmad, F.; Manganiello, V. C.; Movsesian, M. A. Isoforms of Cyclic Nucleotide Phosphodiesterase PDE3A in Cardiac Myocytes. *Journal of Biological Chemistry* 2002, 277, 38072-38078.

41. Nilsson, R.; Ahmad, F.; Swärd, K.; Andersson, U.; Weston, M.; Manganiello, V.; Degerman, E. Plasma membrane cyclic nucleotide phosphodiesterase 3B (PDE3B) is associated with caveolae in primary adipocytes. *Cellular Signalling* 2006, 18, 1713-1721.

42. Razani, B.; Combs, T. P.; Wang, X. B.; Frank, P. G.; Park, D. S.; Russell, R. G.; Li, M.; Tang, B.; Jelicks, L. A.; Scherer, P. E.; Lisanti, M. P. Caveolin-1-deficient Mice Are Lean, Resistant to Diet-induced Obesity, and Show Hypertriglyceridemia with Adipocyte Abnormalities. *Journal of Biological Chemistry* 2002, 277, 8635-8647.

43. Cohen, A. W.; Combs, T. P.; Scherer, P. E.; Lisanti, M. P. Role of caveolin and caveolae in insulin signaling and diabetes. *American Journal of Physiology - Endocrinology And Metabolism* 2003, 285, E1151-E1160.

44. Lee, M. E.; Markowitz, J.; Lee, J.-O.; Lee, H. Crystal structure of phosphodiesterase 4D and inhibitor complex. *FEBS letters* 2002, 530, 53-58.

45. Scapin, G.; Patel, S. B.; Chung, C.; Varnerin, J. P.; Edmondson, S. D.; Mastracchio, A.; Parmee, E. R.; Singh, S. B.; Becker, J. W.; Van der Ploeg, L. H.; Tota, M. R. Crystal structure of human phosphodiesterase 3B: atomic basis for substrate and inhibitor specificity. *Biochemistry* 2004, 43, 6091-100.

46. Enoksson, S.; Degerman, E.; Hagström-Toft, E.; Large, V.; Arner, P. Various phosphodiesterase subtypes mediate the in vivo antilipolytic effect of insulin on adipose tissue and skeletal muscle in man. *Diabetologia* 1998, 41, 560-568.

47. Beebe, S. J.; Redmon, J. B.; Blackmore, P. F.; Corbin, J. D. Discriminative insulin antagonism of stimulatory effects of various cAMP analogs on adipocyte lipolysis and hepatocyte glycogenolysis. *Journal of Biological Chemistry* 1985, 260, 15781-15788.

48. Ahmad, F.; Cong, L.-N.; Stenson Holst, L.; Wang, L.-M.; Rahn Landstrom, T.; Pierce, J. H.; Quon, M. J.; Degerman, E.; Manganiello, V. C. Cyclic Nucleotide Phosphodiesterase 3B Is a Downstream Target of Protein Kinase B and May Be Involved in Regulation of Effects of Protein Kinase B on Thymidine Incorporation in FDCP2 Cells. *The Journal of Immunology* 2000, 164, 4678-4688.

49. Boyes, S.; Loten, E. G. Purification of an insulin-sensitive cyclic AMP phosphodiesterase from rat liver. *European Journal of Biochemistry* 1988, 174, 303-309.

50. Pyne, N. J.; Cooper, M. E.; Houslay, M. D. The insulin- and glucagon-stimulated 'dense-vesicle' high-affinity cyclic AMP phosphodiesterase from rat liver. Purification, characterization and inhibitor sensitivity. *The Biochemical journal* 1987, 242, 33-42.

51. Degerman, E.; Belfrage, P.; Manganiello, V. C. Structure, localization, and regulation of cGMP-inhibited phosphodiesterase (PDE3). *Journal of Biological Chemistry* 1997, 272, 6823-6826.

52. Resjo, S.; Oknianska, A.; Zolnierowicz, S.; Manganiello, V.; Degerman, E. Phosphorylation and activation of phosphodiesterase type 3B (PDE3B) in adipocytes in response to serine/threonine phosphatase inhibitors: deactivation of PDE3B in vitro by protein phosphatase type 2A. *The Biochemical journal* 1999, 341, 839-845.

53. Zhang, W.; Colman, R. W. Thrombin regulates intracellular cyclic AMP concentration in human platelets through phosphorylation/activation of phosphodiesterase 3A. *Blood* 2007, 110, 1475-1482.

54. Pozuelo Rubio, M.; Campbell, D. G.; Morrice, N. A.; Mackintosh, C. Phosphodiesterase 3A binds to 14-3-3 proteins in response to PMA-induced phosphorylation of Ser428. *The Biochemical journal.* 2005, 392, 163-172.

55. Hunter, R. W.; MacKintosh, C.; Hers, I. Protein Kinase C-mediated Phosphorylation and Activation of PDE3A Regulate cAMP Levels in Human Platelets. *Journal of Biological Chemistry* 2009, 284, 12339-12348.

56. Elbatarny, H. S.; Maurice, D. H. Leptin-mediated activation of human platelets: involvement of a leptin receptor and phosphodiesterase 3A-containing cellular signaling complex. *American Journal of Physiology - Endocrinology And Metabolism* 2005, 289, E695-E702.

57. Movsesian, M. A. PDE3 cyclic nucleotide phosphodiesterases and the compartmentation of cyclic nucleotide-mediated signalling in cardiac myocytes. *Basic Research in Cardiology* 2002, 97, 1/83-1/90.

58. Jiang, H.; Colbran, J. L.; Francis, S. H.; Corbin, J. D. Direct evidence for cross-activation of cGMP-dependent protein kinase by cAMP in pig coronary arteries. *Journal of Biological Chemistry* 1992, 267, 1015-1019.

59. Takahashi, S.; Oida, K.; Fujiwara, R.; Maeda, H.; Hayashi, S.; Takai, H.; Tamai, T.; Nakai, T.; Miyabo, S. Effect of Cilostazol, a Cyclic AMP Phosphodiesterase Inhibitor, on the Proliferation of Rat Aortic Smooth Muscle Cells in Culture. *Journal of Cardiovascular Pharmacology* 1992, 20, 900-906.

60. Take, M. D. S.; Matsutani, M. D. M.; Ueda, M. D. H.; Hamaguchi, M. D. H.; Konishi, M. D. H.; Baba, M. D. Y.; Kawaratani, M. D. H.; Suguira, M. D. T.; Iwasaka, M. D. T.; Inada, M. D. M. Effect of Cilostazol in Preventing Restenosis After Percutaneous Transluminal Coronary Angioplasty. *The American Journal of Cardiology* 1997, 79, 1097-1099.

61. Tsuchikane, E.; Katoh, O.; Sumitsuji, S.; Fukuhara, A.; Funamoto, M.; Otsuji, S.; Tateyama, H.; Awata, N.; Kobayashi, T. Impact of cilostazol on intimal proliferation after directional coronary atherectomy. *American Heart Journal* 1998, 135, 495-502.

62. Myou, S.; Fujimura, M.; Kamio, Y.; Ishiura, Y.; Tachibana, H.; Hirose, T.; Hashimoto, T.; Matsuda, T. Bronchodilator Effect of Inhaled Olprinone, a Phosphodiesterase 3 Inhibitor, in Asthmatic Patients. *American Journal of Respiratory and Critical Care Medicine* 1999, 160, 817-820.

63. Palmer, D.; Maurice, D. H. Dual Expression and Differential Regulation of Phosphodiesterase 3A and Phosphodiesterase 3B in Human Vascular Smooth Muscle: Implications for Phosphodiesterase 3 Inhibition in Human Cardiovascular Tissues. *Molecular Pharmacology* 2000, 58, 247-252.

64. Begum, N.; Hockman, S.; Manganiello, V. C. Phosphodiesterase 3A (PDE3A) deletion suppresses proliferation of cultured murine vascular smooth muscle cells (VSMCs) via inhibition of mitogen-activated protein kinase (MAPK) signaling and alterations in critical cell cycle regulatory proteins. *Journal of Biological Chemistry* 2011, 286, 26238-26249.

65. Masciarelli, S.; Horner, K.; Liu, C. Y.; Park, S. H.; Hinckley, M.; Hockman, S.; Nedachi, T.; Jin, C.; Conti, M.; Manganiello, V. Cyclic nucleotide phosphodiesterase 3A-deficient mice as a model of female infertility. *Journal of Clinical Investigation* 2004, 114, 196-205.

66. Boden, G. Role of fatty acids in the pathogenesis of insulin resistance and NIDDM. *Diabetes* 1997, 46, 3-10.

67. McGarry, J. D.; Dobbins, R. L. Fatty acids, lipotoxicity and insulin secretion. *Diabetologia* 1999, 42, 128-138.

68. Nagaoka, T.; Shirakawa, T.; Balon, T. W.; Russell, J. C.; Fujita-Yamaguchi, Y. Cyclic nucleotide phosphodiesterase 3 expression in vivo: Evidence for tissue-specific expression of phosphodiesterase 3A or 3B mRNA and activity in the aorta and adipose tissue of atherosclerosis-prone insulin-resistant rats. *Diabetes* 1998, 47, 1135-44.

69. Engfeldt, P.; Arner, P.; Bolinder, J.; Ostman, J. Phosphodiesterase Activity in Human Subcutaneous Adipose Tissue in Insulin- and Noninsulin-Dependent Diabetes Mellitus. *Journal of Clinical Endocrinology & Metabolism* 1982, 55, 983-988.

70. Cheung, P.; Yang, G.; Boden, G. Milrinone, a selective phosphodiesterase 3 inhibitor, stimulates lipolysis, endogenous glucose production, and insulin secretion. *Metabolism: clinical and experimental* 2003, 52, 1496-1500.

71. El-Metwally, M.; Shafiee-Nick, R.; Pyne, N. J.; Furman, B. L. The effect of selective phosphodiesterase inhibitors on plasma insulin concentrations and insulin secretion in vitro in the rat. *European Journal of Pharmacology* 1997, 324, 227-232.

72. Allan, Z.; Lena Stenson, H. Regulation of cAMP Level by PDE3B - Physiological Implications in Energy Balance and Insulin Secretion. In *Cyclic Nucleotide Phosphodiesterases in Health and Disease*, CRC Press: 2006.

73. Cohn, J. N.; Goldstein, S. O.; Greenberg, B. H.; Lorell, B. H. A dose-dependent increase in mortality with vesnarinone among patients with severe heart failure. *The New England Journal of Medicine* 1998, 339, 1810-6.

74. Feldman, A. M.; Bristow, M. R.; Parmley, W. W.; Carson, P. E.; Pepine, C. J.; Gilbert, E. M.; Strobeck, J. E.; Hendrix, G. H.; Powers, E. R.; Bain, R. P.; White, B. G. Effects of Vesnarinone on Morbidity and Mortality in Patients with Heart Failure. *New England Journal of Medicine* 1993, 329, 149-155.

75. Nony, P.; Boissel, J. P.; Lievre, M.; Leizorovicz, A.; Haugh, M. C.; Fareh, S.; De Breyne, B. Evaluation of the effect of phosphodiesterase inhibitors on mortality in chronic heart failure patients. *European Journal of Clinical Pharmacology* 1994, 46, 191-196.

76. Packer, M.; Carver, J. R.; Rodeheffer, R. J.; Ivanhoe, R. J.; DiBianco, R.; Zeldis, S. M.; Hendrix, G. H.; Bommer, W. J.; Elkayam, U.; Kukin, M. L.; Mallis, G. I.; Sollano, J. A.; Shannon, J.; Tandon, P. K.; DeMets, D. L. Effect of Oral Milrinone on Mortality in Severe Chronic Heart Failure. *New England Journal of Medicine* 1991, 325, 1468-1475.

77. Uretsky, B. F.; Jessup, M.; Konstam, M. A.; Dec, G. W.; Leier, C. V.; Benotti, J.; Murali, S.; Herrmann, H. C.; Sandberg, J. A. Multicenter trial of oral enoximone in patients with moderate to moderately severe congestive heart failure. Lack of benefit compared with placebo. *Circulation* 1990, 82, 774-780.

78. Ding, B.; Abe, J.-i.; Wei, H.; Huang, Q.; Walsh, R. A.; Molina, C. A.; Zhao, A.; Sadoshima, J.; Blaxall, B. C.; Berk, B. C.; Yan, C. Functional role of phosphodiesterase 3 in cardiomyocyte apoptosis: implication in heart failure. *Circulation* 2005, 111, 2469-76.

79. Feldman, M. D.; Copelas, L.; Gwathmey, J. K.; Phillips, P.; Warren, S. E.; Schoen, F. J.; Grossman, W.; Morgan, J. P. Deficient production of cyclic AMP: pharmacologic evidence of an important cause of contractile dysfunction in patients with end-stage heart failure. *Circulation* 1987, 75, 331-9.

80. Yan, C.; Miller, C. L.; Abe, J.-i. Regulation of Phosphodiesterase 3 and Inducible cAMP Early Repressor in the Heart. *Circ. Res.* 2007, 100, 489-501.

81. Ding, B.; Abe, J.-i.; Wei, H.; Xu, H.; Che, W.; Aizawa, T.; Liu, W.; Molina, C. A.; Sadoshima, J.; Blaxall, B. C.; Berk, B. C.; Yan, C. A positive feedback loop of phosphodiesterase 3 (PDE3) and inducible cAMP early repressor (ICER) leads to cardiomyocyte apoptosis. *Proceedings of the National Academy of Sciences of the United States of America* 2005, 102, 14771-14776.

82. Tomita, H.; Nazmy, M.; Kajimoto, K.; Yehia, G.; Molina, C. A.; Sadoshima, J. Inducible cAMP early repressor (ICER) is a negative-feedback regulator of cardiac hypertrophy and an important mediator of cardiac myocyte apoptosis in response to β-adrenergic receptor stimulation. *Circulation Research* 2003, 93, 12-22.

83. Bohm, M.; Reiger, B.; Schwinger, R. H. G.; Erdmann, E. cAMP concentrations, cAMP dependent protein kinase activity, and phospholamban in non-failing and failing myocardium. *Cardiovascular Research* 1994, 28, 1713-1719.

84. Benotti, J. R.; Grossman, W.; Braunwald, E.; Davolos, D. D.; Alousi, A. A. Hemodynamic assessment of amrinone. A new inotropic agent. *New England Journal of Medicine* 1978, 299, 1373-7.

85. Dibianco, R.; Shabetai, R.; Silverman, B. D.; Leier, C. V.; Benotti, J. R. Oral amrinone for the treatment of chronic congestive heart failure: Results of a multicenter randomized double-blind and placebo-controlled withdrawal study. *Journal of the American College of Cardiology* 1984, 4, 855-866.

86. Massie, B.; Bourassa, M.; DiBianco, R.; Hess, M.; Konstam, M.; Likoff, M.; Packer, M. Long-term oral administration of amrinone for congestive heart failure: lack of efficacy in a multicenter controlled trial. *Circulation* 1985, 71, 963-971.

87. Lowes, B. D.; Higginbotham, M.; Petrovich, L.; DeWood, M. A.; Greenberg, M. A.; Rahko, P. S.; Dec, G. W.; LeJemtel, T. H.; Roden, R. L.; Schleman, M. M.; Robertson, A. D.; Gorczynski, R. J.; Bristow, M. R. Low-dose enoximone improves exercise capacity in chronic heart failure. *Journal of the American College of Cardiology* 2000, 36, 501-508.

88. Packer, M. The search for the ideal positive inotropic agent. *New England Journal of Medicine* 1993, 329, 201-2.

89. Kieback, A. G.; Iven, H.; Stolzenburg, K.; Eichner, E.; Ruckdeschel, W.; Baumann, G. Pharmacokinetics and hemodynamic effects of the phosphodiesterase III inhibitor saterinone in patients with chronic heart failure. *International Journal of Cardiology* 2003, 91, 201-8.

90. Mebazaa, A.; Nieminen, M. S.; Packer, M.; Cohen-Solal, A.; Kleber, F. X.; Pocock, S. J.; Thakkar, R.; Padley, R. J.; Põder, P.; Kivikko, M. Levosimendan vs Dobutamine for Patients With Acute Decompensated Heart Failure. *JAMA: The Journal of the American Medical Association* 2007, 297, 1883-1891.

91. Mebazaa, A.; Nieminen, M. S.; Filippatos, G. S.; Cleland, J. G.; Salon, J. E.; Thakkar, R.; Padley, R. J.; Huang, B.; Cohen-Solal, A. Levosimendan vs. dobutamine: outcomes for acute heart failure patients on β-blockers in SURVIVEâ€ *European Journal of Heart Failure* 2009, 11, 304-311.

92. Liu, Y.; Fong, M.; Cone, J.; Wang, S.; Yoshitake, M.; Kambayashi, J.-I. Inhibition of adenosine uptake and augmentation of ischemia-induced increase of interstitial adenosine by cilostazol, an agent to treat intermittent claudication. *Journal of Cardiovascular Pharmacology* 2000, 36, 351-360.

93. Liu, Y.; Shakur, Y.; Yoshitake, M.; Kambayashi, J.-I. Cilostazol (Pletal): a dual inhibitor of cyclic nucleotide phosphodiesterase type 3 and adenosine uptake. *Cardiovascular Drug Reviews* 2001, 19, 369-386.

94. Wang, S.; Cone, J.; Fong, M.; Yoshitake, M.; Kambayashi, J.-I.; Liu, Y. Interplay between inhibition of adenosine uptake and phosphodiesterase type 3 on cardiac function by cilostazol, an agent to treat intermittent claudication. *Journal of Cardiovascular Pharmacology* 2001, 38, 775-783.

95. Sun, B.; Le, S. N.; Lin, S.; Fong, M.; Guertin, M.; Liu, Y.; Tandon, N. N.; Yoshitake, M.; Kambayashi, J.-i. New Mechanism of Action for Cilostazol: Interplay Between Adenosine and Cilostazol in Inhibiting Platelet Activation. *Journal of Cardiovascular Pharmacology* 2002, 40, 577-585.

96. Kambayashi, J.; Liu, Y.; Sun, B.; Shakur, Y.; Yoshitake, M.; Czerwiec, F. Cilostazol as a unique antithrombotic agent. *Current Pharmaceutical Design* 2003, 9, 2289-2302.

97. Shakur, Y.; Liu, Y.; Kambayashi, J. Bench to Bedside. In *Cyclic Nucleotide Phosphodiesterases in Health and Disease*, CRC Press: 2006.

98. Igawa, T.; Tani, T.; Chijiwa, T.; Shiragiku, T.; Shimidzu, S.; Kawamura, K.; Kato, S.; Unemi, F.; Kimura, Y. Potentiation of anti-platelet aggregating activity of cilostazol with vascular endothelial cells. *Thrombosis Research* 1990, 57, 617-623.

99. Kim, J.-S.; Lee, K.-S.; Kim, Y.-I.; Tamai, Y.; Nakahata, R.; Takami, H. A randomized crossover comparative study of aspirin, cilostazol and clopidogrel in normal controls: analysis with quantitative bleeding time and platelet aggregation test. *Journal of Clinical Neuroscience* 2004, 11, 600-602.

100. Shimizu, E.; Kobayashi, Y.; Oki, Y.; Kawasaki, T.; Yoshimi, T.; Nakamura, H. OPC-13013, a cyclic nucleotide phosphodiesterase type III inhibitor, inhibits cell proliferation and transdifferentiation of cultured rat hepatic stellate cells. *Life Sciences* 1999, 64, 2081-2088.

101. Lee, J. H.; Lee, Y.-K.; Ishikawa, M.; Koga, K.; Fukunaga, M.; Miyakoda, G.; Mori, T.; Hosokawa, T.; Hong, K. W. Cilostazol reduces brain lesion induced by focal cerebral ischemia in rats - an MRI study. *Brain Research* 2003, 994, 91-98.

102. Nakamura, N.; Hamazaki, T.; Johkaji, H.; Minami, S.; Yamazaki, K.; Satoh, A.; Sawazaki, S.; Urakaze, M.; Kobayashi, M.; Osawa, H.; Yamabe, H.; Okomura, K. Effects of cilostazol on serum lipid concentrations and plasma fatty acid composition in type 2 diabetic patients with peripheral vascular disease. *Clinical and Experimental Medicine* 2003, 2, 180-184.

103. Gotoh, F.; Tohgi, H.; Hirai, S.; Terashi, A.; Fukuuchi, Y.; Otomo, E.; Shinohara, Y.; Itoh, E.; Matsuda, T.; Sawada, T.; Yamaguchi, T.; Nishimaru, K.; Ohashi, Y. Cilostazol stroke prevention study: A placebo-controlled double-blind trial for secondary prevention of cerebral infarction. *Journal of Stroke and Cerebrovascular Diseases* 2000, 9, 147-157.

104. Shakur, Y.; Fong, M.; Hensley, J.; Cone, J.; Movsesian, M. A.; Kambayashi, J.-i.; Yoshitake, M.; Liu, Y. Comparison of the Effects of Cilostazol and Milrinone on cAMP-PDE Activity, Intracellular cAMP and Calcium in the Heart. *Cardiovascular Drugs and Therapy* 2002, 16, 417-427.

105. Lehnart, S. E.; Wehrens, X. H. T.; Reiken, S.; Warrier, S.; Belevych, A. E.; Harvey, R. D.; Richter, W.; Jin, S. L. C.; Conti, M.; Marks, A. R. Phosphodiesterase 4D deficiency in the ryanodine-receptor complex promotes heart failure and arrhythmias. *Cell* 2005, 123, 25-35.

106. Sudo, T.; Tachibana, K.; Toga, K.; Tochizawa, S.; Inoue, Y.; Kimura, Y.; Hidaka, H. Potent effects of novel anti-platelet aggregatory cilostamide analogues on recombinant cyclic nucleotide phosphodiesterase isozyme activity. *Biochemical Pharmacology* 2000, 59, 347-356.

107. Fleming, J. S.; Buyniski, J. P. A potent new inhibitor of platelet aggregation and experimental thrombosis, anagrelide (BL-4162A). *Thrombosis Research* 1979, 15, 373-388.

108. Andes, W. A.; Noveck, R. J.; Fleming, J. S. Inhibition of platelet production induced by an antiplatelet drug, anagrelide, in normal volunteers. *Thrombosis and haemostasis* 1984, 52, 325-8.

109. Alvarez, R.; Banerjee, G. L.; Bruno, J. J.; Jones, G. L.; Liittschwager, K.; Strosberg, A. M.; Venuti, M. C. A potent and selective inhibitor of cyclic AMP phosphodiesterase with potential cardiotonic and antithrombotic properties. *Mol. Pharmacol.* 1986, 29, 554-60.

110. Venuti, M. C.; Alvarez, R.; Bruno, J. J.; Strosberg, A. M.; Gu, L.; Chiang, H. S.; Massey, I. J.; Chu, N.; Fried, J. H. Inhibitors of cyclic AMP phosphodiesterase. 4. Synthesis and evaluation of potential prodrugs of lixazinone (N-cyclohexyl-N-methyl-4-[(1,2,3,5-tetrahydro-2- oxoimidazo[2,1-b]quinazolin-7-yl)-oxy]butyramide, RS-82856). *Journal of Medicinal Chemistry* 1988, 31, 2145-52.

111. Venuti, M. C.; Jones, G. H.; Alvarez, R.; Bruno, J. J. Inhibitors of cyclic AMP phosphodiesterase. 2. Structural variations of N-cyclohexyl-N-methyl-4-[(1,2,3,5-tetrahydro- 2-oxoimidazo[2,1-b]quinazolin-7-yl)-oxy]butyramide (RS-82856). *Journal of Medicinal Chemistry* 1987, 30, 303-18.

112. Beverung, W. N., Jr.; Partyka, A. Optionally substituted 1,2,3,5-tetrahydroimidezo(2,1-b)-quinazolin-2-ones and 6(H)-1,2,3,4-tetrahydropyimido(2,1-b)quinazolin-2-ones. US3932407A, 1976.

113. Ishikawa, F.; Saegusa, J.; Inamura, K.; Sakuma, K.; Ashida, S. Cyclic guanidines. 17. Novel (N-substituted amino)imidazo[2,1-b]quinazolin-2-ones: water-soluble platelet aggregation inhibitors. *Journal of Medicinal Chemistry* 1985, 28, 1387-93.

114. Ishikawa, F.; Yamaguchi, H.; Saegusa, J.; Inamura, K.; Mimura, T.; Nishi, T.; Sakuma, K.; Ashida, S. Cyclic guanidines. XVI. Synthesis and biological activities of tetracyclic imidazo[2,1-b]quinazolinone derivatives. *Chemical & Pharmaceutical Bulletin* 1985, 33, 3336-48.

115. Kienzle, F.; Kaiser, A.; Chodnekar, M. S. 1,5-Dihydroimidazoquinazolinones as blood platelet aggregation inhibitors. *Eur. J. Med. Chem.* 1982, 17, 547-556.

116. Edmondson, S. D.; Mastracchio, A.; He, J. F.; Chung, C. C.; Forrest, M. J.; Hofsess, S.; MacIntyre, E.; Metzger, J.; O'Connor, N.; Patel, K.; Tong, X. C.; Tota, M. R.; Van der Ploeg, L. H. T.; Varnerin, J. P.; Fisher, M. H.; Wyvratt, M. J.; Weber, A. E.; Parmee, E. R. Benzyl vinylogous amide substituted aryldihydropyridazinones and aryldimethylpyrazolones as potent and selective PDE3B inhibitors. *Bioorganic & Medicinal Chemistry Letters* 2003, 13, 3983-3987.

117. Snyder, P. B.; Beaton, G.; Rueter, J. K.; Fanning, D. L.; Warren, S. D.; Hadida-Ruah, S. S. Preparation of substituted sulfonylalkylcarboxamides as selective pde3b inhibitors and use of the same in therapy. WO2002070469A2, 2002.

118. Nikpour, M.; Sadeghian, H.; Saberi, M. R.; Nick, R. S.; Seyedi, S. M.; Hosseini, A.; Parsaee, H.; Bozorg, A. T. D. Design, synthesis and biological evaluation of 6-(benzyloxy)-4-methylquinolin-2(1H)-one derivatives as PDE3 inhibitors. *Bioorganic & Medicinal Chemistry* 2010, 18, 855-862.

119. Snyder, P. B. The adipocyte cGMP-inhibited cyclic nucleotide phosphodiesterase (PDE3B) as a target for lipolytic and thermogenic agents for the treatment of obesity. *Expert Opinion on Therapeutic Targets* 1999, 3, 587-599.

120. Kim, K. Y.; Lee, H.; Yoo, S.-E.; Kim, S. H.; Kang, N. S. Discovery of new inhibitor for PDE3 by virtual screening. *Bioorganic & Medicinal Chemistry Letters* 2011, 21, 1617-1620.

121. Skoumbourdis, A. P.; LeClair, C. A.; Stefan, E.; Turjanski, A. G.; Maguire, W.; Titus, S. A.; Huang, R.; Auld, D. S.; Inglese, J.; Austin, C. P.; Michnick, S. W.; Xia, M.; Thomas, C. J. Exploration and optimization of substituted triazolothiadiazines and triazolopyridazines as PDE4 inhibitors. *Bioorganic & Medicinal Chemistry Letters* 2009, 19, 3686-3692.

122. Mongillo, M.; McSorley, T.; Evellin, S.; Sood, A.; Lissandron, V.; Terrin, A.; Huston, E.; Hannawacker, A.; Lohse, M. J.; Pozzan, T.; Houslay, M. D.; Zaccolo, M. Fluorescence Resonance Energy Transfer - Based Analysis of cAMP Dynamics in Live Neonatal Rat Cardiac Myocytes Reveals Distinct Functions of Compartmentalized Phosphodiesterases. *Circulation Research* 2004, 95, 67-75.

123. Patrucco, E.; Notte, A.; Barberis, L.; Selvetella, G.; Maffei, A.; Brancaccio, M.; Marengo, S.; Russo, G.; Azzolino, O.; Rybalkin, S. D.; Silengo, L.; Altruda, F.; Wetzker, R.; Wymann, M. P.; Lembo, G.; Hirsch, E. PI3Kγ modulates the cardiac response to chronic pressure overload by distinct kinase-dependent and -independent effects. *Cell* 2004, 118, 375-87.

124. Beverung, W. N., Jr.; Partyka, R. A. Antihypertensive and blood coagulation inhibiting 1H-2,3,4,5-tetrahydroimidazo[2,1-b]quinazolin-2-ones and 1,2,3,4,5,6-hexahydropyrimido[2,1-b]quinazolin-2-ones. 73-2305575
2305575, 19730205., 1973.

125. Beverung, W. N.; Partyka, R. A. 6-Methyl-1,2,3,5-tetrahydroimidazo[2,1-b]quinazolin-2-one, a potent inhibitor of ADP-induced platelet aggregation. *Journal of Medicinal Chemistry* 1975, 18, 224-225.

126. Ishikawa, F.; Kosasayama, A.; Yamaguchi, H.; Watanabe, Y.; Saegusa, J.; Shibamura, S.; Sakuma, K.; Ashida, S.; Abiko, Y. Cyclic guanidines. 14. Imidazo[1,2-a]thienopyrimidin-2-one derivatives as blood platelet aggregation inhibitors. *Journal of Medicinal Chemistry* 1981, 24, 376-382.

127. Jones, G. H.; Venuti, M. C.; Alvarez, R.; Bruno, J. J.; Berks, A. H.; Prince, A. Inhibitors of cyclic AMP phosphodiesterase. 1. Analogues of cilostamide and anagrelide. *Journal of Medicinal Chemistry* 1987, 30, 295-303.

128. Bristol, J. A.; Sircar, I.; Moos, W. H.; Evans, D. B.; Weishaar, R. E. Cardiotonic agents. 1. 4,5-Dihydro-6-[4-(1H-imidazol-1-yl)phenyl]-3(2H)-pyridazinones: novel positive inotropic agents for the treatment of congestive heart failure. *Journal of Medicinal Chemistry* 1984, 27, 1099-1101.

129. Venuti, M. C.; Stephenson, R. A.; Alvarez, R.; Bruno, J. J.; Strosberg, A. M. Inhibitors of Cyclic AMP Phosphodiesterase. 3. Synthesis and Biological Evaluation of Pyrido and Imidazolyl Analogues of 1,2,3,5-Tetrahydro-2-oxoimidazo[2,1-b]quinazoline. *Journal of Medicinal Chemistry* 1988, 31, 2136-2145.

130. Meanwell, N. A.; Roth, H. R.; Smith, E. C. R.; Wedding, D. L.; Wright, J. J. K.; Fleming, J. S.; Gillespie, E. 1,3-Dihydro-2H-imidazo[4,5-b]quinolin-2-ones - inhibitors of blood platelet cAMP phosphodiesterase and induced aggregation. *Journal of Medicinal Chemistry* 1991, 34, 2906-2916.

131. Meanwell, N. A.; Pearce, B. C.; Roth, H. R.; Smith, E. C. R.; Wedding, D. L.; Wright, J. J. K.; Buchanan, J. O.; Baryla, U. M.; Gamberdella, M. Inhibitors of blood platelet cAMP phosphodiesterase. 2. Structure-activity relationships associated with 1,3-dihydro-2H-imidazo[4,5-b]quinolin-2-ones substituted with functionalized side chains. *Journal of Medicinal Chemistry* 1992, 35, 2672-2687.

132. Meanwell, N. A.; Dennis, R. D.; Roth, H. R.; Rosenfeld, M. J.; Smith, E. C. R.; Wright, J. J. K.; Buchanan, J. O.; Brassard, C. L.; Gamberdella, M.; Gillespie, E.; Seiler, S. M.; Zavoico, G. B.; Fleming, J. S. Inhibitors of Blood Platelet cAMP Phosphodiesterase. 3. 1,3-Dihydro-*2H*-imidazo[4,5-*b*]quinolin-2-one Derivatives with Enhanced Aqueous Solubility. *Journal of Medicinal Chemistry* 1992, 35, 2688-2696.

133. Meanwell, N. A.; Hewawasam, P.; Thomas, J. A.; Wright, J. J. K.; Russell, J. W.; Gamberdella, M.; Goldenberg, H. J.; Seiler, S. M.; Zavoico, G. B. Inhibitors of Blood Platelet cAMP Phosphodiesterase. 4. Structural Variation of the Side-Chain Terminus of Water-Soluble 1,3-Dihydro-*2H*-imidazo[4,5-*b*]quinolin-2-one Derivatives. *Journal of Medicinal Chemistry* 1993, 36, 3251-3264.

134. Golding, B. Process for the preparation of anagrelide and analogues. WO2010070318A1, 2010.

135. Srivastava, G. K.; Kesarwani, A. P.; Grover, R. K.; Roy, R.; Srinivasan, T.; Kundu, B. Solid Phase Synthesis of 2-Aminoquinazoline-Based Compounds. *Journal of Combinatorial Chemistry* 2003, 5, 769-774.

136. Kesarwani, A. P.; Grover, R. K.; Roy, R.; Kundu, B. Solid-phase synthesis of imidazoquinazolinone derivatives with three-point diversity. *Tetrahedron* 2005, 61, 629-635.

137. Yamaguchi, H.; Fumiyoshi, I. Synthesis and Reactions of 2-Chloro-3,4-dihydrothienopyrimidines and -quinazolines. *Journal of Heterocyclic Chemistry* 1981, 18, 67-70.

138. Borch, R. F.; Bernstein, M. D.; Durst, H. D. Cyanohydridoborate anion as a selective reducing agent. *Journal of the American Chemical Society* 1971, 93, 2897-2904.

139. Diedrich, C. L.; Haase, D.; Christoffers, J. New octahydropyrido[3,4-b]acridine scaffolds for combinatorial chemistry. *Synthesis-Stuttgart* 2008, 2199-2210.

140. Davis, A.; Warrington, B. H.; Vinter, J. G. Strategic approaches to drug design. II. Modelling studies on phosphodiesterase substrates and inhibitors. *Journal of Computer-Aided Molecular Design* 1987, 1, 97-119.

141. Moos, W. H.; Humblet, C. C.; Sircar, I.; Rithner, C.; Weishaar, R. E.; Bristol, J. A.; McPhail, A. T. Cardiotonic agents. 8. Selective inhibitors of adenosine 3',5'-cyclic phosphate phosphodiesterase III. Elaboration of a five-point model for positive inotropic activity. *Journal of Medicinal Chemistry* 1987, 30, 1963-72.

142. Apaya, R. P.; Lucchese, B.; Price, S. L.; Vinter, J. G. The matching of electrostatic extrema: a useful method in drug design? A study of phosphodiesterase III inhibitors. *Journal of Computer-Aided Molecular Design* 1995, 9, 33-43.

143. Fossa, P.; Boggia, R.; Mosti, L. Toward the identification of the cardiac cGMP inhibited-phosphodiesterase catalytic site. *Journal of Computer-Aided Molecular Design* 1998, 12, 361-372.

144. Klebe, G. Virtual ligand screening: strategies, perspectives and limitations. *Drug Discovery Today* 2006, 11, 580-594.

145. Fossa, P.; Giordanetto, F.; Menozzi, G.; Mosti, L. Structural basis for selective PDE 3 inhibition: a docking study. *Quantitative Structure-Activity Relationships* 2002, 21, 267-275.

146. Xu, R. X.; Hassell, A. M.; Vanderwall, D.; Lambert, M. H.; Holmes, W. D.; Luther, M. A.; Rocque, W. J.; Milburn, M. V.; Zhao, Y.; Ke, H.; Nolte, R. T. Atomic Structure of PDE4: Insights into Phosphodiesterase Mechanism and Specificity. *Science* 2000, 288, 1822-1825.

147. Salter, E. A.; O'Brien, K. A.; Edmunds, R. W.; Wierzbicki, A. ONIOM investigation of nucleotide selectivity in phosphodiesterases 3 and 4. *International Journal of Quantum Chemistry* 2008, 108, 1189-1199.

148. Thompson, P. E.; Manganiello, V.; Degerman, E. Re-Discovering PDE3 Inhibitors - New Opportunities for a Long Neglected Target. *Current Topics in Medicinal Chemistry* 2007, 7, 421-436.

149. Hung, S. H.; Zhang, W.; Pixley, R. A.; Jameson, B. A.; Huang, Y. C.; Colman, R. F.; Colman, R. W. New insights from the structure-function analysis of the catalytic region of human platelet phosphodiesterase 3A - A role for the unique 44-amino acid insert. *Journal of Biological Chemistry* 2006, 281, 29236-29244.

150. Hung, S. H.; Madhusoodanan, K. S.; Beres, J. A.; Boyd, R. L.; Baldwin, J. L.; Zhang, W.; Colman, R. W.; Colman, R. F. A New Nonhydrolyzable Reactive cAMP Analog, (Sp)-Adenosine-3',5'-cyclic-S-(4-bromo-2,3-dioxobutyl)monophosphorothioate Irreversibly Inactivates Human Platelet cGMP-Inhibited cAMP Phosphodiesterase. *Bioorganic Chemistry* 2002, 30, 16-31.

151. Sadeghian, H.; Seyedi, S. M.; Saberi, M. R.; Nick, R. S.; Hosseini, A.; Bakavoli, M.; Mansouri, S. M. T.; Parsaee, H. Design, synthesis and pharmacological evaluation of 6-hydroxy-4-methylquinolin-2(1H)-one derivatives as inotropic agents. *Journal of Enzyme Inhibition and Medicinal Chemistry* 2009, 24, 918-929.

152. Gonnet, G. H.; Cohen, M. A.; Benner, S. A. Exhaustive matching of the entire protein sequence database. *Science* 1992, 256, 1443-5.

153. *Prime*, version 3.1; Schrödinger, LLC, New York, NY: 2012.

154. *Glide*, version 5.7; Schrödinger, LLC, New York, NY: 2012.

155. Friesner, R. A.; Banks, J. L.; Murphy, R. B.; Halgren, T. A.; Klicic, J. J.; Mainz, D. T.; Repasky, M. P.; Knoll, E. H.; Shelley, M.; Perry, J. K.; Shaw, D. E.; Francis, P.; Shenkin, P. S. Glide: A New Approach for Rapid, Accurate Docking and Scoring. 1. Method and Assessment of Docking Accuracy. *Journal of Medicinal Chemistry* 2004, 47, 1739-1749.

156. Zhou, Z.; Felts, A. K.; Friesner, R. A.; Levy, R. M. Comparative Performance of Several Flexible Docking Programs and Scoring Functions: Enrichment Studies for a Diverse Set of Pharmaceutically Relevant Targets. *Journal of Chemical Information and Modeling* 2007, 47, 1599-1608.

157. Yang, B. H.; Buchwald, S. L. Palladium-catalyzed amination of aryl halides and sulfonates. *Journal of Organometallic Chemistry* 1999, 576, 125-146.

158. *Reactor was used for enumeration and reaction modeling*, JChem 5.3.5, 2010; ChemAxon (http://www.chemaxon.com): 2010.

159. Tanaka, M.; Ishikawa, F.; Hakusui, H. Isolation and identification of seven metabolites of a water-soluble platelet aggregation inhibitor in rat urine. *Xenobiotica* 1995, 25, 1247-57.

160. Campbell, S. F.; Roberts, D. A. Tetrahydroimidazoquinazolinone inotropic agents. EP 205 280, 17 Dec 1986, 1987.

161. Wang, L.; Chai, Y.; Tu, P.; Sun, C.; Pan, Y. Formation of [M + 15]+ ions from aromatic aldehydes by use of methanol: in-source aldolization reaction in electrospray ionization mass spectrometry. *Journal of Mass Spectrometry* 2011, 46, 1203-1210.

162. Surry, D. S.; Buchwald, S. L. Dialkylbiaryl phosphines in Pd-catalyzed amination: a user's guide. *Chemical Science* 2011, 2, 27-50.

163. Maiti, D.; Fors, B. P.; Henderson, J. L.; Nakamura, Y.; Buchwald, S. L. Palladium-catalyzed coupling of functionalized primary and secondary amines with aryl and heteroaryl halides: two ligands suffice in most cases. *Chemical Science* 2011, 2, 57-68.

164. Fors, B. P.; Krattiger, P.; Strieter, E.; Buchwald, S. L. Water-Mediated Catalyst Preactivation: An Efficient Protocol for C-N Cross-Coupling Reactions. *Organic Letters* 2008, 10, 3505-3508.

165. Amatore, C.; Jutand, A. Role of dba in the reactivity of palladium(0) complexes generated in situ from mixtures of Pd(dba)2 and phosphines. *Coordination Chemistry Reviews* 1998, 178-180, Part 1, 511-528.

166. Su, M.; Buchwald, S. L. A Bulky Biaryl Phosphine Ligand Allows for Palladium-Catalyzed Amidation of Five-Membered Heterocycles as Electrophiles. *Angewandte Chemie International Edition* 2008, 51, 4710-4713.

167. Torraca, K. E.; Kuwabe, S.-I.; Buchwald, S. L. A High-Yield, General Method for the Catalytic Formation of Oxygen Heterocycles. *Journal of the American Chemical Society* 2000, 122, 12907-12908.

168. Kuethe, J. T.; Childers, K. G.; Humphrey, G. R.; Journet, M.; Peng, Z. A Rapid, Large-Scale Synthesis of a Potent Cholecystokinin (CCK) 1R Receptor Agonist. *Organic Process Research & Development* 2008, 12, 1201-1208.

169. Blackmore, T. R.; Thompson, P. E. Imidazolidin-4-ones, their syntheses and applications. *Heterocycles* 2011, 83, 1953-1975.

170. Card, G. L.; Blasdel, L.; England, B. P.; Zhang, C.; Suzuki, Y.; Gillette, S.; Fong, D.; Ibrahim, P. N.; Artis, D. R.; Bollag, G.; Milburn, M. V.; Kim, S.-H.; Schlessinger, J.; Zhang, K. Y. J. A family of phosphodiesterase inhibitors discovered by cocrystallography and scaffold-based drug design. *Nature Biotechnology* 2005, 23, 201-207.

171. Teague, S. J.; Davis, A. M.; Leeson, P. D.; Oprea, T. The Design of Leadlike Combinatorial Libraries. *Angewandte Chemie International Edition* 1999, 38, 3743-3748.

172. Hajduk, P. J.; Greer, J. A decade of fragment-based drug design: strategic advances and lessons learned. *Nature Reviews Drug Discovery* 2007, 6, 211-219.

173. Schuffenhauer, A.; Ruedisser, S.; Marzinzik, A.; Jahnke, W.; Selzer, P.; Jacoby, E. Library Design for Fragment Based Screening. *Current Topics in Medicinal Chemistry* 2005, 5, 751-762.

174. Dickopf, S.; Frank, M.; Junker, H.-D.; Maier, S.; Metz, G. n.; Ottleben, H.; Rau, H.; Schellhaas, N.; Schmidt, K.; Sekul, R.; Vanier, C.; Vetter, D.; Czech, J. r.; Lorenz, M.; Matter, H.; Schudok, M.; Schreuder, H.; Will, D. W.; Nestler, H. P. Custom chemical microarray production and affinity fingerprinting for the S1 pocket of factor VIIa. *Analytical Biochemistry* 2004, 335, 50-57.

175. Boehm, H.-J.; Boehringer, M.; Bur, D.; Gmuender, H.; Huber, W.; Klaus, W.; Kostrewa, D.; Kuehne, H.; Luebbers, T.; Meunier-Keller, N.; Mueller, F. Novel Inhibitors of DNA Gyrase: 3D Structure Based Biased Needle Screening, Hit Validation by Biophysical Methods, and 3D Guided Optimization. A Promising Alternative to Random Screening. *Journal of Medicinal Chemistry* 2000, 43, 2664-2674.

176. Carr, R. A. E.; Congreve, M.; Murray, C. W.; Rees, D. C. Fragment-based lead discovery: leads by design. *Drug Discovery Today* 2005, 10, 987-992.

177. Congreve, M.; Carr, R.; Murray, C.; Jhoti, H. A 'rule of three' for fragment-based lead discovery? *Drug Discovery Today* 2003, 8, 876-7.

178. Chen, I. J.; Hubbard, R. E. Lessons for fragment library design: analysis of output from multiple screening campaigns. *Journal of Computer-Aided Molecular Design* 2009, 23, 603-620.

179. Siegel, M. G.; Vieth, M. Drugs in other drugs: a new look at drugs as fragments. *Drug Discovery Today* 2007, 12, 71-79.

180. Pfeiffer, U.; Riccaboni, M. T.; Erba, R.; Pinza, M. A Short Synthesis of 4-imidazolidinone. *Liebigs Annalen der Chemie* 1988, 993-995.

181. Suwinski, J.; Wagner, P. Hydride reduction of 4-nitro-1-phenylazoles. *Pol. J. Chem.* 2000, 74, 1575-1580.

182. Granados, R.; Alvarez, M.; Lopez-Calahorra, F.; Salas, M. An approach to simple aminal synthesis: preparation of N-(6-aminohexyl)-N-benzyl-N-methylmethylenediamine. *Synthesis* 1983, 329-30.

183. Topliss, J. G. Utilization of operational schemes for analog synthesis in drug design. *Journal of Medicinal Chemistry* 1972, 15, 1006-11.

184. Nguyen, W. Development of Novel Kv1.3 Ion Channel Blockers Based Upon Diphenoxylate. Monash University, Melbourne, 2012.

185. Edward, J. T.; Martlew, E. F. Action of Raney nickel on 2-thiohydantoins. *Chemistry & Industry* 1954, 193-4.

186. Freter, K.; Rabinowitz, J. C.; Witkop, B. Labile Stoffwechselprodukte V. Zur Biogenese Des Formiminoglycins Aus 4(5H)-Imidazolon. *Justus Liebigs Annalen der Chemie* 1957, 607, 174-187.

187. Schulze, V. K.; Eis, K.; Wortmann, L.; Kosemund, D.; Prien, O.; Siemeister, G.; Hess-Stumpp, H.; Eberspaecher, U. Preparation of thiazolidinones as polo-like kinase (Plk1) inhibitors. WO2006063806A1, 2006.

188. Selvakumar, N.; Das, J.; Trehan, S.; Iqbal, J.; Kumar, M. S.; Rajagopalan, R.; Rao, M. N. V. S. Preparation of novel heterocyclic compounds having antibacterial activity. US20040102494A1, 2004.

189. Ley, S. V.; Thomas, A. W. Modern Synthetic Methods for Copper-Mediated C(aryl)-O, C(aryl)-N, and C(aryl)-S Bond Formation. *Angewandte Chemie International Edition* 2003, 42, 5400-5449.

190. Sapountzis, I.; Ettmayer, P.; Klein, C.; Mantoulidis, A.; Steurer, S.; Waizenegger, I. Preparation of triazolylbenzamides as B-Raf inhibitors for treating cancer. WO2009003999A2, 2009.

191. Abdel-Magid, A. F.; Carson, K. G.; Harris, B. D.; Maryanoff, C. A.; Shah, R. D. Reductive Amination of Aldehydes and Ketones with Sodium Triacetoxyborohydride. Studies on Direct and Indirect Reductive Amination Procedures. *The Journal of Organic Chemistry* 1996, 61, 3849-3862.

192. Kumar, V.; Kaushik, M. P.; Mazumdar, A. An Efficient Approach for the Synthesis of N-1 Substituted Hydantoins. *European Journal of Organic Chemistry* 2008, 2008, 1910-1916.

193. *JChem for Excel was used for structure generation*, JChem 5.3.5, 2010; ChemAxon (http://www.chemaxon.com): 2010.

194. Breslin, H. J.; Kukla, M. J.; Kromis, T.; Cullis, H.; De Knaep, F.; Pauwels, R.; Andries, K.; De Clercq, E.; Janssen, M. A. C.; Janssen, P. A. J. Synthesis and anti-HIV activity of 1,3,4,5-tetrahydro-2H-1,4-benzodiazepin-2-one (TBO) derivatives. truncated 4,5,6,7-tetrahydro-5-methylimidazo[4,5,1-jk][1,4]benzodiazepin-2(1H)-ones (TIBO) analogues. *Bioorganic & Medicinal Chemistry* 1999, 7, 2427-2436.

195. Iyobe, A.; Uchida, M.; Kamata, K.; Hotei, Y.; Kusama, H.; Harada, H. Studies on New Platelet Aggregation Inhibitors 1. Synthesis of 7-Nitro-3, 4-dihydroquinoline-2(1H)-one Derivatives. *Chemical & Pharmaceutical Bulletin* 2001, 49, 822-829.

196. Hu, Y.-Z.; Zhang, G.; Thummel, R. P. Friedländer Approach for the Incorporation of 6-Bromoquinoline into Novel Chelating Ligands. *Organic Letters* 2003, 5, 2251-2253.

197. Searcey, M.; Pye, P. L.; Lee, J. B. Improved syntheses of N-substituted nitroimidazoles. *Synthetic Communications* 1989, 19, 1309-15.

198. Perree-Fauvet, M.; Verchere-Beaur, C.; Tarnaud, E.; Anneheim-Herbelin, G.; Bone, N.; Gaudemer, A. New amino acid porphyrin derivatives. Part I: Synthesis. *Tetrahedron* 1996, 52, 13569-13588.

199. Cope, A. C.; Hancock, E. M. Benzoates, p-aminobenzoates and phenylurethans of 2-alkylaminoethanols. *Journal of the American Chemical Society* 1944, 66, 1448-53.

Appendix A

A.1 Molecular docking of PDE3A inhibitors into the PDE3A homology model

It was of interest to determine how docking experiments using the PDE3A and PDE3B models would perform across different classes of PDE3 inhibitors. This was investigated by docking a series of known PDE3A inhibitors into the binding site. The results from this docking experiment failed to show any correlation between gScores and IC_{50} values.

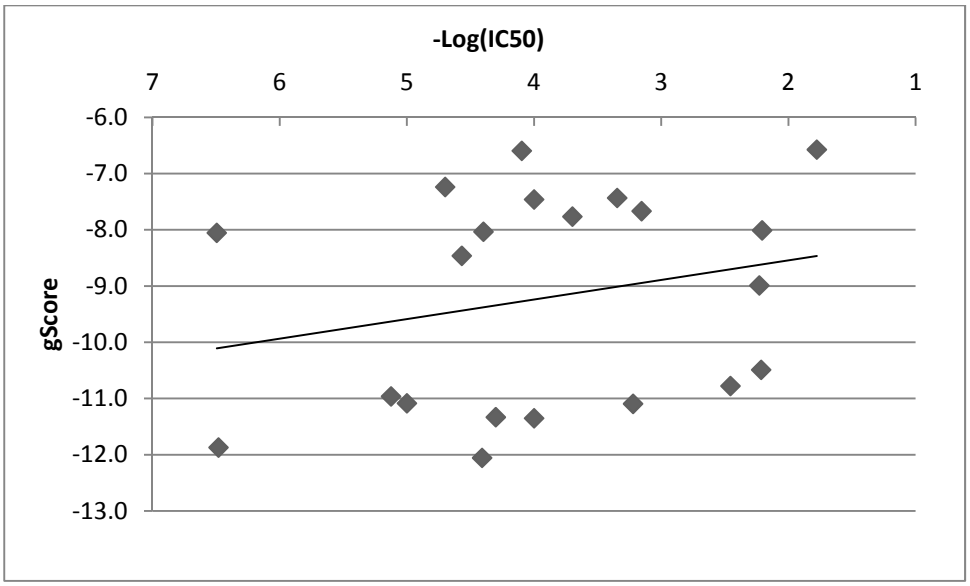

Figure 47 Literature compound IC_{50} data vs. gScores from XP docking into PDE3A

The results summarized in Figure 47, and detailed in Table 13, suggest that this approach is ill suited for predicting the potency of a diverse set of PDE3A inhibitors. There is the potential that the crystal structure represents an enzyme conformation that is induced by MERCK1 (**6**) which may not be accessed by structurally unrelated PDE3 inhibitors. Alternate docking methods that allow the enzyme to adapt and accommodate the ligand are available however they were not examined.

Name	IC50 (nM)	XP PDE3A gScore
OPC-33540	0.32	-8.22
MERCK1	0.33	-13.07
Levosimendan	7.5	-11.74
Lixazinone	10	-13.05
Saterinone	20	-7.64
Cilostamide	27	-8.66
NSP-513	39	-11.41
Trequinsin	40	-6.20
OPC-3911	50	-9.02
Indolidan	80	-7.52
Anagrelide	100	-8.15
Org-9935	100	-11.32
Cilostazol	200	-8.27
Milrinone	450	-6.69
CI930	600	-12.56
Siguazodan	700	-9.09
Pimobendan	3500	-9.85
Enoximone	5900	-10.41
Imazodan	6100	-11.78
Vesnarinone	6200	-9.38
Amrinone	16700	-6.61

Table 13 Reported PDE3A IC_{50} values and PDE3A gScores of docked PDE3 inhibitors

A.2 Docking of reported MERCK1 analogues.

In the next series of experiments the focus was placed on testing analogues within a series, and the selectivity of an analogue between the two isoforms. A series of 38 analogues of MERCK1 (Figure 48)[116] were docked into both the PDE3A and PDE3B models. The analogues can be divided into two classes by the nature of their heterocyclic ring. The first class, which includes MERCK1, incorporate an (R)-5-methyl-4,5-dihydropyridazin-3(2H)-one or MDP ring, while the second class possess a 4,4-dimethyl-1H-pyrazol-5(4H)-

one or DMP ring. Analogues of the MDP class were substituted around either the central or distal aryl ring, while the DMP class analogues are substituted around both the central and distal aryl rings.

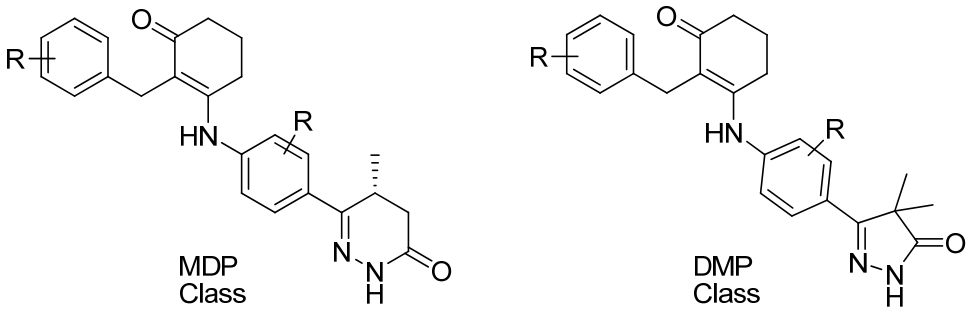

Figure 48 PDE3B selective analogues that were docked into the PDE3A and PDE3B models

The gScores of the 38 analogues docked into the PDE3A and PDE3B models were compared with their literature PDE3A and PDE3B IC_{50} values. In both cases the correlation was poor (PDE3A $R^2 = 0.04$, PDE3B $R^2 = 0.05$) although some of the potent compounds did receive notably better docking scores.

In addition there was no correlation between gScore and isoform selectivity, in fact linear regression gave the opposite relationship. However, predicting isoform selectivity was an extremely difficult task given that there were only marginal differences in potency of even the most isoform selective ligand (**7**) (33 fold for PDE3B) and across the entire series (average of 8 fold, all for PDE3B).

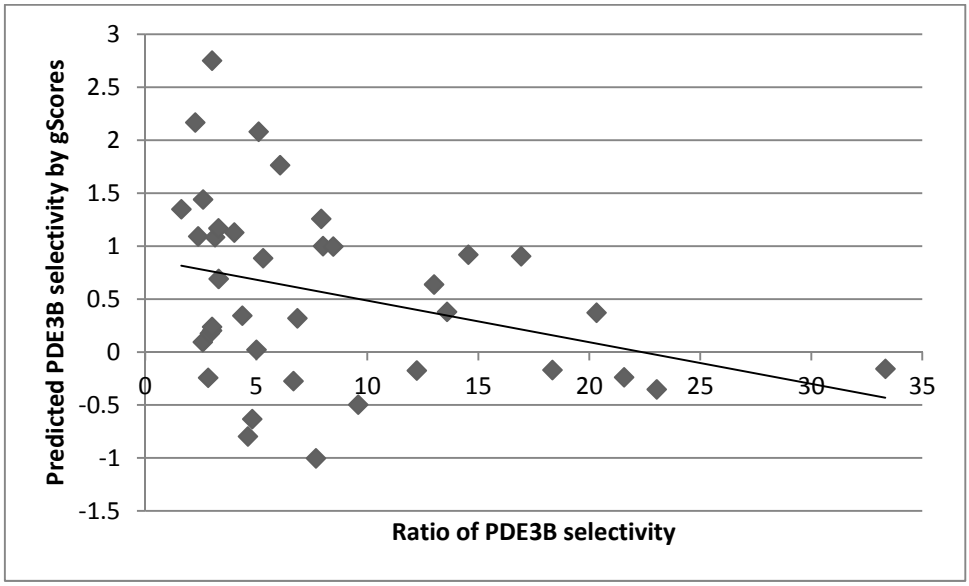

Figure 49 Reported selectivity (PDE3A IC_{50} / PDE3B IC_{50}) vs. predicted selectivity (PDE3A gScore – PDE3B gScore)

This result was not entirely surprising; docking the same analogue with the same features into two almost identical models was likely to give similar results. These experiments did demonstrate that the docking program can produce the expected binding mode consistently for a series of analogues.

Appendix B

Monash University Declaration for Thesis Appendix B

Declaration by candidate

In the case of Appendix B, the nature and extent of my contribution to the work was the following:

Nature of contribution	Contribution (%)
Literature review and Manuscript preparation	75%

The following co-authors contributed to the work. Co-authors who are students at Monash University must also indicate the extent of their contribution in percentage terms:

Name	Nature of contribution
Dr Philip Thompson	Manuscript preparation and editing

Candidate's Signature ---------- **Date**

Declaration by co-authors

The undersigned hereby certify that:

(1) the above declaration correctly reflects the nature and extent of the candidate's contribution to this work, and the nature of the contribution of each of the co-authors.
(2) they meet the criteria for authorship in that they have participated in the conception, execution, or interpretation, of at least that part of the publication in their field of expertise;
(3) they take public responsibility for their part of the publication, except for the responsible author who accepts overall responsibility for the publication;
(4) there are no other authors of the publication according to these criteria;
(5) potential conflicts of interest have been disclosed to (a) granting bodies, (b) the editor or publisher of journals or other publications, and (c) the head of the responsible academic unit; and
(6) the original data are stored at the following location(s) and will be held for at least five years from the date indicated below:

Location **Department of Medicinal Chemistry, Monash Institute of Pharmaceutical Sciences, 381 Royal Pde, Parkville, Vic, 3052, Australia**

Signed  **Date: 29/8/2012**

HETEROCYCLES, Vol. 83, No. 9, pp. 1953 - 1975. © The Japan Institute of Heterocyclic Chemistry
Received, 21st March, 2011, Accepted, 13th May, 2011, Published online, 30th May, 2011
DOI: 10.3987/REV-11-707

IMIDAZOLIDIN-4-ONES: Their Syntheses and Applications

Timothy R. Blackmore* and Philip E. Thompson

Medicinal Chemistry and Drug Action, Monash Institute of Pharmaceutical Sciences, 381 Royal Parade, Parkville, VIC 3052, Australia

Abstract – This review focuses on the synthesis and use of the imidazolidin-4-one ring in synthetic and medicinal chemistry studies. It has remained remarkably under-utilized as a motif in drug discovery despite its obvious similarity to the widely encountered lactam pyrrolidinone, its isomer imidazolin-2-one and its oxidation state variants, the hydantoins (imidazolidendiones), imidazolidines, and imidazoles, as well as fused bicyclic ring systems. The synthesis of imidazolidin-4-one is reported in only 3 journal articles and a search for the explicit use of it in synthesis resulted in just 5 patents, and no academic journals. The specific sub-structure motif is reported in 296 journal articles and 65 patents. The different methods reported for creating substituted analogues will be discussed, as well as the application of the moiety in medicinal chemistry projects and alternative uses of these analogues as organic catalysts and prodrugs.

Early Reports:

The history of imidazolidin-4-one starts with investigations into the synthesis of diphenylhydantoin (phenytoin, Dilantin) described by Heinrich Biltz in 1908,[1] and later found to have antiseizure effects.[2] In the first reported synthesis of an imidazolidin-4-one, (**Scheme 1**), the phenytoin analogue, 5,5-diphenylthiohydantoin (**1**), was shown to react with sodium in amyl alcohol to produce 5,5-diphenylimidazolidin-4-one (**2**).[3,4] Carrington *et al.* later reported that the same reduction of the thiocarbonyl intermediate (**1**) can also be achieved using Raney nickel.[5] Biltz's findings were later reinvestigated by Edward *et al*., while the key structures were in agreeance, there was a difference between the structures of some derivatives.[6] Whalley *et al*. found that the desulfurization step could also yield a variety of stable intermediates or by-products including 5,5-diphenyl-2-hydroxy-4-imidazolidone (**3**) and 4,4-diphenyl-5-oxo-2-imidazoline (**4**).[7] Such additional complexity may have limited the application of this route to imidazolidin-4-ones.

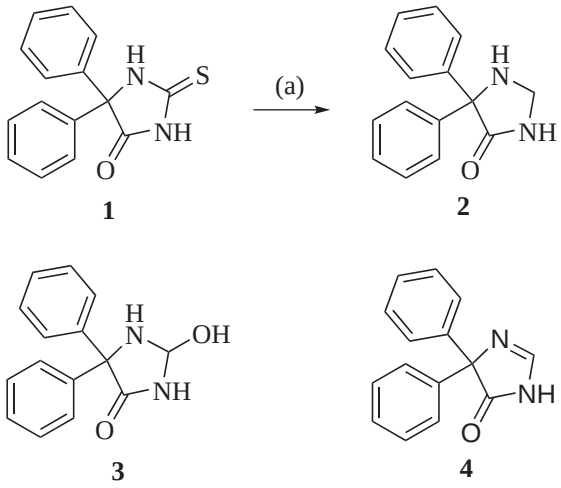

Scheme 1. *(a) Raney Ni, EtOH, 30 min, reflux*

Synthesis of Imidazolidin-4-ones

Condensation of carbonyl compounds and aminoacetamide equivalents

One of the principle synthetic routes to imidazolidin-4-one derivatives incorporates a reaction between an aldehyde or ketone and an aminoacetamide. The unsubstituted imidazolidin-4-one itself can be produced this way, from simple starting materials (**Scheme 2**).[8] Treatment of 2-(benzylamino)-acetamide (**5**) with

formaldehyde gave 1-benzyl-3-(hydroxymethyl)imidazolidin-4-one (**6**). The hydroxymethyl group can be removed by careful distillation at low pressure, giving a 1-benzylimidazolidin-4-one (**7**). The benzyl group can then be hydrogenolysed to give the unsubstituted imidazolidin-4-one (**8**). This represents the simplest reported access to the title compound.

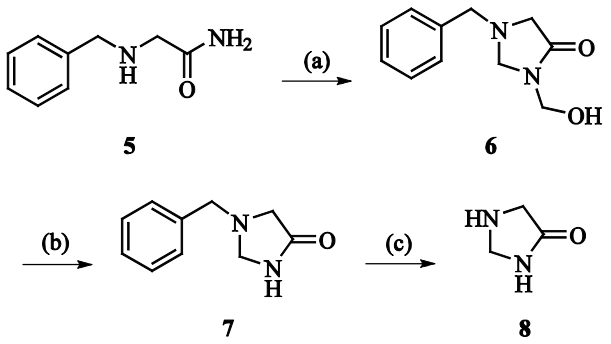

Scheme 2. *(a) H_2O, CH_2O, 30 min, reflux (b) 4 h, 150 ^oC (c) EtOH, 5% Pd-C, H_2, 4 h, RT*

A study of imidazolidin-4-one cyclisation by Pascal *et al*. found that when formaldehyde is used to cyclize 2-(methylamino)propanamide (**9**) there are two products formed, the desired 1,5-dimethylimidazolidin-4-one (**10**) and the by-product 3-(hydroxymethyl)-1,5-dimethylimidazolidin-4-one (**11**) that exist in equilibrium (**Scheme 3**) .[9,10] While the hydroxy methyl may be removable in some cases, it can represent a significant obstacle to the usefulness of this approach.

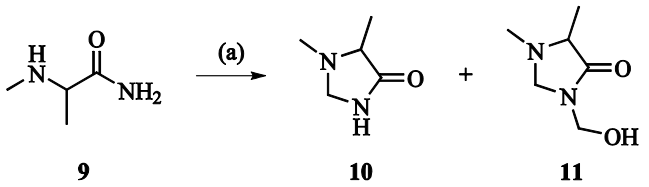

Scheme 3. *(a) H_2O, CH_2O*

Analogously, Harmon *et al*. had previously investigated the synthesis of 3-hydroxyimidazolidin-4-ones by condensing α-amino hydroxamic acids with aldehydes.[11] For example, glycine hydroxamic acid (**12**) and formaldehyde combine to form 3-hydroxyimidazolidin-4-one (**13**) (**Scheme 4**), which was reported to be a ligand for the strychnine-insensitive glycine binding site of the NMDA receptor.[12]

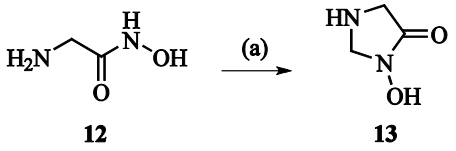

12 **13**

Scheme 4. *(a) CH_2O, EtOH, H_2O, 3 h, reflux*

The general reaction actually dates back to 1951 where Davis *et al*. reported the synthesis of 2,2-dimethylimidazolidin-4-one (**Scheme 5**). Aminoacetamide (**14**) and acetone were combined to form the Schiff base (**15**) which exists in equilibrium with the corresponding imino-oxazolidine (**16**). Rearrangement occurs to yield the more stable imidazolidin-4-one product (**17**)**.** This product is still labile in basic or hot acidic solution, and is hydrolyzed back to aminoacetamide (**14**).[13]

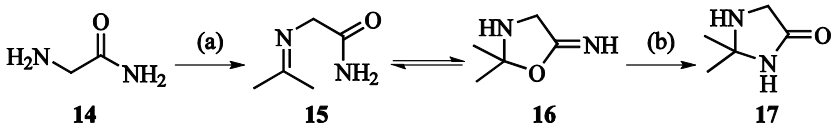

14 **15** **16** **17**

Scheme 5. *(a) acetone, benzene, 30 min, reflux (b) pyridine, 30 min, reflux*

Spiroimidazolidin-4-ones can be prepared by utilizing cyclic ketones (**Scheme 6**). Condensing cyclohexanone (**18**) with aminoacetonitrile (**19**) using sodium methoxide as a catalyst gives 1,4-diazaspiro[4.5]decan-2-one (**20**).[13] This compound is more stable than dimethylimidazolidin-4-one (**17**). These examples suggest that using substituted ketones give cleaner or more stable products than using formaldehyde. A separate publication concluded that some of the reported compounds, specifically the 2-hydroxyimidazolidin-4-ones, actually existed as open chain tautomers.[14]

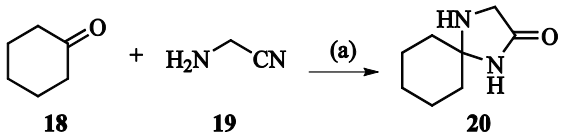

18 **19** **20**

Scheme 6. *(a) NaOMe, MeOH, 15 min, 100 °C*

Khalaj *et al*. reported where a variety of 2-aminoacetamide analogues will cyclize with carbonyl compounds to imdazolidin-4-ones, but only by refluxing in methanol with a p-toluenesulfonic acid catalyst.[15] Another

report indicated that H-Y zeolite is also a useful catalyst, which has the advantage of being heterogeneous and can therefore be easily removed from the reaction by filtration.[16] These reports show the scope of this reaction, proceeding with both aryl and alkyl derivatives on the acetamide and carbonyl reagents. A series of such compounds were patented for their anti-inflammatory and analgesic effects.[17]

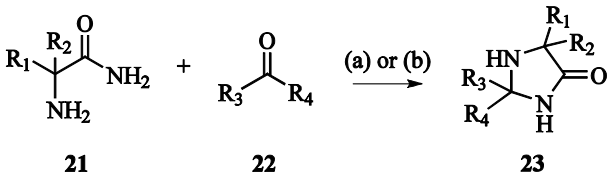

21 **22** **23**

Scheme 7. *(a) p-TsOH, MeOH, 6 h, reflux (b) HY zeolite, MeOH, 12 h, reflux*

Published methods exist for synthesizing a wide variety of diversely substituted imidazolidin-4-ones from a resin bound aminoacetamide. This presents an ideal opportunity for parallel synthesis of large libraries with significant diversity and this has been successfully demonstrated.

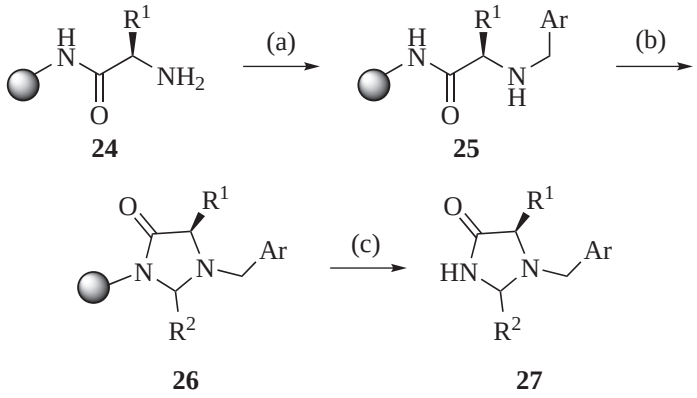

24 **25** **26** **27**

Scheme 8. *(a)ArCHO, trimethylorthoformate, AcOH, $NaBH_3CN$, 1 h, RT (b) benzotriazole, R^2CHO, benzene, 16 h, reflux (c) HF, 1.5 h, -5 ^oC*

Rinnová *et al*. developed a solid phase synthesis of 1,2,5-trisubstituted imidazolidin-4-ones (**27**), that was used to synthesize an extensive series of analogues. **Scheme 8** begins with reductive amination of a resin bound aminoacetamide (**24**), with benzaldehyde to give (**25**), which can then be cyclised with another aldehyde (**26**).

The resin cleavage step requires the use of hydrofluoric acid and produces diastereomeric products.

This methodology was used to create a library of compound mixtures.[18] A similar report using a modified synthetic scheme reported making a library of 180 different spiroimidazolidin-4-ones.[19,20] An alternate method was published by Qin *et al*. including a solid phase synthesis of 1,2,5-trisubstituted imidazolidin-4-ones, that uses a photo cleavable linker, avoiding the hazards of using hydrofluoric acid.[21]

Cyclization by addition of Nitrogen

A less well documented synthetic approach exists where ammonia is inserted to cyclize a carbonyl containing compound. The Schiff base of an amino acid ester and an aldehyde can be cyclized to give a 2,5 substituted imidazolidin-4-ones. The precursor and imidizolidin-4-ones are achieved in high yields, using mild conditions (**Scheme 9**).[22] Amino acids esters can react with benzylidenemethylamine (**31**) to give tri-substituted imidazolidin-4-ones (**Scheme 10**).[23] This is somewhat analogous to an intermolecular version of the Schiff base cyclisation above. Two molecules of acetone can be combined to yield a 2,2,5,5-tetramethylimidazolidin-4-one, through a reaction with sodium cyanide and ammonium chloride (**Scheme 11**).[24] It has been supposed that this method would allow for large scale synthesis of relatively simple imidazolidin-4-ones.[25]

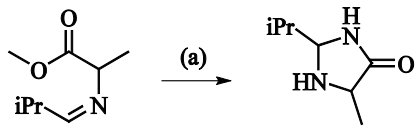

28 **29**

Scheme 9. *(a) NH_4OH, 15 – 20 h, RT*

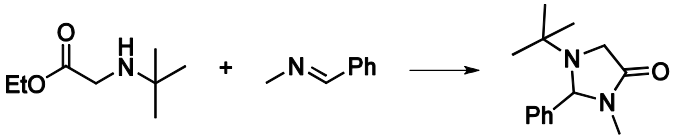

30 **31** **32**

Scheme 10.

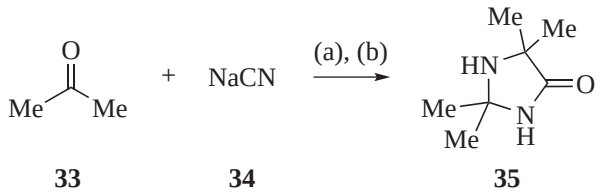

33 **34** **35**

Scheme 11. *(a) NH_4Cl, H_2O, 5 h, 40 °C (b) NaOH, MeOH, H_2O, 8 h, 30 °C*

In another variation, treatment of α-haloacetamidobenzophenones (**36**) with hexamine yields 1,1'-methylenebis(3-(4-halophenyl)imidazolidin-4-ones) (**37**) which can be acid hydrolyzed to give corresponding imidazolidin-4-ones (**38**).[26]

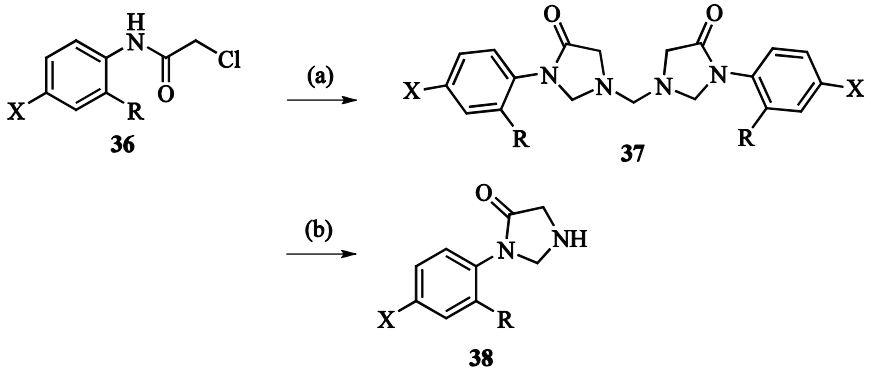

Scheme 12. *(a) Hexamine, EtOH, 2 h, reflux (b) HCl, $CHCl_3$, EtOH, 15 min, RT*

Imidazolidin-4-one by ring expansion and contraction

Other general synthetic routes to imidazolidin-4-one and analogues, rely on ring expansion reactions. Imidazolidin-4-one structures have been reported by ring expansion of precursor β-lactams. In another explicit synthesis of imidazolidin-4-one itself, the azetidin-3-one (**39**) is converted to an oxime and then mesylated to give **41**. Beckmann rearrangement gives the carbamate which can be deprotected to yield the desired compound (**43**).[27]

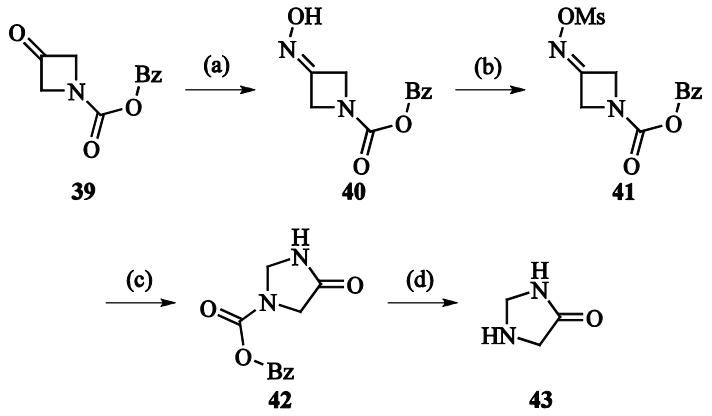

Scheme 13. *(a) NH_4Cl, H_2O (b) Methanesulfonyl chloride (c) Al_2O_3, benzene (d) H_2, Pd*

Bird *et al.* described the conversion of β-lactam (**44**) to imidazolidin-4-one (**45**) (**Scheme 14**). The benzylacetamide function was shown to play some role in the transformation. This was shown by as replacing it with *p*-methylbenzenesulfonamide and observing that it does not react in the same manner.[28] This suggested that the reactions usefulness could be limited to only a smaller range of compounds.

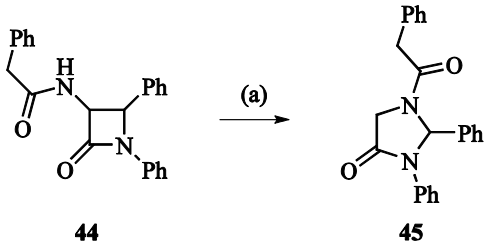

Scheme 14. *(a) I_2, xylene, reflux*

Oxaziridine (**46**) reacts with substituted *N*-arylketenimine (**47**) and to produce a complex imidazolidin-4-one (**48**) (**Scheme 15**). The nature of this product was confirmed by several subsequent reactions. Acidic hydrolysis yielded anilide and benzaldehyde. Treatment with lithium aluminium hydride with an acidic workup gave an acyclic diamine and benzaldehyde, yet with a basic workup gave a 1,3-diazolidine.[29] The reaction in **Scheme 16** produced imidazolidin-4-ones (**51**) from nitrones (**49**) and isocyanides (**50**) in a conceptually similar manner.[30]

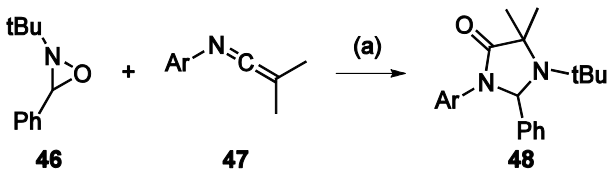

Scheme 15. *(a) benzene, 50 h, 80 °C*

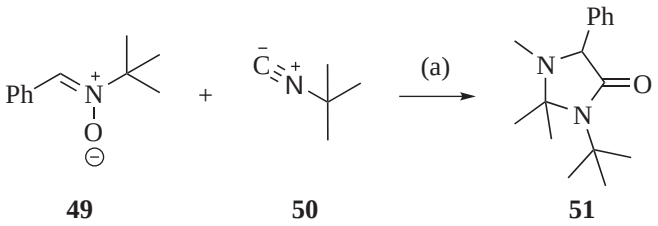

Scheme 16. *(a) CH_2Cl_2, 10 h, RT*

A number of examples where aziridine precursors have been converted to imidazolidin-4-ones exist in the literature. In **Scheme 17** 2-cyanoaziridine (**52**) interconverts to compound (**53**) which reacts with phenylisocyanate to form 4-imidazolidinone (**54**).[31] A similar reaction is shown in **Scheme 18**, substituted 2-(alkoxycarbonyl)aziridines (**55**) ring open to give azomethine ylides (**56**) which can react with vinyl isocyanates and give rise to imidazolidin-4-ones (**57**). This shows that a variety of functional groups are tolerated in this transformation.[32]

Finally in **Scheme 19** 3-aryl-1-methylaziridine-2-carboxamides (**59**) convert to intermediates (**58**) and react with 1-aryl-2-bromoethenes to give functionalized imidazolidin-4-ones (**60**).[33]

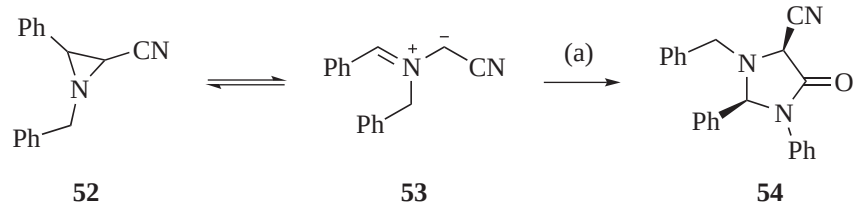

Scheme 17. *(a) PhNCO, toluene, 24 h, RT*

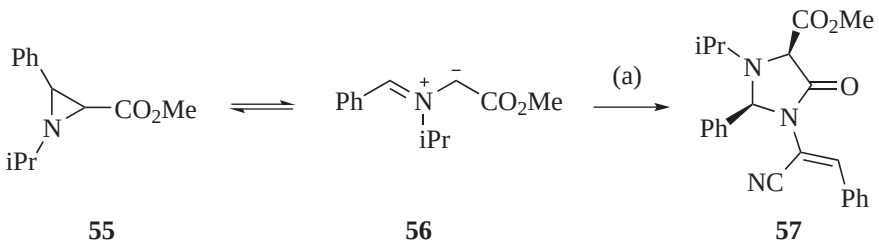

Scheme 18. *(a) PhCHC(CN)NCO, toluene*

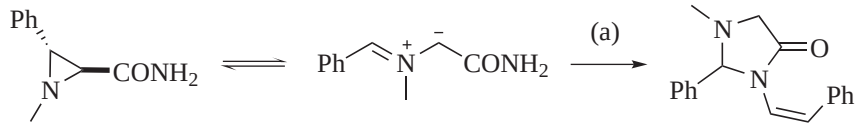

58 **59** **60**

Scheme 19. *(a) PhCHCHBr, CuI, N,N-dimethylglycine, Cs_2CO_3, dioxane, 12 h, reflux*

A remarkably fast ring expansion occurs when adding LDA to a solution of 1-benzhydryl-2,4-dimethyl-1,2-diazetidin-3-one (**61**), where the *N*-methyl carbon is incorporated into the imidazolidin-4-one ring of **62** (**Scheme 20**).[34] The suggested mechanism was supported by deuterium incorporation experiments.

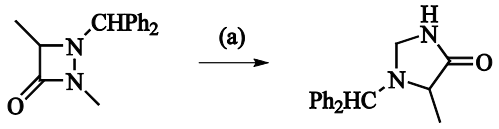

61 **62**

Scheme 20. *(a) LDA, THF, 1 min, -78 °C*

In an attempt to synthesize a range of substituted β-lactam ring systems Shevtsov and coworkers discovered **Scheme 21** where 1,2-dialkyldiaziridines (**64**) react with arylketenes (**63**) to give imidazolidin-4-ones (**65**).[35]

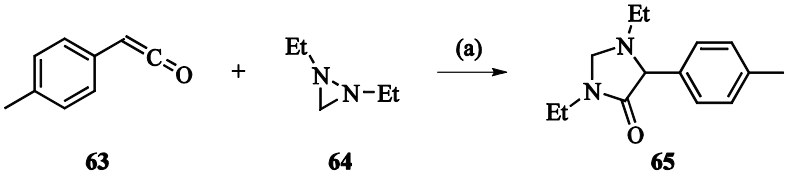

63 **64** **65**

Scheme 21. *(a) TEA, Et_2O, 17 h, -30 °C to RT*

Imidazolin-4-ones have also been obtained by ring contraction. Photochemical irradiation of 3,6,6-trimethyl-5,6-dihydropyrazin-2(1*H*)-one (**66**) (450W mercury lamp) in aqueous solution gave 5-methylimidazolidin-4-one (**67**) (**Scheme 22**). The by-product of this reaction is acetone and a corresponding mechanism has been suggested, however the practical scope of this reaction is yet to be reported.[36]

Another interesting ring contraction (**Scheme 23**) to highly derivatized imidazolidin-4-ones (**69**) arises from the desulfurization of hexahydrotriazines (**68**), however this approach also yields hydantoins. A complex six step mechanism is proposed for this reaction.[37]

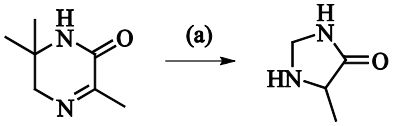

Scheme 22. *(a) hv, H_2O, 96 h, RT*

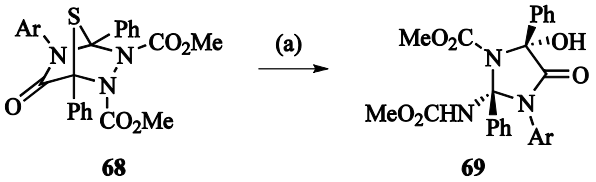

Scheme 23. *(a) Raney Ni, acetone, 4 h, RT*

Other routes to imidazolin-4-ones

Several other routes have been taken to imidazolidin-4-one derivatives and are summarized here. First, 4-nitro-1-phenylazoles (**70**) treated with reducing aluminium give an intermediate oxime (**71**), and that converts to an imidazolidin-4-one (**72**) in fair yields. The versatility of this pathway has yet to be significantly investigated (**Scheme 24**).[38]

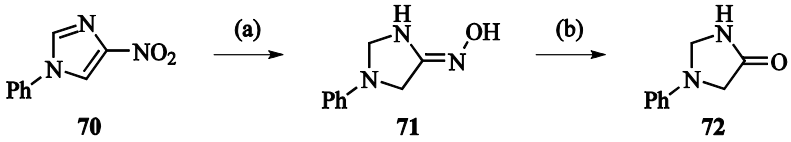

Scheme 24. *(a) Red-Al, MeOH (b) NaOH, H_2O_2, MeOH, H_2O*

The Weinreb amide (**73**) in **Scheme 25** reacts with potassium hexamethyldisilazide and cyclopentyl bromide to give a substituted imidazolidin-4-one (**74**). However the cyclisation reaction is dependent on the exact nature of the substituents, and can yield alternate 5-membered rings, therefore may not be useful in other synthetic schemes.[39]

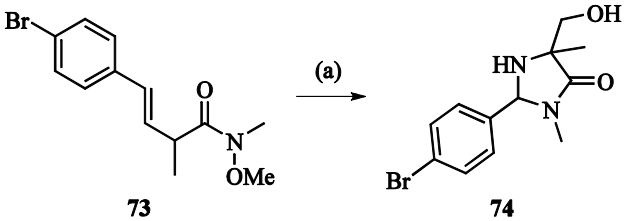

Scheme 25. *(a) potassium hexamethyldisilazide, cyclopentyl bromide, 20 h, -78 ^oC to RT*

As shown in **Scheme 26**, 2-vinylimidazolidin-4-ones (**76**) can be prepared from α-amino allenylamides (**75**). Microwave heating decreased the yield of imidazolidin-4-ones in favor of a 6-membered ring product.[40] Use of a gold catalyst can greatly increase the yield of imidazolidin-4-ones in this reaction.[41]

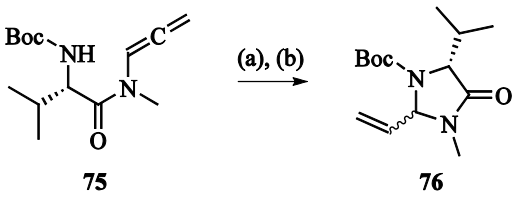

75 **76**

Scheme 26. *(a) t-BuOK, THF, 4 h, RT (b) $AuCl_3$, MeCN, 12 min, reflux*

The reaction in **Scheme 27** of diethyl zinc with a α-aldiminoester (**77**) yields a substituted imidazolidin-4-one (**78**) albeit as a side product of (**79**). The reaction is enantioselective but the imidazolidin-4-one was the minor product in all but one reported case.[42] Perhaps this would be amenable to optimization.

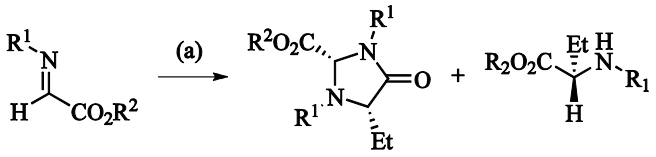

77 **78** **79**

Scheme 27. *(a) Et_2Zn, Ti-cat, Toluene, -40 ^oC*

Another method of combining an aminoacetamide and carbonyl containing compound is a three-component aza-Micheal addition reaction (**Scheme 28**). The example below uses (*S*)-2-amino-*N*-alkyl-3-methylbutanamide (**80**), 4-nitrobenzaldehyde (**81**) and but-3-en-2-one (**82**) produces imidazolidin-4-ones (**83**) in a highly stereoselective manner (up to >50 : 1).[43] The usefulness of chiral imidazolidin-4-ones as organic catalysts will be discussed further.

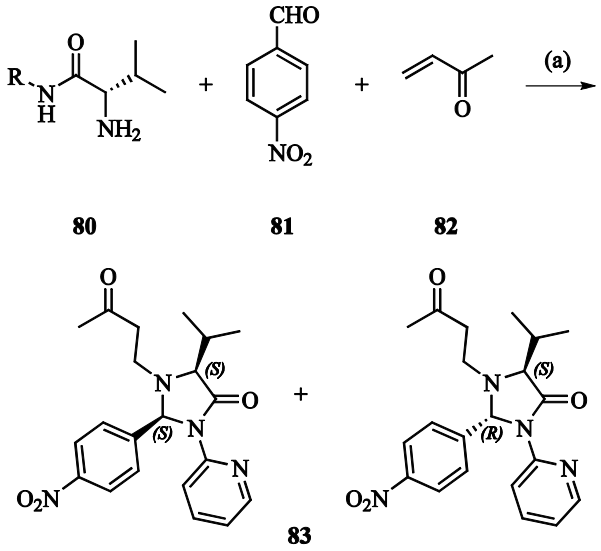

Scheme 28. *(a) TFA, iPrOH, 48 h, RT*

Imidazolidin-4-ones in synthesis

There are rather fewer reported reactions that use imidazolidin-4-ones as reactants reported in the literature. This may reflect the simplicity of making these compounds with the desired functionalities already in place or the difficulty of modifying them post-cyclization.

The facile nature of imidazolidin-4-one ring cyclisation and opening has been exploited in the synthesis of modified amino acids, via alkylation or substitution at an existing chiral center with stereocontrol.[44]

Glycinamide hydrochloride is converted to racemic 2-*tert*-butylimidazolidin-4-one by treatment with pivaldehyde followed by TFA. This racemic mix can be resolved by chiral HPLC or by two rounds of crystallization, the first with camphor sulfonic acid and then with *N*-acetyl-(*R*)-valine to give an enantiomeric ratio of greater than 99.5:0.5. The enantiopure imidazolidin-4-one (**86**) is protected with Boc and methylated to give (**88**). Activation with lithum diisopropylamide allows for substitution with an electrophile in a highly stereoselective manner. The monosubstituted imidazolidin-4-one (**90**) can then be deprotected, hydrolyzed without racemization. The resultant amino acid methyl ester is treated with benzylchloroformate to protect the amine, and for ease of purification. Alternatively a second round of activation, this time with *N*-butyl lithium and another stereoselective reaction with an electrophile gives di-substituted imidazolidin-4-one (**92**).

Following deprotection and hydrolysis an α,α-disubstituted amino acid methyl ester is revealed (**Scheme 29**).[45,46]

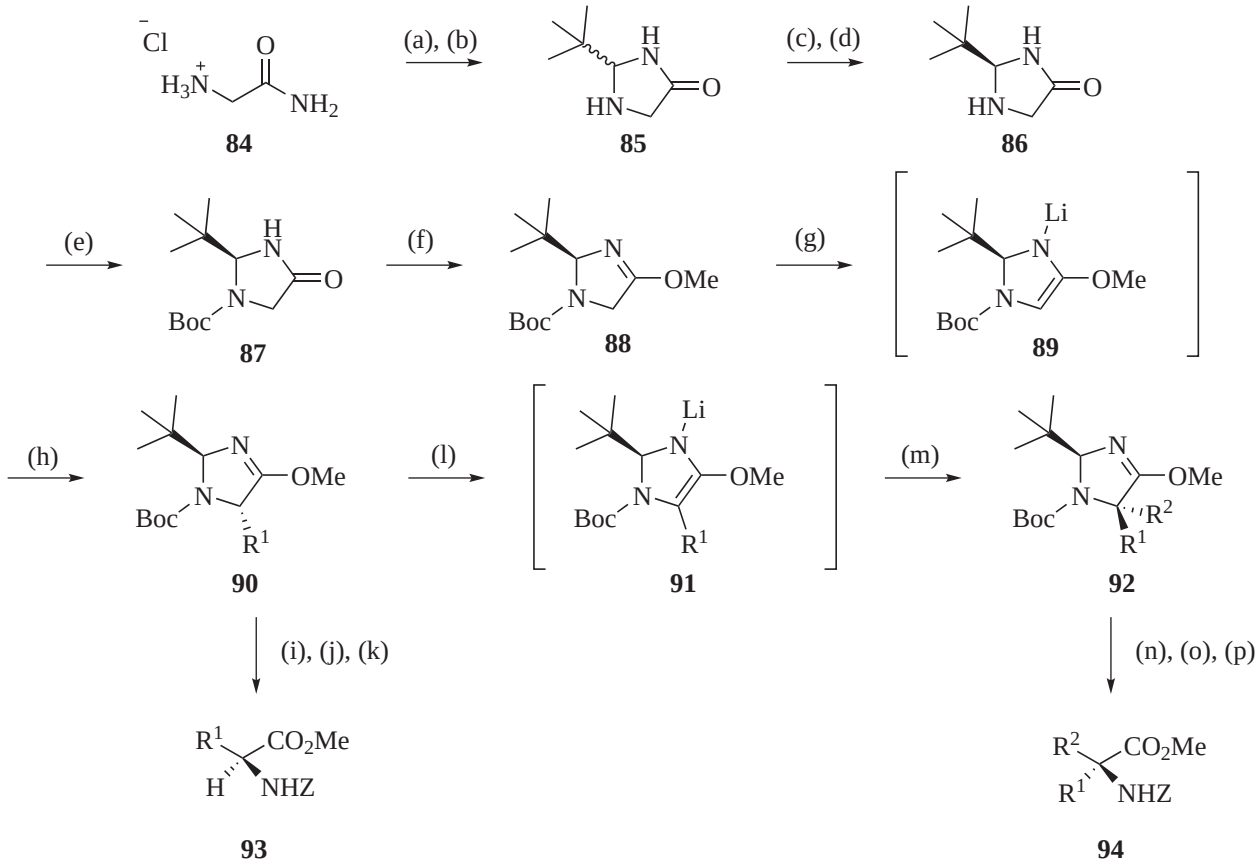

Scheme 29. *(a) tBuCHO, Et_3N, CH_2Cl_2, 16 h, reflux (b) TFA, CH_2Cl_2, 24 h, RT (c) (S)-(+)-CSA, acetone/MeOH, 16 h, reflux to RT (d) N-acetyl-(R)-valine, EtOAc, 16 h, reflux to RT (e) Boc_2O, Et_3N, CH_2Cl_2, 3 h, RT (f) Me_3OBF_4, CH_2Cl_2, 24 h, 0 °C (g) LDA, THF, 40 min, -78 °C (h) R^1X, 12 h, -78 °C to RT (i) TMSO-Tf, CH_2Cl_2, 12 h, -15 °C (j) 0.1M aq. TFA, THF, 4 d, 4 °C (k) Z-Cl, 2M NaOH, CH_2Cl_2, 1 d, RT (l) BuLi, THF, 40 min, -78 °C (m) R^2X, 12 h, -78 °C to RT (n) TFA, CH_2Cl_2, 8 h, RT (o) 2M aq. TFA, THF, 4 d, RT, (p) Z-Cl, 2M NaOH, CH_2Cl_2, 1 d, RT*

In a truncated **Scheme 30** (*S*)-1-benzoyl-2-(*tert*-butyl)-3-methyl-4-imidazolidinone (**95**) is a key precursor in the stereospecific synthesis of the antibiotic (+)-obafluorin (**96**).[47] A related method has also been used in a pilot plant scale synthesis of a cell adhesion inhibitor BIRT-377 (**97**).[48]

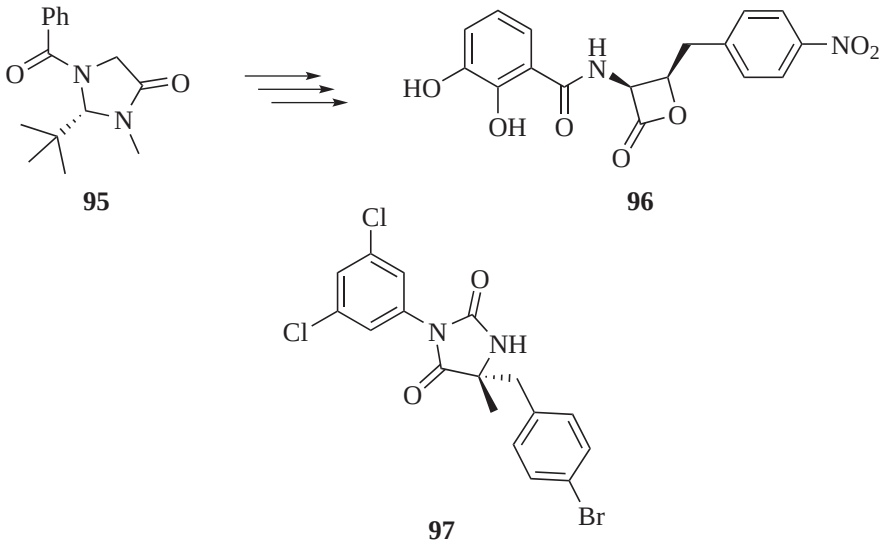

Scheme 30.

Several other works that include imidazolidin-4-one in some way have been published, some examples of which will be examined here.

Scheme 31 shows substituted imidazolidin-4-ones (**98**) can undergo 4+4 cycloaddition reactions with tetrachloro-*o*-benzoquinone (**99**) to give complex tricyclic systems (**100**).[49]

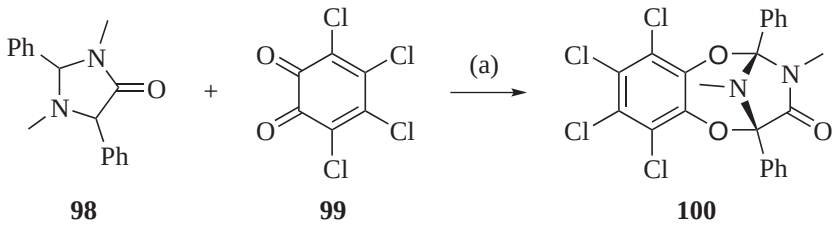

Scheme 31. *(a) CH_2Cl_2, 20 min, RT*

Whilst looking for novel nitrogen containing analogues of imidazolidin-4-ones, Blass *et al*. found that imidazolidin-4-ones (**101**) undergo nitrosation (**102**) at the amine function as expected. Reduction to the corresponding amine was found to be more challenging, proceeding only in the presence of zinc dust and ammonium chloride, yielding 1-amino imidazolidin-4-one (**103**) (**Scheme 32**).[50]

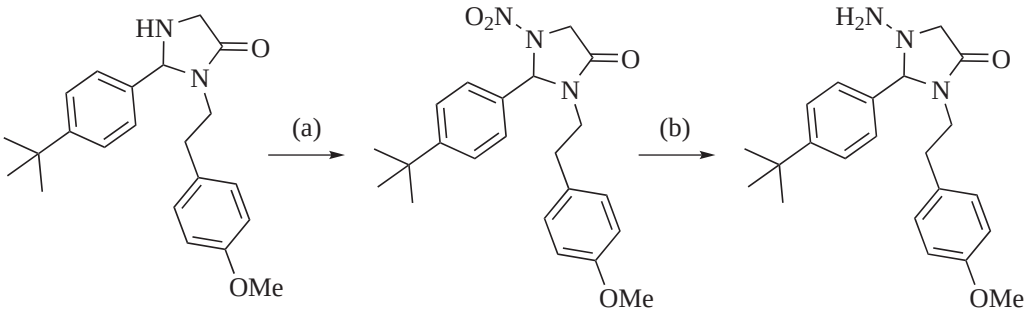

101 **102** **103**

Scheme 32. *(a) $NaNO_2$, AcOH, MeOH, 18 h, 0 °C to RT (b) Zn, NH_4Cl, MeOH, 10 min, 80 °C, microwave*

An investigation into the optical properties and geometry of imidazolidin-4-ones derived from α-amino acids concluded that circular dichroism spectrometry is a useful method for analyzing such compounds.[51] A series of NMR experiments were also undertaken in an effort to better characterize these substituted ring systems.[52,53] Hydrolysis of the imidazolidin-4-one ring can be achieved by refluxing in 6 M hydrochloric acid.[54] Some 2,2,5,5-substituted imidazolidin-4-ones can form stable nitroxide radicals, and can be used to stabilize synthetic polymers against light.[55]

There are a number of other medicinal chemistry projects that used imidazolidin-4-one in some way that will be discussed later.

As Organic Catalysts

Imidazolidin-4-ones make up a family of very useful organic catalysts generally referred to as iminium catalysts. They have a well understood activation mode that can be utilized in a number of different stereoselective reactions.[56] MacMillan *et al.* first reported highly enantioselective organocatalysis of the Diels-Alder reaction **Scheme 33**. Finding that (*S*)-5-benzyl-2,2,3-trimethylimidazolidin-4-one (**104**) is an efficient asymmetric catalyst that can be used in place of older Lewis acid type catalysts.[56]

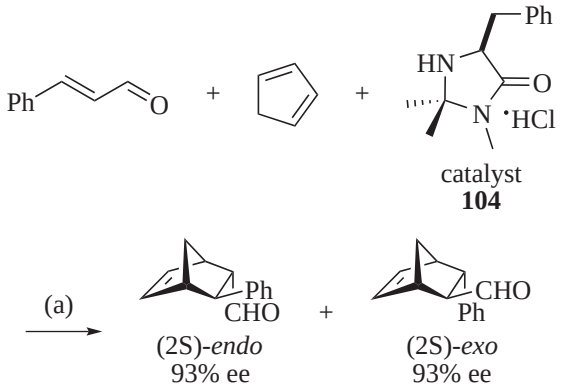

Scheme 33. *(a) cat. 5 mol%, MeOH, H_2O, RT, 21 h*

This catalytic strategy was also applied to a 1,3-dipolar cycloaddition reaction in **Scheme 34** between a α,β-unsaturated aldehyde (**106**) and a nitrone (**105**) giving **108** with a high *ee*. This reaction was not viable with traditional metal catalysis, possibly due to metal chelation by the nitrone group, which is not an issue when using this organic catalyst (**107**).[57]

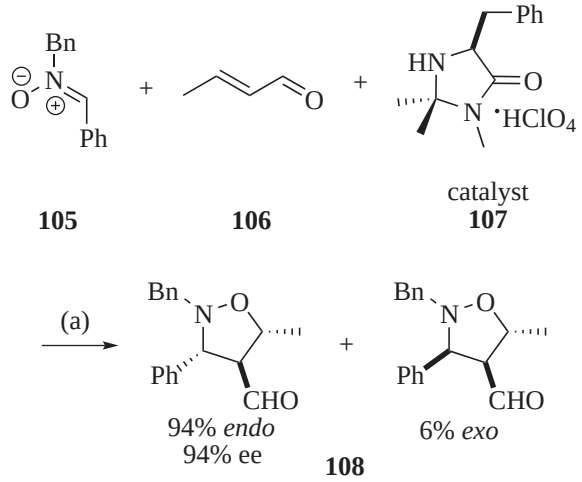

Scheme 34. *(a) cat. 20 mol%, $MeNO_2$, H_2O, 21 h, -20 °C*

Scheme 35 uses singly occupied molecular orbital activation catalysis which allows for asymmetric functionalization alpha to a carbonyl group. This unique organocatalytic mechanism utilizes the same class of imidazolidin-4-one organic catalysts (**109**) as iminium catalysis but involves a radical cation.[58,59]

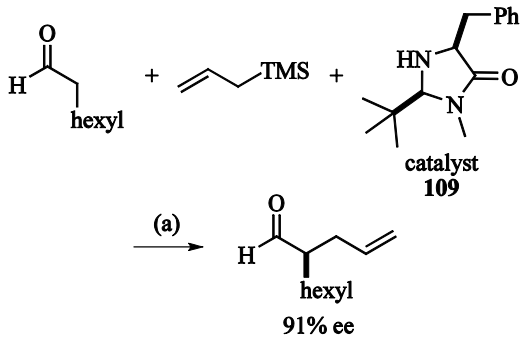

Scheme 35. *(a) cat. 20 mol%, ceric ammonium nitrate, $NaHCO_3$, DME, 24 h, -20 ^oC*

A solid phase equivalent of the iminium catalyst, used in the enantioselective Diels-Alder reaction, has been synthesized attached to a PEG polymer matrix. This allows the catalyst to function as it does in solution, and for easier catalyst recycling.[60] It has also been shown that different solid supports (e.g. amide resin, silica) can be used to tune the activity of the catalyst.[61-63]

Imidazolidin-4-ones in Medicinal Chemistry

The prevalence of imidazolidin-4-one in medicinal chemistry journals and patents has risen significantly in recent years. This could be due to a number of reasons, including the need for pharmaceutical companies to constantly be moving into new chemical space, rising interest in structurally related compounds such as Rolipram (**110**) or simply that a small rise in interest, promoted awareness and research in this motif.

The imidazolidin-4-one scaffold has appeared in a number of recent patents and medicinal chemistry journals for a wide variety of disease states. There have been patents filed for their use as CCR1 antagonists with possible anti-inflammatory effects (**111**),[64] and as sodium channel inhibitors which are typically used to treat cardiac arrythmia (**112**).[65] A series of spiroimidazolidin-4-ones (**113**) were patented by Pfizer as a treatment for diabetes related conditions.[66] A short series of compounds utilizing an imidazolidin-4-one scaffold (**114**) were synthesized and tested for inhibitory activity at human leukocyte elastase for a possible treatment of emphysema.[67] Simple *N*,*N*-Dihaloimidazolidin-4-ones (**115**) have been patented for being biocidal at low concentrations.[25]

There is a similar variety of imidazolidin-4-one containing compounds that have been reported as BBB penetrating agents with various activities. One patent claimed a series of analogs as CNS penetrating agents (**116**).[68] Another series has been patented as inhibitors of β-secretase for treatment for Alzheimer's disease (**117**),[69]. Analogues of Spiperone (**118**) were originally patented in 1975 and have become useful as radiolabels for imaging dopamine receptor subtypes.[70,71] In work related to the synthesis of an unsubstituted imidazolidin-4-one ring by Pfieffer *et al*. a patent has been filed for a series of nootropic compounds (**119**).[72] A related paper by Pinza *et al*, utilizes imidazolidin-4-ones as an intermediate to get to a related series of bicyclic compounds that could also be used as cognition enhancers.[73] This vast breadth of applications in medicinal chemistry highlights both the novelty and versatility of this motif.

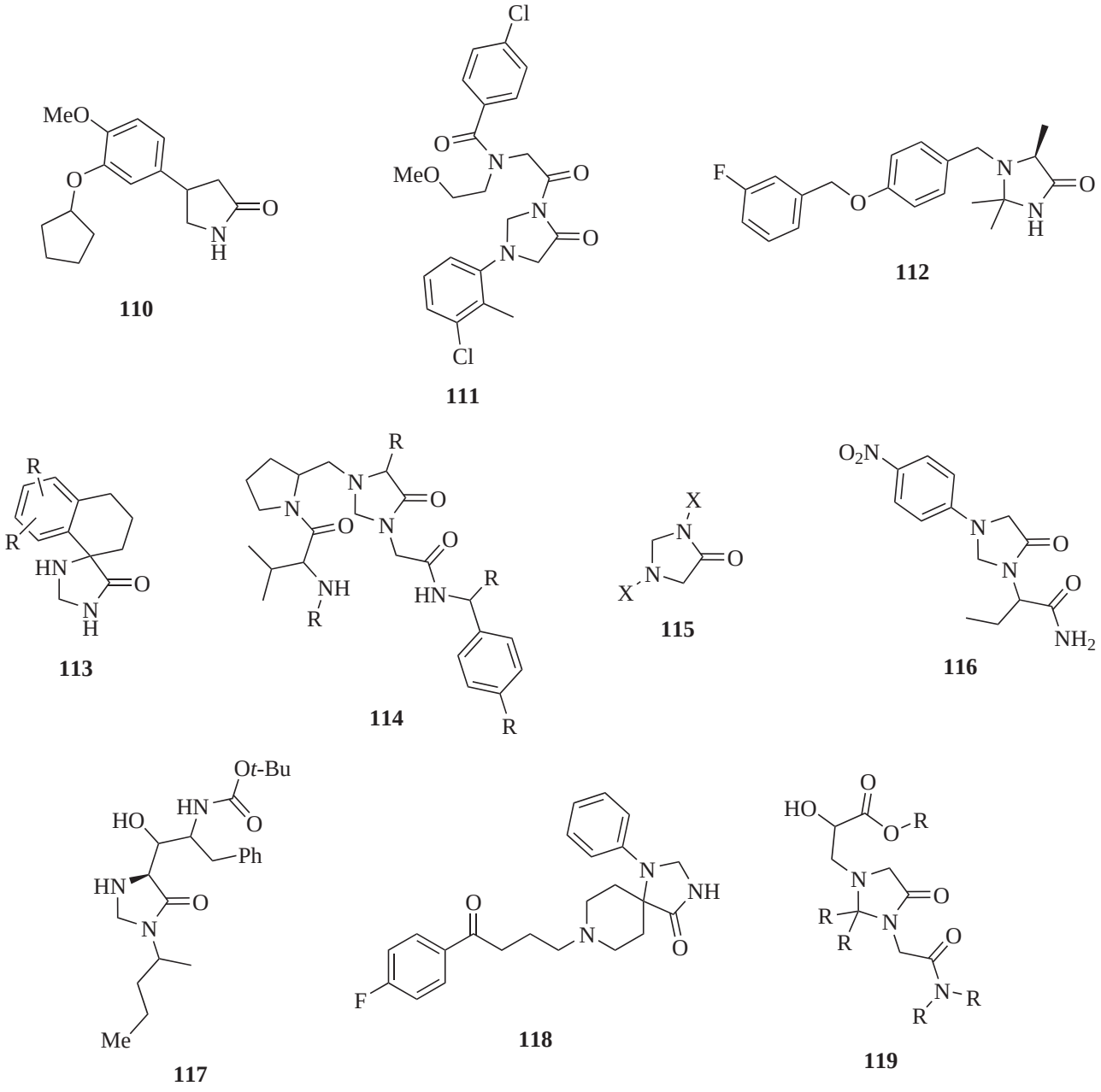

Figure 1

Pro drugs

Imidazolidin-4-ones can be labile to hydrolysis under physiological conditions; this has lead to several investigations into prodrugs containing this motif. A prime example is Hetacillin (**Figure 2, 120**), a prodrug of ampicillin, contains an imidazolidin-4-one ring that is cleaved in the body.[74]

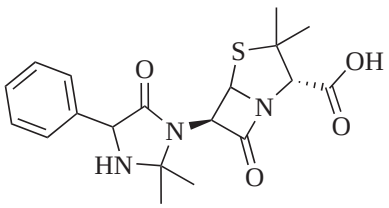

120

Figure 2

Ethanol is metabolized to acetaldehyde, it was hypothesized that this could react with a metabolite of lidnocaine to form a stable imidazolidin-4-one species.[75] The equivalent condensation with prilocaine (**121**) and formaldehyde to form an imidazolidin-4-one prodrug (**122**) was investigated along with the kinetics of its degradation (**Scheme 36**).[76]

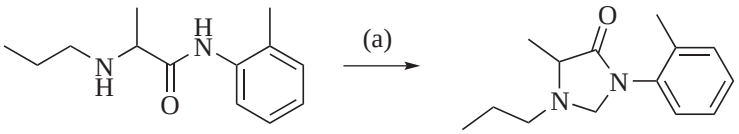

121 **122**

Scheme 36. *(a) CH_2O, toluene, 3 h, reflux*

An analogous study **Scheme 37** was conducted on imidazolidin-4-one prodrugs (**124**) of primaquine derivatives (**123**), further studies found that these prodrugs were active anti-malarial agents in their own right.[77,78] It was also found that formation of such prodrugs can occur in an enantioselective manner.[79]

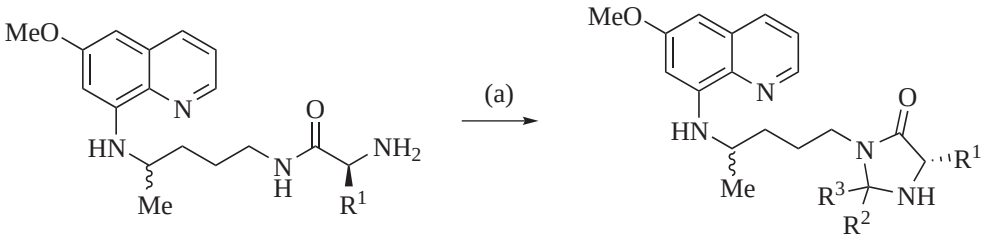

123 **124**

Scheme 37. *(a) R^2R^3CO, Et_3N, sieves, MeOH, 3 d, reflux*

To improve the metabolic stability of a peptide the amino terminus can be condensed with an aldehyde such as acetone and form an imidazolidin-4-one. This peptide motif has been reported to occur naturally. The open side chain of cyclopeptide alkaloid Nummularine-B (**125**) was converted to a imidazolidin-4-one (**126**) by treatment with formaldehyde in ethanol (**Scheme 38**), this was used to confirm the existence of a natural equivalent peptide.[80]

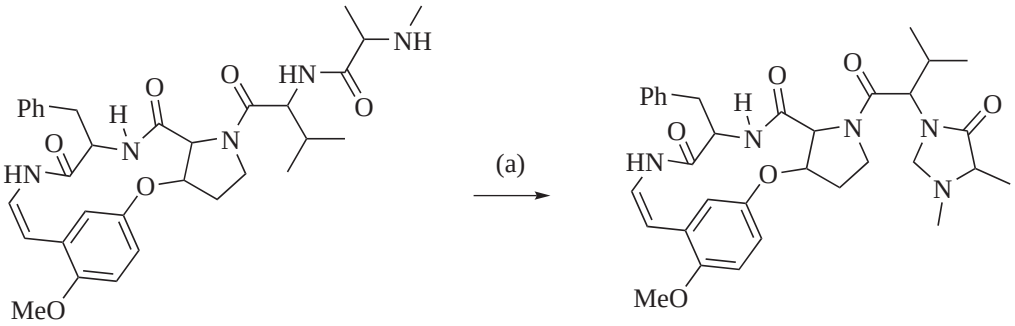

125 **126**

Scheme 38. *(a) formaldehyde, H_2O, < 24 h, RT*

In the presence of formaldehyde or acetaldehyde the N-terminus of glycopeptide antibiotic Vancomycin will spontaneously convert to an imidazolidin-4-one. This modification is reversible but while in the cyclized state the drugs potency is significantly reduced.[81] Similarly enkephalin peptides can resist metabolism by adding an imidazolidin-4-one ring into the peptide backbone. The peptide will be spontaneously hydrolyzed back to its native state in physiological conditions.[82] Cyclizing the N-terminus with acetone increases the half life of leu-enkephalin from 6 minutes to 23.5 hours.[82] The activity and stability of leu-enkephalin with imidazolidin-4-one rings installed at different positions have been studied.[83]

Conclusion

In this review, we have identified the surprising number of different synthetic approaches that can be taken to the synthesis of imidazolidin-4-one derivatives, and the variety of applications in which they can be exploited as reagents, catalysts, bioactive molecules and prodrugs.

While the imidazolin-4-one ring has in many respects been neglected as a functional moiety in medicinal chemistry, it has been appearing more often in recent times particularly in the patent literature. This would

seem to be logical as the ring system has multiple points of substitution and within its own structure multiple means by which it could participate in interactions with macromolecular targets. As such simply substituted imidazolin-4-ones can be envisaged as excellent components of fragment-based screening libraries likely to possess high ligand efficiency as well as chemical novelty. The variety of synthetic approaches should see numerous new compounds and interesting applications of this class of heterocycle developed in the future.

References and Notes

[1] H. Biltz, *Berl. Dtsch. Chem. Gesamte.*, 1908, **41**, 1379.

[2] T. J. Putnam and H. H. Merritt, *Science*, 1937, **85**, 525.

[3] H. Biltz, *Chem. Ber.*, 1909, **42**, 1792.

[4] H. Biltz and K. Seydel, *Liebigs. Annalen.*, 1912, **391**, 215.

[5] H. C. Carrington, C. H. Vasey and W. S. Waring, *J. Chem. Soc.*, 1953, 3105.

[6] J. T. Edward and I. Lantos, *Can. J. Chem.*, 1967, **45**, 1925.

[7] W. B. Whalley, E. L. Anderson, F. Dugan, J. W. Wilson and G. E. Ullyot, *J. Am. Chem. Soc.*, 1955, **77**, 745.

[8] U. Pfeiffer, M. T. Riccaboni, R. Erba and M. Pinza, *Liebigs. Annalen.*, 1988, 993.

[9] R. Pascal, M. Lasperas, J. Taillades, A. Commeyras and A. Perez-Rubalcaba, *Bull. Soc. Chim. Fr. II*, 1984, **7**, 329.

[10] R. Pascal, J. Taillades and A. Commeyras, *Tetrahedron*, 1978, **34**, 2275.

[11] R. E. Harmon, V. L. Rizzo and S. K. Gupta, *J. Heterocycl. Chem.*, 1970, **7**, 439.

[12] A. Cordi, J. M. Lacoste, V. Audinot and M. Millan, *Bioorg. Med. Chem. Lett.*, 1999, **9**, 1409.

[13] A. C. Davis and A. L. Levy, *J. Chem. Soc.*, 1951, 3479.

[14] E. Schipper and E. Chinery, *J. Org. Chem.*, 1961, **26**, 4480.

[15] A. Khalaj, R. D. Bazaz and M. Shekarchi, *Monatshe. Chem.*, 1997, **128**, 395.

[16] M. A. Nooshabadi, K. Aghapoor, M. Bolourtchian and M. M. Heravi, *J. Chem. Res., Synop.*, 1999, 498.

[17] F. Kusuda, Y. Matsuo and E. Seto. 1966, US3284447

[18] M. Rinnova, A. Vidal, A. Nefzi and R. Houghten, *J. Comb. Chem.*, 2002, **4**, 209.

[19] L. Feliu, G. Subra, J. Martinez and M. Amblard, *J. Comb. Chem.*, 2003, **5**, 356.

[20] P. Bedos, L. Feliu, J. Martinez and M. Amblard, *Tetrahedron Lett.*, 2003, **44**, 4937.

[21] L.-Y. Qin, *Tetrahedron Lett.*, 2009, **50**, 419.

[22] P. G. Wiering and H. Steinberg, *Recl. Trav. Chim. Pays-Bas*, 1971, **90**, 284.

[23] Y. G. Gololobov and L. I. Nesterova, *Khim. Geterotsikl. Soedin.*, 1980, 706.

[24] R. Anzai and K. Kikuchi. 2002, JP 2002265453

[25] S. D. Worley, T. Tsao and D. E. Williams. 1991, WO 9110623

[26] M. Hannoun, M. Zinic, D. Kolbah, N. Blazevic and F. Kajfez, *J. Heterocycl. Chem.*, 1981, **18**, 963.

[27] Y. Nitta, *Heterocycles*, 1986, **24**, 25.

[28] C. W. Bird, *Tetrahedron Lett.*, 1964, 609.

[29] N. Murai, M. Komatsu, Y. Ohshiro and T. Agawa, *J. Org. Chem.*, 1977, **42**, 448.

[30] D. Moderhack, M. Lorke and D. Schomburg, *Liebigs. Annalen.*, 1984, 1685.

[31] H. Benhaoua, F. Texier and R. Carrie, *Tetrahedron*, 1986, **42**, 2283.

[32] O. Mamoun and H. Benhaoua, *Bull. Soc. Chim. Belg.*, 1994, **103**, 753.

[33] J.-Y. Wang, Y. Hu, D.-X. Wang, J. Pan, Z.-T. Huang and M.-X. Wang, *Chem. Comm.*, 2009, 422.

[34] E. C. Taylor, R. J. Clemens, H. M. L. Davies and N. F. Haley, *J. Am. Chem. Soc.*, 1981, **103**, 7659.

[35] A. V. Shevtsov, V. Y. Petukhova, Y. A. Strelenko, K. A. Lyssenko, I. V. Fedyanin and N. N. Makhova, *Mendeleev Commun.*, 2003, **13**, 221.

[36] D. L. Kleyer and T. H. Koch, *J. Org. Chem.*, 1982, **47**, 3145.

[37] T. Sheradsky and N. Itzhak, *J. Chem. Soc. Perkin. Trans. 1*, 1989, 33.

[38] J. Suwinski and P. Wagner, *Pol. J. Chem.*, 2000, **74**, 1575.

[39] C. L. Gibson, A. R. Kennedy, R. R. Morthala, J. A. Parkinson and C. J. Suckling, *Tetrahedron*, 2008, **64**, 7619.

[40] G. Broggini, S. Galli, M. Rigamonti, S. Sottocornola and G. Zecchi, *Tetrahedron Lett.*, 2009, **50**, 1447.

[41] A. Manzo, *Tetrahedron Lett.*, 2009, **50**, 4696.

[42] S. Basra, M. W. Fennie and M. C. Kozlowski, *Org. Lett.*, 2006, **8**, 2659.

[43] Z. Xu, T. Buechler, K. Wheeler and H. Wang, *Chem. Eur. J.*, 2010, **16**, 2972.

[44] D. Seebach, D. D. Miller, S. Mueller and T. Weber, *Helv. Chim. Acta*, 1985, **68**, 949.

[45] M. Hoffmann, S. Blank, D. Seebach, E. Küsters and E. Schmid, *Chirality*, 1998, **10**, 217.

[46] D. Seebach and M. Hoffmann, *Eur. J. Med. Chem.*, 1998, **7**, 1337.

[47] C. Lowe, Y. Pu and J. C. Vederas, *J. Org. Chem.*, 1992, **57**, 10.

[48] N. K. Yee, L. J. Nummy, R. P. Frutos, J. J. Song, E. Napolitano, D. P. Byrne, P.-J. Jones and V. Farina, *Tetrahedron: Asymmetry*, 2003, **14**, 3495.

[49] W. Friedrichsen, W. D. Schroeer and T. Debaerdemaeker, *Liebigs. Annalen.*, 1980, 1850.

[50] B. E. Blass, K. Coburn, N. Fairweather, A. Fluxe, S. Hodson, C. Jackson, J. Janusz, W. Lee, J. Ridgeway, R. White and S. Wu, *Tetrahedron Lett.*, 2006, **47**, 7497.

[51] T. Polonski, *Tetrahedron*, 1985, **41**, 611.

[52] T. Połoński, *Org. Magn. Reson.*, 1984, **22**, 176.

[53] C. Garcia-Martinez, H. Cervantes-Cuevas and J. Escalante-Garcia, *Chirality*, 2003, **15**, S74.

[54] D. Seebach, E. Juaristi, D. D. Miller, C. Schickli and T. Weber, *Helvetica Chimica Acta*, 1987, **70**, 237.

[55] T. Toda, S. Morimura, E. Mori, H. Horiuchi and K. Murayama, *Bull. Chem. Soc. Jap.*, 1971, **44**, 3445.

[56] K. A. Ahrendt, C. J. Borths and D. W. C. Macmillan, *J. Am. Chem. Soc.*, 2000, **122**, 4243.

[57] W. S. Jen, J. J. M. Wiener and D. W. C. Macmillan, *J. Am. Chem. Soc.*, 2000, **122**, 9874.

[58] T. D. Beeson, A. Mastracchio, J.-B. Hong, K. Ashton and D. W. C. Macmillan, *Science*, 2007, **316**, 582.

[59] H.-Y. Jang, J.-B. Hong and D. W. C. Macmillan, *J. Am. Chem. Soc.*, 2007, **129**, 7004.

[60] M. Benaglia, G. Celentano, M. Cinquini, A. Puglisi and F. Cozzi, *Adv. Synth. Catal.*, 2002, **344**, 149.

[61] S. A. Selkala, J. Tois, P. M. Pihko and A. M. P. Koskinen, *Adv. Synth. Catal.*, 2002, **344**, 941.

[62] A. Puglisi, M. Benaglia, M. Cinquini, F. Cozzi and G. Celentano, *Eur. J. Org. Chem.*, 2004, 567.

[63] C. S. Pecinovsky, G. D. Nicodemus and D. L. Gin, *Chem. Mater.*, 2005, **17**, 4889.

[64] P. Zhang, A. M. K. Pennell, L. Li and E. J. Sullivan. 2008, US 7786157

[65] C. Cattaneo, R. Fariello and R. Maj. 2009, EP2093218

[66] J. L. Belletire and R. Sarges. 1981, EP0028485B1

[67] L. Wei, *Bioorg. Med. Chem.*, 2003, **11**, 5149.

[68] B. Kenda, L. Turet, L. Quesnel, P. Michel and A. Ates. 2008, WO 2008132142

[69] J. C. Barrow, K. E. Rittle and P. L. Bondiskey. 2007, WO2007058862

[70] K. Sasajima, K. Ono, M. Nakao, I. Maruyama, M. Takayama, S. Katayama, J. Katsube, S. Inaba and H. Yamamoto. 1975, JP 50005385A

[71] V. Bakthavachalam, N. Baindur, B. K. Madras and J. L. Neumeyer, *J. Med. Chem.*, 1991, **34**, 3235.

[72] M. Pinza, U. Pfeiffer, C. Farina and S. Banfi. 1987, EP0207681A2

[73] M. Pinza, C. Farina, A. Cerri, U. Pfeiffer, M. T. Riccaboni, S. Banfi, R. Biagetti, O. Pozzi, M. Magnani and L. Dorigotti, *J. Med. Chem.*, 1993, **36**, 4214.

[74] G. A. Hardcastle, Jr., D. A. Johnson, C. A. Panetta, A. I. Scott and S. A. Sutherland, *J. Org. Chem.*, 1966, **31**, 897.

[75] S. D. Nelson, G. D. Breck and W. F. Trager, *J. Med. Chem.*, 1973, **16**, 1106.

[76] S. W. Larsen, M. Sidenius, M. Ankersen and C. Larsen, *Eur. J. Pharm. Sci.*, 2003, **20**, 233.

[77] P. Gomes, M. J. Araújo, M. Rodrigues, N. Vale, Z. Azevedo, J. Iley, P. Chambel, J. Morais and R. Moreira, *Tetrahedron*, 2004, **60**, 5551.

[78] M. J. Araujo, J. Bom, R. Capela, C. Casimiro, P. Chambel, P. Gomes, J. Iley, F. Lopes, J. Morais, R. Moreira, O. E. De, R. V. Do and N. Vale, *J. Med. Chem.*, 2005, **48**, 888.

[79] R. Ferraz, J. R. B. Gomes, O. E. De, R. Moreira and P. Gomes, *J. Org. Chem.*, 2007, **72**, 4189.

[80] A. H. Shah, V. B. Pandey, G. Eckhardt and R. Tschesche, *Phytochemistry*, 1985, **24**, 2765.

[81] A. J. R. Heck, P. J. Bonnici, E. Breukink, D. Morris and M. Wills, *Chem. Eur. J.*, 2001, **7**, 910.

[82] G. J. Rasmussen and H. Bundgaard, *Int. J. Pharm.*, 1991, **76**, 113.

[83] M. Rinnová, A. Nefzi and R. A. Houghten, *Bioorg. Med. Chem. Lett.*, 2002, **12**, 3175.